

University of Central Florida

STARS

Electronic Theses and Dissertations, 2020-

2021

Reliable and Efficient Cognitive Radio Communications Using Directional Antennas

Hassan Yazdani

University of Central Florida



Part of the [Electrical and Computer Engineering Commons](#)

Find similar works at: <https://stars.library.ucf.edu/etd2020>

University of Central Florida Libraries <http://library.ucf.edu>

This Doctoral Dissertation (Open Access) is brought to you for free and open access by STARS. It has been accepted for inclusion in Electronic Theses and Dissertations, 2020- by an authorized administrator of STARS. For more information, please contact STARS@ucf.edu.

STARS Citation

Yazdani, Hassan, "Reliable and Efficient Cognitive Radio Communications Using Directional Antennas" (2021). *Electronic Theses and Dissertations, 2020-*. 1164.

<https://stars.library.ucf.edu/etd2020/1164>

RELIABLE AND EFFICIENT COGNITIVE RADIO COMMUNICATIONS USING DIRECTIONAL ANTENNAS

by

HASSAN YAZDANI

B.S. in Electrical Engineering, Shiraz University of Technology, Shiraz, Iran, 2009

M.S. in Electrical Engineering, University of Tehran, Tehran, Iran, 2012

A dissertation submitted in partial fulfilment of the requirements
for the degree of Doctor of Philosophy
in the Department of Electrical and Computer Engineering
in the College of Engineering and Computer Science
at the University of Central Florida
Orlando, Florida

Summer Term
2021

Major Professor: Azadeh Vosoughi

© 2021 Hassan Yazdani

ABSTRACT

Cognitive Radio (CR) is a promising solution that enhances spectrum utilization by allowing an unlicensed or Secondary User (SU) to access licensed bands in a such way that its imposed interference on a license holder Primary User (PU) is limited, and hence fills the spectrum holes in time and/or frequency domains. Resource allocation, which involves scheduling of available time and transmit power, represents a crucial problem for the performance evaluation of CR systems. In this dissertation, we study the spectral efficiency maximization problem in an opportunistic CR system. Specifically, in the first part of the dissertation, we consider an opportunistic CR system where the SU transmitter (SU_{tx}) is equipped to a Reconfigurable Antenna (RA). RA, with the capabilities of dynamically modifying their characteristics can improve the spectral efficiency, via beam steering and utilizing the spectrum white spaces in spatial (angular) domain. In our opportunistic CR system, SU_{tx} relies on the beam steering capability of RA to detect the direction of PU's activity and also to select the strongest beam for data transmission to SU receiver (SU_{rx}). We study the combined effects of spectrum sensing error and channel training error as well as the beam detection error and beam selection error on the achievable rates of an opportunistic CR system with a RA at SU_{tx} . We also find the best duration for spectrum sensing and channel training as well as the best transmit power at SU_{tx} such that the throughput of our CR system is maximized subject to the Average Transmit Power Constraint (ATPC) and Average Interference Constraint (AIC).

In the second part of the dissertation, we consider an opportunistic Energy Harvesting (EH)-enabled CR network, consisting of multiple SUs and an Access Point (AP), that can access a wideband spectrum licensed to a primary network. Assuming that each SU is equipped with a finite size rechargeable battery, we study how the achievable sum-rate of SUs is impacted by the combined effects of spectrum sensing error and imperfect Channel State Information (CSI) of SUs-AP links. We also design an energy management strategy that maximizes the achievable sum-rate of SUs, subject to a constraint on the average interference that SUs can impose on the PU.

To my love, Ghazaleh, who never gave up on me, for her endless support,
and to my parants and my sisters.

ACKNOWLEDGMENTS

I would like to express my sincere gratitude to my advisor Prof. Azadeh Vosoughi of the Electrical and Computer Engineering department at UCF for her insightful guidance, immense knowledge, and continuous support of my PhD study and research. She was incessantly encouraging, supportive, and ready to provide practical help and advice.

I am also grateful to my committee members for their great support and invaluable advice: Dr. Xun Gong, Dr. Murat Yuksel, Dr. Nazanin Rahnavard of the Electrical and Computer Engineering program and Dr. Marianna Pensky of Department of Mathematics.

I am grateful to my close friends for providing support and friendship that I needed in my PhD life. I also want to thank my lab mates for the stimulating discussions and brainstorms we did and for sharing their valuable ideas in research related problems I encountered along the way.

I would like to thank my parents and my sisters who have provided me through moral and emotional support in my life.

Words cannot express how grateful I am to my beloved wife, who always supports me with her unconditional love through thick and thin.

Last but not least, thanks are also due to the National Science Foundation (NSF) for supporting this research under grants CCF-1341966, CCF-1319770, ECCS-1418710, CCF-1718195, ECCS-1443942, and CISE-CNS-2006683.

TABLE OF CONTENTS

LIST OF FIGURES	xi
LIST OF TABLES	xiv
LIST OF ACRONYMS	xv
CHAPTER 1: INTRODUCTION AND LITERATURE REVIEW	1
1.1 Cognitive Radio Systems	1
1.1.1 Transmit Power Control	2
1.1.2 Spectrum Sensing	3
1.1.3 Channel Estimation	4
1.1.4 Combined effects of Spectrum Sensing, Channel Estimation and Transmit Power Control in Opportunistic CR Systems	5
1.2 Energy Harvesting in CR Systems	6
1.3 Integration of Directional Antennas in Opportunistic CR Systems	7
1.3.1 Reconfigurable Antenna	8
1.4 Motivation, Contributions and Dissertation Organization	10
CHAPTER 2: BEAM SELECTION AND DISCRETE POWER ALLOCATION IN OPPORTUNISTIC COG- NITIVE RADIO SYSTEMS WITH LIMITED FEEDBACK USING ESPAR ANTENNAS	16
2.1 System Model and Problem Statement	16

2.1.1	Background on ESPAR Antennas	16
2.1.2	Geometry of Our Opportunistic CR System	18
2.1.3	Our Problem Statement	19
2.2	Characterizing Objective Function and Constraints in (2.P1)	24
2.2.1	Energy-Based Binary Detector for Spectrum Sensing Using ESPAR Antenna	24
2.2.2	Determining the Beam Corresponding to PU	26
2.2.3	Determining the Beam Corresponding to SU_{rx}	29
2.3	Formalizing and Solving (2.P1)	30
2.3.1	Formalizing (2.P1) with Modified Objective Function and Constraints	31
2.3.2	Solving (2.P2)	33
2.4	Outage and Symbol Error Probabilities	34
2.5	Simulation Results	36
2.6	Conclusions	41
CHAPTER 3: ACHIEVABLE RATES OF OPPORTUNISTIC COGNITIVE RADIO SYSTEMS USING RE- CONFIGURABLE ANTENNAS WITH IMPERFECT SENSING AND CHANNEL ESTIMA- TION		43
3.1	System Model	44
3.1.1	Structure of a RA	44
3.1.2	Description of Our Opportunistic CR System	44
3.2	Spatial Spectrum Sensing Phase	47

3.2.1	Eigenvalue-Based Detector for Spatial Spectrum Sensing	47
3.2.2	Determining the Beam Corresponding to PU Direction	49
3.3	Channel Training Phase	50
3.3.1	Channel Estimation at SU_{rx}	50
3.3.2	Determining the Beam Corresponding to SU_{rx} Direction	52
3.4	Data Transmission Phase	54
3.5	Constrained Maximization of Rate Lower Bound	59
3.5.1	Scheme 1	62
3.5.2	Scheme 2	63
3.5.3	Discussion on Computational Complexity of Proposed Algorithms	63
3.6	Simulation Results	65
3.7	Conclusions	68
CHAPTER 4: STEADY-STATE RATE-OPTIMAL POWER ADAPTATION IN ENERGY HARVESTING OP- PORTUNISTIC COGNITIVE RADIOS WITH SPECTRUM SENSING AND CHANNEL ESTI- MATION ERRORS		70
4.1	System Model	71
4.1.1	Battery and Energy Harvesting Models	71
4.1.2	Slot Structure of SUs	73
4.1.3	Transmission Model and Battery Dynamics	74
4.2	Spectrum Sensing Phase	78

4.3	Channel Probing Phase	80
4.4	Data Transmission Phase	82
4.5	Simulation Results	88
4.6	Conclusion	98
CHAPTER 5: THROUGHPUT-OPTIMAL D2D MMWAVE COMMUNICATION: JOINT COALITION FOR-		
MATION, POWER, AND BEAM OPTIMIZATION		99
5.1	System Overview	99
5.1.1	System Model	99
5.1.2	Antenna Model	102
5.1.3	Problem Formulation	102
5.2	Solving Problem	104
5.2.1	Solving Sub-problem (5.SP1)	105
5.2.2	Solving Sub-problem (5.SP2)	106
5.2.3	Solving Sub-problem (5.SP3)	108
5.3	Numerical Performance Evaluations	108
5.4	Conclusion	112
CHAPTER 6: CONCLUSION		113
6.1	Conclusions	113
APPENDIX A: APPENDIX FOR CHAPTER 3		116

A.1	Showing that $\partial R_{LB}/\partial T_{se} = 0$ has one solution in the interval $(0, T_f - T_{tr})$	117
A.2	Showing that $\partial R_{LB}/\partial T_{tr} = 0$ has one solution in the interval $(0, T_f - T_{se})$	118
APPENDIX B: BIOGRAPHICAL SKETCH		119
APPENDIX C: PUBLICATIONS		121
APPENDIX D: COPYRIGHT PERMISSIONS		124
LIST OF REFERENCES		131

LIST OF FIGURES

1.1	The structure of frame employed by SU_{tx}	2
2.1	The ESPAR antenna structure and its beampatterns, (a) The ESPAR antenna structure, (b) Beam-patterns of an ESPAR with 8 parasitic elements, assuming the Gaussian radiation pattern in (2.1).	18
2.2	Our CR system with an $(M+1)$ -element ESPAR antenna at SU_{tx} and omni-directional antennas at SU_{rx} and PU.	19
2.3	The structure of frame employed by SU_{tx}	20
2.4	A schematic to show how different beams can be selected to indicate the orientation of SU_{tx} with respect to PU and SU_{rx} (a) $m_{PU}^* = 3$, (b) $m_{SR}^* = 2$	27
2.5	Δ_1 versus ϕ_{PU} for $M = 8$ and $SNR_{PU} = 0$ dB (a) $N_{se} = 20$, $\phi_{3dB} = 20^\circ, 30^\circ$ (b) $\phi_{3dB} = 20^\circ$, $N_{se} = 10, 30, 200$	28
2.6	$\bar{\Delta}_{1,m}$ versus the index beam m for $\phi_{3dB} = 20^\circ$ (a) $SNR_{PU} = 0$ dB, (b) $SNR_{PU} = -5$ dB.	29
2.7	Parameters $A_0 = 0.97$, $A_1 = 0.03$, which correspond to $E_A = 0.145$. For a fair comparison, we set the gain of the omni-directional antenna $p^{Om}(\phi) = E_A$ for $\phi \in (-\pi, \pi)$, to ensure that the equality in (2.45) holds true. (a) polar coordinate, (b) Cartesian coordinate.	37
2.8	C_{Opt}^{LB} and $C_{Opt}^{LB,Om}$ versus \bar{P}_{av} for $m_{SR}^* = m_{PU}^* = 1$ and (a) $M = 8$, (b) $M = 12$	38
2.9	C_{Opt}^{LB} and $C_{Opt}^{LB,Om}$ versus \bar{P}_{av} for $M = 8$, $m_{SR}^* = 1$ and (a) $m_{PU}^* = 2$, (b) $m_{PU}^* = 3$	39
2.10	(a) $\overline{C_{Opt}^{LB}}$ and $C_{Opt}^{LB,Om}$ versus \bar{P}_{av} , (b) Λ versus \bar{P}_{av}	39
2.11	$\overline{C_{Opt}^{LB}}$ and $C_{Opt}^{LB,Om}$ versus \bar{P}_{av}	40
2.12	(a) \bar{P}_{out} and P_{out}^{Om} versus \bar{P}_{av} , (b) \bar{P}_e and P_e^{Om} versus \bar{P}_{av}	41

3.1	Our opportunistic CR system with an M -beam RA at SU_{tx} and omni-directional antennas at SU_{rx} and PU.	45
3.2	The structure of frame employed by SU_{tx}	46
3.3	$\bar{\Delta}_{1,m}$ versus the index beam m for $\phi_{3dB}=20^\circ$ (a) $SNR_{PU}=0$ dB, (b) $SNR_{PU}=-5$ dB.	51
3.4	The optimized P obtained from (3.45a) versus $\hat{\nu}^*$ (and c) for $\bar{P}_{av} = 2$ dB.	60
3.5	P versus $\hat{\nu}^*$ for $\bar{P}_{av} = 2$ dB, $\bar{I}_{av} = -12$ dB.	66
3.6	For $\bar{P}_{av} = 2$ dB, $\bar{I}_{av} = -15$ dB, (a) Rate versus T_{se} , (b) Rate versus T_{tr}	66
3.7	(a) Rate versus \bar{I}_{av} for $M = 7, 11$ and $\bar{P}_{av} = 2$ dB, (b) Rate versus \bar{P}_{av} for $M = 7, 11$ and $\bar{I}_{av} = -14$ dB.	67
3.8	P_{out} versus \bar{P}_{av} for $\bar{I}_{av} = -8$ dB.	68
4.1	Schematics of the uplink CR network.	71
4.2	Our CR system model corresponding to SU_n for $n = 1, \dots, N_u$	72
4.3	Slot structure of SUs.	73
4.4	Schematics of Markov chain corresponding to the battery state random process $\mathcal{B}_n^{(t)}$	77
4.5	This example shows how many energy units ($\alpha_{k,n}$) SU_n spends for data transmission, given its battery state and the received information about its channel gain via feedback link. (a) $\Omega_n^{(a)} = 0.75, \theta_n^{(a)} = 0.02$, (b) $\Omega_n^{(b)} = 0.95, \theta_n^{(b)} = 0.02$	78
4.6	(a) R_{LB} versus T_{se} for $K = 80, \theta = 0.25, \Omega = 0.35, \sigma_w^2 = \sigma_v^2 = 1$, (b) R_{LB} versus α_t for $K = 200, \theta = 0.25, \Omega = 0.35, \sigma_w^2 = \sigma_v^2 = 5$	90
4.7	(a) R_{LB} versus Ω for $K = 80, \theta = 0.2$, (b) R_{LB} versus θ for $K = 80, \Omega = 0.35$	91
4.8	ζ_k versus k for $K = 80, \rho = 15, \theta = 0.2$, (a) $\Omega = 0.45$, (b) $\Omega = 0.30$	92

4.9	ζ_k versus k for $K = 80, \rho = 15, \Omega = 0.35$, (a) $\theta = 0.1$, (b) $\theta = 0.5$	92
4.10	(a) P_b^{Out} versus Ω for $K = 80, \theta = 0.05$, (b) P_b^{Out} versus θ for $K = 80, \Omega = 0.35$	93
4.11	(a) η_{EE} versus η_{SE} for different values of Ω and $\theta = 0.02$, (b) η_{EE} versus η_{SE} for different values of θ and $\Omega = 0.6$	94
4.12	(a) Z versus Ω for $\theta = 0.02$, (b) Z versus θ for $\Omega = 0.6$	95
4.13	R_{LB} versus \bar{I}_{av} for $K = 60, \rho = 10, N_u = 3$	95
4.14	R_{LB}^* versus K for $\bar{I}_{\text{av}} = 2$ dB.	96
4.15	R_{LB}^* versus \bar{I}_{av} for $N_u = 3, K = 80$	96
4.16	$P_{b_1}^{\text{Out}}$ for SU_1 versus K when $\bar{I}_{\text{av}} = 2$ dB.	97
4.17	$P_{\alpha_1}^{\text{Out}}$ for SU_1 versus \bar{I}_{av} for SU_1 when $K = 100$	97
5.1	An example of 5 transmitter-receiver pairs in a coalition. In each pair, the directional antennas of transmitter and receiver are exactly along the center of their main lobes (which is not necessarily throughput-optimal).	101
5.2	An example of $A_\ell(\phi)$	102
5.3	Network throughput versus P_{max} for $N = 20, N_c = 4$	109
5.4	Network throughput versus P_{max} for $N = 20, N_c = 4$	110
5.5	Network throughput versus P_{max} for $N_c = 4$	110
5.6	Network throughput versus N_c for $N = 30, P_{\text{max}} = 30$ dB.	111
5.7	Network throughput versus $\phi_{3\text{dB}}$ for $N = 20, N_c = 4$	111

LIST OF TABLES

2.1	Most commonly used symbols.	20
2.2	Sequential steps within each three phases.	22
2.3	Simulation Parameters	37
3.1	Most commonly used symbols.	46
3.2	$\Pr(\hat{\nu}^* \geq c m_{\hat{\nu}^*})$ in terms of c , given $m_{\hat{\nu}^*} = 0.1484$	61
3.3	Simulation Parameters	65
4.1	Most commonly used symbols.	79
4.2	Simulation Parameters	89
5.1	Simulation Parameters	109

LIST OF ACRONYMS

- AIC** Average Interference Constraint. iii, 11, 12, 14, 18, 21–24, 32, 33, 38, 40–43, 47, 56–59, 62, 63, 65, 67–69, 85, 113, 114
- AP** Access Point. iii, 13–15, 70, 71, 74, 78–80, 82, 83, 86, 114
- ATPC** Average Transmit Power Constraint. iii, 11, 12, 18, 21–24, 33, 38–43, 47, 56–59, 62, 63, 65, 67–69, 113, 114
- AWGN** Additive White Gaussian Noise. 79, 80
- BCD** Block Coordinate Descent. 33, 42, 59, 62, 63, 69, 104, 112–115
- BER** Bit Error Rate. 8
- CDF** Cumulative Distribution Function. 23, 26, 27, 29, 30, 35, 49, 50, 53, 67, 68, 75, 76, 79
- CLT** Central Limit Theorem. 25, 49
- CR** Cognitive Radio. iii, 1–14, 16–18, 22, 34, 36–38, 40–44, 68, 70, 77, 78, 113, 114
- CSI** Channel State Information. iii, 4–8, 11–13, 15, 37, 43, 70, 114
- D2D** Device-to-Device. 15, 99, 112, 115
- EE** Energy-Efficiency. 3
- EH** Energy Harvesting. iii, 6, 7, 13, 70, 114
- ESPAR** Electrically Steerable Parasitic Array Radiator. 9–11, 16–19, 22, 24, 28, 34, 36–42, 113
- GLRT** Generalized Likelihood Ratio Test. 4, 48
- KKT** Karush-Kuhn-Tucker. 33, 59, 104, 107
- LLR** Logarithm of Likelihood Ratio. 48

LMMSE Linear Minimum Mean Square Error. 51, 52, 55, 56, 80, 84, 85

LRT Likelihood Ratio Test. 3, 4

MDP Markov Decision Process. 14

MIMO Multiple-Input Multiple-Output. 9

ML Maximum Likelihood. 48

MMSE Minimum Mean Square Error. 5, 55, 56, 84, 85

MMWAVE Millimeter Wave. 15, 99, 105, 112, 115

MRC Maximum Ratio Combining. 8

MSE Mean Square Error. 55, 84

PDF Probability Density Function. 4, 26, 27, 29, 30, 48, 50, 52, 53, 55, 83, 117

PMF Probability Mass Function. 72, 73, 75

PU Primary User. iii, 1–14, 16, 18–24, 26, 27, 30–32, 36, 38, 40, 41, 43–50, 56–58, 68, 70, 113, 114

RA Reconfigurable Antenna. iii, 8–13, 43–45, 68, 114

RF Radio Frequency. 1, 6, 8, 9, 16

RX Receiver. 7, 13

SEP Symbol Error Probability. 3, 5, 11, 34, 35

SINR Signal-to-Interference-plus-Noise Ratio. 5

SNR Signal-to-Noise Ratio. 9, 10, 36

SU Secondary User. iii, 1–5, 7–11, 13–15, 19, 31, 45, 46, 70, 71, 78, 79, 85, 86, 114

TX Transmitter. 7, 13, 70

CHAPTER 1: INTRODUCTION AND LITERATURE REVIEW¹²³⁴⁵⁶

1.1 Cognitive Radio Systems

With the increasing demands for ubiquitous high data rate wireless access and smart mobile devices with bandwidth consuming wireless applications, Radio Frequency (RF) spectrum is becoming more and more crowded. Contrasting the general belief which says “we are running out of bandwidth,” the results of empirical measurements on electromagnetic spectrum occupancy show that a large portion of the licensed spectrum is not utilized for significant periods of time. These findings suggest that spectrum scarcity is largely due to the inefficient utilization of the spectrum, rather than the shortage of the spectrum. CR is a promising solution which addresses this challenge by allowing an unlicensed or SU to access licensed bands in a such way that its imposed interference on a license holder PU is limited, and hence fills the spectrum holes in time and/or frequency domains [7–11].

CR systems are mainly classified as *underlay CR*, *opportunistic (or interweave) CR*, and *overlay CR* systems. The *underlay CR* approach allows concurrent primary and secondary transmissions if the interference imposed on PUs is below a given threshold. In *opportunistic CR* approach, the SUs periodically monitor the radio spectrum and opportunistically exploit spectral holes (in time and/or frequency domains) to communicate with minimal interference to PUs. The *overlay CR* approach allows concurrent primary and secondary transmissions. The SUs are allowed to access the licensed bands in return for improving the quality-of-service of primary transmissions by acting as a relay to convey the messages form Primary User Transmitter (PU_{tx}) to Primary User Receiver (PU_{rx}). Inspired by the inherent benefits of the above approaches, *hybrid CR* approaches, e.g., overlay-underlay [12] and interweave-underlay [13] CR approaches have been proposed to improve the performance of CR systems. While underlay CR systems do not require spectrum sensing to detect PU’s activities, they demand coordination between PUs and SUs (to obtain channel gain of PU links at SUs) that is not always feasible. The enabling premise for overlay CR systems is that the Secondary User Transmitter (SU_{tx}) has knowledge of the PUs’ codebooks, messages and channel gains which requires coordination

¹© 2017 IEEE. Part of this chapter is reprinted, with permission, from [1].

²© 2018 IEEE. Part of this chapter is reprinted, with permission, from [2].

³© 2019 IEEE. Part of this chapter is reprinted, with permission, from [3].

⁴© 2020 IEEE. Part of this chapter is reprinted, with permission, from [4].

⁵© 2021 IEEE. Part of this chapter is reprinted, with permission, from [5].

⁶© 2021 IEEE. Part of this chapter is reprinted, with permission, from [6].

between PUs and SUs. On the other hand, opportunistic CR systems utilize spectrum sensing to enable SUs to use a licensed frequency band during a time interval, only if PUs are not using that frequency band within that time interval, implying that coordination between PUs and SUs to acquire channel gain of PU links is not needed.

In this dissertation, we consider an *opportunistic* CR system where SUs are required to monitor the spectrum and to identify transmission opportunities (spectrum holes) accurately. Our opportunistic CR system works in three main phases, including “*spatial spectrum sensing phase*”, “*channel training phase*” and “*data transmission phase*”. SUs Each SU_{tx} employs a frame with a fixed duration of T_f seconds which is used for spectrum sensing, channel training and data transmission (see Fig. 1.1). When a SU_{tx} discovers a transmission opportunity, it can access the spectrum for

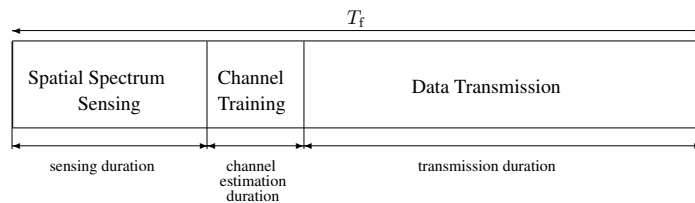


Figure 1.1: The structure of frame employed by SU_{tx} .

channel training and data transmission, in such a way that their imposed interference on the PUs does not exceed the maximum allowed interference level. While doing so, SUs also need to monitor the channels they occupy and vacate them whenever PUs become active on these channels. Within this context, the available resources must be adaptively allocated to the SUs to achieve a high system performance without interrupting the primary transmissions. In the following we briefly review the three phases mentioned above and their corresponding challenges.

1.1.1 Transmit Power Control

To enhance the performance of CR systems while providing sufficient protection for PUs, the transmit power of SUs must be adapted for different types of data traffic and channel statistics. Developing adaptive transmit power control strategies has drawn a great interest in the literature of CR systems design. Researchers have developed different transmit power control policies that are optimized considering various CR system performance metrics, transmit power constraints and interference constraints [14–18]. For delay-insensitive data traffic such as email and file transfer, the proper performance metric is the ergodic capacity⁷. The authors in [18] designed transmit power adaptation policies

⁷Ergodic capacity is the maximum achievable long-term data rate averaged over the channel fading states.

that maximize the ergodic capacity of a CR system subject to both average and peak transmit power constraints. For delay-sensitive data traffic such as video and VoIP, the proper system performance metric is the outage capacity⁸. For instance, the authors in [16] developed optimal transmit power control schemes, considering both the ergodic capacity and the outage capacity of an underlay CR system, subject to peak/average transmit power constraint and peak/average interference constraint. In [19] the Energy-Efficiency (EE) is considered as the system performance metric and the optimal transmit power control scheme is obtained subject to peak/average transmit power constraint and peak/average interference constraint. A novel transmit power control policy is derived in [20] to minimize the Symbol Error Probability (SEP) subject to an average interference constraint or an interference outage probability constraint⁹ at PU_{rx} .

1.1.2 Spectrum Sensing

In opportunistic CR systems, spectrum sensing is necessary for detecting PUs' activities and protecting PUs against harmful interference. The SUs need to regularly sense and monitor the spectrum and reliably detect the spectrum holes and utilize them opportunistically. Upon the detection of a PU's presence, SUs must vacate the occupied spectrum immediately.

Spectrum sensing can be formulated as a binary hypothesis testing problem in statistics in which the binary hypotheses \mathcal{H}_0 and \mathcal{H}_1 denote the PU is truly inactive and truly active in the monitored spectrum, respectively, i.e.,

$$\begin{aligned}\mathcal{H}_0 &: \text{PU is inactive} \\ \mathcal{H}_1 &: \text{PU is active}\end{aligned}\tag{1.1}$$

When adopting the Neyman-Pearson optimality criterion for the detection performance, the Neyman-Pearson theorem says that for a given probability of false alarm, the test statistic that maximizes the probability of detection is the Likelihood Ratio Test (LRT) defined as [21]

$$T_{\text{LRT}} = \frac{f(\mathbf{y}|\mathcal{H}_1)}{f(\mathbf{y}|\mathcal{H}_0)}\tag{1.2}$$

⁸Outage capacity is maximum achievable rate at a certain outage probability.

⁹This constraint mandates that the probability that the instantaneous interference at PU_{rx} exceeds a threshold is less than a target outage probability P_{out} .

where \mathbf{y} is the received signal vector and $f(\cdot)$ is the Probability Density Function (PDF). The major difficulty in using the LRT is that it requires the exact knowledge of the conditional distribution of \mathbf{y} . Depending on the level of information available at SUs about the PUs' signal, different LRT-based spectrum sensing methods have been introduced in the literature, including energy detection, matched filter detection, cyclostationary feature detection [8, 22–24]. Among these spectrum sensing methods, energy detection [25] is the most common method due to its low computational complexity and not requiring any knowledge on PUs' signal and channel gains at SUs. Matched filter detection is the optimum method when perfect information about the PUs' signal (including bandwidth, operating frequency, modulation type and order, pulse shaping, etc) is available at SUs. Obtaining such information requires advanced signal processing techniques, which makes the implementation cost and complexity of this detection method very high. Cyclostationary feature detector exploits the cyclostationary feature of the received signals (which is caused by the periodicity in the PUs' signals) to differentiate modulated signal from additive noise. This detection method requires SUs to know the frequencies in the PUs' signals, which increases the implementation cost and complexity. When no knowledge about the PUs' signal and communication channel statistics is not available at SUs, the LRT-based spectrum sensing methods cannot be applied. The main approach to tackle spectrum sensing problem in the presence of the aforementioned uncertainty is the Generalized Likelihood Ratio Test (GLRT). In [26], a GLRT detector for a multiple antenna CR system is derived assuming that the channel gain, the additive noise variance and the PU's signal power are unknown. Based on the GLRT detection, other variations, including maximum eigenvalue detection, maximum-minimum eigenvalue detection, and energy with minimum eigenvalue detection approaches are investigated in [27–29]. In general, any spectrum sensing technique is prone to error, that can be described as mis-detection and false alarm probabilities. This error can affect the opportunistic CR system performance and should be considered in the CR system design.

1.1.3 Channel Estimation

An important factor that impacts the performance of opportunistic CR systems is the level of assumption made regarding the availability of CSI. In opportunistic CR systems, although CSI corresponding to SU–PU link is not required (which is a major advantage), still CSI corresponding to SU_{tx} – SU_{tx} link is needed for properly adapting the data transmission. The CR literature mainly assumes that each SU_{tx} has access to full CSI of all communication links for its operation. However, in practice, SU_{tx} has access only to partial CSI, due to several factors including channel estimation error, mobility of PU or SU, and limitation of feedback channel. Partial (imperfect) CSI has deteriorating

effects on the fundamental performance limits of CRs and should not be overlooked. The authors in [30] considered a pilot-based channel estimation in a CR system. During the training phase, SU_{tx} sends training symbols to enable channel estimation at Secondary User Receiver (SU_{rx}). Different Minimum Mean Square Error (MMSE) estimation methods are considered for channel estimation at SU_{rx} . We note that the impact of partial CSI on the performance of underlay and opportunistic CR systems are different, due to inherent distinctions between these two CR systems. In underlay CR systems, the additive noise is the only randomness that affects the quality of channel estimation. Several researchers have studied the impact of imperfect CSI on the ergodic capacity [31–37] and the SEP [20] corresponding to different modulation schemes for underlay CR systems. The authors in [35] investigated the effect of five different levels of CSI on the capacity of a CR system under a minimum Signal-to-Interference-plus-Noise Ratio (SINR) constraint for PU_{rx} . However, in opportunistic CR (where spectrum sensing is necessary to detect the spectrum holes), the quality of channel estimation is affected by the accuracy of spectrum sensing as well as the additive noise. Hence, studying the problem of channel estimation is more challenging in opportunistic CR systems. We note that imperfect CSI due to channel estimation error (even under perfect spectrum sensing) has negative influence on the link capacity. Imperfect spectrum sensing exacerbates the negative effect of imperfect CSI on the link capacity.

1.1.4 Combined effects of Spectrum Sensing, Channel Estimation and Transmit Power Control in Opportunistic CR Systems

Spectrum sensing is crucial in the detection of PUs' signals and protecting them from harmful interference. However, it has an incurred cost for high rate data transmission. As the time duration for spectrum sensing increases, the accuracy of the employed spectrum sensing method increases, i.e., the false alarm probability decreases and the detection probability increases. On the other hand, given the fixed length frame structure in Fig. 1.1, the available time for data transmission decreases. Therefore, a trade-off exists between the spectrum sensing duration and the data rate of opportunistic CR systems. [38–46]. Motivated by this fact, the authors in [41] formulated the sensing-throughput tradeoff problem mathematically, and showed that their formulated problem indeed has an optimal spectrum sensing time duration which yields the highest throughput. The authors in [38] obtained the jointly optimal transmit power and spectrum sensing duration to maximize the energy efficiency of SUs, subject to peak interference constraint and a minimum data rate constraint. The authors in [47] obtained the jointly optimal detection threshold (for spectrum sensing) and transmit power of SUs, obtained to minimize the total energy consumption with the constraints on SUs' quality-of-service and the detection probability of PU' signals.

Besides spectrum sensing, channel estimation also induces a cost for high data rate transmission. As the allocated transmission resources for channel estimation (i.e., time and power for sending training symbols to SU_{rx}) increases, the channel estimation becomes more accurate and the channel estimation error decreases. On the other hand, the average interference imposed on the PUs during transmission of training symbols increases, the available time for data transmission and hence, the data rate decrease. Therefore, a trade-off exists between the time duration of channel estimation and the data rate of CR systems. Hence, for opportunistic CR systems, we need to study the combined effects of imperfect spectrum sensing and imperfect CSI as well as adaptive transmit power control policies on the CR system performance. For example in [48], SU_{tx} monitors the PU's activity and estimates the PU's signal power based on its received signal during sensing-estimation time. If the spectrum is sensed idle, SU_{tx} sends data to SU_{rx} with a fixed transmit power. The authors showed that the constrained capacity of SU_{tx} - SU_{rx} link can be significantly enhanced (subject to a constraint on the detection probability corresponding to the spectrum sensing detector), via optimizing the duration of sensing-estimation time. The work in [19] considered different levels of CSI corresponding to SU_{tx} - SU_{rx} and SU_{tx} -PU links, and studied the optimal transmit power levels at SU_{tx} , such that the capacity of SU_{tx} - SU_{rx} link is maximized.

1.2 Energy Harvesting in CR Systems

In addition to spectral efficiency, energy efficiency is another important metric to consider when designing communication systems [38, 49–53]. EH has been recognized as an effective approach for improving the energy efficiency. EH-powered devices can operate without the need for external power cables or periodic battery replacements [54–56]. EH-enabled CR systems have received substantial attention as a promising solution for increasing both energy efficiency and spectral efficiency [57–59]. EH-enabled communication systems can harvest energy from ambient energy sources (e.g., solar, wind, thermal, vibration) or RF signals [60, 61]. In practice, the energy arrival of ambient energy sources, including ambient RF signal sources, is intrinsically time-variant and often sporadic. This natural factor degrades the performance of the battery-free EH-enabled communication systems in which a “harvest-then-transmit” strategy is adopted, i.e., users can only transmit when the energy harvested in one time slot is sufficient for data transmission [62]. To flatten the randomness of the energy arrival, the harvested energy is stored in a battery, to balance the energy arrival and the energy consumption [54]. In practice, the capacity of the batteries is limited, and this can result in an energy overflow.

Power/energy management in EH-enabled communication systems with finite size batteries is necessary, in order to

adapt the rate of energy consumption with the rate of energy harvesting. If the energy management policy is overly aggressive, such that the rate of energy consumption is greater than the rate of energy harvesting, the transmitter may stop functioning, due to energy outage. On the other hand, if the energy management policy is overly conservative, the transmitter may fail to utilize the excess energy, due to energy overflow, and the data transmission would become limited in each energy allocation interval.

Focusing on opportunistic EH-enabled CR systems, we realize that power control strategies, aiming at optimizing the performance of SUs, should be designed such that spectrum sensing (and its corresponding errors), as well as spectrum sensing-data transmission trade-offs are incorporated in the design process [53, 63–66]. For instance, the authors in [63] considered a system model, where SU_{tx} can perform energy harvesting and spectrum sensing simultaneously. Depending on the results of spectrum sensing, SU_{tx} continues to harvest energy (when the spectrum is sensed busy) or transmits data (when the spectrum is sensed idle), and studied maximizing SU_{tx} – SU_{rx} channel capacity, via optimizing the threshold of the energy detector (employed for spectrum sensing).

In general, the power control strategies designed for opportunistic EH-enabled CR systems should depend on the level of assumption made regarding the availability of CSI corresponding to SU_{tx} – SU_{rx} link, and whether the adapted transmit power levels are continuous or discrete values. In practice, only partial CSI can be available at SU_{tx} and SU_{rx} due to several factors (e.g., channel estimation error and limitation of feedback channel from SU_{rx} to SU_{tx}). Partial CSI has deteriorating effects on the performance of communication systems (including EH-enabled CR systems), and should not be overlooked [67–70]. Assuming perfect CSI at the Receiver (RX) and partial CSI at the Transmitter (TX) (due to channel estimation error), the authors in [68, 69] analyzed maximizing the TX’s average throughput, in two asymptotic regimes (where the rate of energy harvesting is very small or very large), via optimizing continuous-valued data transmit power.

1.3 Integration of Directional Antennas in Opportunistic CR Systems

All the cited works so far on developing spectrum sensing and data transmission approaches for CR systems are built upon the main assumption that SUs are equipped with an omni-directional antenna. Consequently, these approaches can identify transmission and reception opportunities only across two dimensions of frequency and time. When a SU_{tx} with an omni-directional antenna detects PU’s activity (in either of these domains) it cannot extract any information about the directionality of the PU’s signal, i.e., SU_{tx} fails to identify transmission and reception opportunities

across spatial domain. A *steerable directional antenna* enables SU_{tx} to sense the spectrum in all directions (so-called directional spectrum sensing) and to identify the angular directions that are vacant of the PUs' activities in a certain frequency band [1, 2, 71–73]. The spatial-spectral holes discovered by the steerable directional antenna present new transmission and reception opportunities that would be missed if using an omni-directional antenna. One can significantly enhance the spectrum utilization via employing a steerable directional antenna and enabling transmission and reception in the unoccupied angular directions and also providing spatial filtering for mitigating in-band interference to and from PUs (by properly steering the antenna beam and creating nulls toward certain directions).

There is a rich literature provided by the researchers on optimizing transmission strategies for opportunistic spectrum access of SUs, that are equipped with directional antennas, in the presence of PUs' activities [74–81]. These works have considered multi-antenna CR systems and focused on designing beamforming weights that optimize certain system performance metrics. Multiple antennas, and in particular transmit beamforming techniques, have been utilized to ameliorate the performance degradation due to the interference imposed on PUs in underlay CR systems [75, 78, 79] and opportunistic CR systems [80] when perfect CSI of SU_{tx} – SU_{rx} link is available at SU_{tx} . The authors in [81] considered an opportunistic CR system, where SU_{tx} has a single antenna and SU_{rx} has multiple antennas and applies Maximum Ratio Combining (MRC) technique to combine the received signals at multiple antennas, and studied the combined effects of spectrum sensing error and imperfect CSI of SU_{tx} – SU_{rx} link at SU_{tx} on the CR system Bit Error Rate (BER) performance. The authors in [81] obtained the optimal spectrum sensing time, channel estimation time, and SU_{tx} transmit power, such that BER is minimized, subject to average transmit power and peak interference constraints. These works assume that transmit antennas use multiple RF chains connected to the antenna elements, and hence the weight of each antenna element can be digitally adjusted to generate the desired beam pattern. We note that the benefits of multi-antenna techniques come at the cost of requiring an expensive and power-hungry RF chain per antenna, which consists of digital-to-analog converters, filters, mixers, and amplifiers. While multi-antenna techniques are affordable for base station and access points, where cost, size, power, and complexity are of less concern, they are not directly applicable to portable lightweight devices.

1.3.1 Reconfigurable Antenna

RA [82,83], with the capabilities of dynamically modifying their characteristics (e.g., operating frequency, beamwidth, radiation pattern, polarization) can improve the spectral efficiency (well beyond what is attainable with omni-directional antennas), via beam steering and utilizing the spectrum white spaces in spatial (angular) domain. RA, which has only

one RF chain, is a low-complexity and low-cost technology that addresses the aforementioned challenges in the multi-antenna systems [84–86]. RAs have been used to design directional wireless and 5G millimeter-wave communication systems to combat the significant path-loss and reduce the number of RF chains in massive Multiple-Input Multiple-Output (MIMO) systems [87, 88]. For both underlay and opportunistic CR systems, RAs are used to increase Signal-to-Noise Ratio (SNR) for transmission and reception of directional signals [89], enhance the accuracy of spectrum sensing [89–91], and limit interference to and from PUs [3–5].

An Electrically Steerable Parasitic Array Radiator (ESPAR) antenna is a special kind of RAs, that has been used for identifying the spectral holes in spatial domain in CR systems. ESPAR divides the angular domain into several sectors (beams) and switches between beampatterns of sectors in a time-division fashion (only one of M beams is active at a time) [92]. The ESPAR antenna relies on a single RF front end (an active element) coupled to several passive or parasitic elements (mutually coupled to the active one) to steer beams in prescribed directions [92, 93]. The active element is connected to the transmitter/receiver circuit and the parasitic elements are reactively loaded. Since only one RF chain is needed, the power consumption, cost, and hardware complexity are significantly reduced. The mutual coupling between the ESPAR antenna elements is created by reducing the spacing between them, which makes this antenna suitable for small mobile devices.

For CR systems, the ESPAR antennas provide an improved *spectrum sensing*, due to a SNR increase for transmission and reception of directional signals, and limit out-of-band interference to and from PUs [89]. Considering the ESPAR antennas, the authors in [89–91, 94] designed spectrum sensing energy detectors, based on the received signal energy in different beams, and also eigenvalue-based detectors, based on the covariance matrix constructed from the received signals in different beams. The advantages of spectrum sensing using ESPAR antennas are twofold. First, the SNR gain from the directional beampatterns increases the probability of detecting PU’s activities within that beam, and hence decreases the chance of causing interference on the PU. Second, the discovered unoccupied beams in spatial (angular) domain during spectrum sensing represents directional transmission and reception opportunities for SUs, which can be utilized to increase spectral efficiency (opportunities that would be missed when using an omni-directional antenna at SU_{tx}).

The ESPAR antennas have the capability of *transmitting multiple data streams* by signal projection on beamspace basis [95]. Also, they can be used for blind interference alignment through beampattern switching [96]. ESPAR antennas have been used in [97], to provide an end-to-end solution for practically implementable cloud radio access networks. RAs can enhance performance of MIMO systems, via enabling beam and antenna selection optimiza-

tion [98–102]. The work in [101] shows that comparing RA and traditional antenna selection, the former can offer significant improvements in SNR.

A related research thrust in the context of ESPAR antennas for design of CR systems is developing *adaptive beam patterns* (also called beamforming) [89, 103–106]. Designing an adaptive beam pattern algorithm for an ESPAR antenna from a mathematical perspective is very challenging, due to the tunable reactive loads, which renders a non-convex optimization problem with respect to the optimization parameters, without any closed form solution. Furthermore, implementing such design incurs high computational complexity.

1.4 Motivation, Contributions and Dissertation Organization

Our literature survey indicates that the studies on optimizing spectrum sensing and optimizing data communication have been pursued as two separate research thrusts: the works cited in [89–91, 94] focus on spectrum sensing in opportunistic CR systems, whereas the works in [98–102] focus on data communication in underlay CR systems. The developed beam selection and beamforming schemes in [98–102] are specifically tailored for underlay CR systems, which do not require spectrum sensing to detect PU’s activities, and rely on the knowledge obtained from coordination between PUs and SUs. Evidently, the literature lacks a holistic system design, that integrates spectrum sensing and data communication in a cohesive manner for opportunistic CR systems. Such a holistic system design needs to take into consideration the effect of imperfect spectrum sensing on data communication optimization, while taking full advantage of beam steering capability of the ESPAR antennas. This is the motivation behind our work presented in chapters 2 and 3.

In Chapter 2 we consider an opportunistic CR system consisting of a PU, a SU_{tx} , and a SU_{rx} , where SU_{tx} is equipped with an ESPAR antenna with the capability of choosing one sector among M sectors for its data transmission to SU_{rx} . We leverage on the beam steering capability of the ESPAR antenna for both spectrum sensing and data communication optimization and we propose an integrated design for opportunistic CR systems. Different from the state-of-the-art, our proposed integrated design incorporates induced errors due to: (i) imperfect spectrum sensing and determining the correct beam corresponding to the PU’s location, such errors affect the interference imposed on the PU; (ii) selecting the best beam for data communication over SU_{tx} – SU_{rx} link.

During the initial *spatial spectrum sensing phase* SU_{tx} senses the channel and monitors the PU’s activity. While being in this phase, SU_{tx} determines the beam corresponding to the location (orientation) of the PU based on the received

signal energy from all directions. SU_{tx} stays in this phase as long as the spectrum is sensed busy. It leaves this phase and enters transmission phase when the spectrum is sensed idle. The transmission phase itself consists of two phases: *channel estimation phase* followed by *data transmission phase*. During the former phase, SU_{tx} sends training symbols to enable channel estimation at SU_{rx} as well as selection of the strongest channel among all beams between SU_{tx} – SU_{rx} for data transmission. Also, SU_{rx} employs an n_b -bit quantizer to quantize the gain of the selected beam. Then, SU_{rx} feeds back the index of the selected beam as well as the n_b -bit representation of the index of the quantization interval over an error-free bandwidth limited feedback link to SU_{tx} , so SU_{tx} can optimally adapt its discrete power level accordingly. To the best of our knowledge, this is the first work that adopts a holistic approach to design an opportunistic CR system using ESPAR antennas and integrates sector-based spectrum sensing and sector-based data communication. All previous works use RAs for enhanced communication in underlay CR systems. Utilizing ESPAR antennas in opportunistic CR systems for spectrum sharing is a highly promising solution to enhance the data rate of SUs' links, while satisfying the AIC and ATPC [102].

The main contributions of Chapter 2 can be summarized as follows:

- Given our system model, we formulate a novel optimization problem, aiming at maximizing the constrained ergodic capacity of SU_{tx} – SU_{rx} link, subject to AIC and ATPC.
- Our problem formulation takes into consideration the effect of imperfect spectrum sensing as well as the error due to incorrect determination of the beam corresponding to PU's location (and its corresponding effect on imposed average interference) occurred during *spatial spectrum sensing phase*.
- Our problem formulation also takes into account the probability of correct determination of the strongest beam for data transmission from SU_{tx} to SU_{rx} , occurred during *channel estimation phase*. It also incorporates the impact of CSI quantization on the constrained optimization problem in hand.
- We solve the formulated problem and optimize the time duration of spectrum sensing, thresholds of CSI quantizer, and discrete transmit power levels (to be employed at SU_{tx}) corresponding to CSI quantization intervals. We also provide closed form expressions for outage probability¹⁰ and SEP.
- Taking advantage of the additional degrees of freedom offered by ESPAR antennas with variable beam directions, we improve the spectral efficiency and reduce implementation complexity of opportunistic spectrum sharing systems. Our simulations demonstrate and quantify the capacity improvement provided by the ESPAR

¹⁰We define the outage probability as the probability of SU_{tx} not transmitting data due to the weak SU_{tx} – SU_{rx} channel.

antenna, in terms of average transmit power \bar{P}_{av} and average interference \bar{I}_{av} constraints. For instance, at $\bar{P}_{av} = 12$ dB, $\bar{I}_{av} = -6$ dB, the capacity of our CR system is 1.83 times larger than the capacity of a CR system that its SU_{tx} has an omni-directional antenna. Also, we show that with only a small number of feedback bits the capacity of our opportunistic CR system approaches to its baseline, which assumes the full knowledge of unquantized SU_{tx} – SU_{rx} channel gain at SU_{tx} .

In Chapter 3, we consider the combined effects of spectrum sensing error and imperfect CSI of SU_{tx} – SU_{rx} link on the achievable rates of an opportunistic CR system with a RA at SU_{tx} . In our opportunistic CR system, SU_{tx} relies on the beam steering capability of RA to detect the direction of PU’s activity and also to select the strongest beam for data transmission to SU_{rx} . We assume SU_{tx} sends training symbols to enable channel estimation at SU_{rx} , and employs Gaussian input signaling for transmitting its data symbols to SU_{rx} . Also, SU_{rx} shares its imperfect CSI of SU_{tx} – SU_{rx} link with SU_{tx} through an error-free low-rate feedback channel.

Assuming that there are ATPC and AIC, we provide answers to the following research questions: How does spectrum sensing error affect accuracy of detecting the direction of PU’s activity, estimating SU_{tx} – SU_{rx} channel, and selecting the strongest beam for data transmission? How do training symbol transmission and beam detection error (error in obtaining the true direction of PU’s activity) affect interference imposed on PU? How do the combined effects of spectrum sensing error and channel estimation error, as well as beam detection error and beam selection error (error in finding the true strongest beam for data communication to SU_{rx}) impact the achievable rates for reliable communication over SU_{tx} – SU_{rx} link? How do the trade-offs between spatial spectrum sensing time, channel training time, data transmission time, training and data symbol transmission powers affect the achievable rates? How can we utilize these trade-offs to design transmit power control strategies, such that the achievable rates subject to ATPC and AIC are maximized? Our main contributions follow:

- Given this system model, we establish a lower bound on the achievable rates of SU_{tx} – SU_{rx} link, in the presence of both spectrum sensing error and channel estimation error. We formulate a novel constrained optimization problem, aiming at maximizing the derived lower bound subject to AIC and ATPC.
- Our problem formulation takes into consideration the combined effects of imperfect spectrum sensing and channel estimation as well as the errors due to (i) incorrect detection of the beam corresponding to PU’s location (and its corresponding effect on average interference imposed on the PU) occurred during spatial spectrum sensing phase, (ii) incorrect selection of the strongest beam for data transmission from SU_{tx} to SU_{rx} , occurred during

channel estimation phase. These beam detection and beam selection errors are introduced by the RA at SU_{tx} .

- Given a fixed-length frame, we optimize the durations of spatial spectrum sensing and channel training as well as data symbol transmission power. Based on the structure of the optimized transmit power, we propose alternative power adaptation schemes that are simpler to implement and yield lower bounds on the achievable rates that are very close to the one produced by the optimized transmit power.

In Chapter 4 we consider an opportunistic EH-enabled CR network, consisting of N_u SUs and an AP, that can access a wideband spectrum licensed to a primary network. Each SU is capable of harvesting energy from natural ambient energy sources, and is equipped with a finite size rechargeable battery, to store the harvested energy. Our main *objectives* are (i) to study how the achievable sum-rate of SUs is impacted by the *combined effects* of spectrum sensing error and imperfect CSI of SUs–AP links (due to channel estimation error), and (ii) to design an energy management strategy that maximizes the achievable sum-rate of SUs, subject to a constraint on the average interference that SUs can impose on the PU. To the best of our knowledge, our work in Chapter 4 is the first to study the impact of these combined effects on the performance of an opportunistic EH-enabled CR network.

The importance of our study in Chapter 4 is evident by the works in [107–112], which demonstrate the significance of considering the effect of imperfect CSI at the RX, due to channel estimation, on the TX achievable rate. We note that the TX in these works is a primary transmitter (not a secondary transmitter in a CR system) and has a traditional stable power supply. One expects that spectrum sensing error, combined with random energy arrival at the TX, exacerbates the effect of imperfect CSI on the TX achievable rate. The challenges of our study are twofold: first, it requires integration of energy harvesting, spectrum sensing, and channel estimation. Successful achievement of this integration entails stochastic modeling of energy arrival, energy storage, and PU’s activities. These stochastic models are utilized to establish an achievable sum-rate of SUs that takes into account both spectrum sensing error and channel estimation error. Second, one needs to properly design energy control strategies for SUs, that strike a balance between the energy harvesting and the energy consumption, and adapt transmit power according to the available CSI and the battery state.

We assume that SUs operate under a time-slotted scheme, and SU_n is capable of harvesting energy during the entire time slot. Each time slot consists of three sub-slots corresponding to spectrum sensing phase (during which SU_n senses the spectrum), channel estimation phase (during which SU_n sends training symbols to the AP, when the spectrum is sensed idle, for estimating the fading coefficient corresponding to SU_n –AP link), and data transmission phase (during

which SU_n sends data symbols to the AP). Assuming that the AP feeds back its estimate of the fading coefficient to SU_n , SU_n adapts its transmit power based on this information as well as the available energy in its battery.

Our main contributions can be summarized as follow:

- Our system model encompasses the stochastic energy arrival model for harvesting energy, the stochastic energy storage model for the finite size battery, the stochastic model of PU's activities, spectrum sensing error, and channel estimation error (both at SUs and the AP). We model the randomly arriving energy packets during a time slot as a Poisson process, and the dynamics of the battery as a finite state Markov chain.
- We propose a power adaptation strategy for SU_n that mimics the behavior of the rate-optimal power adaptation scheme with respect to the estimated channel power gain \hat{g}_n available at SU_n and the AP, i.e., when \hat{g}_n is below a cut-off threshold θ_n , the transmit energy is zero, and when \hat{g}_n exceeds θ_n , the transmit energy increases monotonically in proportion to a parameter Ω_n , as \hat{g}_n increases. The parameters Ω_n and θ_n play key roles in balancing the energy harvesting and the energy consumption.
- Given our system model, we establish a lower bound on the achievable sum-rate of SUs–AP links, in the presence of both spectrum sensing error and channel estimation error (both at SUs and the AP). We formulate a novel constrained optimization problem with the optimization variables $\{\Omega_n, \theta_n\}_{n=1}^{N_u}$, aiming at maximizing the derived sum-rate lower bound, subject to the AIC imposed on the PU and the causality constraint of the battery. We solve the formulated constrained optimization problem assuming that the battery reaches its steady-state.
- We derive closed form expressions for the battery outage probability and transmission outage probability and demonstrate their behaviors, in terms of the average number of harvesting energy packets and the AIC. We also study the existing trade-offs between spectrum sensing-channel estimation-data transmission and how these trade-offs impact the sum-rate of our CR network.

Our work in Chapter 4 is different from [62, 67, 68, 70]. In particular, these works view the energy management policy design as a sequential decision making problem, and hence, they adopt the Markov Decision Process (MDP) framework to solve the problem. In this framework, the goal is typically optimizing a specific metric over a horizon spanning several time slots. The solutions (obtained using dynamic programming) are dependent across time slots, and also depend on the initial condition (i.e., the initial state of the battery). Here, we assume that the battery operates at its steady-state, and hence, our proposed constrained optimization problem can be solved for each time slot. Furthermore,

the problem can be solved *offline* and the optimized transmission parameters $\{\Omega_n, \theta_n\}_{n=1}^{N_u}$ (that do *not* depend on the initial condition of the battery) can become available *a priori* at the AP and SUs. During the data transmission phase, SU_n chooses its symbol power, using its optimized transmission parameters Ω_n, θ_n , and based on its partial CSI of SU_n -AP link (received via the feedback channel) as well as the available energy in its battery.

In Chapter 5, we explore a throughput-optimal design for a Device-to-Device (D2D) Millimeter Wave (MMWAVE) network, where the nodes employ *directional antennas* for wireless communication. In particular, we consider a MMWAVE network with a total available bandwidth of B_c Hz, that supports communication of N cooperative pairs of transmitters and receivers over fading channels. We assume the available spectrum band is divided into N_c non-overlapping sub-bands, where each sub-band has a bandwidth of $W = B_c/N_c$ Hz. Also, we assume $N_c \ll N$. Each node is capable of steering its beam within the range of its field of view (FOV) [1, 5]. Also, each transmitter node can adjust its transmit power. The transmitter-receiver pairs can form up to N_c disjoint coalitions, such that the pairs in a particular coalition share the same sub-band for communication. Therefore, the pairs within a coalition cause co-channel interference, whereas the pairs in different coalitions do not interfere.

The questions we address are: What is the best coalition among the pairs? What are the optimal beam steering angles of directional antennas of the pairs within each coalition, and what are the optimal transmit powers such that the network throughput, defined as the sum-rate of all N transmitter-receiver pairs in N_c coalitions, is maximized?

We combine the concepts of coalition formation among cooperative transmitter-receiver pairs and directional MMWAVE bands, and we take full advantage of adaptive beam steering and adaptive transmit power to improve the spectral efficiency and maximize the network throughput.

Finally, Chapter 6 concludes the dissertation.

CHAPTER 2: BEAM SELECTION AND DISCRETE POWER ALLOCATION IN OPPORTUNISTIC COGNITIVE RADIO SYSTEMS WITH LIMITED FEEDBACK USING ESPAR ANTENNAS¹

In this chapter, we consider an opportunistic CR system consisting of a PU, SU_{tx} , and SU_{rx} , where SU_{tx} is equipped with an ESPAR antenna with the capability of choosing one sector among M sectors for its data transmission to SU_{rx} . During the initial *spatial spectrum sensing phase* SU_{tx} senses the channel and monitors the activity of PU. While being in this phase, SU_{tx} determines the beam corresponding to the location (orientation) of PU based on the received signal energy. SU_{tx} stays in this phase as long as the channel is sensed busy. It leaves this phase and enters transmission phase when the channel is sensed idle. The transmission phase itself consists of two phases: *channel training phase* followed by *data transmission phase*. During the former phase, SU_{tx} sends training symbols to enable channel estimation at SU_{rx} as well as selection of the strongest channel among all beams between SU_{tx} – SU_{rx} for data transmission. Also, SU_{rx} employs an n_b -bit quantizer to quantize the gain of the selected beam. Then, SU_{rx} feeds back the index of the selected beam as well as the n_b -bit representation of the index of the quantization interval over an error-free bandwidth limited feedback link to SU_{tx} , so SU_{tx} can optimally adapt its discrete power level accordingly.

2.1 System Model and Problem Statement

2.1.1 Background on ESPAR Antennas

The ESPAR antenna is a circular array, comprised of one active element and M parasitic elements symmetrically surrounding the active element, and the radius of the array is $r < \lambda_c/2$, where λ_c is the carrier wavelength [92]. Fig. 2.1a depicts an ESPAR structure. The active element is connected to the single RF chain, while M parasitic elements (which are mutually coupled to the active element) are short-circuited and loaded by M variable reactive loads. Let x_m be the reactive load of m -th element and vector $\mathbf{x} = [x_1, \dots, x_M]$ denote the reactive loads of all M parasitic elements. By adjusting these reactive loads, the beampatterns of the ESPAR antenna are designed such that the angular space is divided into M spatial sectors or beams². In particular, to design the beampattern corresponding to

¹© 2020 IEEE. Part of this chapter is reprinted, with permission, from [4].

²Throughout this dissertation, “sector” and “beam” are used interchangeably.

the first beam, entries of vector \mathbf{x}_1 are optimized such that the beam gain is maximized at an angle (for example angle 0°) [92]. Since the ESPAR antenna structure is symmetric, the beampattern corresponding to the second beam can be obtained by circularly shifting the entries of \mathbf{x}_1 , such that the beam gain is maximized at angle $\kappa_2 = \frac{2\pi}{M}$. Repeating this M times one can obtain M beampatterns corresponding to M beams such that the beampattern corresponding to the m -th beam achieves its maximum at angle $\kappa_m = \frac{2\pi(m-1)}{M}$ for $m = 1, \dots, M$. It is noteworthy that the ESPAR antenna can provide an omni-directional beampattern if the reactive loads of all parasitic elements are chosen equal (omni-directional mode).

Similar to [113], to mathematically model the radiation pattern (antenna pattern) of the ESPAR antenna, we adopt the Gaussian pattern in $x-y$ azimuth plane in terms of angle ϕ given by

$$p(\phi) = A_1 + A_0 e^{-B \left(\frac{\mathcal{M}(\phi)}{\phi_{3\text{dB}}} \right)^2}, \quad (2.1)$$

$$\mathcal{M}(\phi) = \text{mod}_{2\pi}(\phi + \pi) - \pi, \quad (2.2)$$

$\text{mod}_{2\pi}(\phi)$ denotes the remainder of $\frac{\phi}{2\pi}$, constant $B = \ln(2)$, $\phi_{3\text{dB}}$ is the 3-dB beamwidth, A_1 and A_0 are two constant antenna parameters. The radiation pattern of m -th sector at angle ϕ is

$$p_m(\phi) = p(\phi - \kappa_m) \quad \text{for } m = 1, \dots, M. \quad (2.3)$$

In Fig. 2.1b, the beampatterns of an ESPAR antenna with 8 parasitic elements are shown. In this chapter, we discuss the received or transmitted signal at m -th sector of SU_{tx} . This means that, during the signal reception or transmission, the reactive loads of all M parasitic elements (i.e., the entries of vector \mathbf{x}) are set and tuned such that the beampattern corresponding to the m -th beam is generated. Note that in our work we assume the reactive loads (i.e., the entries of vector \mathbf{x} and thus the shapes of beampatterns or equivalently the radiation patterns of M sectors) are determined by the ESPAR antenna designer. Given the antenna design, we focus on how the sector-based structure of this ESPAR antenna can be exploited to enhance the system performance of our opportunistic CR system, in which SU_{tx} optimizes its sector-based data communication to SU_{rx} according to the results of its sector-based spectrum sensing.

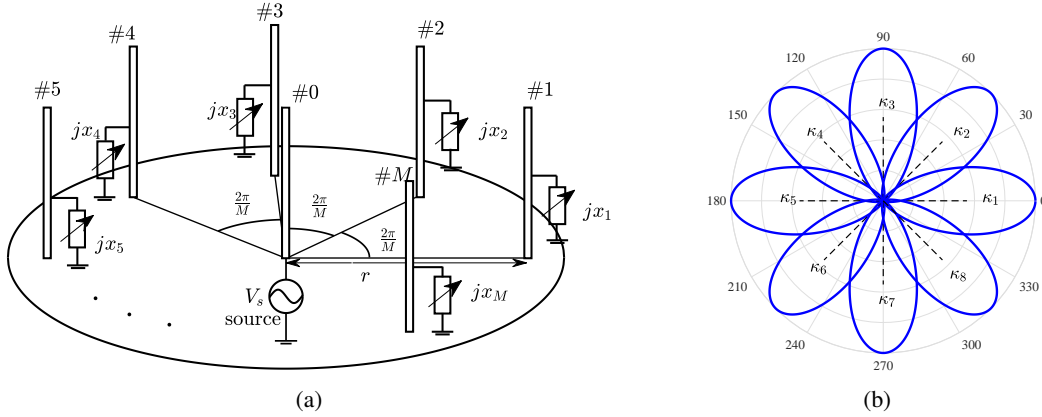


Figure 2.1: The ESPAR antenna structure and its beampatterns, (a) The ESPAR antenna structure, (b) Beampatterns of an ESPAR with 8 parasitic elements, assuming the Gaussian radiation pattern in (2.1).

2.1.2 Geometry of Our Opportunistic CR System

Our CR system model is illustrated in Fig. 2.2, consisting of a PU and a pair of SU_{tx} and SU_{rx} . We note that PU in our system model can be a primary transmitter or receiver. We assume when PU is active it is engaged in a bidirectional communication with another PU, which is located far from SU_{tx} and hence its activity does not impact our analysis. We assume SU_{tx} is equipped with an $(M + 1)$ -element ESPAR antenna (for spectrum sensing and communication) with the capability of choosing one sector among M sectors for its data transmission to SU_{rx} , while SU_{rx} and PU use omni-directional antennas. The reason for this assumption is to focus on quantifying the capacity improvement provided by the ESPAR antenna at SU_{tx} , in the presence of spectrum sensing error as well as ATPC and AIC. We also assume there is an error-free bandwidth limited feedback channel from SU_{rx} to SU_{tx} (where the channel bandwidth is measured in terms of the number of bits sent over the channel [15, 114], to help SU_{tx} select the best sector for its data transmission to SU_{rx} and also to provide SU_{tx} with the quantized channel gain of the selected beam, so SU_{tx} can adapt its discrete power level accordingly. The direction (orientation) of PU and SU_{rx} with respect to SU_{tx} are denoted by angles ϕ_{PU} , and ϕ_{SR} , respectively. Clearly, in our problem SU_{tx} does not know these directions or angles (otherwise, the beam selection at SU_{tx} for data transmission would become trivial).

Let h , h_{ss} , h_{sp} denote the fading coefficients of channels between SU_{tx} and PU, SU_{tx} and SU_{rx} , and SU_{rx} and PU, respectively, when the ESPAR antenna of SU_{tx} is in omni-directional mode. We model these fading coefficients as independent circularly symmetric complex Gaussian random variables. We assume $g = |h|^2$, $g_{ss} = |h_{ss}|^2$ and

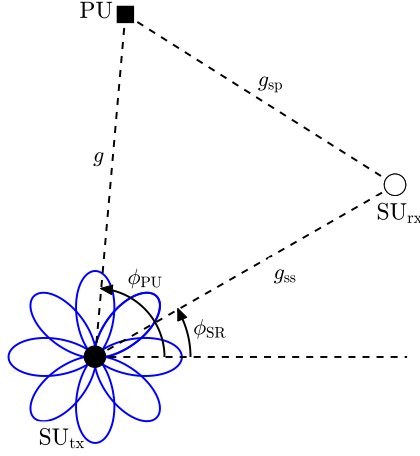


Figure 2.2: Our CR system with an $(M+1)$ -element ESPAR antenna at SU_{tx} and omni-directional antennas at SU_{rx} and PU.

$g_{sp} = |h_{sp}|^2$ are independent exponentially distributed random variables with mean γ , γ_{ss} and γ_{sp} , respectively³. Since in our problem SUs and PU cannot cooperate, SUs cannot estimate g and g_{sp} . However, we assume that SU_{tx} knows the channel statistics, i.e., the mean values γ and γ_{sp} . Let ψ_m and χ_m denote the fading coefficients of channel between m -th sector of SU_{tx} and PU, and between m -th sector of SU_{tx} and SU_{rx} , respectively, when the ESPAR antenna of SU_{tx} is in directional mode, where $\psi_m = h\sqrt{p_m(\phi_{PU})}$, $\chi_m = h_{ss}\sqrt{p_m(\phi_{SR})}$. We assume the channel gain $\nu_m = |\chi_m|^2$ is an exponential random variable with mean δ_m , and SU_{tx} knows δ_m , for all m [102]. For the readers' convenience, we have collected the most commonly used symbols in Table 2.1.

2.1.3 Our Problem Statement

Suppose, SUs employ a frame with a fixed duration of T_f seconds, depicted in Fig. 2.3. We assume SU_{tx} first senses the channel and monitors the activity of PU. We refer to this period as *spatial spectrum sensing phase* (with a variable duration of T_{se} seconds). Depending on the outcome of this phase, SU_{tx} stays in this phase or enters the next phase, which we refer to as *transmission phase*. The transmission phase itself consists of two phases: *channel training phase* (with a fixed duration of T_{tr} seconds) followed by *data transmission phase* (with a variable duration of $T_f - T_{se} - T_{tr}$ seconds). During the former phase, SU_{tx} sends training symbols to enable channel estimation at SU_{rx} . During the

³ We note that the distances between users are included in the small scale fading model [115]. In particular, we assume that the mean values are $\gamma = (d_0/d)^\epsilon$, $\gamma_{ss} = (d_0/d_{ss})^\epsilon$, $\gamma_{sp} = (d_0/d_{sp})^\epsilon$, where d_0 is the reference distance, ϵ is the path-loss exponent, and d , d_{ss} and d_{sp} are the distances between SU_{tx} and PU, SU_{tx} and SU_{rx} , and SU_{rx} and PU, respectively.

Table 2.1: Most commonly used symbols.

Symbol	Description
M	Number of beams
N_{se}	Number of samples used for spectrum sensing
n_b	Number of bits for quantization at SU_{rx}
$p_m(\phi)$	Radiation pattern of m -th beam at angle ϕ
ψ_m	Fading coefficient of channel between m -th beam of SU_{tx} and PU
χ_m	Fading coefficient of channel between m -th beam of SU_{tx} and SU_{rx}
δ_m	Mean of channel gain between m -th beam of SU_{tx} and SU_{rx}
ν^*	Channel gain of selected beam for data transmission from SU_{tx} to SU_{rx}
ϕ_{PU}, ϕ_{SR}	Directions of PU and SU_{rx} with respect to SU_{tx}
m_{PU}^*, m_{SR}^*	Indices of selected beam for PU and SU_{rx}
π_0, π_1	Prior probabilities of \mathcal{H}_0 and \mathcal{H}_1
$\hat{\pi}_0, \hat{\pi}_1$	Probabilities of channel being sensed idle or busy
T_f	Duration of frame employed by SU_{tx}
T_{se}	Duration of <i>spatial spectrum sensing phase</i>

latter phase, SU_{tx} sends data symbols to SU_{rx} . Given T_f and T_{tr} we have $0 < T_{se} < (T_f - T_{tr})$. In the following, we describe how SU_{tx} operates in directional mode during these three distinct phases. Based on these descriptions, we provide our problem statement.

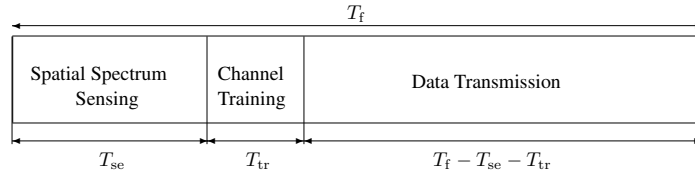


Figure 2.3: The structure of frame employed by SU_{tx} .

• **Spatial Spectrum Sensing Phase:** During this phase SU_{tx} senses the channel and monitors the activity of PU. Suppose \mathcal{H}_1 and \mathcal{H}_0 represent the binary hypotheses of PU being active and inactive, respectively, with prior probabilities $\Pr\{\mathcal{H}_1\} = \pi_1$ and $\Pr\{\mathcal{H}_0\} = \pi_0$. SU_{tx} applies a binary detection rule, as will be described in Section 2.2.1, to decide whether or not PU is active. Let $\hat{\mathcal{H}}_1$ and $\hat{\mathcal{H}}_0$ denote the detector outcome, i.e., the detector finds PU active (channel is sensed busy and occupied) and inactive (channel is sensed idle and unoccupied and thus can be used by SU_{tx} for transmission), respectively. The accuracy of this binary detector is characterized by its false alarm probability $P_{fa} = \Pr\{\hat{\mathcal{H}}_1|\mathcal{H}_0\}$ and detection probability $P_d = \Pr\{\hat{\mathcal{H}}_1|\mathcal{H}_1\}$. Therefore, the probabilities of events $\hat{\mathcal{H}}_0$ and $\hat{\mathcal{H}}_1$ become $\hat{\pi}_0 = \Pr\{\hat{\mathcal{H}}_0\} = \pi_1(1 - P_d) + \pi_0(1 - P_{fa})$ and $\hat{\pi}_1 = \Pr\{\hat{\mathcal{H}}_1\} = \pi_1 P_d + \pi_0 P_{fa}$, respectively. Furthermore,

the joint probabilities are $\beta_0 = \Pr\{\mathcal{H}_0, \hat{\mathcal{H}}_0\} = \pi_0(1 - P_{\text{fa}})$ and $\beta_1 = \Pr\{\mathcal{H}_1, \hat{\mathcal{H}}_0\} = \pi_1(1 - P_{\text{d}})$. The accuracy of spectrum sensing impacts the maximum information rate that SU_{tx} can transmit reliably to SU_{rx} . Our problem formulation incorporates the effect of imperfect spectrum sensing on the constrained ergodic capacity maximization. As long as the channel is sensed busy, SU_{tx} stays in *spatial spectrum sensing phase*. While being in this phase, SU_{tx} determines the beam corresponding to the location (orientation) of PU based on the received signal energy. We denote the sector index corresponding to PU's location by m_{PU}^* . SU_{tx} uses m_{PU}^* for adapting its discrete power level during *data transmission phase*. We note that, there is a non-zero error probability when SU_{tx} determines the beam index m_{PU}^* , i.e., it is possible that m_{PU}^* is not the true beam index corresponding to PU. Our problem formulation takes into account the impact of this error probability on the constrained ergodic capacity maximization.

- Channel Training Phase:** When the channel is sensed idle, SU_{tx} leaves *spatial spectrum sensing phase* and enters this new phase and sends training symbols over all beams. Based on the received training signal, SU_{rx} estimates the channel gain $\nu_m = |\chi_m|^2$ for all beams and determines the strongest channel $\nu^* = \max\{\nu_m\}$ among all beams, and the corresponding beam index $m_{\text{SR}}^* = \arg \max\{\nu_m\}$. Also, SU_{rx} employs an n_b -bit quantizer to quantize ν^* . The quantizer has $N_b = 2^{n_b}$ thresholds, denoted by $\{\mu_k\}_{k=1}^{N_b}$, satisfying $\mu_0 = 0 < \mu_1 < \dots < \mu_{N_b+1} = \infty$, and has $N_b + 1$ quantization intervals $\mathcal{I}_k = [\mu_k, \mu_{k+1})$ for $k = 0, \dots, N_b$. The quantization mapping rule follows: if the quantizer input ν^* lies in the interval \mathcal{I}_k then the quantizer output is μ_k , for $k = 0, \dots, N_b$. The index of quantization interval k can be represented by n_b -bits. Then, SU_{rx} feeds back m_{SR}^* as well as the n_b -bit representation of the index of the quantization interval to which ν^* belongs, over an error-free bandwidth limited feedback link to SU_{tx} , so SU_{tx} can optimally adapt its discrete power level accordingly. We take into account the probability of determining the true beam corresponding to SU_{rx} as well as the probability of selecting the true strongest channel among all beams between SU_{tx} and SU_{rx} , on the constrained capacity maximization.

- Data Transmission Phase:** After *channel training phase*, SU_{tx} enters *data transmission phase* and transmits data to SU_{rx} over the selected beam m_{SR}^* . During this phase, SU_{tx} adapts its discrete power level P_k , where $P_k \in \{P_0, P_1, P_2, \dots, P_{N_b}\}$, using m_{PU}^* and the information received from SU_{rx} through the feedback channel, such that the ergodic capacity of $\text{SU}_{\text{tx}}\text{-SU}_{\text{rx}}$ link is maximized, subject to ATPC and AIC. We let $P_0 = 0$ to indicate that when $\nu^* \in \mathcal{I}_0 = [0, \mu_1)$ then SU_{tx} does not transmit data to SU_{rx} , since the channel is too weak.

Table 2.2 enumerates the sequential steps we take within each of the three phases: *spatial spectrum sensing phase*, *channel training phase*, and *data transmission phase*.

Table 2.2: Sequential steps within each three phases.

Phase	Sequential steps in each phase
1. Spatial Spectrum Sensing Phase	1.1. SU _{tx} senses the channel and monitors the activity of PU. 1.2. As long as the channel is sensed busy, SU _{tx} stays in this phase. 1.3. While being in this phase, SU _{tx} determines the beam corresponding to the orientation of PU denoted by m_{PU}^* (based on the received signal energy). 1.4. When the channel is sensed idle, SU _{tx} leaves this phase and enters the next phase.
2. Channel Training Phase	2.1. SU _{tx} sends training symbols over all beams. 2.2. SU _{rx} estimates the channel gain ν_m for all beams and determines the strongest channel ν^* among all beams and the corresponding beam index m_{SR}^* . 2.3. SU _{rx} employs an n_b -bit quantizer to quantize ν^* . 2.4. SU _{rx} feeds back m_{SR}^* as well as the n_b -bit representation of the index of the quantization interval to which ν^* belongs, over a feedback link to SU _{tx} . 2.5 SU _{tx} leaves this phase and enters the next phase.
3. Data Transmission Phase	3.1. SU _{tx} adapts its discrete power level P_k , using m_{PU}^* and the information received from SU _{rx} through the feedback channel, such that the constrained ergodic capacity is maximized. 3.2. SU _{tx} transmits data to SU _{rx} with power P_k over the selected beam m_{SR}^* .

Remark: It is worth emphasizing that in our problem, SU_{tx} does not know the angles ϕ_{PU} and ϕ_{SU} , defined in Section 2.1.2 (otherwise, the beam selection at SU_{tx} for data transmission would become trivial). We take full advantage of beam steering capability of the ESPAR antenna that enables sector-based spectrum sensing and communication at SU_{tx}. In this work, SU_{tx} does not estimate the angles ϕ_{PU} and ϕ_{SR} . Instead it determines the indices of the sectors corresponding to PU and SU_{rx} (i.e., SU_{tx} finds m_{PU}^* and learns m_{SR}^* during *spatial spectrum sensing phase* and *channel training phase*, respectively). For mathematical tractability, we assume that these sectors are unchanged during a frame duration. Comparing with a CR system design that is based on angle (or directional of arrival) estimation at SU_{tx}, using the sector-based sensing and communication improves the system design resilience against the mobility of users (as long as the determined sectors do not change due to mobility).

When spectrum sensing is imperfect, the capacity of SU_{tx}-SU_{rx} link can be written as [3]

$$C = D_d \mathbb{E} \left\{ \beta_0 C_{0,0} + \beta_1 C_{1,0} \right\}, \quad (2.4)$$

where $C_{i,0}$ is the instantaneous capacity of this link corresponding to the event \mathcal{H}_i and \hat{H}_0 , $D_d = (T_f - T_{\text{se}} - T_{\text{tr}})/T_f$ and $\mathbb{E}\{\cdot\}$ is the statistical expectation operator. Let \bar{I}_{av} indicate the maximum allowed interference imposed on PU and \bar{P}_{av} denote the maximum allowed average transmit power of SU_{tx}. Given our aforementioned system model description and to enable mathematically expressing the AIC and ATPC in our problem, we let $P(\nu^*)$ indicate SU_{tx} transmit power in terms of the channel gain of the selected beam ν^* between SU_{tx} and SU_{rx}. To satisfy the AIC, we have

$$D_d \beta_1 \mathbb{E} \left\{ g_{\text{sp}} p(\kappa_{\text{SR}}^* - \kappa_{\text{PU}}^*) P(\nu^*) \right\} \leq \bar{I}_{\text{av}}, \quad (2.5)$$

and to satisfy the ATPC, we have

$$D_d \widehat{\pi}_0 \mathbb{E} \left\{ P(\nu^*) \right\} \leq \bar{P}_{\text{av}}. \quad (2.6)$$

Notice that, had spectrum sensing have been ideal, $\beta_1 = 0$ and data communication between SU_{tx} and SU_{rx} would cause no interference on PU. The more accurate spectrum sensing is, the smaller is the power of interference signal imposed on PU. On the other hand, increasing the accuracy of spectrum sensing requires a longer T_{se} and a shorter D_d , given the frame duration T_f . Reducing D_d decreases the capacity C in (2.4). Therefore, there is a tradeoff between increasing C and decreasing the power of interference signal imposed on PU. Let $F_{\nu^*}(\cdot)$ be the Cumulative Distribution Function (CDF) of ν^* (will be derived in Section 2.2.3). Given the discrete power levels P_k 's and the quantization thresholds μ_k 's, $\mathbb{E} \{ P(\nu^*) \}$ can be written as

$$\mathbb{E} \left\{ P(\nu^*) \right\} = \sum_{k=1}^{N_b} P_k \left[F_{\nu^*}(\mu_{k+1}) - F_{\nu^*}(\mu_k) \right]. \quad (2.7)$$

Therefore, the constraints in (2.5) and (2.6) can be rewritten as

$$D_d \beta_1 \gamma_{\text{sp}} \mathbb{E} \left\{ p(\kappa_{\text{SR}}^* - \kappa_{\text{PU}}^*) \right\} \sum_{k=1}^{N_b} P_k \left[F_{\nu^*}(\mu_{k+1}) - F_{\nu^*}(\mu_k) \right] \leq \bar{I}_{\text{av}}, \quad (2.8)$$

$$D_d \widehat{\pi}_0 \sum_{k=1}^{N_b} P_k \left[F_{\nu^*}(\mu_{k+1}) - F_{\nu^*}(\mu_k) \right] \leq \bar{P}_{\text{av}}. \quad (2.9)$$

Our main objective is to find the optimal spectrum sensing phase duration T_{se} , the optimal quantization thresholds μ_k 's for the channel gain quantizer employed at SU_{rx} , and the optimal discrete power levels P_k 's corresponding to each quantization interval $\mathcal{I}_k = [\mu_k, \mu_{k+1})$, such that the ergodic capacity C in (2.4) is maximized, subject to AIC and ATPC given in (2.8) and (2.9), respectively. In other words, we are interested in solving the following constrained optimization problem

$$\underset{T_{\text{se}}, \{\mu_k, P_k\}_{k=1}^{N_b}}{\text{Maximize}} \quad C = D_d \mathbb{E} \left\{ \beta_0 C_{0,0} + \beta_1 C_{1,0} \right\} \quad (2.P1)$$

$$\text{s.t.} \quad 0 < T_{\text{se}} < (T_f - T_{\text{tr}}),$$

$$0 < \mu_1 < \dots < \mu_{N_b} < \infty,$$

$$P_k > 0 \quad \forall k,$$

$$(2.8) \text{ and } (2.9) \text{ are satisfied.}$$

2.2 Characterizing Objective Function and Constraints in (2.P1)

Characterizing the objective function and the constraints in (2.P1) requires addressing the following three components. First, the performance of the binary detector employed by SU_{tx} to detect PU activity during *spatial spectrum sensing phase* plays role in the objective function and the AIC in (2.8) via β_1 , and in the ATPC in (2.9) via $\hat{\pi}_0$. Obviously, this performance depends on the choice of the detector. Section 2.2.1 describes our proposed binary detector, which is based on the energy of the collected measurements from all sectors of the ESPAR antenna at SU_{tx} during this phase, and provides closed form expressions for P_d and P_{fa} of this detector. Second, the error probability of finding the sector index m_{pU}^* corresponding to PU at SU_{tx} during *spatial spectrum sensing phase* affects the AIC in (2.8). This error probability depends on the mechanism through which SU_{tx} determines this sector index. Section 2.2.2 explains how SU_{tx} finds this beam index, using the received signal energy from all sectors of the ESPAR antenna during this phase, and derives closed form expression of the corresponding error probability. Third, the probability of finding the sector index m_{sR}^* corresponding to SU_{rx} during *channel training phase* impacts the AIC in (2.8). During *data transmission phase* SU_{tx} sends data to SU_{rx} over the selected beam m_{sR}^* . Section 2.2.3 discusses the method utilized by SU_{rx} to find this beam index, using the received training signal transmitted by all sectors of SU_{tx} antenna, and derives a closed form expression for the corresponding probability.

2.2.1 Energy-Based Binary Detector for Spectrum Sensing Using ESPAR Antenna

Spectrum sensing at SU_{tx} (detecting the activity of PU) during *spatial spectrum sensing phase* can be formulated as a binary hypothesis testing problem. Suppose when PU is active (present), it transmits signal $s(t)$ with power P_p . Let $y_m(n)$ denote the discrete-time representation of received signal at m -th sector of SU_{tx} at time instant $t = nT_s$ where T_s is the sampling period. Assuming SU_{tx} collects $N_{se} = \lfloor T_{se}/(MT_s) \rfloor$ samples corresponding to each sector we can write

$$y_m(n) = \psi_m(n)s(n) + w_m(n), \quad \text{for } n = 1 + (m-1)N_{se}, \dots, mN_{se}, \quad m = 1, \dots, M$$

We model the transmitted signal $s(n)$ by PU as a zero-mean complex Gaussian random variable with variance P_p and we assume SU_{tx} knows P_p . The term $w_m(n)$ is the additive noise at m -th sector of SU_{tx} antenna and is modeled as $w_m(n) \sim \mathcal{CN}(0, \sigma_w^2)$. We assume that $\psi_m(n)$, $s(n)$ and $w_m(n)$ are mutually independent random variables. Since SU_{tx} takes samples of the received signal for different sectors sequentially (in different time instants), $\psi_m(n)$

and noise samples $w_m(n)$ are independent and thus uncorrelated both in time and space (sector) domains. Under hypothesis \mathcal{H}_1 , given ψ_m , we have $y_m(n) \sim \mathcal{CN}(0, \sigma_m^2 + \sigma_w^2)$ where $\sigma_m^2 = |\psi_m|^2 P_p$. Under hypothesis \mathcal{H}_0 , we have $y_m(n) \sim \mathcal{CN}(0, \sigma_w^2)$. The hypothesis testing problem at discrete time instant n for m -th sector is then given by

$$\begin{cases} \mathcal{H}_0 : & y_m(n) = w_m(n), \\ \mathcal{H}_1 : & y_m(n) = \psi_m(n)s(n) + w_m(n). \end{cases} \quad (2.10)$$

Our proposed energy-based binary detector uses all the collected samples from M sectors (total of $N_{\text{eq}} = MN_{\text{se}}$ collected samples). Let ε_m be the energy of received signal at sector m . We have

$$\varepsilon_m = \frac{1}{N_{\text{se}}} \sum_{n=1+(m-1)N_{\text{se}}}^{mN_{\text{se}}} |y_m(n)|^2. \quad (2.11)$$

Under hypothesis \mathcal{H}_0 and also under \mathcal{H}_1 (given ψ_m), the sector energy ε_m is distributed as a central chi-square random variable with $2N_{\text{se}}$ degrees of freedom. We consider the summation of energies of received signals over all sectors as the decision statistics T given below

$$T = \frac{1}{M} \sum_{m=1}^M \varepsilon_m \underset{\hat{\mathcal{H}}_0}{\overset{\hat{\mathcal{H}}_1}{\geq}} \eta. \quad (2.12)$$

where η is the decision threshold. We can rewrite T as

$$T = \frac{1}{MN_{\text{se}}} \sum_{m=1}^M \sum_{n=1+(m-1)N_{\text{se}}}^{mN_{\text{se}}} |y_m(n)|^2. \quad (2.13)$$

Note that T is the summation of N_{eq} random variables. When N_{eq} is large enough T can be approximated as a Gaussian random variable. Thus, Under hypothesis \mathcal{H}_0 , for large N_{eq} we invoke the Central Limit Theorem (CLT), to approximate T as Gaussian with distribution $T \sim \mathcal{N}(\sigma_w^2, \sigma_{T|\mathcal{H}_0}^2)$, where $\sigma_{T|\mathcal{H}_0}^2 = \sigma_w^4/N_{\text{eq}}$. Similarly, under hypothesis \mathcal{H}_1 for large N_{eq} , T can be approximated with another Gaussian with distribution $T \sim \mathcal{N}(\zeta, \sigma_{T|\mathcal{H}_1}^2)$ where $\zeta = P_p \gamma E_A + \sigma_w^2$, and $\sigma_{T|\mathcal{H}_1}^2$ is given below

$$\sigma_{T|\mathcal{H}_1}^2 = \frac{1}{N_{\text{eq}}} \left[\sigma_w^4 + 2\gamma P_p E_A \sigma_w^2 + \gamma^2 P_p^2 \left(3E_B - MNE_A^2 \right) \right] + \frac{\gamma^2 P_p^2}{M^2} \sum_{m=1}^M \sum_{m'=1}^M E_{mm'}, \quad (2.14)$$

where

$$E_{mm'} = \frac{1}{2\pi} \int_0^{2\pi} p_m(\theta)p_{m'}(\theta)d\theta, \quad (2.15a)$$

$$E_A = \frac{1}{2\pi} \int_0^{2\pi} p(\theta)d\theta, \quad (2.15b)$$

and $E_B = E_{mm}$. Then, the false alarm and detection probabilities of this detector are given as the following

$$P_{\text{fa}} = Q\left(\frac{\eta - \sigma_w^2}{\sigma_{T|\mathcal{H}_0}}\right), \quad P_d = Q\left(\frac{\eta - \zeta}{\sigma_{T|\mathcal{H}_1}}\right), \quad (2.16)$$

where $Q(\cdot)$ is the Q-function. For a given value of $P_d = \bar{P}_d$, the false alarm probability can be written as

$$P_{\text{fa}} = Q\left(\frac{\sigma_{T|\mathcal{H}_1} Q^{-1}(\bar{P}_d) + \zeta - \sigma_w^2}{\sigma_{T|\mathcal{H}_0}}\right). \quad (2.17)$$

2.2.2 Determining the Beam Corresponding to PU

During *spatial spectrum sensing phase* when the channel is sensed busy, SU_{tx} determines the beam corresponding to the orientation of PU based on the received signal energy $\varepsilon_m, m = 1, \dots, M$. Ordering these calculated energies, SU_{tx} selects the beam index corresponding to the largest energy $m_{\text{PU}}^* = \arg \max\{\varepsilon_m\}$ among all sectors. For example, in Fig. 2.4a, we have $m_{\text{PU}}^* = 3$, that is, the third beam has received the largest amount of energy. As we mentioned, under hypothesis \mathcal{H}_1 , given ψ_m (or equivalently given g and ϕ_{PU}), the sector energy ε_m is distributed as a central chi-square random variable with $2N_{\text{se}}$ degrees of freedom and its conditional PDF and CDF expressions are

$$f_{\varepsilon_m}\left(x|g, \phi_{\text{PU}}\right) = \frac{x^{N_{\text{se}}-1} e^{-\frac{x}{\sigma_{\varepsilon_m}^2}}}{\sigma_{\varepsilon_m}^{2N_{\text{se}}} \Gamma(N_{\text{se}})}, \quad (2.18a)$$

$$F_{\varepsilon_m}\left(x|g, \phi_{\text{PU}}\right) = \frac{\gamma(N_{\text{se}}, \frac{x}{\sigma_{\varepsilon_m}^2})}{\Gamma(N_{\text{se}})}, \quad (2.18b)$$

where $\sigma_{\varepsilon_m}^2 = (\sigma_m^2 + \sigma_w^2)/N_{\text{se}}$ and $\gamma(\cdot, \cdot)$ is the lower incomplete gamma function

$$\gamma(s, x) = x^s e^{-x} \Gamma(s) \sum_{j=0}^{\infty} \frac{x^j}{\Gamma(j + s + 1)}. \quad (2.19)$$

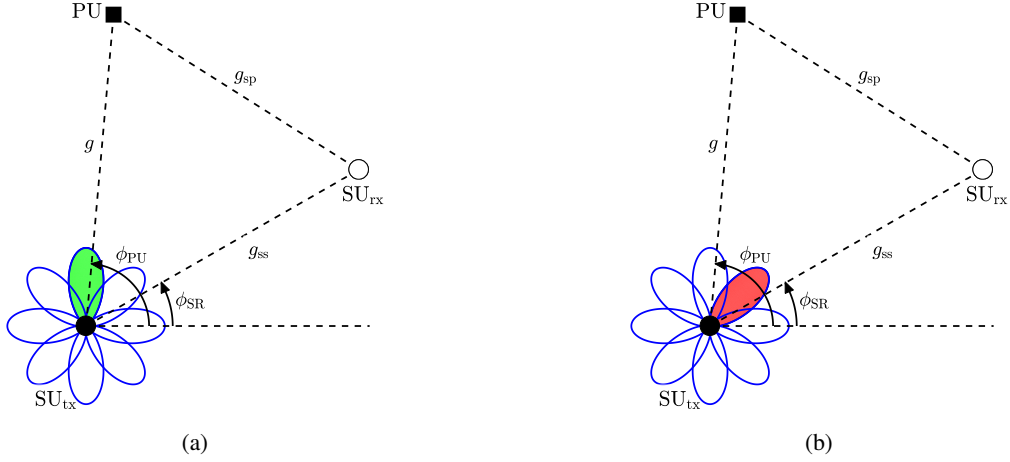


Figure 2.4: A schematic to show how different beams can be selected to indicate the orientation of SU_{tx} with respect to PU and SU_{rx} (a) $m_{PU}^* = 3$, (b) $m_{SR}^* = 2$.

Let $\bar{\Delta}_{i,m}$ represent the average error probability of finding the sector index corresponding to PU, i.e., the probability that $m_{PU}^* = i$ while the true orientation of PU belongs to the angular domain of m -th sector, $\phi_{PU} \in \Phi_m = \left[\frac{2\pi(m-3/2)}{M}, \frac{2\pi(m-1/2)}{M} \right)$, for $i \neq m, i, m = 1, \dots, M$. To find $\bar{\Delta}_{i,m}$ we start with finding $\Omega_i = \Pr\{m_{PU}^* = i | g, \phi_{PU}\}$, which is the probability that the index of selected sector, given g and ϕ_{PU} , is i . We have

$$\begin{aligned} \Omega_i &= \Pr \left\{ m_{PU}^* = i \mid g, \phi_{PU} \right\} = \Pr \left\{ \varepsilon_1 < \varepsilon_i, \dots, \varepsilon_{i-1} < \varepsilon_i, \varepsilon_{i+1} < \varepsilon_i, \dots, \varepsilon_M < \varepsilon_i \right\} \\ &= \mathbb{E}_{\varepsilon_i} \left\{ \prod_{\substack{m=1 \\ m \neq i}}^M F_{\varepsilon_m} \left(x | g, \phi_{PU} \right) \right\} = \int_0^\infty f_{\varepsilon_i} \left(y | g, \phi_{PU} \right) \prod_{\substack{m=1 \\ m \neq i}}^M F_{\varepsilon_m} \left(y | g, \phi_{PU} \right) dy. \end{aligned} \quad (2.20)$$

in which $f_{\varepsilon_m}(x|g, \phi_{PU})$ and $F_{\varepsilon_m}(x|g, \phi_{PU})$ are the conditional PDF and CDF of ε_m given in (2.18). Without loss of generality, suppose $i = 1$. After some mathematical manipulations and taking expectation with respect to ε_1 , Ω_1 in (2.20) can be written as

$$\Omega_1 = \frac{G^{-MN_{se}}}{\Gamma(N_{se}) \prod_{m=1}^M \sigma_{e_m}^{2N_{se}}} \widetilde{\sum}_{k_2:k_M} \frac{\Gamma \left(MN_{se} + \sum_{j=2}^M k_j \right)}{E_k G^{\sum_{j=2}^M k_j}}, \quad (2.21)$$

where

$$\widetilde{\sum}_{k_2:k_M} = \sum_{k_2=0}^{\infty} \sum_{k_3=0}^{\infty} \dots \sum_{k_M=0}^{\infty},$$

$$E_k = \prod_{j=2}^M \sigma_{e_j}^{2k_j} \Gamma(k_j + N_{\text{se}} + 1), \quad G = \sum_{m=1}^M \frac{1}{\sigma_{e_m}^2}.$$

To illustrate the behavior of Ω_1 (averaged over fading gain g) we define $\Delta_1 = \mathbb{E}_g\{\Omega_1\} = \Pr\{m_{\text{PU}}^* = 1 | \phi_{\text{PU}}\}$ and plot Δ_1 versus ϕ_{PU} for $M = 8$ and $\text{SNR}_{\text{PU}} = \gamma P_p / \sigma_w^2 = 0$ dB. Fig. 2.5a shows Δ_1 versus ϕ_{PU} for $N_{\text{se}} = 20$ and $\phi_{3\text{dB}} = 20^\circ, 30^\circ$. We observe that when $\phi_{3\text{dB}}$ decreases from 30° to 20° , beam selection becomes more accurate, i.e., Δ_1 increases for $\phi_{\text{PU}} \in \Phi_1 = [-22.5^\circ, 22.5^\circ)$, however, it decreases outside this angular interval. Fig. 2.5b plots Δ_1 versus ϕ_{PU} for $N_{\text{se}} = 10, 30, 200$ and $\phi_{3\text{dB}} = 20^\circ$. We observe that as N_{se} increases beam selection becomes more accurate. For large N_{se} , we can see that Δ_1 approaches one for $\phi_{\text{PU}} \in \Phi_1$ and it is approximately zero outside this angular interval. Now, we are ready to find $\bar{\Delta}_{i,m}$ using $\Delta_i = \Pr\{m_{\text{PU}}^* = i | \phi_{\text{PU}}\}$. We have

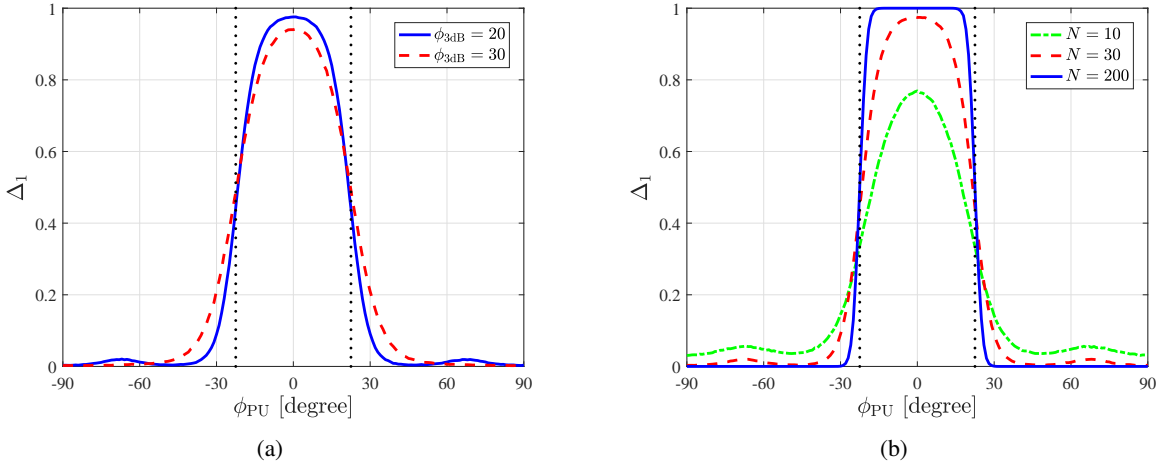


Figure 2.5: Δ_1 versus ϕ_{PU} for $M = 8$ and $\text{SNR}_{\text{PU}} = 0$ dB (a) $N_{\text{se}} = 20$, $\phi_{3\text{dB}} = 20^\circ, 30^\circ$ (b) $\phi_{3\text{dB}} = 20^\circ$, $N_{\text{se}} = 10, 30, 200$.

$$\bar{\Delta}_{i,m} = \int_{\phi_{\text{PU}} \in \Phi_m} \Delta_i \Pr\{\phi_{\text{PU}} \in \Phi_m\} d\phi_{\text{PU}}. \quad (2.22)$$

Due to the symmetrical structure of the ESPAR antenna we have $\bar{\Delta}_{i,m} = \bar{\Delta}_{m,i}$. Note that $\bar{\Delta}_{i,i}$ is the probability of selecting the correct beam and $\bar{\Delta}_{i,m}$ for $i \neq m$ is the probability of selecting the incorrect beam, leading to error probability in beam selection. The average error probability $\bar{\Delta}_{1,m}$ versus the index beam m is shown in Figs. 2.6a and 2.6b for $\text{SNR}_{\text{PU}} = 0, -5$ dB. As expected, $\bar{\Delta}_{1,1}$ increases and $\bar{\Delta}_{1,m}, m \neq 1$ decreases as N_{se} increases.

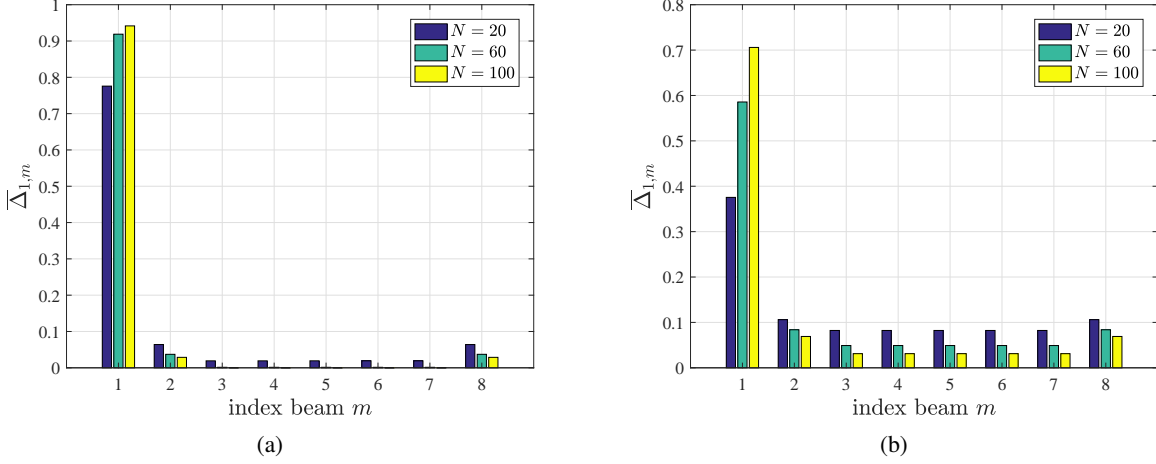


Figure 2.6: $\bar{\Delta}_{1,m}$ versus the index beam m for $\phi_{3\text{dB}} = 20^\circ$ (a) $\text{SNR}_{\text{PU}} = 0$ dB, (b) $\text{SNR}_{\text{PU}} = -5$ dB.

2.2.3 Determining the Beam Corresponding to SU_{rx}

When the channel is sensed idle, SU_{tx} leaves *spatial spectrum sensing phase* and enters *channel training phase*. During this phase, SU_{tx} sends training symbols over all beams to enable channel estimation at SU_{rx} . Using the received training signal, SU_{rx} estimates the channel gains $\nu_m = |\chi_m|^2$ corresponding to all sectors and determines the strongest channel $\nu^* = \max\{\nu_m\}$ among all beams and the corresponding beam index $m_{\text{SR}}^* = \arg \max\{\nu_m\}$. For example, in Fig. 2.4b, we have $m_{\text{SR}}^* = 2$, i.e., the second beam has the largest channel gain. SU_{rx} employs an n_b -bit quantizer, with quantization thresholds $\{\mu_k\}_{k=0}^{N_b}$ and quantization intervals $\{\mathcal{I}_k\}_{k=0}^{N_b}$, to quantize ν^* and to find the quantization interval to which ν^* belongs to. Then, SU_{rx} feeds back m_{SR}^* as well as the n_b -bit representation of the index of the quantization interval to which ν^* belongs, over the feedback link to SU_{tx} . Let $\Psi_i = \Pr\{m_{\text{SR}}^* = i\}$ denote the probability that $m_{\text{SR}}^* = i$. To characterize Ψ_i we need to find the CDF and PDF of ν^* , denoted as $F_{\nu^*}(\cdot)$ and $f_{\nu^*}(\cdot)$, respectively. Note that given our assumptions, ν_m 's are independent across sectors, however, not necessarily identically distributed. Therefore, $F_{\nu^*}(x)$ can be written as

$$F_{\nu^*}(x) = \prod_{m=1}^M F_{\nu_m}(x), \quad (2.23)$$

where $F_{\nu_m}(x) = 1 - e^{-\frac{x}{\delta_m}}$. After simplification, (2.23) can be written as

$$F_{\nu^*}(x) = 1 + \sum_{m=1}^M (-1)^m \sum_m \exp(-xA_{j_1:j_m}), \quad (2.24)$$

where

$$A_{j_1:j_m} = \sum_{i=1}^m \frac{1}{\delta_{j_i}}, \quad \sum_m = \sum_{j_1=1}^{M-m+1} \sum_{j_2=j_1+1}^{M-m+2} \cdots \sum_{j_m=j_{m-1}+1}^M .$$

From the CDF in (2.24), we can find the PDF

$$f_{\nu^*}(x) = \sum_{m=1}^M (-1)^{m+1} \sum_m A_{j_1:j_m} \exp(-xA_{j_1:j_m}). \quad (2.25)$$

Similar to section 2.2.2, we can express Ψ_i as the following

$$\Psi_i = \Pr \left\{ m_{\text{SR}}^* = i \right\} = \int_0^\infty f_{\nu_i}(y) \prod_{\substack{m=1 \\ m \neq i}}^M F_{\nu_m}(y) dy. \quad (2.26)$$

Without loss of generality, suppose $i = 1$. After some mathematical simplification, Ψ_1 can be expressed as

$$\Psi_1 = \Pr \left\{ m_{\text{SR}}^* = 1 \right\} = 1 + \sum_{m=1}^{M-1} (-1)^m \sum'_m \frac{1}{1 + \delta_1 B_{j_1:j_m}}, \quad (2.27)$$

where

$$B_{j_1:j_m} = \sum_{i=1}^m \frac{1}{\delta_{(1+j_i)}}, \quad \sum'_m = \sum_{j_1=1}^{M-m} \sum_{j_2=j_1+1}^{M-m+1} \cdots \sum_{j_m=j_{m-1}+1}^{M-1} .$$

2.3 Formalizing and Solving (2.P1)

After *channel training phase*, SU_{tx} enters *data transmission phase*. Going through the previous two phases, at this point SU_{tx} knows the beam indices m_{PU}^* , m_{SR}^* as well as the index of quantization interval to which the largest channel gain ν^* belongs to. Knowing the quantization interval index, SU_{tx} infers the quantized value of ν^* and adopts its discrete power level accordingly. For instance, if $\nu^* \in \mathcal{I}_k$ then the quantized ν^* is μ_k and the associated discrete power level is P_k . From a system-level design perspective, one can optimize the quantization thresholds μ_k 's and the associated discrete power levels P_k 's, such that the constrained capacity is maximized. Furthermore, the capacity expression itself and the power of interference signal imposed on PU during this phase depend on the accuracy of the

energy-based binary detector in Section 2.2.1, in a way that increasing the detector accuracy has a positive effect on lowering the interference and a negative impact on enhancing the capacity itself. This implies that an optimal T_{se} can exist that maximizes the constrained capacity. In the following we express $C_{0,0}$ and $C_{1,0}$ in terms of the optimization variables $\{\mu_k, P_k\}_{k=1}^{N_b}$ and we find the term $\mathbb{E}\{p(\kappa_{\text{SR}}^* - \kappa_{\text{PU}}^*)\}$ in (2.8) using the analysis we have conducted in sections 2.2.2 and 2.2.3. We modify the objective function and the constrains in terms of the optimization variables in Section 2.3.1. Then, we provide our solution to the problem in Section 2.3.2.

2.3.1 Formalizing (2.P1) with Modified Objective Function and Constraints

Starting with the continuous valued ν^* and its corresponding continuous valued transmit power $P(\nu^*)$, we can write the expressions for the instantaneous capacity $C_{0,0}$ and $C_{1,0}$ in (2.4) as [1]

$$C_{0,0} = \log_2 \left(1 + \frac{\nu^* P(\nu^*)}{\sigma_w^2} \right), \quad C_{1,0} = \log_2 \left(1 + \frac{\nu^* P(\nu^*)}{\sigma_w^2 + P_p g_{\text{sp}}} \right). \quad (2.28)$$

Since SUs and PU cannot cooperate, SU_{tx} cannot estimate the channel gain g_{sp} and thus $C_{1,0}$ cannot be directly maximized at SU_{tx} . Instead, we consider a lower bound on its average over g_{sp} , denoted as $\mathbb{E}_{g_{\text{sp}}}\{C_{1,0}\}$. Using the Jensen's inequality [116], the lower bound on $\mathbb{E}_{g_{\text{sp}}}\{C_{1,0}\}$ becomes

$$\mathbb{E}_{g_{\text{sp}}}\{C_{1,0}\} \geq \log_2 \left(1 + \frac{\nu^* P(\nu^*)}{\sigma_w^2 + \sigma_p^2} \right) = C_{1,0}^{\text{LB}} \quad (2.29)$$

where $\sigma_p^2 = P_p \mathbb{E}\{g_{\text{sp}}\} = P_p \gamma_{\text{sp}}$. Let $C^{\text{LB}} = D_d \mathbb{E}_{\nu^*} \left\{ \beta_0 C_{0,0} + \beta_1 C_{1,0}^{\text{LB}} \right\}$ where C^{LB} is the lower bound on C in (2.4). From now on, we focus on C^{LB} . Let $R_{0,0}^{(k)}$ and $R_{1,0}^{(k)}$ denote the discrete transmission rates when the quantization interval index of ν^* is k , i.e., $\nu^* \in \mathcal{I}_k$, quantized ν^* is μ_k , and discrete power level is P_k . From (2.28) we have

$$R_{0,0}^{(k)} = \log_2 \left(1 + \frac{\mu_k P_k}{\sigma_w^2} \right), \quad R_{1,0}^{(k)} = \log_2 \left(1 + \frac{\mu_k P_k}{\sigma_w^2 + \sigma_p^2} \right). \quad (2.30)$$

Recall that the probability of quantized ν^* being in the interval \mathcal{I}_k is equal to $F_{\nu^*}(\mu_{k+1}) - F_{\nu^*}(\mu_k)$. By averaging over all possible quantization intervals, we can rewrite C^{LB} in terms of the discrete transmission rates as the following:

$$C^{\text{LB}} = D_d \sum_{k=1}^{N_b} \left(\beta_0 R_{0,0}^{(k)} + \beta_1 R_{1,0}^{(k)} \right) \left[F_{\nu^*}(\mu_{k+1}) - F_{\nu^*}(\mu_k) \right]. \quad (2.31)$$

Next, we focus on the constraint in (2.8) and find the term $\mathbb{E}\{p(\kappa_{\text{SR}}^* - \kappa_{\text{PU}}^*)\}$. Using the average probabilities derived in (2.22) and (2.26) we have

$$\mathbb{E}\left\{p(\kappa_{\text{SR}}^* - \kappa_{\text{PU}}^*)\right\} = \sum_{j=1}^M \sum_{i=1}^M \Psi_j \bar{\Delta}_{m_{\text{PU}}^*, i} p(\kappa_j - \kappa_i). \quad (2.32)$$

Then, the constraint in (2.8) can be written as

$$D_d b_0 \sum_{k=1}^{N_b} P_k \left[F_{\nu^*}(\mu_{k+1}) - F_{\nu^*}(\mu_k) \right] \leq \bar{I}_{\text{av}}, \quad (2.33)$$

where b_0 is

$$b_0 = \beta_1 \gamma_{\text{sp}} \sum_{j=1}^M \sum_{i=1}^M \Psi_j \bar{\Delta}_{m_{\text{PU}}^*, i} p(\kappa_j - \kappa_i). \quad (2.34)$$

We end this section with the statement of the constrained optimization problem we solve. In Section 2.3.2 we solve the following constrained optimization problem

$$\begin{aligned} \text{Maximize}_{T_{\text{se}}, \{\mu_k, P_k\}_{k=1}^{N_b}} \quad & C^{\text{LB}} = D_d \sum_{k=1}^{N_b} \left(\beta_0 R_{0,0}^{(k)} + \beta_1 R_{1,0}^{(k)} \right) \left[F_{\nu^*}(\mu_{k+1}) - F_{\nu^*}(\mu_k) \right] \\ \text{s.t.:} \quad & 0 < T_{\text{se}} < (T_f - T_{\text{tr}}), \\ & 0 < \mu_1 < \dots < \mu_{N_b} < \infty, \\ & P_k > 0 \quad \forall k, \end{aligned} \quad (2.P2)$$

(2.33) and (2.9) are satisfied.

It is worth mentioning that (2.P2) includes the special case where the locations (orientations) of PU and SU_{rx} are such that they belong to the same beam, with respect to SU_{tx} . First, suppose $m_{\text{PU}}^* = m_{\text{SR}}^*$. In this case, the interference imposed on PU increases and SU_{tx} uses a small transmit power level P_k , such that the AIC in (2.33) is satisfied. Next, suppose $m_{\text{PU}}^* \neq m_{\text{SR}}^*$. In this case SU_{tx} uses a larger P_k , compared with the case where $m_{\text{PU}}^* = m_{\text{SR}}^*$ (because SU_{tx} wrongly assumes that PU and SU_{rx} lie in two different beams/sectors). Although the instantaneous interference in this case becomes larger (compared with the case where $m_{\text{PU}}^* = m_{\text{SR}}^*$), the AIC in (2.33) is still satisfied.

2.3.2 Solving (2.P2)

We note that (2.P2) is a non-convex problem and can be solved using exhaustive search, which can be computationally expensive. Therefore we develop an iterative suboptimal algorithm with a much less computational complexity, to find the local optimal solution using the Lagrangian method. The Lagrangian is

$$\begin{aligned} \mathcal{L} = & -D_d \sum_{k=1}^{N_b} \left(\beta_0 R_{0,0}^{(k)} + \beta_1 R_{1,0}^{(k)} \right) \left[F_{\nu^*}(\mu_{k+1}) - F_{\nu^*}(\mu_k) \right] \\ & + \lambda \left(D_d \hat{\pi}_0 \sum_{k=1}^{N_b} P_k \left[F_{\nu^*}(\mu_{k+1}) - F_{\nu^*}(\mu_k) \right] - \bar{P}_{av} \right) + \vartheta \left(D_d b_0 \sum_{k=1}^{N_b} P_k \left[F_{\nu^*}(\mu_{k+1}) - F_{\nu^*}(\mu_k) \right] - \bar{I}_{av} \right) \end{aligned} \quad (2.35)$$

where λ and ϑ are the nonnegative Lagrange multipliers, associated with the ATPC and AIC, respectively. The Lagrangian multipliers can be obtained using the subgradient method. Our iterative algorithm is based on the Block Coordinate Descent (BCD) algorithm which relies on the following principle: all variables except one are assumed to be fixed and the optimal variable that minimizes (2.35) is found. This process is iterated for all the variables until the final solution is reached. Convergence is achieved if there exists a single solution that minimizes (2.35) at each iteration [15]. To apply the principle of BCD algorithm in our problem, we consider the following. Assuming fixed μ_k 's and T_{se} , the problem (2.P2) becomes convex with respect to P_k . Therefore, the optimal P_k 's that minimize (2.35) are the solutions to the Karush-Kuhn-Tucker (KKT) optimality necessary and sufficient conditions

$$\begin{aligned} P_k &= \left[\frac{F_k + \sqrt{\Upsilon_k}}{2} \right]^+, \quad \text{for } k = 1, 2, \dots, N_b \\ F_k &= \frac{\hat{\pi}_0}{\ln(2)(\lambda \hat{\pi}_0 + \vartheta b_0)} - \frac{2\sigma_w^2 + \sigma_p^2}{\mu_k}, \quad \Upsilon_k = F_k^2 - \frac{4}{\mu_k} \left(\frac{\sigma_w^2(\sigma_w^2 + \sigma_p^2)}{\mu_k} - \frac{\hat{\pi}_0 \sigma_w^2 + \beta_1 \sigma_p^2}{\ln(2)(\lambda \hat{\pi}_0 + \vartheta b_0)} \right), \end{aligned} \quad (2.36)$$

where $[x]^+ = \max(x, 0)$. On the other hand, assuming fixed P_k 's and T_{se} , the optimal μ_k 's that minimize (2.35) are the solutions to $\partial \mathcal{L} / \partial \mu_k = 0$ for $k = 1, \dots, N_b$, which is the first derivative of \mathcal{L} with respect to μ_k . Setting $\partial \mathcal{L} / \partial \mu_k = 0$ we reach to

$$F_{\nu^*}(\mu_{k+1}) = F_{\nu^*}(\mu_k) + \frac{f_{\nu^*}(\mu_k) \left[\beta_0 \left(R_{0,0}^{(k)} - R_{0,0}^{(k-1)} \right) + \beta_1 \left(R_{1,0}^{(k)} - R_{1,0}^{(k-1)} \right) - (\lambda \hat{\pi}_0 + \vartheta b_0)(P_k - P_{k-1}) \right]}{\frac{P_k}{\ln(2)} \left(\frac{\beta_0}{\sigma_w^2 + \mu_k P_k} + \frac{\beta_1}{\sigma_w^2 + \sigma_p^2 + \mu_k P_k} \right)} \quad (2.37)$$

Note the values of λ and ϑ in (2.36) and (2.37) are obtained by applying the constraints given in (2.33) and (2.9). Recall that $\mu_0 = 0$ and $\mu_{N_b+1} = \infty$ and hence $F_{\nu^*}(\mu_0) = 0$ and $F_{\nu^*}(\mu_{N_b+1}) = 1$.

We are now ready to state our iterative algorithm to find the local optimal solution of (2.P2). In the first step, let T_{se} be a value in the interval $(0, T_f - T_{tr})$. We initiate $\mu_1 > 0$ and find P_1 using (2.36). Having $P_1, P_0 = 0$ and μ_1 we obtain μ_2 using (2.37). We repeat this and iterate between (2.36) and (2.37) until we find $\{P_k, \mu_k\}_{k=1}^{N_b}$. At this point, we check whether or not $F_{\nu^*}(\mu_{N_b+1}) = 1$. If $F_{\nu^*}(\mu_{N_b+1})$ is less (greater) than one, we increase (decrease) the initial value of μ_1 and find a new set of values for $\{P_k, \mu_k\}_{k=1}^{N_b}$ and check for the condition $F_{\nu^*}(\mu_{N_b+1}) = 1$. We continue changing the initial value of μ_1 and finding new values for $\{P_k, \mu_k\}_{k=1}^{N_b}$ and checking for the condition $F_{\nu^*}(\mu_{N_b+1}) = 1$, until we find the set of values such that this condition is satisfied. In the second step, given $\{P_k, \mu_k\}_{k=1}^{N_b}$ values reached at the end of the first step, we find T_{se} that minimizes (2.35), using search methods such as bisection method⁴. A summary of our proposed iterative algorithm for solving (2.P2) is given in Algorithm 1.

Algorithm 1: Our proposed iterative algorithm for solving (2.P2)

- 1: Initialize $T_{se} \in (0, T_f - T_{tr}), \mu_1, \lambda, \vartheta$.
 - 2: Set $P_0 = 0$.
 - 3: **repeat**
 - 4: **repeat**
 - 5: Find P_1 using (2.36).
 - 6: **for** $k = 2 : N_b$
 - 7: Having P_0, \dots, P_{k-1} , obtain μ_k using (2.37).
 - 8: Having μ_k , obtain P_k using (2.36).
 - 9: **end**
 - 10: Update λ and ϑ using subgradient method.
 - 11: **until** Constraints in (2.33) and (2.9) are satisfied.
 - 12: Find $F_{\nu^*}(\mu_{N_b+1})$ using (2.37).
 - 13: **if** $F_{\nu^*}(\mu_{N_b+1}) < 1$
 - 14: increase μ_1 .
 - 15: **elseif** $F_{\nu^*}(\mu_{N_b+1}) > 1$
 - 16: decrease μ_1 .
 - 17: **end**
 - 18: **until** $F_{\nu^*}(\mu_{N_b+1}) = 1$
 - 19: Find T_{se}^{Opt} that maximizes C^{LB} using bisection method.
-

2.4 Outage and Symbol Error Probabilities

Two other relevant metrics to evaluate the performance of our opportunistic CR system with the ESPAR antenna at SU_{tx} are outage probability and SEP, denoted as P_{out} and P_e , respectively. We define P_{out} as the probability of

⁴The problem in (2.P2) can be solved offline, based on the statistical information of the channels between SU_{tx} -PU and SU_{tx} - SU_{rx} , the number of sectors M , and the number of feedback bits n_b . In particular, given each pair $m_{PU}^*, m_{SR}^* \in \{1, \dots, M\}$ there is a set of optimal solution for T_{se} , $\{\mu_k, P_k\}_{k=1}^{N_b}$. These M^2 sets of solutions are available a priori at SU_{tx} . Also, the M^2 sets of $\{\mu_k\}_{k=1}^{N_b}$ are available a priori at SU_{rx} . During channel training phase, SU_{tx} can also send its finding m_{PU}^* to SU_{rx} . With the knowledge of m_{PU}^* and m_{SR}^* , SU_{rx} would know which set of quantization thresholds to use for quantizing ν^* . The idea of offline power allocation optimization with a limited feedback channel has been used before for distributed detection systems in wireless sensor networks [114].

SU_{tx} not transmitting data due to the weak $SU_{\text{tx}}-SU_{\text{rx}}$ channel. In the following, we derive closed-form expressions for P_{out} and P_e , based on the solutions provided in Section 2.3.2. The outage probability P_{out} can be directly obtained using the CDF of ν^* as

$$P_{\text{out}} = \Pr \left\{ P(\nu^*) = 0 \right\} = \Pr \left\{ \nu^* < \mu_1 \right\} = F_{\nu^*}(\mu_1). \quad (2.38)$$

For many digital modulation schemes SEP can be written as $P_e = \mathbb{E} \left\{ Q(\sqrt{\rho \text{SNR}}) \right\}$ where ρ is a constant parameter related to the type of modulation [100]. Considering the noise (plus interference) imposed on SU_{rx} under hypotheses $\hat{\mathcal{H}}_0$ and $\hat{\mathcal{H}}_1$, we can write P_e as

$$P_e = \beta_0 \mathbb{E} \left\{ Q \left(\sqrt{\frac{\rho \nu^* P(\nu^*)}{\sigma_w^2}} \right) \right\} + \beta_1 \mathbb{E} \left\{ Q \left(\sqrt{\frac{\rho \nu^* P(\nu^*)}{\sigma_w^2 + \sigma_p^2}} \right) \right\}. \quad (2.39)$$

Let focus on the expectation in the first term of (2.39). Since $P(\nu^*) = P_k$ when $\nu^* \in \mathcal{I}_k = [\mu_k, \mu_{k+1})$, we have

$$\mathbb{E} \left\{ Q \left(\sqrt{\frac{\rho \nu^* P(\nu^*)}{\sigma_w^2}} \right) \right\} = \int_0^\infty Q \left(\sqrt{\frac{\rho x P(x)}{\sigma_w^2}} \right) f_{\nu^*}(x) dx = \sum_{k=0}^{N_b} \int_{\mu_k}^{\mu_{k+1}} Q \left(\sqrt{\frac{\rho x P_k}{\sigma_w^2}} \right) f_{\nu^*}(x) dx. \quad (2.40)$$

Similarly, we can find the expectation in the second term of (2.39). Using the following equation

$$\int_\mu^\infty Q(\sqrt{bx}) e^{-Ax} dx = \frac{1}{A} \left[e^{-A\mu} Q(\sqrt{b\mu}) - \frac{Q\left(\sqrt{\mu(2A+b)}\right)}{\sqrt{1 + \frac{2A}{b}}} \right], \quad (2.41)$$

and after some manipulation, the P_e in (2.39) can be written as

$$P_e = \sum_{m=1}^M (-1)^{m+1} \sum_m \sum_{k=0}^{N_b} \left[\beta_0 \left(V(\mu_{k+1}, \text{SNR}_k^{(0)}) - V(\mu_k, \text{SNR}_k^{(0)}) \right) + \beta_1 \left(V(\mu_{k+1}, \text{SNR}_k^{(1)}) - V(\mu_k, \text{SNR}_k^{(1)}) \right) \right] \quad (2.42)$$

where

$$V(\mu, \text{SNR}) = \frac{Q\left(\sqrt{\mu(\text{SNR} + 2A_{j_1:j_m})}\right)}{\sqrt{1 + \frac{2A_{j_1:j_m}}{\text{SNR}}}} - e^{-\mu A_{j_1:j_m}} Q\left(\sqrt{\mu \text{SNR}}\right) \quad (2.43)$$

In (2.42), $\text{SNR}_k^{(0)}$ and $\text{SNR}_k^{(1)}$ are the received SNR at SU_{rx} when $\nu^* \in \mathcal{I}_k$ and the channel is sensed idle and busy, respectively, defined as

$$\text{SNR}_k^{(0)} = \frac{\rho P_k}{\sigma_w^2}, \quad \text{SNR}_k^{(1)} = \frac{\rho P_k}{\sigma_w^2 + \sigma_p^2}. \quad (2.44)$$

2.5 Simulation Results

We corroborate our analysis on constrained maximization of ergodic capacity as well as outage probability and SEP derivations with Matlab simulations. To illustrate the advantage of ESPAR antennas on increasing constrained capacity, we compare the performance of our CR system with another CR system in which SU_{tx} has an omni-directional antenna. Different from an ESPAR antenna that concentrates the electromagnetic power in specific directions (so-called sector or beam), an omni-directional antenna spreads the power equally in all angles. To fairly compare the performance of our CR system (in which SU_{tx} has an ESPAR antenna) with the other CR system (in which SU_{tx} has an omni-directional antenna), we let $p^{\text{Om}}(\phi) = E_A$ for $\phi \in (-\pi, \pi)$, i.e., we set the gain of the omni-directional antenna to be E_A . Note that, with this setting, we have the following equality⁵

$$\frac{1}{2\pi} \int_0^{2\pi} p(\phi) d\phi = \frac{1}{2\pi} \int_0^{2\pi} p^{\text{Om}}(\phi) d\phi, \quad (2.45)$$

Fig. 2.7a shows the beampatterns of omni-directional and ESPAR antennas in polar coordinate, where $A_0 = 0.97$, $A_1 = 0.03$ (corresponding to $E_A = 0.145$). Note that the radius of the red beampattern is 0.145 and the blue beampattern has the maximum value of $p(0) = A_1 + A_0 = 1$ at angle $\phi = 0$ radians. The area covered by the solid blue beampattern is equal to the area covered by the dashed red beampattern, in the sense that the equality in (2.45) holds true. Fig. 2.7b plots the same beampatterns in Cartesian coordinate. For the CR system with the omni-directional antenna at SU_{tx} , we consider a modified procedure for *spatial spectrum sensing, channel training and data transmission* phases⁶ (with respect to the description in Section 2.1.3) and denote the constrained capacity in (2.P2) evaluated at the optimized variables T_{se}, μ_k 's, P_k 's, by $C_{\text{Opt}}^{\text{LB,Om}}$. For our CR system let $C_{\text{Opt}}^{\text{LB}}$ denote the constrained capacity in (2.P2), that is evaluated at the optimized variables T_{se}, μ_k 's, P_k 's. Obviously, the optimized variables obtained from

⁵ We note that comparing an ESPAR antenna with the omni-directional antenna obtained from the same ESPAR antenna is not a fair comparison for the following reason. The omni-directional beampattern obtained from the same ESPAR antenna (when reactive loads of all parasitic elements are equal) becomes $p^{\text{Om}}(\phi) = A_1 + A_0$ for $\phi \in (-\pi, \pi)$. Clearly, this beampattern does not satisfy the equality in (2.45) and hence the comparison between the two CR systems is not fair.

⁶ Since the omni-directional antenna has only one beampattern, there is no beam selection corresponding to the orientations of PU and SU_{rx} . Thus, step 1.3 of Table 2.2 will be removed. The following steps in Table 2.2 are modified: in step 2.2, SU_{rx} estimates only one channel gain ν , in step 2.4, SU_{rx} feeds back only the n_b -bit representation of the index of the quantization interval to which ν belongs to SU_{rx} , in step 3.1, SU_{tx} adapts its discrete power level P_k , using the information received from SU_{rx} .

solving (2.P2) for omni-directional and ESPAR antennas can be different.

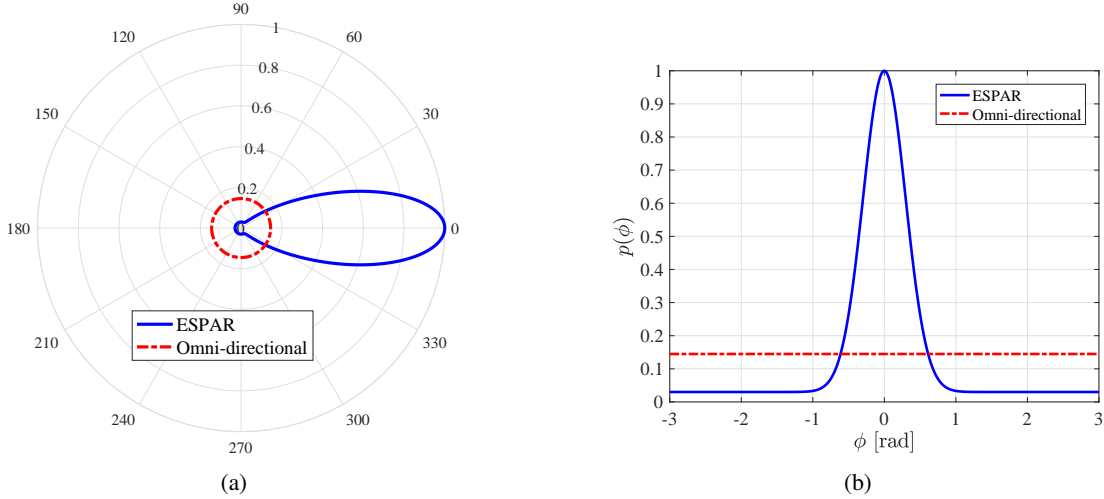


Figure 2.7: Parameters $A_0 = 0.97, A_1 = 0.03$, which correspond to $E_A = 0.145$. For a fair comparison, we set the gain of the omni-directional antenna $p^{\text{Om}}(\phi) = E_A$ for $\phi \in (-\pi, \pi)$, to ensure that the equality in (2.45) holds true. (a) polar coordinate, (b) Cartesian coordinate.

Table 2.3: Simulation Parameters

Parameter	Value	Parameter	Value	Parameter	Value
A_0	1, 2	γ_{ss}	3	σ_{w}^2	1
A_1	0.01	$\gamma; \gamma_{\text{sp}}$	1	P_{p}	1 watts
$\phi_{3\text{dB}}$	20°	π_1	0.3	T_{f}	20 ms
ρ	4	\bar{P}_{d}	0.9	\bar{I}_{av}	-6 dB

Our simulation parameters are given in Table 2.3. First, we explore the effect of increasing the number of quantization bits n_b . Fig. 2.8a shows $C_{\text{Opt}}^{\text{LB}}$ and $C_{\text{Opt}}^{\text{LB,Om}}$ versus \bar{P}_{av} for different n_b , when $M = 8, m_{\text{PU}}^* = 1$ ($\phi_{\text{PU}} = 12^\circ$), $m_{\text{SR}}^* = 1$ ($\phi_{\text{SR}} = 0^\circ$) and $A_0 = 1, A_1 = 0.01$ (corresponding to $E_A = 0.127$). As a baseline we also plot the capacity when perfect CSI (for $\text{SU}_{\text{tx}}\text{-SU}_{\text{rx}}$ link) is available for both CR systems (labeled as $n_b = \infty$ in the figures). Clearly, our CR system with the ESPAR antenna at SU_{tx} yields a higher capacity than the CR system with the omni-directional antenna at SU_{tx} . This figure also shows that as n_b increases, $C_{\text{Opt}}^{\text{LB}}$ increases and for $n_b = 4$ bits $C_{\text{Opt}}^{\text{LB}}$ is very close to the baseline capacity. To observe the impact of increasing the number of beams (the number of parasitic elements of the ESPAR antenna), Fig. 2.8b plots $C_{\text{Opt}}^{\text{LB}}$ and $C_{\text{Opt}}^{\text{LB,Om}}$ versus \bar{P}_{av} for different n_b , when $M = 12$. Comparing Figs.

2.8a and 2.8b we observe that as M increases a higher capacity can be achieved.

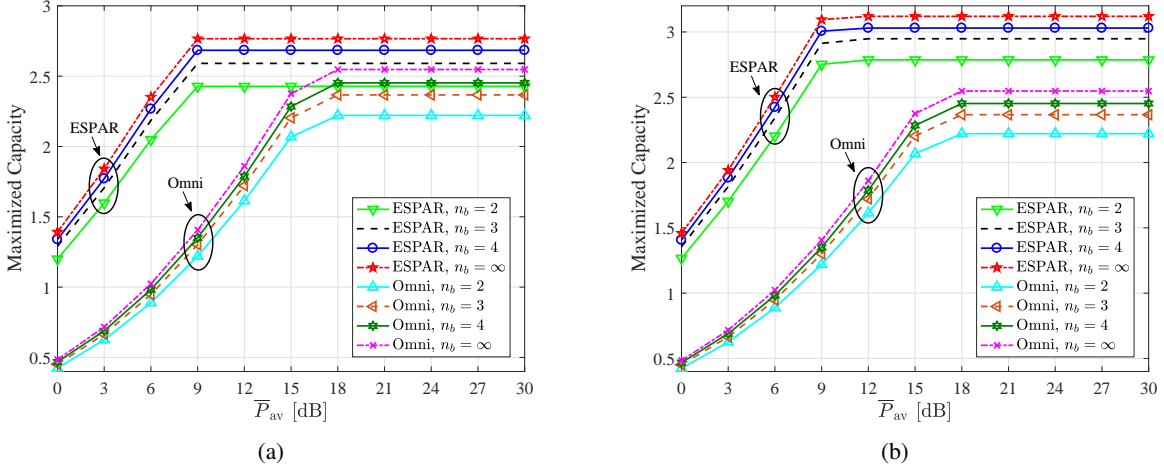


Figure 2.8: $C_{\text{Opt}}^{\text{LB}}$ and $C_{\text{Opt}}^{\text{LB,Om}}$ versus \bar{P}_{av} for $m_{\text{SR}}^* = m_{\text{PU}}^* = 1$ and (a) $M = 8$, (b) $M = 12$.

To explore the effect of changes in PU orientation, Figs. 2.9a and 2.9b illustrate $C_{\text{Opt}}^{\text{LB}}$ and $C_{\text{Opt}}^{\text{LB,Om}}$ versus \bar{P}_{av} for $M = 8$ when $m_{\text{PU}}^* = 2$ and $m_{\text{PU}}^* = 3$, respectively (with fixed $m_{\text{SR}}^* = 1$). Comparing Figs. 2.8a, 2.9a, 2.9b we observe that as m_{PU}^* becomes further away from m_{SR}^* , the imposed interference on PU from SU_{tx} decreases and SU_{tx} can transmit at a higher transmit power level, leading to an increase in $C_{\text{Opt}}^{\text{LB}}$. Note that $C_{\text{Opt}}^{\text{LB,Om}}$ in Figs. 2.8a, 2.8b, 2.9a, 2.9b are the same. Let $\overline{C_{\text{Opt}}^{\text{LB}}}$ denote $C_{\text{Opt}}^{\text{LB}}$ that is averaged over all possible ϕ_{SR}^* and ϕ_{PU}^* . Fig. 2.10a plots $\overline{C_{\text{Opt}}^{\text{LB}}}$ and $C_{\text{Opt}}^{\text{LB,Om}}$ versus \bar{P}_{av} for $n_b = 2, 3, 4, \infty$. Clearly, our CR system with the ESPAR antenna at SU_{tx} yields a higher capacity on average, compared to the CR system with the omni-directional antenna at SU_{tx} .

To quantify the capacity improvement provided with the ESPAR antenna, we define the ratio $\Lambda = \overline{C_{\text{Opt}}^{\text{LB}}} / C_{\text{Opt}}^{\text{LB,Om}}$. Fig. 2.10b shows Λ versus \bar{P}_{av} for $\bar{I}_{\text{av}} = -6, -2, 2$ dB and $n_b = \infty$. First, we consider how Λ behaves as \bar{P}_{av} increases, for a given \bar{I}_{av} value. Fig. 2.10b shows that, as \bar{P}_{av} increases from zero to a certain value, Λ decreases. As \bar{P}_{av} increases beyond that certain value, Λ increases, however, it becomes constant after \bar{P}_{av} reaches a certain point. For instance, given $\bar{I}_{\text{av}} = -6$ dB, Λ decreases from 2.9 to 1.65, as \bar{P}_{av} increases from zero to 15 dB, it increases from 1.65 to 2.22, as \bar{P}_{av} increases from 15 dB to 27 dB, and it becomes constant afterward. The reason for this behavior is that, when $\bar{P}_{\text{av}} \leq 15$ dB, the ATPC in (2.9) is dominant for both ESPAR and omni-directional antennas. For $15 \text{ dB} \leq \bar{P}_{\text{av}} \leq 27$ dB, the ATPC is dominant for the ESPAR antenna and the AIC in (2.33) is dominant for the omni-directional antenna. For $\bar{P}_{\text{av}} \geq 27$ dB, the AIC is dominant for both ESPAR and omni-directional antennas. Next, we

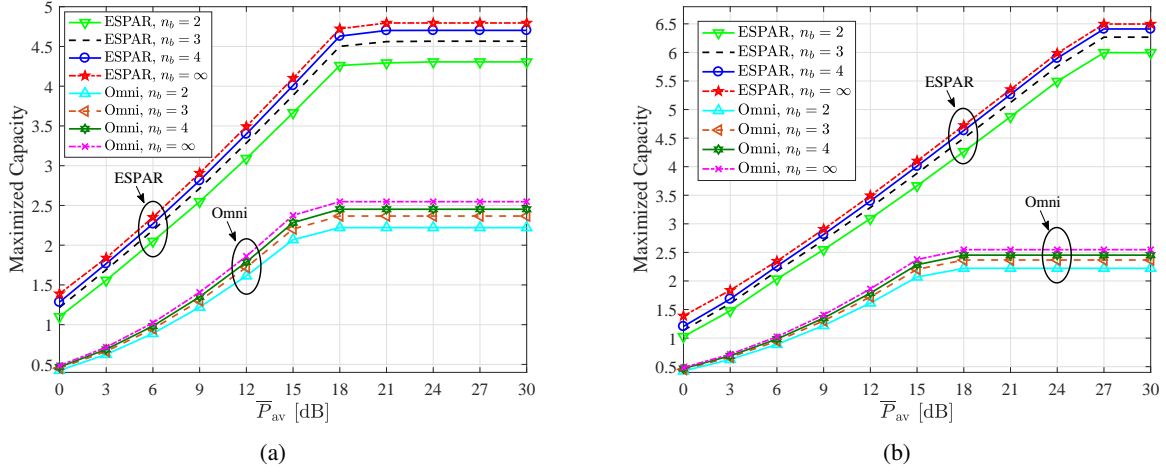


Figure 2.9: $C_{\text{Opt}}^{\text{LB}}$ and $C_{\text{Opt}}^{\text{LB,Om}}$ versus \bar{P}_{av} for $M=8$, $m_{\text{SR}}^*=1$ and (a) $m_{\text{PU}}^*=2$, (b) $m_{\text{PU}}^*=3$.

examine how Λ behaves as \bar{I}_{av} decreases, for a given \bar{P}_{av} value. Fig. 2.10b shows that, for $\bar{P}_{\text{av}} \leq 15$ dB Λ does not vary much as \bar{I}_{av} decreases, since the ATPC is dominant. However, this behavior changes as \bar{P}_{av} increases beyond 15 dB, where we note Λ increases as \bar{I}_{av} decreases. Overall, we observe that the ESPAR antenna can provide a high capacity improvement (Λ varies between 1.4 and 2.9 in Fig. 2.10b), compared with the omni-directional antenna, and the capacity improvement changes as \bar{P}_{av} and \bar{I}_{av} vary.

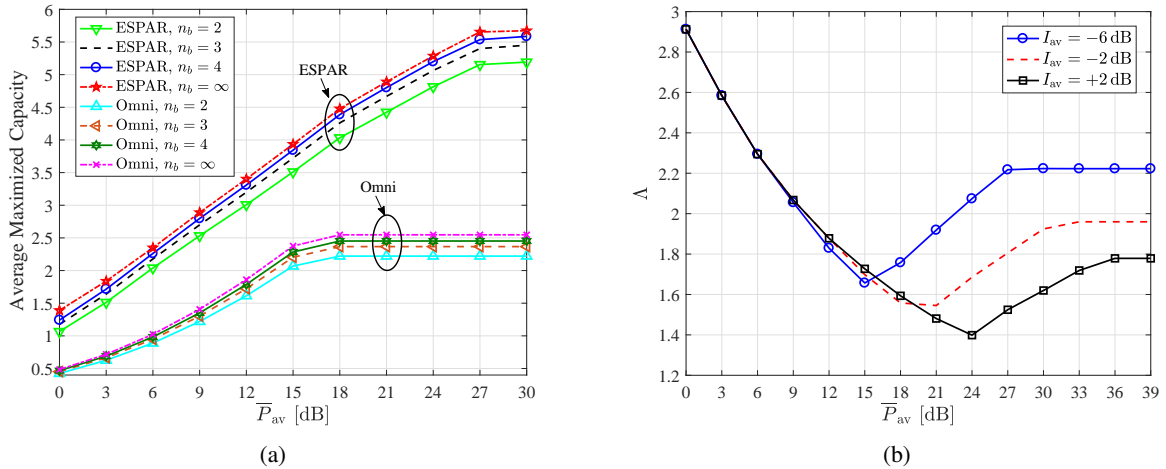


Figure 2.10: (a) $\overline{C_{\text{Opt}}^{\text{LB}}}$ and $C_{\text{Opt}}^{\text{LB,Om}}$ versus \bar{P}_{av} , (b) Λ versus \bar{P}_{av} .

Next, we explore the influence of parameter E_A defined in (2.15b). Fig. 2.11 plots $\overline{C_{\text{Opt}}^{\text{LB}}}$ and $C_{\text{Opt}}^{\text{LB,Om}}$ versus \overline{P}_{av} for $A_1 = 0.01$, $n_b = \infty$ and two choices of A_0 : $A_0 = 1$ (corresponding to $E_A = 0.127$) and $A_0 = 2$ (corresponding to $E_A = 0.245$). We observe that, for a given \overline{P}_{av} value, when we increase $A_0 = 1$ to $A_0 = 2$, the capacity enhancement for the ESPAR antenna is higher than that of the omni-directional antenna. To explain this observation, let $L = A_0/A_1$ denote the ESPAR beampattern attenuation in side-lobe with respect to its maximum value (main-lobe). Increasing L positively affects $\overline{C_{\text{Opt}}^{\text{LB}}}$ in two ways. First, the ESPAR antenna can reduce the imposed interference on PU more effectively, and hence SU_{tx} can transmit at higher power levels, without violating the AIC. Second, $\text{SU}_{\text{tx}}\text{-SU}_{\text{rx}}$ link becomes a stronger link for data communication. Increasing L , however, affects $C_{\text{Opt}}^{\text{LB,Om}}$ differently. We note that, although increasing L renders $\text{SU}_{\text{tx}}\text{-SU}_{\text{rx}}$ link a stronger link for data communication (positive impact), it increases the imposed interference on PU (negative impact), and hence SU_{tx} is enforced to transmit at lower power levels to satisfy the AIC.

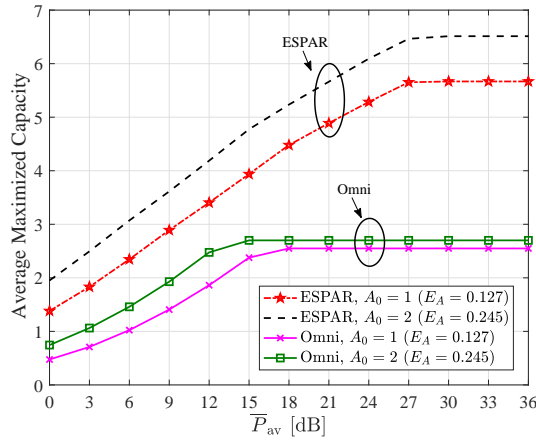


Figure 2.11: $\overline{C_{\text{Opt}}^{\text{LB}}}$ and $C_{\text{Opt}}^{\text{LB,Om}}$ versus \overline{P}_{av} .

Let $\overline{P}_{\text{out}}$ and \overline{P}_e denote P_{out} and P_e that are averaged over all possible ϕ_{SR}^* and ϕ_{PU}^* , respectively. For comparison, we also include the outage and symbol error probabilities $P_{\text{out}}^{\text{Om}}$ and P_e^{Om} corresponding to the CR system that its SU_{tx} has an omni-directional antenna. Fig. 2.12a illustrates $\overline{P}_{\text{out}}$ and $P_{\text{out}}^{\text{Om}}$ versus \overline{P}_{av} . We observe that given an n_b value, both outage and symbol error probabilities decrease as \overline{P}_{av} increases. However, they remain constant as \overline{P}_{av} increases beyond a certain point (they reach error floors). These behaviors can be explained as the following. For low \overline{P}_{av} , the ATPC in (2.9) is dominant and $\overline{P}_{\text{out}}$ and \overline{P}_e decrease as \overline{P}_{av} increases, since SU_{tx} can transmit at higher power levels. On the other hand, for high \overline{P}_{av} , the AIC in (2.33) is dominant and SU_{tx} cannot increase its transmit power level, regardless of how high \overline{P}_{av} becomes. As a result, $\overline{P}_{\text{out}}$ and \overline{P}_e remain constant. Compared

with the ESPAR antenna, the omni-directional antenna imposes a larger interference on PU. Thus, the AIC for the omni-directional antenna becomes active at a smaller \bar{P}_{av} value, compared with the ESPAR antenna. As a result both outage and symbol error probabilities reach error floors at smaller \bar{P}_{av} values, compared with the ESPAR antenna. Also, we note that as n_b increases \bar{P}_{out} decreases. Fig. 2.12b plots \bar{P}_e and P_e^{Om} versus \bar{P}_{av} . Similar observations to those of Fig. 2.12a can be made here. In a nutshell, Figs. 2.12a and 2.12b show that our proposed CR system yields lower outage and symbol error probabilities, compared with the CR system that its SU_{tx} has an omni-directional antenna.

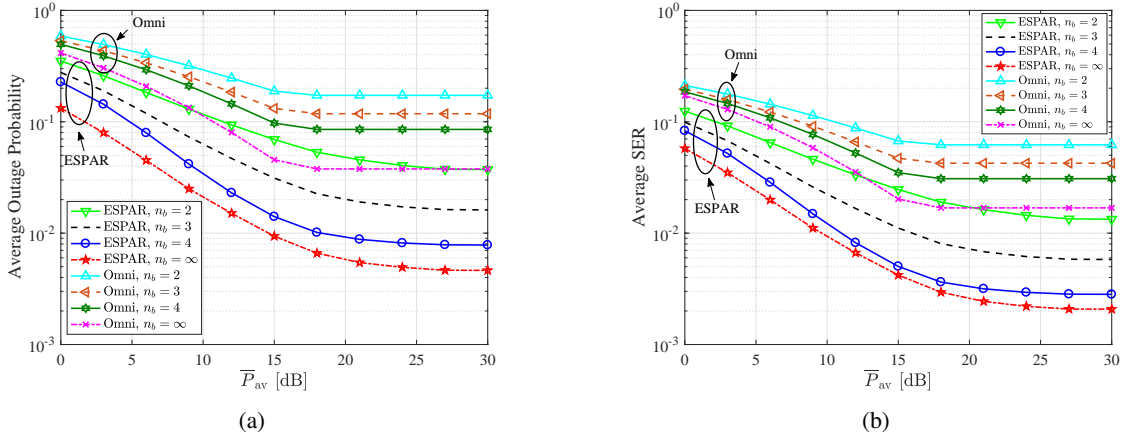


Figure 2.12: (a) \bar{P}_{out} and P_{out}^{Om} versus \bar{P}_{av} , (b) \bar{P}_e and P_e^{Om} versus \bar{P}_{av} .

2.6 Conclusions

We proposed a holistic system design for integrated sector-based spectrum sensing and sector-based data communication for an opportunistic CR system consisting of a PU, SU_{tx} , and SU_{rx} , where SU_{tx} is equipped with an ESPAR antenna that has M parasitic elements, and there is an error-free bandwidth limited feedback channel from SU_{rx} to SU_{tx} . We formulated a constrained optimization problem, where the ergodic capacity for SU_{tx} - SU_{rx} link is maximized, subject to ATPC and AIC, and the optimization variables are spectrum sensing duration, quantization thresholds at SU_{rx} , and discrete power levels at SU_{tx} . Our problem formulation takes into consideration the effect of imperfect spectrum sensing, the error in determining the true orientation of PU, the error in selecting the strongest channel for data communication, and the impact of channel gain quantization. We developed an iterative suboptimal algorithm

with a low computational complexity, based on the BCD algorithm, that finds a unique and locally optimal solution for the constrained problem. In addition, we derived closed form expressions for outage and symbol error probabilities of our opportunistic CR system. We corroborated our mathematical analyses with extensive simulations. Our numerical results demonstrate that our proposed CR system with the ESPAR antenna at SU_{tx} yields a significantly higher capacity, a lower outage probability, and a lower symbol error probability, compared with a CR system that its SU_{tx} has an omni-directional antenna. The capacity improvement varies as the ATPC and AIC change. For instance, at $\bar{P}_{av} = 12$ dB, $\bar{I}_{av} = -6$ dB, the capacity of our CR system is 1.83 times larger than the capacity of the CR system with omni-directional antenna. Furthermore, we showed that with only a small number of feedback bits the capacity of our CR system approaches to its baseline, which assumes the full knowledge of unquantized channel gain.

CHAPTER 3: ACHIEVABLE RATES OF OPPORTUNISTIC COGNITIVE RADIO SYSTEMS USING RECONFIGURABLE ANTENNAS WITH IMPERFECT SENSING AND CHANNEL ESTIMATION¹

In this chapter, we consider the combined effects of spectrum sensing error and imperfect CSI of SU_{tx} - SU_{rx} link on the achievable rates of an opportunistic CR system with a RA at SU_{tx} . In our opportunistic CR system, SU_{tx} relies on the beam steering capability of RA to detect the direction of PU's activity and also to select the strongest beam for data transmission to SU_{rx} . We assume SU_{tx} sends training symbols to enable channel estimation at SU_{rx} , and employs Gaussian input signaling for transmitting its data symbols to SU_{rx} . Also, SU_{rx} shares its imperfect CSI of SU_{tx} - SU_{rx} link with SU_{tx} through an error-free low-rate feedback channel.

Assuming that there are ATPC and AIC, we provide answers to the following research questions: How does spectrum sensing error affect accuracy of detecting the direction of PU's activity, estimating SU_{tx} - SU_{rx} channel, and selecting the strongest beam for data transmission? How do training symbol transmission and beam detection error (error in obtaining the true direction of PU's activity) affect interference imposed on PU? How do the combined effects of spectrum sensing error and channel estimation error, as well as beam detection error and beam selection error (error in finding the true strongest beam for data communication to SU_{rx}) impact the achievable rates for reliable communication over SU_{tx} - SU_{rx} link? How do the trade-offs between spatial spectrum sensing time, channel training time, data transmission time, training and data symbol transmission powers affect the achievable rates? How can we utilize these trade-offs to design transmit power control strategies, such that the achievable rates subject to ATPC and AIC are maximized?

¹© 2021 IEEE. Part of this chapter is reprinted, with permission, from [5].

3.1 System Model

3.1.1 Structure of a RA

We consider a RA which can generate M *beampatterns* and these beampatterns cover the angular plane from ϕ_1 to ϕ_2 , i.e., the angular space from ϕ_1 to ϕ_2 is divided into M spatial *sectors* or beams². One can extend this angular space to cover the entire azimuth plane. The beampattern corresponding to m -th beam achieves its maximum at angle $\kappa_m = \frac{2\pi(m-1)}{M}$ for $m = 1, \dots, M$. Fig. 3.1 shows the beampatterns of a RA with $M = 7$ beams. It is noteworthy that the RA can also reconfigure itself to generate an omni-directional pattern. To mathematically model the radiation pattern of beams, we adopt the Gaussian pattern in x - y azimuth plane in terms of angle ϕ given by [4]

$$p(\phi) = A_1 + A_0 e^{-B\left(\frac{\mathcal{M}(\phi)}{\phi_{3\text{dB}}}\right)^2}, \quad \mathcal{M}(\phi) = \text{mod}_{2\pi}(\phi + \pi) - \pi, \quad (3.1)$$

where $\text{mod}_{2\pi}(\phi)$ denotes the remainder of $\frac{\phi}{2\pi}$, $B = \ln(2)$, $\phi_{3\text{dB}}$ is the 3-dB beamwidth, A_1 and A_0 are two constant antenna parameters. The radiation pattern of m -th beam at angle ϕ is

$$p_m(\phi) = p(\phi - \kappa_m), \quad \text{for } m = 1, \dots, M. \quad (3.2)$$

In this chapter, we discuss the received or transmitted signal at m -th beam of SU_{tx} . This implies that, during the signal reception or transmission, the SU_{tx} 's antenna parameters are set and tuned such that the beampattern corresponding to m -th beam is generated. Given the antenna design, we focus on how the sector-based structure of this RA can be exploited to enhance the system performance of our opportunistic CR system, in which SU_{tx} optimizes its sector-based data communication to SU_{rx} according to the results of its sector-based spectrum sensing.

3.1.2 Description of Our Opportunistic CR System

Our opportunistic CR system model is illustrated in Fig. 3.1, consisting of a PU and a pair of SU_{tx} and SU_{rx} . We note that PU in our system model can be a primary transmitter or receiver. We assume when PU is active it is engaged in a bidirectional communication with another PU, which is located far from SU_{tx} and hence its activity does not impact our analysis. We assume SU_{tx} is equipped with an M -beam RA (for spatial spectrum sensing, channel

²Throughout this chapter, "sector" and "beam" are used interchangeably.

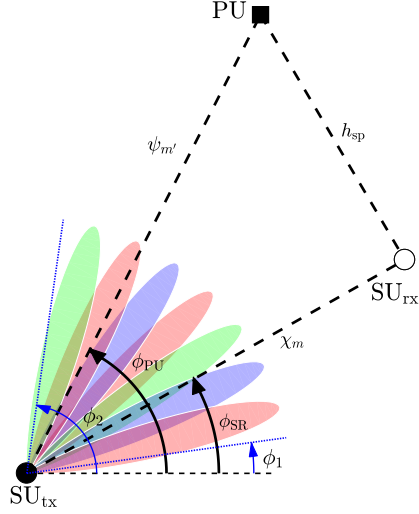


Figure 3.1: Our opportunistic CR system with an M -beam RA at SU_{tx} and omni-directional antennas at SU_{rx} and PU.

training and data transmission) with the capability of choosing one out of M sectors for its data transmission to SU_{rx} , while SU_{rx} and PU use omni-directional antennas. We assume there is an error-free low-rate feedback channel³ from SU_{rx} to SU_{tx} , to enable SU_{tx} select the best sector for its data transmission to SU_{rx} , and to adapt its transmit power according to the SU_{tx} – SU_{rx} channel information. The direction (orientation) of PU and SU_{rx} with respect to SU_{tx} are denoted by angles ϕ_{PU} , and ϕ_{SR} , respectively, where $\phi_{SR}, \phi_{PU} \in (\phi_1, \phi_2)$. Clearly, in our problem SU_{tx} does not know these directions or angles (otherwise, the beam selection at SU_{tx} for data transmission would become trivial).

Let h , h_{ss} , h_{sp} denote the fading coefficients of channels between SU_{tx} and PU, SU_{tx} and SU_{rx} , and SU_{rx} and PU, respectively, when the RA of SU_{tx} is in omni-directional mode. We model these fading coefficients as independent zero mean circularly symmetric complex Gaussian random variables. Equivalently, $g = |h|^2$, $g_{ss} = |h_{ss}|^2$ and $g_{sp} = |h_{sp}|^2$ are independent exponentially distributed random variables with mean γ , γ_{ss} and γ_{sp} , respectively⁴. In our problem we assume that SUs and PU cannot cooperate, and hence SUs cannot estimate g and g_{sp} . However, SU_{tx} knows the channel statistics, i.e., the mean values γ and γ_{sp} . Let $\psi_{m'}$ and χ_m denote the fading coefficients of channel between m' -th sector of SU_{tx} and PU, and between m -th sector of SU_{tx} and SU_{rx} , respectively, when the RA of SU_{tx} is in directional mode. Using the radiation pattern expression in (3.2) we can relate $\psi_{m'}$ to h and χ_m to h_{ss} as $\psi_{m'} = h\sqrt{p_{m'}(\phi_{PU})}$, $\chi_m = h_{ss}\sqrt{p_m(\phi_{SR})}$. We assume the channel gain $\nu_m = |\chi_m|^2$ is an exponentially

³Given a low rate feedback, the error-free feedback channel is a reasonable assumption [78].

⁴We note that the distances between users are included in the small scale fading model [115], i.e., the mean values $\gamma, \gamma_{ss}, \gamma_{sp}$ encompass distance-dependent path loss.

distributed random variable with mean α_m , and SU_{tx} knows α_m , for all m [4, 102]. For the readers' convenience, we have collected the most commonly used symbols in Table 3.1.

Table 3.1: Most commonly used symbols.

Symbol	Description
M	Number of beams
N_{se}	Number of samples used for <i>spatial spectrum sensing</i>
N_t	Number of samples used for <i>channel training</i>
P_{tr}	Power of training symbols
$\psi_{m'}$	Fading coefficient of channel between m' -th beam of SU_{tx} and PU
$\chi_m, \hat{\chi}_m, \tilde{\chi}_m$	Fading coefficient of channel between m -th beam of SU_{tx} and SU_{rx} , LMMSE channel estimate, and its corresponding estimation error
$\alpha_m, \hat{\alpha}_m, \tilde{\alpha}_m$	Variances of $\chi_m, \hat{\chi}_m, \tilde{\chi}_m$
m_{PU}^*, m_{SR}^*	Indices of selected beam for PU and SU_{rx}
\hat{d}^*	Channel gain of selected beam for data transmission from SU_{tx} to SU_{rx}

Suppose, SUs employ a frame with a fixed duration of T_f seconds, depicted in Fig. 3.2. We assume the SU_{tx} – SU_{rx} channel remains constant over the frame duration. SU_{tx} first senses the spectrum and monitors PU's activity. We refer to this period as *spatial spectrum sensing* phase with a variable duration of $T_{se} = MN_{se}T_s$ seconds, where T_s is the sampling period and N_{se} is the number of collected samples during this phase per beam. Suppose \mathcal{H}_1 and \mathcal{H}_0 represent the binary hypotheses of PU being active and inactive, respectively, with prior probabilities $\Pr\{\mathcal{H}_1\} = \pi_1$ and $\Pr\{\mathcal{H}_0\} = \pi_0$. SU_{tx} applies a binary detection rule to decide whether or not PU is active. The details of the binary detector are presented in Section 3.2.1. While being in this phase, SU_{tx} determines the beam corresponding to the orientation of PU based on the received signal energy as we describe in Section 3.2.2.

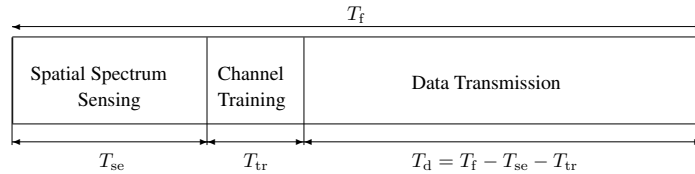


Figure 3.2: The structure of frame employed by SU_{tx} .

Depending on the outcome of spectrum sensing, SU_{tx} stays in spatial spectrum sensing phase or enters the next phase, which we refer to as *channel training phase* with a variable duration of $T_{tr} = MN_tT_s$ seconds. In this phase, SU_{tx} sends N_t training symbols with fixed symbol power P_{tr} per beam to enable channel estimation at SU_{rx} , as we

explain in Section 3.3.1. Based on the results of channel estimation for all beams, SU_{rx} selects the beam with the largest SU_{tx} - SU_{rx} fading gain, as we describe in Section 3.3.2. This information as well as the corresponding beam index are shared with SU_{tx} via the feedback channel. Next, SU_{tx} enters *data transmission phase* with a variable duration of $T_d = T_f - T_{se} - T_{tr}$ seconds. During this phase, SU_{tx} sends $N_d = T_d/T_s$ Gaussian data symbols with adaptive symbol power P to SU_{rx} over the selected strongest beam. SU_{tx} adapts P aiming at maximizing the achievable rates, subject to ATPC and AIC as we describe in Section 3.4. In the following sections, we describe how SU_{tx} operates during spatial spectrum sensing phase, channel training phase, and data transmission phase.

3.2 Spatial Spectrum Sensing Phase

3.2.1 Eigenvalue-Based Detector for Spatial Spectrum Sensing

Let $\hat{\mathcal{H}}_1$ and $\hat{\mathcal{H}}_0$ denote the detector outcome, i.e., the detector finds PU active (spectrum is sensed busy and occupied) and inactive (spectrum is sensed idle and unoccupied and thus can be used by SU_{tx} for data transmission), respectively. Suppose when PU is active, it transmits signal $s(t)$ with power P_p . Let $y_m(n)$ denote the discrete-time representation of received signal at m -th sector of SU_{tx} at time instant $t = nT_s$. We model PU's transmitted signal $s(n)$ as a zero-mean complex Gaussian random variable with variance P_p and we assume SU_{tx} knows P_p . Since SU_{tx} collects N_{se} samples per beam during spatial spectrum sensing phase, the hypothesis testing problem at discrete time instant n for m -th sector is

$$\begin{aligned} \mathcal{H}_0: \quad & y_m(n) = w_m(n), \\ \mathcal{H}_1: \quad & y_m(n) = \psi_m(n)s(n) + w_m(n). \end{aligned} \tag{3.3}$$

The term $w_m(n)$ is the additive noise at m -th sector of SU_{tx} antenna and is modeled as $w_m(n) \sim \mathcal{CN}(0, \sigma_w^2)$. We assume that $\psi_m(n)$, $s(n)$ and $w_m(n)$ are mutually independent random variables. Since SU_{tx} takes samples of the received signal for different sectors sequentially (in different time instants), $\psi_m(n)$ and $w_m(n)$ are independent and thus uncorrelated both in time and space (sector) domains. Under hypothesis \mathcal{H}_1 , given ψ_m , we have $y_m(n) \sim \mathcal{CN}(0, \sigma_m^2 + \sigma_w^2)$ where $\sigma_m^2 = |\psi_m|^2 P_p$. Under hypothesis \mathcal{H}_0 , we have $y_m(n) \sim \mathcal{CN}(0, \sigma_w^2)$.

Our proposed binary detector uses all the collected samples from M sectors. To facilitate the signal processing needed for the binary detection, we define an $M \times N_{se}$ sample matrix $\mathbf{Z} = [z_1, \dots, z_{N_{se}}]$, where the first row of \mathbf{Z} is the N_{se} samples collected from the first sector, the second row of \mathbf{Z} is the N_{se} samples collected from the second sector, and

so forth. Given our assumptions, the columns of \mathbf{Z} are orthogonal under both hypotheses, that is

$$\mathbb{E}\left\{z_i z_j^H | \mathcal{H}_0\right\} = \mathbf{0}, \quad \mathbb{E}\left\{z_i z_j^H | \mathcal{H}_1\right\} = \mathbf{0}, \quad \text{for } i \neq j, \quad i, j = 1, \dots, N_{\text{se}} \quad (3.4)$$

where $\mathbb{E}\{\cdot\}$ is the statistical expectation operator and have the below covariance matrices

$$\mathbf{\Gamma}_0 = \mathbb{E}\left\{z_j z_j^H | \mathcal{H}_0\right\} = \sigma_w^2 \mathbf{I}_M, \quad \mathbf{\Gamma}_1 = \mathbb{E}\left\{z_j z_j^H | \mathcal{H}_1, \boldsymbol{\psi}\right\} = P_p \boldsymbol{\psi} \boldsymbol{\psi}^H + \sigma_w^2 \mathbf{I}_M, \quad (3.5)$$

where vector $\boldsymbol{\psi} = [\psi_1, \psi_2, \dots, \psi_M]^T$. Therefore the sample covariance matrix $\widehat{\mathbf{R}}$ becomes $\widehat{\mathbf{R}} = \frac{1}{N_{\text{se}}} \mathbf{Z} \mathbf{Z}^H$. Let $f(\mathbf{Z} | \mathcal{H}_0)$ and $f(\mathbf{Z} | \mathcal{H}_1, \boldsymbol{\psi})$ denote the PDF of \mathbf{Z} under \mathcal{H}_0 and \mathcal{H}_1 (given $\boldsymbol{\psi}$), respectively. These PDF expressions are

$$f(\mathbf{Z} | \mathcal{H}_0) = \frac{1}{(\pi \sigma_w^2)^{N_{\text{eq}}}} \exp\left\{\frac{\text{tr}(\mathbf{Z} \mathbf{Z}^H)}{-\sigma_w^2}\right\}, \quad f(\mathbf{Z} | \mathcal{H}_1, \boldsymbol{\psi}) = \frac{1}{\pi^{N_{\text{eq}}} \det(\mathbf{\Gamma}_1)^{N_{\text{se}}}} \exp\left\{\frac{\text{tr}(\mathbf{\Gamma}_1^{-1} \mathbf{Z} \mathbf{Z}^H)}{-\sigma_w^2}\right\}, \quad (3.6)$$

where $N_{\text{eq}} = M N_{\text{se}}$. The optimal detector would compare the Logarithm of Likelihood Ratio (LLR) against a threshold η_0 to detect the PU's activity as below

$$\text{LLR} = \ln \frac{f(\mathbf{Z} | \mathcal{H}_1, \boldsymbol{\psi})}{f(\mathbf{Z} | \mathcal{H}_0)} \underset{\widehat{\mathcal{H}}_0}{\overset{\widehat{\mathcal{H}}_1}{\geq}} \eta_0. \quad (3.7)$$

In the absence of the knowledge of the fading coefficients vector $\boldsymbol{\psi}$, SU_{tx} obtains the GLRT [26–29, 41] which uses the Maximum Likelihood (ML) estimate of $\boldsymbol{\psi}$ under \mathcal{H}_1 . Let $\mathcal{L}_1(\mathbf{Z}) = \ln f(\mathbf{Z} | \mathcal{H}_1, \boldsymbol{\psi})$. To find the maximum of $\mathcal{L}_1(\mathbf{Z})$ with respect to $\boldsymbol{\psi}$, we take the derivative of $\mathcal{L}_1(\mathbf{Z})$ with respect to $\boldsymbol{\psi}$ and solve $\frac{\partial}{\partial \boldsymbol{\psi}} \mathcal{L}_1(\mathbf{Z}) = \mathbf{0}$ for $\boldsymbol{\psi}$. The obtained solution is the ML estimate of $\boldsymbol{\psi}$. Substituting this solution into (3.7) and after some mathematical manipulation, we reach the following decision rule $T = \frac{\lambda_{\text{max}}}{\sigma_w^2} \underset{\widehat{\mathcal{H}}_0}{\geq} \widehat{\mathcal{H}}_1 \eta$ [26], where T is the test statistics, λ_{max} is the maximum eigenvalue of $\widehat{\mathbf{R}}$, and η is the threshold. For large N_{se} , T under \mathcal{H}_0 is distributed as Tracy-Widom distribution of order 2 [26, Lemma 1] and the probability of false alarm $P_{\text{fa}} = \Pr(\widehat{\mathcal{H}}_1 | \mathcal{H}_0) = \Pr(T > \eta | \mathcal{H}_0)$ is

$$P_{\text{fa}} = 1 - F_{\text{TW2}}\left(\frac{\eta - \theta_{\text{sen}}}{\sigma_{\text{sen}}}\right), \quad (3.8)$$

where $F_{\text{TW}2}(\cdot)$ is the CDF of Tracy-Widom distribution of order 2 and θ_{sen} and σ_{sen} in (3.8) are given below

$$\theta_{\text{sen}} = \left(1 + \sqrt{\frac{M}{N_{\text{se}}}}\right)^2, \quad \sigma_{\text{sen}} = \frac{1}{\sqrt{N_{\text{se}}}} \left(1 + \sqrt{\frac{M}{N_{\text{se}}}}\right) \left(\frac{1}{\sqrt{N_{\text{se}}}} + \frac{1}{\sqrt{M}}\right)^{\frac{1}{3}}. \quad (3.9)$$

For large N_{se} , T under \mathcal{H}_1 is Gaussian distributed [26, Lemma 2] and the probability of detection $P_d = \Pr(\widehat{\mathcal{H}}_1|\mathcal{H}_1) = \Pr(T > \eta|\mathcal{H}_1)$ is [26, 29]

$$P_d = Q\left(\frac{\eta\sqrt{N_{\text{se}}}}{1+\delta_{\text{sen}}} - \frac{M-1}{\delta_{\text{sen}}\sqrt{N_{\text{se}}}} - \sqrt{N_{\text{se}}}\right), \quad (3.10)$$

where $\delta_{\text{sen}} = \frac{P_p\|\psi\|^2}{\sigma_w^2}$. The average detection probability \bar{P}_d can be computed by averaging (3.10) over vector ψ , $\bar{P}_d = \mathbb{E}_\psi\{P_d\}$. For a given \bar{P}_d , we can numerically find η and obtain \bar{P}_{fa} using (3.8). We can also compute the probabilities of events $\widehat{\mathcal{H}}_0$ and $\widehat{\mathcal{H}}_1$ as $\hat{\pi}_0 = \Pr\{\widehat{\mathcal{H}}_0\} = \beta_0 + \beta_1$ and $\hat{\pi}_1 = \Pr\{\widehat{\mathcal{H}}_1\} = 1 - \hat{\pi}_0$, respectively, where

$$\beta_0 = \Pr\{\mathcal{H}_0, \widehat{\mathcal{H}}_0\} = \pi_0(1 - \bar{P}_{\text{fa}}), \quad \beta_1 = \Pr\{\mathcal{H}_1, \widehat{\mathcal{H}}_0\} = \pi_1(1 - \bar{P}_d). \quad (3.11)$$

3.2.2 Determining the Beam Corresponding to PU Direction

During spatial spectrum sensing phase when the spectrum is sensed busy, SU_{tx} determines the beam corresponding to the direction of PU based on the received signal energy. Let ε_m be the energy of received signal at m -th beam. We have

$$\varepsilon_m = \frac{1}{N_{\text{se}}} \sum_{n=1+(m-1)N_{\text{se}}}^{mN_{\text{se}}} \left|y_m(n)\right|^2. \quad (3.12)$$

SU_{tx} determines the beam with the largest amount of received energy $m_{\text{PU}}^* = \arg \max\{\varepsilon_m\}$ among all beams. For large N_{se} , we invoke CLT to approximate ε_m 's as Gaussian random variables under both hypotheses. Thus, under \mathcal{H}_0 we approximate ε_m as a Gaussian with distribution $\varepsilon_m \sim \mathcal{N}(\sigma_w^2, \sigma_w^4/N_{\text{se}})$. Similarly, under \mathcal{H}_1 , given ϕ_{PU} we approximate ε_m as another Gaussian with distribution $\varepsilon_m \sim \mathcal{N}(\varrho_m, \sigma_{\varepsilon_m|\mathcal{H}_1}^2)$, where the mean $\varrho_m = \gamma P_p p_m(\phi_{\text{PU}}) + \sigma_w^2$, and the variance $\sigma_{\varepsilon_m|\mathcal{H}_1}^2$ is given below

$$\sigma_{\varepsilon_m|\mathcal{H}_1}^2 = \frac{1}{N_{\text{se}}} \left[\sigma_w^4 + 3P_p^2\gamma^2 p_m^2(\phi_{\text{PU}}) + 2\sigma_w^2 P_p \gamma p_m(\phi_{\text{PU}}) \right]. \quad (3.13)$$

We note that, there is a non-zero error probability when SU_{tx} determines the beam index m_{PU}^* , i.e., it is possible that m_{PU}^* is not the true beam index corresponding to PU direction.

Let $\bar{\Delta}_{i,m}$ represent the average error probability of finding the sector index corresponding to PU direction, i.e., the probability that $m_{\text{PU}}^* = i$ while the true PU direction lies in the angular domain of m -th sector, $\phi_{\text{PU}} \in \Phi_m = \left[\frac{2\pi(m-3/2)}{M}, \frac{2\pi(m-1/2)}{M} \right)$, for $i \neq m, i, m = 1, \dots, M$. To find $\bar{\Delta}_{i,m}$ we start with finding $\Delta_i = \Pr\{m_{\text{PU}}^* = i | \phi_{\text{PU}}, \hat{\mathcal{H}}_1\}$, which is the probability that the index of selected sector is i , given ϕ_{PU} and $\hat{\mathcal{H}}_1$ (the binary detector in Section 3.2.1 finds PU active). Note that under both hypotheses, ε_m 's are independent. Also, under \mathcal{H}_0 , ε_m 's are identically distributed. Therefore, we have

$$\begin{aligned} \Delta_i &= \Pr \left\{ \varepsilon_i > \varepsilon_m \mid \phi_{\text{PU}}, \hat{\mathcal{H}}_1 \right\} \\ &= \varsigma_1 \int_0^\infty f_{\varepsilon_i | \mathcal{H}_1}(y | \phi_{\text{PU}}) \prod_{\substack{m=1 \\ m \neq i}}^M F_{\varepsilon_m | \mathcal{H}_1}(y | \phi_{\text{PU}}) dy + \varsigma_0 \int_0^\infty f_{\varepsilon_m | \mathcal{H}_0}(y) F_{\varepsilon_m | \mathcal{H}_0}^{M-1}(y) dy \end{aligned} \quad (3.14)$$

where $f_{\varepsilon_m | \mathcal{H}_\ell}(x)$ and $F_{\varepsilon_m | \mathcal{H}_\ell}(x)$ are the PDF and CDF expressions of ε_m under $\mathcal{H}_\ell, \ell = 0, 1$ and

$$\varsigma_0 = \Pr\{\mathcal{H}_0 | \hat{\mathcal{H}}_1\} = \frac{\pi_0 \bar{P}_{\text{fa}}}{\hat{\pi}_1}, \quad \varsigma_1 = \Pr\{\mathcal{H}_1 | \hat{\mathcal{H}}_1\} = \frac{\pi_1 \bar{P}_{\text{d}}}{\hat{\pi}_1}. \quad (3.15)$$

Using Δ_i , we find $\bar{\Delta}_{i,m}$ as the following

$$\bar{\Delta}_{i,m} = \int_{\phi_{\text{PU}} \in \Phi_m} \Delta_i \Pr\left\{ \phi_{\text{PU}} \in \Phi_m \right\} d\phi_{\text{PU}}. \quad (3.16)$$

Note that $\bar{\Delta}_{i,i}$ is the probability of selecting the correct beam and $\bar{\Delta}_{i,m}$ for $i \neq m$ is the probability of selecting the incorrect beam, leading to error probability in beam selection. The average error probability $\bar{\Delta}_{1,m}$ versus the index beam m is shown in Figs. 3.3a and 3.3b for $\text{SNR}_{\text{PU}} = \gamma P_{\text{p}} / \sigma_{\text{w}}^2 = 0, -5$ dB. As expected, $\bar{\Delta}_{1,1}$ increases and $\bar{\Delta}_{1,m}, m \neq 1$ decreases as N_{se} increases.

3.3 Channel Training Phase

3.3.1 Channel Estimation at SU_{rx}

During this phase, SU_{tx} sends the training vector \mathbf{x}_t over all beams to enable channel estimation at SU_{rx} . Without loss of generality, we assume $\mathbf{x}_t = \sqrt{P_{\text{tr}}} \mathbf{1}$, where $\mathbf{1}$ is an $N_t \times 1$ all-ones vector and P_{tr} is given. Let $\mathbf{r}_m = [r_m(1), \dots, r_m(N_t)]^T$ denote the discrete-time representation of received training symbols at SU_{rx} from m -th sector

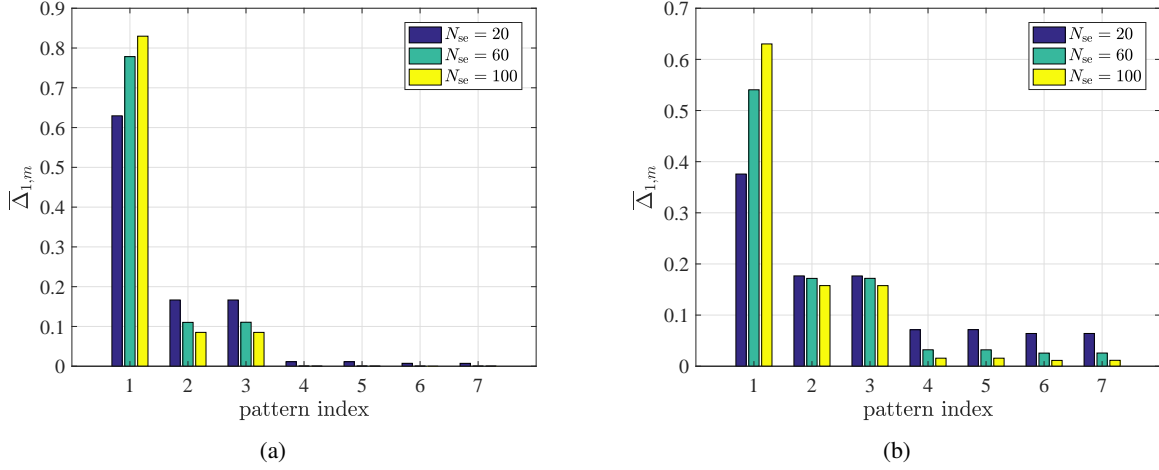


Figure 3.3: $\bar{\Delta}_{1,m}$ versus the index beam m for $\phi_{3\text{dB}} = 20^\circ$ (a) $\text{SNR}_{\text{PU}} = 0$ dB, (b) $\text{SNR}_{\text{PU}} = -5$ dB.

of SU_{tx} . We note that SU_{tx} enters this phase when the outcome of the binary detector in Section 3.2.1 is $\hat{\mathcal{H}}_0$. Due to error in spatial spectrum sensing, we need to differentiate the signal model for r_m under \mathcal{H}_0 and \mathcal{H}_1 . Assuming the fading coefficient χ_m is unchanged during the frame, we have

$$\begin{aligned} \mathcal{H}_0, \hat{\mathcal{H}}_0: r_m(n) &= \chi_m \sqrt{P_{\text{tr}}} + q_m(n), \\ \mathcal{H}_1, \hat{\mathcal{H}}_0: r_m(n) &= \chi_m \sqrt{P_{\text{tr}}} + h_{\text{sp}}(n) s(n) + q_m(n), \end{aligned} \quad (3.17)$$

where $q_m(n)$ is the additive noise at SU_{rx} antenna and is modeled as $q_m(n) \sim \mathcal{CN}(0, \sigma_q^2)$. The Linear Minimum Mean Square Error (LMMSE) estimation of fading coefficient χ_m when the spectrum sensing result is $\hat{\mathcal{H}}_0$ can be obtained as [117]

$$\hat{\chi}_m = C_{\chi_m \mathbf{r}_m} C_{\mathbf{r}_m}^{-1} \mathbf{r}_m, \quad (3.18a)$$

$$C_{\chi_m \mathbf{r}_m} = \mathbb{E}\{\chi_m \mathbf{r}_m^H | \hat{\mathcal{H}}_0\} = \sqrt{P_{\text{tr}}} \alpha_m \mathbf{1}, \quad (3.18b)$$

$$C_{\mathbf{r}_m} = \mathbb{E}\left\{ \mathbf{r}_m \mathbf{r}_m^H | \hat{\mathcal{H}}_0 \right\} = \omega_0 \mathbb{E}\left\{ \mathbf{r}_m \mathbf{r}_m^H | \mathcal{H}_0, \hat{\mathcal{H}}_0 \right\} + \omega_1 \mathbb{E}\left\{ \mathbf{r}_m \mathbf{r}_m^H | \mathcal{H}_1, \hat{\mathcal{H}}_0 \right\}, \quad (3.18c)$$

where

$$\omega_0 = \Pr\{\mathcal{H}_0 | \hat{\mathcal{H}}_0\} = \frac{\pi_0(1 - \bar{P}_{\text{fa}})}{\hat{\pi}_0} = \frac{\beta_0}{\hat{\pi}_0}, \quad \omega_1 = \Pr\{\mathcal{H}_1 | \hat{\mathcal{H}}_0\} = \frac{\pi_1(1 - \bar{P}_{\text{d}})}{\hat{\pi}_0} = \frac{\beta_1}{\hat{\pi}_0}. \quad (3.19)$$

Finally, the LMMSE estimation of χ_m when the spectrum sensing result is $\hat{\mathcal{H}}_0$, given in (3.18a), reduces to

$$\hat{\chi}_m = \frac{\alpha_m \sqrt{P_{\text{tr}}}}{\alpha_m P_{\text{tr}} N_t + \sigma_q^2 + \omega_1 \sigma_p^2} \sum_{n=1}^{N_t} r_m(n), \quad (3.20)$$

where $\sigma_p^2 = P_p \gamma_{\text{sp}}$. The estimation error is $\tilde{\chi}_m = \chi_m - \hat{\chi}_m$ where $\hat{\chi}_m$ and $\tilde{\chi}_m$ are orthogonal random variables [117], and $\hat{\chi}_m$ and $\tilde{\chi}_m$ are zero mean. Approximating $h_{\text{sp}}(n)s(n)$ as a zero-mean Gaussian random variable with variance σ_p^2 , we find that the estimate $\hat{\chi}_m$ is distributed as a Gaussian mixture random variable [19, 46]. Let $\hat{\alpha}_m$ and $\tilde{\alpha}_m$, represent the variances of $\hat{\chi}_m$ and $\tilde{\chi}_m$, respectively. Also, Let $\hat{\alpha}_m^0$ and $\hat{\alpha}_m^1$ represent the variances of $\hat{\chi}_m$ under \mathcal{H}_0 and \mathcal{H}_1 , respectively. We have

$$\hat{\alpha}_m^0 = \text{VAR}\{\hat{\chi}_m | \mathcal{H}_0, \hat{\mathcal{H}}_0\} = \frac{\alpha_m^2 P_{\text{tr}} N_t \left(\alpha_m P_{\text{tr}} N_t + \sigma_q^2 \right)}{\left(\alpha_m P_{\text{tr}} N_t + \sigma_q^2 + \omega_1 \sigma_p^2 \right)^2}, \quad (3.21a)$$

$$\hat{\alpha}_m^1 = \text{VAR}\{\hat{\chi}_m | \mathcal{H}_1, \hat{\mathcal{H}}_0\} = \frac{\alpha_m^2 P_{\text{tr}} N_t \left(\alpha_m P_{\text{tr}} N_t + \sigma_q^2 + \sigma_p^2 \right)}{\left(\alpha_m P_{\text{tr}} N_t + \sigma_q^2 + \omega_1 \sigma_p^2 \right)^2}. \quad (3.21b)$$

Therefore, $\hat{\alpha}_m = \omega_0 \hat{\alpha}_m^0 + \omega_1 \hat{\alpha}_m^1$. Also, let $\tilde{\alpha}_m^0$ and $\tilde{\alpha}_m^1$ indicate the variances of $\tilde{\chi}_m$ under \mathcal{H}_0 and \mathcal{H}_1 , respectively.

We have

$$\tilde{\alpha}_m^0 = \text{VAR}\{\tilde{\chi}_m | \mathcal{H}_0, \hat{\mathcal{H}}_0\} = \alpha_m - \hat{\alpha}_m^0, \quad \tilde{\alpha}_m^1 = \text{VAR}\{\tilde{\chi}_m | \mathcal{H}_1, \hat{\mathcal{H}}_0\} = \alpha_m - \hat{\alpha}_m^1. \quad (3.22)$$

Hence, $\tilde{\alpha}_m = \omega_0 \tilde{\alpha}_m^0 + \omega_1 \tilde{\alpha}_m^1$. For perfect spectrum sensing, we get $\omega_0 = 1$ and $\omega_1 = 0$ and $\hat{\chi}_m$ becomes Gaussian.

3.3.2 Determining the Beam Corresponding to SU_{rx} Direction

SU_{rx} finds $\hat{\chi}_m$ for all beams Consider the random variable $\hat{\nu}_m = |\hat{\chi}_m|^2$. Under hypothesis $\mathcal{H}_\ell, \ell = 0, 1$, given $\hat{\mathcal{H}}_0$, $\hat{\nu}_m$ is an exponential random variable with mean $\hat{\alpha}_m^\ell$ and PDF

$$f_{\hat{\nu}_m}^\ell(y) = \frac{1}{\hat{\alpha}_m^\ell} e^{-\frac{y}{\hat{\alpha}_m^\ell}}. \quad (3.23)$$

Hence, the PDF of $\hat{\nu}_m$ can be written as

$$f_{\hat{\nu}_m}(y) = \omega_0 f_{\hat{\nu}_m}^0(y) + \omega_1 f_{\hat{\nu}_m}^1(y). \quad (3.24)$$

SU_{rx} obtains $\hat{\nu}^* = \max\{\hat{\nu}_m\}$ among all beams and the corresponding beam index $m_{\text{SR}}^* = \arg \max\{\hat{\nu}_m\}$ and feeds back this information to SU_{tx}. Let $\Psi_i^\ell = \Pr\{m_{\text{SR}}^* = i | \mathcal{H}_\ell, \hat{\mathcal{H}}_0\}$ denote the probability that $m_{\text{SR}}^* = i$ under hypothesis \mathcal{H}_ℓ and the binary detector outcome is $\hat{\mathcal{H}}_0$. To characterize Ψ_i^ℓ we need to find the CDF and PDF of $\hat{\nu}^*$ given \mathcal{H}_ℓ , denoted as $F_{\hat{\nu}^*}^\ell(\cdot)$ and $f_{\hat{\nu}^*}^\ell(\cdot)$, respectively. Note that given our assumptions, $\hat{\nu}_m$'s are independent across sectors, however, not necessarily identically distributed. Therefore, the CDF $F_{\hat{\nu}^*}^\ell(x)$ can be written as

$$F_{\hat{\nu}^*}^\ell(y) = \prod_{m=1}^M F_{\hat{\nu}_m}^\ell(y) = 1 + \sum_{m=1}^M (-1)^m \sum_m e^{-y A_{j_1:j_m}^\ell} \quad (3.25)$$

$$A_{j_1:j_m}^\ell = \sum_{i=1}^m \frac{1}{\hat{\alpha}_{j_i}^\ell}, \quad \sum_m = \sum_{j_1=1}^{M-m+1} \sum_{j_2=j_1+1}^{M-m+2} \cdots \sum_{j_m=j_{m-1}+1}^M .$$

From the CDF in (3.25), we can find the PDF $f_{\hat{\nu}^*}^\ell(y)$

$$f_{\hat{\nu}^*}^\ell(y) = \sum_{i=1}^M f_{\hat{\nu}_i}^\ell(y) \prod_{\substack{m=1 \\ m \neq i}}^M F_{\hat{\nu}_m}^\ell(y) = \sum_{m=1}^M (-1)^{m+1} \sum_m A_{j_1:j_m}^\ell e^{-y A_{j_1:j_m}^\ell} . \quad (3.26)$$

Similar to section 3.2.2, we obtain Ψ_i^ℓ as

$$\Psi_i^\ell = \int_0^\infty f_{\hat{\nu}_i}^\ell(y) \prod_{\substack{m=1 \\ m \neq i}}^M F_{\hat{\nu}_m}^\ell(y) dy. \quad (3.27)$$

Without loss of generality, suppose $i = 1$. After some mathematical simplification, Ψ_1^ℓ can be expressed as

$$\Psi_1^\ell = 1 + \sum_{m=1}^{M-1} (-1)^m \sum'_m \frac{1}{1 + \hat{\alpha}_1^\ell B_{j_1:j_m}^\ell}, \quad (3.28)$$

where

$$B_{j_1:j_m}^\ell = \sum_{i=1}^m \frac{1}{\hat{\alpha}_{1+j_i}^\ell}, \quad \sum'_m = \sum_{j_1=1}^{M-m} \sum_{j_2=j_1+1}^{M-m+1} \cdots \sum_{j_m=j_{m-1}+1}^{M-1} .$$

Then, we have $\Psi_i = \Pr\{m_{\text{SR}}^* = i | \hat{\mathcal{H}}_0\} = \omega_0 \Psi_i^0 + \omega_1 \Psi_i^1$.

3.4 Data Transmission Phase

During this phase, SU_{tx} sends Gaussian data symbols to SU_{rx} , while data symbol transmission power is adapted based on the information provided by SU_{rx} through the feedback channel. In particular, SU_{tx} transmits $x(n) \sim \mathcal{CN}(0, P)$ over the selected beam $i = m_{\text{SR}}^*$, where P depends on $\hat{\nu}_i$, and symbols are independent and identically distributed (i.i.d). Let $u(n)$ denote the discrete-time representation of received signal at SU_{rx} from i -th beam of SU_{tx} . We note that SU_{tx} enters this phase when the outcome of the binary detector in Section 3.2.1 is $\hat{\mathcal{H}}_0$. Due to error in spatial spectrum sensing, we need to distinguish the signal model for $u(n)$ under \mathcal{H}_0 and \mathcal{H}_1 . We have

$$\begin{aligned} \mathcal{H}_0, \hat{\mathcal{H}}_0 : u(n) &= \chi_i x(n) + q(n), \\ \mathcal{H}_1, \hat{\mathcal{H}}_0 : u(n) &= \chi_i x(n) + h_{\text{sp}}(n) s(n) + q(n), \end{aligned} \quad (3.29)$$

where $q(n) \sim \mathcal{CN}(0, \sigma_q^2)$ and are i.i.d. Substituting $\chi_i = \hat{\chi}_i + \tilde{\chi}_i$ in (3.29), we reach at

$$\begin{aligned} \mathcal{H}_0, \hat{\mathcal{H}}_0 : u(n) &= \hat{\chi}_i x(n) + \overbrace{\tilde{\chi}_i x(n)}^{\text{new noise } \eta_{i,0}(n)} + q(n), \\ \mathcal{H}_1, \hat{\mathcal{H}}_0 : u(n) &= \hat{\chi}_i x(n) + \underbrace{\tilde{\chi}_i x(n) + h_{\text{sp}}(n) s(n)}_{\text{new noise } \eta_{i,1}(n)} + q(n). \end{aligned} \quad (3.30)$$

We obtain an achievable rate expression for a frame by considering symbol-wise mutual information between channel input and output over the duration of N_d data symbols as follows

$$\begin{aligned} R &= \frac{D_d}{N_d} \sum_{n=1}^{N_d} \mathbb{E} \left\{ I \left(x(n); u(n) \mid \hat{\nu}, \hat{\mathcal{H}}_0 \right) \right\} \\ &= \frac{D_d}{N_d} \sum_{n=1}^{N_d} \left[\beta_0 \mathbb{E} \left\{ I \left(x(n); u(n) \mid \hat{\nu}, \mathcal{H}_0, \hat{\mathcal{H}}_0 \right) \right\} + \beta_1 \mathbb{E} \left\{ I \left(x(n); u(n) \mid \hat{\nu}, \mathcal{H}_1, \hat{\mathcal{H}}_0 \right) \right\} \right], \end{aligned} \quad (3.31)$$

where $D_d = T_d/T_f$ is the fraction of the frame used for data transmission and the expectations are taken over $\hat{\nu} = [\hat{\nu}_1, \dots, \hat{\nu}_M]$ given $\hat{\mathcal{H}}_0$ and $\mathcal{H}_\ell, \ell = 0, 1$. To characterize R in (3.31) we need to find $\mathbb{E} \left\{ I \left(x(n); u(n) \mid \hat{\nu}, \mathcal{H}_\ell, \hat{\mathcal{H}}_0 \right) \right\}$

given as the following

$$\begin{aligned}
& \mathbb{E} \left\{ I \left(x(n); u(n) \mid \widehat{\nu}, \mathcal{H}_\ell, \widehat{\mathcal{H}}_0 \right) \right\} \\
&= \int_{\widehat{\nu}_1=0}^{\infty} I \left(x(n); u(n) \mid \widehat{\nu}_1, \widehat{\mathcal{H}}_0, \mathcal{H}_\ell \right) f_{\widehat{\nu}_1}^\ell(\widehat{\nu}_1) \Pr \left(v_1 > v_m \text{ for } m = 2, \dots, M \mid \mathcal{H}_\ell, \widehat{\mathcal{H}}_0 \right) d\widehat{\nu}_1 \\
&+ \dots \\
&+ \int_{\widehat{\nu}_M=0}^{\infty} I \left(x(n); u(n) \mid \widehat{\nu}_M, \widehat{\mathcal{H}}_0, \mathcal{H}_\ell \right) f_{\widehat{\nu}_M}^\ell(\widehat{\nu}_M) \Pr \left(v_M > v_m \text{ for } m = 1, \dots, M-1 \mid \mathcal{H}_\ell, \widehat{\mathcal{H}}_0 \right) d\widehat{\nu}_M \\
&= \sum_{j=1}^M \int_{\widehat{\nu}_j=0}^{\infty} \underbrace{I \left(x(n); u(n) \mid \widehat{\nu}_j, \widehat{\mathcal{H}}_0, \mathcal{H}_\ell \right)}_{\text{Term 1}} f_{\widehat{\nu}_j}^\ell(\widehat{\nu}_j) \underbrace{\prod_{\substack{m=1 \\ m \neq j}}^M F_{\widehat{\nu}_m}^\ell(\widehat{\nu}_j)}_{\text{Term 2}} d\widehat{\nu}_j. \tag{3.32}
\end{aligned}$$

Term 1 in (3.32) is the mutual information between $x(n)$ and $u(n)$ when SU_{tx} transmits over j -th beam, given the estimated channel gain $\widehat{\nu}_j = |\widehat{\chi}_j|^2$, and given \mathcal{H}_ℓ and $\widehat{\mathcal{H}}_0$. Term 2 in (3.32) is the PDF of estimated channel gain $\widehat{\nu}_j = |\widehat{\chi}_j|^2$ when j -th beam is the selected strongest beam, and is characterized by statistics of channel estimation error and beam selection error, occurred during channel training phase. Focusing on Term 1 in (3.32) we have

$$I \left(x(n); u(n) \mid \widehat{\nu}_i, \widehat{\mathcal{H}}_0, \mathcal{H}_\ell \right) = h \left(x(n) \mid \widehat{\nu}_i, \widehat{\mathcal{H}}_0, \mathcal{H}_\ell \right) - h \left(x(n) \mid u(n), \widehat{\nu}_i, \widehat{\mathcal{H}}_0, \mathcal{H}_\ell \right), \tag{3.33}$$

where $h(\cdot)$ is the differential entropy. From now on, we drop the variable n in $x(n)$ and $u(n)$ for brevity. Consider the first term in (3.33). Since $x \sim \mathcal{CN}(0, P)$ we have $h(x \mid \widehat{\nu}_i, \widehat{\mathcal{H}}_0, \mathcal{H}_\ell) = \log_2(\pi e P)$. Consider the second term in (3.33). Due to channel estimation error, the new noises $\eta_{i,\ell}$ in (3.30) are non-Gaussian and this term does not have a closed form expression. Hence, similar to [107, 111, 118] we employ bounding techniques to find an upper bound on this term. This term is upper bounded by the entropy of a Gaussian random variable with the variance $\Theta_M^{i,\ell}$

$$\Theta_M^{i,\ell} = \mathbb{E} \left\{ \left| x - \mathbb{E} \left\{ x \mid \widehat{\nu}_i, \widehat{\mathcal{H}}_0, \mathcal{H}_\ell \right\} \right|^2 \right\}, \tag{3.34}$$

where the expectations are taken over the conditional PDF of x given $u, \widehat{\nu}_i, \widehat{\mathcal{H}}_0, \mathcal{H}_\ell$. In fact, $\Theta_M^{i,\ell}$ is the Mean Square Error (MSE) of the MMSE estimate of x given $u, \widehat{\nu}_i, \widehat{\mathcal{H}}_0, \mathcal{H}_\ell$. Using minimum variance property of MMSE estimator, we have $\Theta_M^{i,\ell} \leq \Theta_L^{i,\ell}$, where $\Theta_L^{i,\ell}$ is the MSE of the LMMSE estimate of x given $u, \widehat{\nu}_i, \widehat{\mathcal{H}}_0, \mathcal{H}_\ell$. Combining all, we find $h(x \mid u, \widehat{\nu}_i, \widehat{\mathcal{H}}_0, \mathcal{H}_\ell) \leq \log_2(\pi e \Theta_L^{i,\ell})$ and $I(x, u \mid \widehat{\nu}_i, \widehat{\mathcal{H}}_0, \mathcal{H}_\ell) \geq \log_2(P / \Theta_L^{i,\ell})$ where

$$\Theta_L^{i,\ell} = \frac{P \sigma_{\eta_{i,\ell}}^2}{\sigma_{\eta_{i,\ell}}^2 + \widehat{\nu}_i P}, \quad \sigma_{\eta_{i,\ell}}^2 = \widetilde{\alpha}_i^\ell P + \sigma_q^2 + \ell \sigma_p^2. \tag{3.35}$$

At the end, we obtain the lower bounds as follow

$$I(x; u | \hat{\nu}_i, \hat{\mathcal{H}}_0, \mathcal{H}_0) \geq \log_2 \left(1 + \frac{\hat{\nu}_i P}{\tilde{\alpha}_i^0 P + \sigma_q^2} \right), \quad (3.36a)$$

$$I(x; u | \hat{\nu}_i, \hat{\mathcal{H}}_0, \mathcal{H}_1) \geq \log_2 \left(1 + \frac{\hat{\nu}_i P}{\tilde{\alpha}_i^1 P + \sigma_q^2 + \sigma_p^2} \right). \quad (3.36b)$$

Substituting equations (3.32) and (3.36) in (3.31) and changing the integration variable (replacing $\hat{\nu}_j$ with y), we reach at

$$R \geq R_{\text{LB}} = D_d \beta_0 R_0 + D_d \beta_1 R_1, \quad (3.37)$$

where

$$R_0 = \sum_{j=1}^M \int_0^\infty \log_2 \left(1 + \frac{yP}{\tilde{\alpha}_j^0 P + \sigma_q^2} \right) f_{\hat{\nu}_j}^0(y) \prod_{\substack{m=1 \\ m \neq j}}^M F_{\hat{\nu}_m}^0(y) dy,$$

$$R_1 = \sum_{j=1}^M \int_0^\infty \log_2 \left(1 + \frac{yP}{\tilde{\alpha}_j^1 P + \sigma_q^2 + \sigma_p^2} \right) f_{\hat{\nu}_j}^1(y) \prod_{\substack{m=1 \\ m \neq j}}^M F_{\hat{\nu}_m}^1(y) dy.$$

We note that the lower bounds in (3.36) are achieved when the new noises $\eta_{m,0}, \eta_{m,1}$ in (3.30) are regarded as worst-case Gaussian noise and hence the MMSE and LMMSE of x given $u, \hat{\nu}_m, \hat{\mathcal{H}}_0, \mathcal{H}_\ell$ coincide.

So far, we have established a lower bound on the achievable rates. Next, we characterize AIC and ATPC. Let \bar{I}_{av} indicate the maximum allowed interference imposed on PU. To satisfy the AIC, we need to have

$$\beta_1 \mathbb{E}\{g\} \left[D_d \mathbb{E} \left\{ p(\kappa_{\text{SR}}^* - \kappa_{\text{PU}}^*) P | \mathcal{H}_1, \hat{\mathcal{H}}_0 \right\} + D_{\text{tr}} P_{\text{tr}} \sum_{j=1}^M \mathbb{E} \left\{ p(\kappa_j - \kappa_{\text{PU}}^*) | \mathcal{H}_1, \hat{\mathcal{H}}_0 \right\} \right] \leq \bar{I}_{\text{av}}, \quad (3.38)$$

where $D_{\text{tr}} = T_{\text{tr}}/T_{\text{f}}$. The first term in (3.38) is the average interference imposed on PU when SU_{tx} transmits data symbols, and the second term is the average interference imposed on PU when SU_{tx} sends training symbols for channel estimation at SU_{rx} . Consider the two conditional expectation terms inside the bracket in (3.38). Using the fact that, given $\mathcal{H}_1, \hat{\mathcal{H}}_0, p(\cdot)$ and P (which depends on $\hat{\nu}^*$) are independent, and also the average probabilities derived in (3.16) and (3.27) we have

$$\mathbb{E} \left\{ p(\kappa_{\text{SR}}^* - \kappa_{\text{PU}}^*) | \mathcal{H}_1, \hat{\mathcal{H}}_0 \right\} = \sum_{j=1}^M \sum_{i=1}^M \Psi_j^1 \bar{\Delta}_{m_{\text{PU}}, i}^* p(\kappa_j - \kappa_i), \quad (3.39)$$

$$\mathbb{E}\left\{p(\kappa_j - \kappa_{\hat{\text{P}}_{\text{U}}^*}) \mid \mathcal{H}_1, \hat{\mathcal{H}}_0\right\} = \sum_{i=1}^M \bar{\Delta}_{m_{\hat{\text{P}}_{\text{U}}^*}, i} p(\kappa_j - \kappa_i). \quad (3.40)$$

Then, the constraint in (3.38) can be written as

$$D_{\text{d}} b_0 \mathbb{E}\left\{P \mid \mathcal{H}_1, \hat{\mathcal{H}}_0\right\} + D_{\text{tr}} u_0 P_{\text{tr}} \leq \bar{I}_{\text{av}}, \quad (3.41)$$

where

$$b_0 = \beta_1 \gamma \sum_{j=1}^M \sum_{i=1}^M \Psi_j^1 \bar{\Delta}_{m_{\hat{\text{P}}_{\text{U}}^*}, i} p(\kappa_j - \kappa_i), \quad (3.42\text{a})$$

$$u_0 = \beta_1 \gamma \sum_{j=1}^M \sum_{i=1}^M \bar{\Delta}_{m_{\hat{\text{P}}_{\text{U}}^*}, i} p(\kappa_j - \kappa_i), \quad (3.42\text{b})$$

$$\mathbb{E}\left\{P \mid \mathcal{H}_1, \hat{\mathcal{H}}_0\right\} = \int_0^\infty P(y) f_{\hat{\mathcal{P}}^*}^1(y) dy. \quad (3.42\text{c})$$

We note that spectrum sensing error, PU beam selection error, and SU_{tx} beam selection error are reflected in AIC through variables β_1 , $\bar{\Delta}_{m_{\hat{\text{P}}_{\text{U}}^*}, i}$ and Ψ_j^1 , respectively. Also, channel estimation error influences AIC through variable P . Let \bar{P}_{av} denote the maximum allowed average transmit power of SU_{tx}. To satisfy the ATPC, we need to have

$$\beta_0 D_{\text{d}} \mathbb{E}\left\{P \mid \mathcal{H}_0, \hat{\mathcal{H}}_0\right\} + \beta_1 D_{\text{d}} \mathbb{E}\left\{P \mid \mathcal{H}_1, \hat{\mathcal{H}}_0\right\} + \hat{\pi}_0 D_{\text{tr}} P_{\text{tr}} \leq \bar{P}_{\text{av}}, \quad (3.43)$$

where $\mathbb{E}\{P \mid \mathcal{H}_0, \hat{\mathcal{H}}_0\} = \int_0^\infty P(y) f_{\hat{\mathcal{P}}^*}^0(y) dy$, and the third term in (3.43) accounts for transmit power used for training symbols. We note that spectrum sensing error affects ATPC through variables β_0 , β_1 and $\hat{\pi}_0$. Also, channel estimation error affects ATPC through variable P .

Now that we have characterized a lower bound on the achievable rates R_{LB} in (3.37), AIC in (3.41), and ATPC in (3.43), we summarize how the four error types, namely, spectrum sensing error, beam detection error, channel estimation error, and beam selection error, affect these expressions. First, spectrum sensing error affects AIC via β_1 , both ATPC and R_{LB} via β_0 and β_1 . Recall β_0, β_1 depend on $\pi_0, \bar{P}_{\text{fa}}, \bar{P}_{\text{d}}$ (see (3.11)). Second, beam detection error affects AIC via $\bar{\Delta}_{m_{\hat{\text{P}}_{\text{U}}^*}, i}$ and does not have a direct impact on ATPC and R_{LB} . Third, channel estimation error affects both AIC and ATPC via T_{tr} , and R_{LB} via $\tilde{\alpha}_m^\ell$. Fourth, beam selection error impacts AIC, ATPC and R_{LB} via P (which depends on the estimation channel gain of the selected beam).

Having the mathematical expressions for R_{LB} , AIC, ATPC, our goal is to allocate transmission resources such that

R_{LB} is maximized, subject to the aforementioned constraints. To determine our optimization variables, we need to examine closely the underlying trade-offs between decreasing average interference and average transmit powers, decreasing four types of errors (i.e., spectrum sensing error, beam detection error, channel estimation error, and beam selection error), and increasing R_{LB} . Within a frame with fixed duration of T_f seconds, time is divided between three phases with variable durations: spatial spectrum sensing with duration T_{se} , channel training with duration T_{tr} , and data transmission with duration of T_d . Suppose T_{se} increases. On the positive side, spectrum sensing error, beam detection error, and average interference imposed on PU decrease (i.e., for ideal spectrum sensing $\beta_1 = 0$ in (3.11) and data transmission from SU_{tx} to SU_{rx} does not cause interference on PU). On the negative side, $T_{tr} + T_d$ decreases, that can lead to increasing channel estimation error (due to decrease in T_{tr}) and/or decreasing R_{LB} (due to decrease in T_d). Given T_{se} , as T_{tr} increases, channel estimation error in (3.22) decreases. However, average interference imposed on PU during transmission of training symbols increases and R_{LB} decreases⁵. Finally, increasing data symbol transmission power P increases R_{LB} , however, it increases average interference and average transmit power. Based on all these existing trade-offs, we seek the optimal T_{se}, T_{tr}, P such that R_{LB} in (3.37) is maximized, subject to AIC and ATPC given in (3.41) and (3.43), respectively. In other words, we are interested in solving the following constrained optimization problem

$$\begin{aligned}
& \underset{T_{se}, T_{tr}, P}{\text{Maximize}} \quad R_{LB} & (3.P1) \\
& \text{s.t.} \quad 0 < T_{se} < T_f - T_{tr} \\
& \quad \quad T_{tr} > 0, \quad P \geq 0 \\
& \quad \quad (3.41) \text{ and } (3.43) \text{ are satisfied.}
\end{aligned}$$

Before delving into the solution of (3.P1), we have a remark on how our adopted fading model in Section 3.1.2 affects our derivations in this section.

Remark: Our theoretical framework can be extended to the more general Nakagami fading model, however, certain expressions need to be re-derived. In particular, $\bar{P}_d = \mathbb{E}_{\psi}\{P_d\}$ in (3.10) changes, since the pdf of ψ changes. Also, the conditional pdf of $\hat{\nu}_m$ given $\{\hat{\mathcal{H}}_0, \mathcal{H}_\ell\}$ in (3.23), and the CDF and pdf of $\hat{\nu}^*$ in (3.25), (3.26) change. Consequently, the expressions for Ψ_i^ℓ in (3.27), $\mathbb{E}\{P|\mathcal{H}_1, \hat{\mathcal{H}}_0\}$ in (3.42c), and R_{LB} in (3.37) must be re-calculated.

⁵Note that as channel estimation error in (3.22) decreases, the lower bounds in (3.36) increase. However, this logarithmic increase is dominated by the linear decrease of D_d in (3.37), which leads into a decrease in R_{LB} .

3.5 Constrained Maximization of Rate Lower Bound

In this section, we address the optimization problem (3.P1). Taking the second derivative of R_{LB} with respect to (w.r.t.) the optimization variables, we note that (3.P1) is not jointly concave over $T_{\text{se}}, T_{\text{tr}}, P$. However, given T_{se} and T_{tr} , (3.P1) is concave⁶ w.r.t. P . We propose an iterative method based on the BCD algorithm to solve (3.P1). The underlying principle of the BCD algorithm is that, at each iteration one variable is optimized, while the remaining variables are fixed. The iteration continues until it converges to a stationary point of (3.P1) [109]. To apply the principle of the BCD algorithm to (3.P1), we consider the following three steps.

Step (i): given $T_{\text{se}}, T_{\text{tr}}$, we optimize P using the Lagrangian method. The Lagrangian is

$$\mathcal{L} = -R_{\text{LB}} + \mu \left[\text{LHS of (3.41)} - \bar{I}_{\text{av}} \right] + \lambda \left[\text{LHS of (3.43)} - \bar{P}_{\text{av}} \right], \quad (3.44)$$

in which LHS stands for left-hand side, λ and μ are the nonnegative Lagrange multipliers, associated with the ATPC and AIC, respectively. Therefore, the optimal P that minimize (3.44) is the solution to the KKT optimality necessary and sufficient conditions. The KKT conditions are the first derivatives of \mathcal{L} w.r.t. P, μ, λ being equal to zero, i.e., $\partial \mathcal{L} / \partial P = 0, \partial \mathcal{L} / \partial \mu = 0, \partial \mathcal{L} / \partial \lambda = 0$. We have

$$-\frac{1}{\ln(2)} \sum_{\ell=0}^1 \beta_{\ell} \sum_{i=1}^M \frac{y (\sigma_{\text{q}}^2 + \ell \sigma_{\text{p}}^2) f_{\hat{v}_i}^{\ell}(y)}{\sigma_{\eta_{i,\ell}}^2 (yP + \sigma_{\eta_{i,\ell}}^2)} \prod_{\substack{m=1 \\ m \neq i}}^M F_{\hat{v}_m}^{\ell}(y) + \lambda \left[\beta_0 f_{\hat{v}^*}^0(y) + \beta_1 f_{\hat{v}^*}^1(y) \right] + \mu b_0 f_{\hat{v}^*}^1(y) = 0, \quad (3.45a)$$

$$\mu \left(\text{LHS of (3.41)} - \bar{I}_{\text{av}} \right) = 0, \quad (3.45b)$$

$$\lambda \left(\text{LHS of (3.43)} - \bar{P}_{\text{av}} \right) = 0. \quad (3.45c)$$

The closed-form analytical solution for (3.45) cannot be found. Hence, we solve these equations numerically for every realization of \hat{v}^* , via the following iterative method. We first initialize the Lagrangian multipliers μ and λ and then find P using (3.45a), and verify that it satisfies (3.45b), (3.45c). Next, we update μ and λ using the subgradient method. Using the updated μ and λ , we find P again using (3.45a). We repeat this procedure until μ and λ converge (i.e., a pre-determined stopping criterion is met).

Step (ii): given P and T_{tr} , we optimize T_{se} . The optimal T_{se} is the solution of the equation $\partial R_{\text{LB}} / \partial T_{\text{se}} = 0$. In

⁶The cost function of (3.P1) given in (3.37) depends on P through the two logarithms, that can be viewed, in terms of P , as $(1 + \frac{aP}{bP+c})$, where a, b, c are positive. Since the arguments of these logarithms are concave, R_{LB} is also concave w.r.t. P .

Appendix A.1, we show that this equation has one solution in the interval $(0, T_f - T_{tr})$. This solution can be found using numerical search methods (e.g., bisection method).

Step (iii): given P and T_{se} , we optimize T_{tr} , via solving $\partial R_{LB}/\partial T_{tr} = 0$. In Appendix A.2, we show that this equation has one solution in the interval $(0, T_f - T_{se})$, which can be found numerically using search methods (e.g., bisection method).

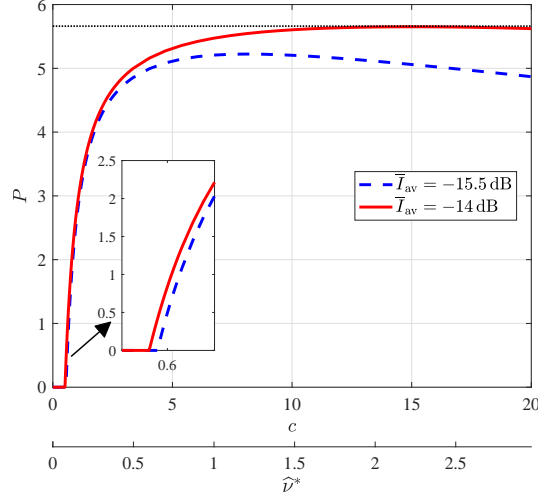


Figure 3.4: The optimized P obtained from (3.45a) versus \hat{v}^* (and c) for $\bar{P}_{av} = 2$ dB.

To gain an insight on the solution of (3.P1), we look into the behavior of the optimized P versus the realizations of the estimated channel gain \hat{v}^* . Fig. 3.4 illustrates the optimized P versus \hat{v}^* (and c , where $\hat{v}^* = c m_{\hat{v}^*}$ and $m_{\hat{v}^*}$ is the mean of \hat{v}^*) for $\bar{I}_{av} = -15.5, -14$ dB and other simulation parameters given in Table 3.3. For these parameters $m_{\hat{v}^*} = 0.1484$. We observe that the optimized P for very small \hat{v}^* (when \hat{v}^* is smaller than a cut-off threshold $\zeta = 3.5 m_{\hat{v}^*}$) is zero. As \hat{v}^* increases the optimized P increases gradually until it reaches a maximum value. As \hat{v}^* increases further, the optimized P decreases, until it reaches a minimum value for very large \hat{v}^* (when $\hat{v}^* > 85 m_{\hat{v}^*}$), not shown in the figure. Comparing the curves for $\bar{I}_{av} = -15.5$ dB and $\bar{I}_{av} = -14$ dB, we note that the optimized P decays faster (after it reaches its maximum value) for lower \bar{I}_{av} . Moreover, the cut-off threshold ζ is lower for higher \bar{I}_{av} . The behavior of the optimized P versus \hat{v}^* is different from our intuitive expectation that expects to see the optimized P increases monotonically as \hat{v}^* increases. We explore this by examining the optimized P , which satisfies (3.45a).

Although for general M the optimized P does not have a closed form expression, for $M = 1$ and under a simplifying

assumption⁷ it can approximated as follows:

$$P \approx \left[\frac{F + \sqrt{\Upsilon}}{2} \right]_+, \quad F = \frac{\beta_0 W(\hat{\nu}^*) + \beta_1}{\ln(2) \left[\lambda \left(\beta_0 W(\hat{\nu}^*) + \beta_1 \right) + \mu b_0 \right]} - \frac{2\sigma_q^2 + \sigma_p^2}{\hat{\nu}^*}, \quad (3.46)$$

$$\Upsilon = F^2 - \frac{4}{\hat{\nu}^*} \left(\frac{\sigma_q^2(\sigma_q^2 + \sigma_p^2)}{\hat{\nu}^*} - \frac{\left(\beta_0 W(\hat{\nu}^*) + \beta_1 \right) \sigma_q^2 + \beta_0 W(\hat{\nu}^*) \sigma_p^2}{\ln(2) \left[\lambda \left(\beta_0 W(\hat{\nu}^*) + \beta_1 \right) + \mu b_0 \right]} \right).$$

where $W(\hat{\nu}^*) = f_{\hat{\nu}^*}^0(\hat{\nu}^*)/f_{\hat{\nu}^*}^1(\hat{\nu}^*) = \hat{\alpha}^1/\hat{\alpha}^0 e^{-\hat{\nu}^*(\frac{1}{\hat{\alpha}^0} - \frac{1}{\hat{\alpha}^1})}$. Considering (3.21) we realize that $\hat{\alpha}^0 < \hat{\alpha}^1$. This implies as $\hat{\nu}^*$ increases, $W(\hat{\nu}^*)$ and Υ decrease. However, the behavior of F changes, i.e., F increases until it reaches a maximum value. As $\hat{\nu}^*$ increases further, F decreases. Considering (3.46) we note that the behavior of P (in terms of $\hat{\nu}^*$) is dominated by the behavior of F . In the ideal scenario when there is no channel estimation error, we have $\hat{\alpha}^0 = \hat{\alpha}^1 = \alpha$ and $W(\hat{\nu}^*) = 1$, F monotonically increases and Υ decreases, i.e., P in (3.46) monotonically increases as $\hat{\nu}^*$ increases, which is what we intuitively expect.

The optimized P we discussed so far requires solving (3.45) several times for each realization of $\hat{\nu}^*$. Integrating the insights we have gained into how this optimized P varies in terms of $\hat{\nu}^*$, we propose two transmit power control schemes that are simpler to implement and yield achievable rate lower bounds that are very close to the maximized R_{LB} values in (3.P1). Since $\Pr(\hat{\nu}^* \geq c m_{\hat{\nu}^*})$ is very small for $c \geq 8$ (see Table 3.2), we focus on the regime when $\hat{\nu}^* < 8 m_{\hat{\nu}^*}$ and develop two schemes, dubbed here scheme 1 and scheme 2, that mimic the behavior of the optimized P in this regime.

Table 3.2: $\Pr(\hat{\nu}^* \geq c m_{\hat{\nu}^*})$ in terms of c , given $m_{\hat{\nu}^*} = 0.1484$.

c	$\Pr(\hat{\nu}^* \geq c m_{\hat{\nu}^*})$
4	3.01×10^{-3}
8	7.04×10^{-6}
12	1.54×10^{-8}
16	4.87×10^{-11}

⁷We assume that the optimized T_{tr} is large enough such that $\tilde{\alpha}P + \sigma_q^2 \approx \sigma_q^2$. This assumption allows us to approximate (3.45a) for $M = 1$ as a quadratic polynomial in P (originally a polynomial of degree 4 in P) and find a closed-form expression for P .

3.5.1 Scheme 1

For scheme 1, when the spectrum is sensed idle, SU_{tx} sends data to SU_{rx} over the selected sector $i = m_{\text{SR}}^*$ according to the following rule:

$$P_{S_1} = \begin{cases} \Pi_1, & \text{if } \hat{\nu}^* \geq \zeta_1 \\ 0, & \text{if } \hat{\nu}^* < \zeta_1 \end{cases} \quad (3.47)$$

i.e., when $\hat{\nu}^*$ is less than a cut-off threshold ζ_1 , SU_{tx} remains silent, when $\hat{\nu}^*$ is larger than ζ_1 , SU_{tx} lets its transmit power be equal to constant Π_1 . The parameter Π_1 can be found in terms of $T_{\text{se}}, T_{\text{tr}}, \zeta_1$, via enforcing AIC in (3.41) and ATPC in (3.43) as the following:

$$\Pi_1 = \frac{1}{D_d} \min \left\{ \frac{\bar{P}_{\text{av}} - \hat{\pi}_0 D_{\text{tr}} P_{\text{tr}}}{\sum_{\ell=0}^1 \beta_{\ell} \left(1 - F_{\hat{\nu}^*}^{\ell}(\zeta_1)\right)}, \frac{\bar{I}_{\text{av}} - u_0 D_{\text{tr}} P_{\text{tr}}}{b_0 \left(1 - F_{\hat{\nu}^*}^1(\zeta_1)\right)} \right\}. \quad (3.48)$$

Let R_{S_1} denote the lower bound on the achievable rates when SU_{tx} adopts the power control scheme in (3.47). We find R_{S_1} expression by substituting P_{S_1} in (3.37) and taking expectation w.r.t. $\hat{\nu}^*$ given as the following

$$R_{S_1} = \frac{D_d}{\ln(2)} \sum_{\ell=0}^1 \beta_{\ell} \sum_{j=1}^M \left[Y\left(\hat{\alpha}_j^{\ell}, \text{SNR}_j^{\ell}\right) + \sum_{\substack{m=1 \\ m \neq j}}^M (-1)^m \sum_m Y\left(d_{j,m}^{\ell}, \text{SNR}_j^{\ell}\right) \right], \quad (3.49)$$

$$Y(a, b) = \int_{\zeta_1}^{\infty} \ln(1 + bx) \frac{1}{a} e^{-\frac{x}{a}} dx = e^{-\zeta_1/a} \ln(1 + b\zeta_1) - e^{1/ab} \text{Ei}(-\zeta_1/a - 1/ab),$$

where $d_{j,m}^{\ell} = (A_{k_1:k_m}^{\ell} + \frac{1}{\hat{\alpha}_j^{\ell}})^{-1}$, $\text{SNR}_i^0 = \frac{\Pi_1}{\hat{\alpha}_i^0 + \sigma_q^2}$, $\text{SNR}_i^1 = \frac{\Pi_1}{\hat{\alpha}_i^1 + \sigma_q^2 + \sigma_p^2}$ and $\text{Ei}(\cdot)$ is the exponential integral. With this transmit power scheme, we consider a modified problem to (3.P1), where the lower bound R_{S_1} in (3.49) is maximized (subject to the same constraints) and the optimization variables are $T_{\text{se}}, T_{\text{tr}}, \zeta_1$. To solve this modified problem, we use an iterative method based on the BCD algorithm and implement the following three steps: **Step (i)**, given $T_{\text{se}}, T_{\text{tr}}$, we optimize ζ_1 , via maximizing R_{S_1} , using bisection search method. **Step (ii)**, given ζ_1, T_{tr} , we optimize T_{se} , using bisection search method. **Step (iii)**, given ζ_1, T_{se} , we optimize T_{tr} , using bisection search method. In Section 3.6 we numerically compare the maximized R_{LB} in (3.P1) and the maximized R_{S_1} .

3.5.2 Scheme 2

For scheme 2, when the spectrum is sensed idle, SU_{tx} sends data symbols to SU_{rx} over the selected sector $i = m_{\text{SR}}^*$ according to the following rule:

$$P_{S_2} = \begin{cases} \Pi_2 \left(1 - \frac{\zeta_2}{\hat{\nu}^*}\right), & \text{if } \hat{\nu}^* \geq \zeta_2 \\ 0, & \text{if } \hat{\nu}^* < \zeta_2 \end{cases} \quad (3.50)$$

Different from scheme 1, in the scheme 2 when $\hat{\nu}^*$ exceeds the cut-off threshold ζ_2 , SU_{tx} transmits at a variable power. The power level increases as $\hat{\nu}^*$ increases, until it reaches its maximum value of Π_2 , i.e., $\lim_{\hat{\nu}^* \rightarrow \infty} P_{S_2} = \Pi_2$. The parameter Π_2 can be found in terms of $T_{\text{se}}, T_{\text{tr}}, \zeta_2$, via enforcing AIC in (3.41) and ATPC in (3.43) as the following:

$$\Pi_2 = \frac{1}{D_d} \min \left\{ \frac{\bar{P}_{\text{av}} - \hat{\pi}_0 D_{\text{tr}} P_{\text{tr}}}{\sum_{\ell=0}^1 \beta_{\ell} [1 - G^{\ell}(\zeta_2)]}, \frac{\bar{I}_{\text{av}} - u_0 D_{\text{tr}} P_{\text{tr}}}{b_0 [1 - G^1(\zeta_2)]} \right\}, \quad (3.51)$$

where $G^{\ell}(\zeta_2) = F_{\hat{\nu}^*}^{\ell}(\zeta_2) + \zeta_2 T^{\ell}(\zeta_2)$ and

$$T^{\ell}(\zeta_2) = \mathbb{E} \left\{ \frac{1}{\hat{\nu}^*} \mid \hat{\nu}^* \geq \zeta_2, \mathcal{H}_{\ell} \right\} = \int_{\zeta_2}^{\infty} \frac{f_{\hat{\nu}^*}^{\ell}(y)}{y} dy = \sum_{m=1}^M (-1)^m \sum_m A_{j_1:j_m}^{\ell} \text{Ei}(-\zeta_2 A_{j_1:j_m}^{\ell}). \quad (3.52)$$

Let R_{S_2} represent the lower bound on the achievable rates when SU_{tx} adopts the power control scheme in (3.50). We find R_{S_2} by substituting P_{S_2} in (3.37) and taking expectation w.r.t. $\hat{\nu}^*$. With this transmit power scheme, we consider a modified problem to (3.P1), where the lower bound R_{S_2} is maximized (subject to the same constraints) and the optimization variables are $T_{\text{se}}, T_{\text{tr}}, \zeta_2$. To solve this modified problem, we use an iterative method based on the BCD algorithm and implement the following three steps: **Step (i)**, given $T_{\text{tr}}, T_{\text{se}}$, we optimize ζ_2 , via maximizing R_{S_2} , using bisection search method. **Step (ii)**, given ζ_2, T_{tr} , we optimize T_{se} , using bisection search method. **Step (iii)**, given ζ_2, T_{se} , we optimize T_{tr} , using bisection search method. In Section 3.6 we numerically compare the maximized R_{LB} in (3.P1) and the maximized R_{S_2} . Note that the closed-form expression for R_{S_2} cannot be obtained.

3.5.3 Discussion on Computational Complexity of Proposed Algorithms

In the following, we discuss the computational complexity of the three proposed algorithms, namely, the first algorithm in Section 3.5, Scheme 1 in Section 3.5.1, and Scheme 2 in Section 3.5.2.

The first algorithm consists of three steps. We discuss the computational complexity of each step. **Step (i)**: given $T_{\text{se}}, T_{\text{tr}}$, we find P via solving (3.45a), (3.45b), (3.45c) numerically. In particular, noting that y in (3.45a) is positive, we partition the real positive line into N_y intervals. Given y is in one of these N_y intervals, we initialize the Lagrangian multipliers μ and λ and then solve (3.45a) for P using bisection method. The computational complexity of bisection method to provide an ϵ_p -accurate solution for each of these N_y intervals is $\mathcal{O}(\log(1/\epsilon_p))$ [119, 120]. Hence, the computational complexity for solving (3.45a) N_y times is $\mathcal{O}(N_y \log(1/\epsilon_p))$. Moving on to (3.45b) and (3.45c), we need to compute LHS of (3.41) and (3.43), respectively, which requires calculating the conditional expectations $\mathbb{E}\{P|\mathcal{H}_1, \widehat{\mathcal{H}}_0\}$ and $\mathbb{E}\{P|\mathcal{H}_0, \widehat{\mathcal{H}}_0\}$ and integrating over y . Hence, the computational complexity for computing (3.45b) and (3.45c) is $\mathcal{O}(N_y)$. Since $N_y \ll N_y \log(1/\epsilon_p)$, we can neglect the computational complexity of solving (3.45b), (3.45c), with respect to that of solving (3.45a). Hence, the computational complexity of solving (3.45), given μ and λ , is $\mathcal{O}(N_y \log(1/\epsilon_p))$. Next, we update μ and λ using the subgradient method. Using the updated μ and λ , we solve (3.45a) for P again. We repeat this procedure until both μ and λ converge. The computational complexity to get $\epsilon_{\mathcal{L}}$ -convergence for μ and λ is $\mathcal{O}(S_1)$, where $S_1 = (N_y \log(1/\epsilon_p))/\epsilon_{\mathcal{L}}$. **Step (ii)**: given P and T_{tr} , we find T_{se} using bisection search method. The computational complexity of bisection search method to provide an ϵ_{se} -accurate solution is $\mathcal{O}(S_2)$, where $S_2 = \log(1/\epsilon_{\text{se}})$. **Step (iii)**: given P and T_{se} , we find T_{tr} using bisection search method. The computational complexity of bisection search method to provide an ϵ_{tr} -accurate solution is $\mathcal{O}(S_3)$, where $S_3 = \log(1/\epsilon_{\text{tr}})$. At each iteration of **Step (iii)**, we execute **Step (ii)** and at each iteration of **Step (ii)**, we execute **Step (i)**. Hence, the overall computational complexity of the first algorithm is $\mathcal{O}(S_1 S_2 S_3)$.

Scheme 1: Similar to the first algorithm, Scheme 1 consists of three steps. At the first step, given $T_{\text{se}}, T_{\text{tr}}$, we optimize ζ_1 using bisection search method. The computational complexity of bisection search method to provide an ϵ_{ζ} -accurate solution is $\mathcal{O}(\log(1/\epsilon_{\zeta}))$. The second and third steps are exactly the same as **Step (ii)** and **Step (iii)** in the first algorithm. Hence, the overall computational complexity of Scheme 1 is $\mathcal{O}(S_2 S_3 \log(1/\epsilon_{\zeta}))$.

Scheme 2: Similar to the first algorithm, Scheme 2 consists of three steps. At the first step, given $T_{\text{se}}, T_{\text{tr}}$, we optimize ζ_2 using bisection search method. The computational complexity of bisection search method to provide an ϵ_{ζ} -accurate solution is $\mathcal{O}(\log(1/\epsilon_{\zeta}))$. The computational complexity of integrating over y in (3.37) within each iteration of bisection search method is $\mathcal{O}(N_y)$. Hence, the computational complexity for the first step of Scheme 2 is $\mathcal{O}(N_y \log(1/\epsilon_{\zeta}))$. The second and third steps are exactly the same as **Step (ii)** and **Step (iii)** in the first algorithm. Hence, the overall computational complexity of Scheme 2 is $\mathcal{O}(N_y S_2 S_3 \log(1/\epsilon_{\zeta}))$.

Comparing the computational complexity of these three schemes, it is clear that Scheme 2 has a higher computational

complexity than that of Scheme 1. Under the assumption $\epsilon_{\zeta} = \epsilon_{\mathcal{L}} = \epsilon_p$, we find that the first scheme has the highest and Scheme 1 has the lowest computational complexity.

3.6 Simulation Results

Table 3.3: Simulation Parameters

Parameter	Value	Parameter	Value	Parameter	Value
A_0	0.98	γ_{ss}	0.1	σ_w^2, σ_q^2	0.5
A_1	0.02	γ, γ_{sp}	0.5	P_p	0.5 watts
ϕ_{3dB}	20°	π_0	0.7	T_f	30 ms
ϕ_1	-55°	\bar{P}_d	0.85	P_{tr}	2 watts
ϕ_2	$+55^\circ$	M	7		

We corroborate our analysis on constrained maximization of achievable rate lower bounds with Matlab simulations. Our simulation parameters are given in Table 3.3. We start by illustrating the behavior of our proposed power allocation schemes versus $\hat{\nu}^*$. Fig. 3.5 shows the optimized P obtained by solving (3.45a) and the two proposed suboptimal schemes P_{S_2} and P_{S_1} versus $\hat{\nu}^*$. We observe that P_{S_2} and P_{S_1} mimic the behavior of the optimized P . Furthermore, for the cut-off thresholds we have $\zeta < \zeta_1 < \zeta_2$.

Next, we explore the effect of spatial spectrum sensing duration T_{se} on the achievable rate lower bounds of our system. Fig. 3.6a shows the maximized R_{LB} , R_{S_2} and R_{S_1} (which we refer in the figures to as ‘‘Rate’’) versus T_{se} . To plot this figure, we maximize the bounds w.r.t. only T_{tr} and P , subject to ATPC and AIC. We note that for all T_{se} values we have $R_{LB} > R_{S_2} > R_{S_1}$. We observe that the achievable rates always have a maximum in the interval $(0, T_f - T_{tr})$. For the simulation parameters in Table 3.3 the optimized $T_{se} = 0.75 \text{ ms} = 2.5\% T_f$. Also, scheme 2 yields a higher achievable rate than that of scheme 1, because its corresponding power P_{S_2} fits better to the optimized power P obtained from solving (3.45a). The achievable rate R_{S_2} is very close to R_{LB} and we do not have a significant performance loss if we choose the simple transmit power control scheme in (3.50).

To investigate the effect of channel training duration T_{tr} on the achievable rate lower bounds, we plot Fig. 3.6b which illustrates the maximized R_{LB} , R_{S_2} and R_{S_1} versus T_{tr} . To plot this figure, we maximize the bounds w.r.t. only T_{se} and P , subject to ATPC and AIC. For all T_{tr} values we have $R_{LB} > R_{S_2} > R_{S_1}$. We observe that the achievable rates always have a maximum in the interval $(0, T_f - T_{se})$. For the simulation parameters in Table 3.3 the optimized $T_{tr} = 0.67 \text{ ms} = 2.23\% T_f$. Comparing Fig. 3.6b and Fig. 3.6a, we notice that the achievable rates are

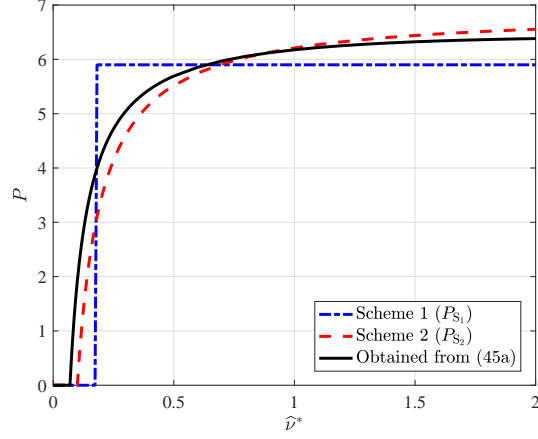


Figure 3.5: P versus $\hat{\nu}^*$ for $\bar{P}_{av} = 2$ dB, $\bar{I}_{av} = -12$ dB.

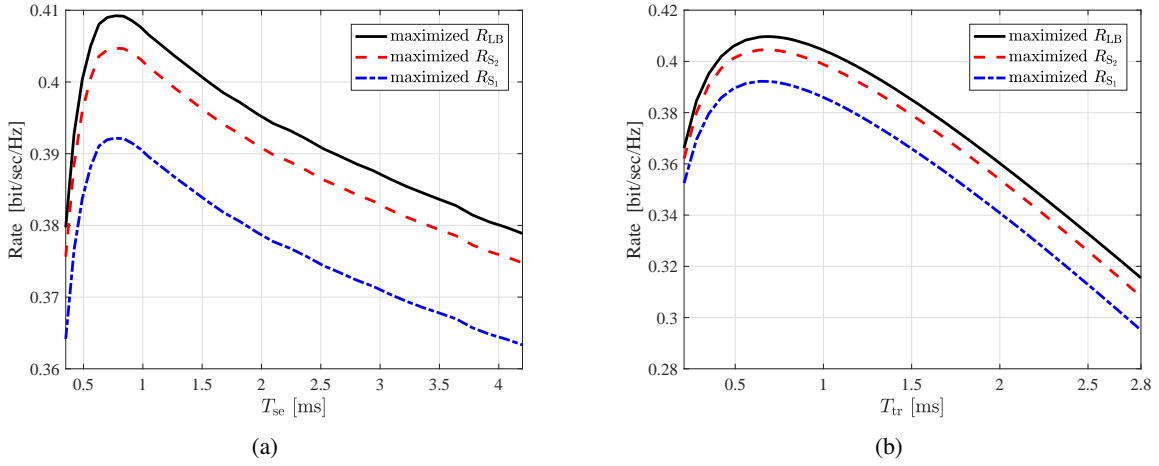


Figure 3.6: For $\bar{P}_{av} = 2$ dB, $\bar{I}_{av} = -15$ dB, (a) Rate versus T_{se} , (b) Rate versus T_{tr} .

more sensitive to the variations of T_{tr} compared to that of T_{se} . To be more specific, considering Fig. 3.6a and Fig. 3.6b, suppose we choose T_{se} and T_{tr} values that are different from their corresponding maximum values by 20%, i.e., $\Delta T_{se} = 20\%$, $\Delta T_{tr} = 20\%$. Then

$$\Delta R_{LB}/\Delta T_{tr} > \Delta R_{LB}/\Delta T_{se}, \quad \Delta R_{S_2}/\Delta T_{tr} > \Delta R_{S_2}/\Delta T_{se}, \quad \Delta R_{S_1}/\Delta T_{tr} > \Delta R_{S_1}/\Delta T_{se}.$$

These indicate that proper allocation of T_{tr} is more important than that of T_{se} , for providing higher achievable rates in

our system.

To explore the effects of the number of beams M and \bar{I}_{av} on the achievable rate lower bounds, Fig. 3.7a illustrates the maximized $R_{\text{LB}}, R_{\text{S}_2}, R_{\text{S}_1}$ versus \bar{I}_{av} for $M = 7, 11$ and $\bar{P}_{\text{av}} = 2$ dB. We observe that as M increases a higher rate can be achieved. For all M and \bar{I}_{av} values we have $R_{\text{LB}} > R_{\text{S}_2} > R_{\text{S}_1}$. We realize that as \bar{I}_{av} increases from -18 dB to -14 dB, the achievable rates are monotonically increasing and the AIC is dominant. However, as \bar{I}_{av} increases beyond -14 dB, the achievable rates remain unchanged and the ATPC is dominant. Fig. 3.7b illustrates the

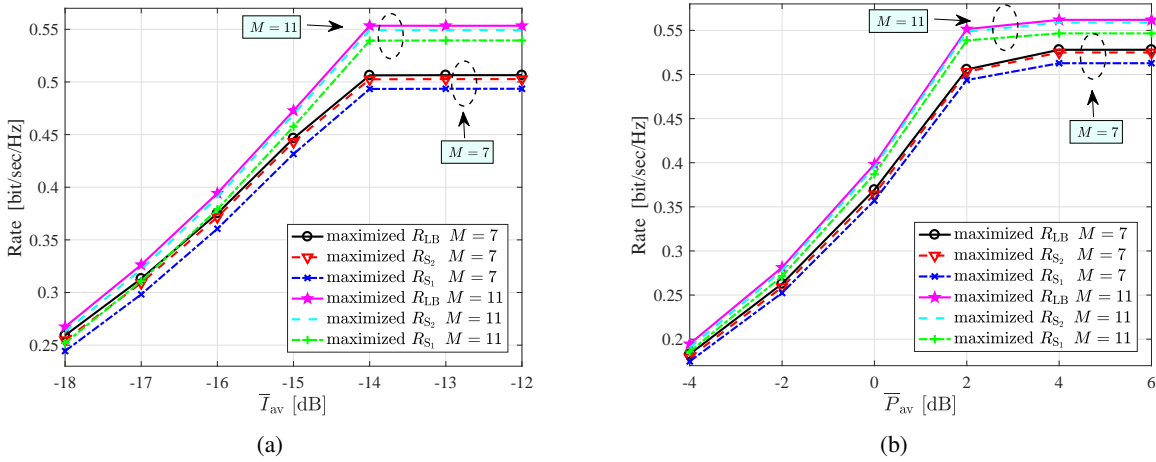


Figure 3.7: (a) Rate versus \bar{I}_{av} for $M = 7, 11$ and $\bar{P}_{\text{av}} = 2$ dB, (b) Rate versus \bar{P}_{av} for $M = 7, 11$ and $\bar{I}_{\text{av}} = -14$ dB.

maximized $R_{\text{LB}}, R_{\text{S}_2}, R_{\text{S}_1}$ versus \bar{P}_{av} for $M = 7, 11$ and $\bar{I}_{\text{av}} = -14$ dB. The behaviors of the achievable rates in terms of M are the same as Fig. 3.7a. We note that as \bar{P}_{av} increases from -4 dB to 2 dB, the achievable rates are monotonically increasing and the ATPC is dominant. However, as \bar{P}_{av} increases beyond 2 dB, the achievable rates remain unchanged and the AIC is dominant.

We also consider outage probability as another performance metric to evaluate our system. We define the outage probability as the probability of SU_{tx} not transmitting data symbols due to the weak $\text{SU}_{\text{tx}}\text{-SU}_{\text{rx}}$ channel when the spectrum is sensed idle, i.e., $P_{\text{out}} = \Pr\{P = 0 \mid \hat{\mathcal{H}}_0\}$. This probability can be directly obtained using the CDF of $\hat{\nu}^*$

evaluated at the cut-off threshold as the following

$$\begin{aligned}
 P_{\text{out}} &= \Pr(\hat{\nu}^* \leq \zeta | \hat{\mathcal{H}}_0) = \omega_0 F_{\hat{\nu}^*}^0(\zeta) + \omega_1 F_{\hat{\nu}^*}^1(\zeta), \\
 P_{\text{out},S_1} &= \Pr(\hat{\nu}^* \leq \zeta_1 | \hat{\mathcal{H}}_0) = \omega_0 F_{\hat{\nu}^*}^0(\zeta_1) + \omega_1 F_{\hat{\nu}^*}^1(\zeta_1), \\
 P_{\text{out},S_2} &= \Pr(\hat{\nu}^* \leq \zeta_2 | \hat{\mathcal{H}}_0) = \omega_0 F_{\hat{\nu}^*}^0(\zeta_2) + \omega_1 F_{\hat{\nu}^*}^1(\zeta_2).
 \end{aligned}$$

Fig. 3.8 illustrates $P_{\text{out}}, P_{\text{out},S_2}, P_{\text{out},S_1}$ versus \bar{P}_{av} for $\bar{I}_{\text{av}} = -8$ dB. We observe that as \bar{P}_{av} increases the outage probabilities decrease. Moreover, for a given \bar{P}_{av} we have $P_{\text{out}} < P_{\text{out},S_2} < P_{\text{out},S_1}$. This is consistent with Fig. 3.5 which shows for a given \bar{P}_{av} , we have $\zeta < \zeta_1 < \zeta_2$. Combined this with the fact that the CDF $F_{\hat{\nu}^*}(\cdot)$ is an increasing function of its argument, we reach the conclusion that $P_{\text{out}} < P_{\text{out},S_2} < P_{\text{out},S_1}$.

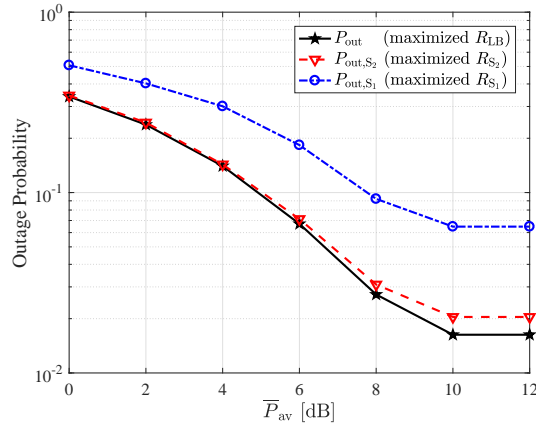


Figure 3.8: P_{out} versus \bar{P}_{av} for $\bar{I}_{\text{av}} = -8$ dB.

3.7 Conclusions

We considered an opportunistic CR system consisting of a PU, SU_{tx} , and SU_{rx} , where SU_{tx} is equipped with a RA that has M beams, and there is an error-free low-rate feedback channel from SU_{rx} to SU_{tx} . We proposed a system design for integrated sector-based spatial spectrum sensing and sector-based data symbol communication. We studied the entangled effects of spectrum sensing error, channel estimation error, and beam detection and beam selection errors (introduced by the RA), on the system achievable rates. We formulated a constrained optimization problem, where a lower bound on the achievable rate of $\text{SU}_{\text{tx}}-\text{SU}_{\text{rx}}$ link is maximized, subject to ATPC and AIC,

with the optimization variables being the durations of spatial spectrum sensing T_{se} and channel training T_{tr} as well as data symbol transmission power at SU_{tx} . Moreover, we proposed two alternative power adaptation schemes that are simpler to implement. We solved the proposed constrained optimization problems using iterative methods based on the BCD algorithm. Our simulation results demonstrate that one can increase the achievable rates of SU_{tx} - SU_{rx} link significantly, via implementing these optimizations, while maintaining the ATPC and AIC. They also showed that the achievable rates obtained from employing simple schemes 1 and 2 are very close to the one produced by the optimized transmit power. Our numerical results also showed that between optimizing T_{se} and T_{tr} , optimizing the latter has a larger effect on increasing the achievable rates in our system.

CHAPTER 4: STEADY-STATE RATE-OPTIMAL POWER ADAPTATION IN ENERGY HARVESTING OPPORTUNISTIC COGNITIVE RADIOS WITH SPECTRUM SENSING AND CHANNEL ESTIMATION ERRORS

In this chapter, we consider an uplink opportunistic EH-enabled CR network, consisting of N_u SUs and an AP, that can access a wideband spectrum licensed to a primary network. Each SU is capable of harvesting energy from natural ambient energy sources, and is equipped with a finite size rechargeable battery, to store the harvested energy. Our main *objectives* are (i) to study how the achievable sum-rate of SUs is impacted by the *combined effects* of spectrum sensing error and imperfect CSI of SUs–AP links (due to channel estimation error), and (ii) to design an energy management strategy that maximizes the achievable sum-rate of SUs, subject to a constraint on the average interference that SUs can impose on the PU. To the best of our knowledge, our work is the first to study the impact of these combined effects on the performance of an opportunistic EH-enabled CR network.

One expects that spectrum sensing error, combined with random energy arrival at the TX, exacerbates the effect of imperfect CSI on the TX achievable rate. The challenges of our study are twofold: first, it requires integration of energy harvesting, spectrum sensing, and channel estimation. Successful achievement of this integration entails stochastic modeling of energy arrival, energy storage, and PU's activities. These stochastic models are utilized to establish an achievable sum-rate of SUs that takes into account both spectrum sensing error and channel estimation error. Second, one needs to properly design energy control strategies for SUs, that strike a balance between the energy harvesting and the energy consumption, and adapt transmit power according to the available CSI and the battery state.

We assume that SUs operate under a time-slotted scheme, and SU_n is capable of harvesting energy during the entire time slot. Each time slot consists of three sub-slots corresponding to spectrum sensing phase (during which SU_n senses the spectrum), channel estimation phase (during which SU_n sends training symbols to the AP, when the spectrum is sensed idle, for estimating the fading coefficient corresponding to SU_n –AP link), and data transmission phase (during which SU_n sends data symbols to the AP). Assuming that the AP feeds back its estimate of the fading coefficient to SU_n , SU_n adapts its transmit power based on this information as well as the available energy in its battery.

4.1 System Model

We consider an uplink opportunistic EH-enabled CR network, operating in FDD mode, that can access a wideband spectrum band licensed to a primary network, consisting of M non-overlapping narrowband spectrum bands, each with a bandwidth of W Hz [121]. The primary network consists of a PU_{tx} and a PU_{rx} . The secondary network consists of an AP and N_{u} SUs (see Fig. 4.1).

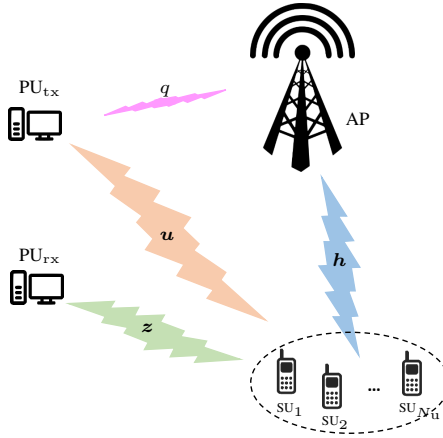


Figure 4.1: Schematics of the uplink CR network.

The AP can serve up to M SUs simultaneously and we assume that $N_{\text{u}} \leq M$. We also assume that narrowband spectrum bands are pre-assigned to SUs and thus each SU knows which band to sense and transmit data over. The SUs are equipped with identical energy harvesting circuits to harvest energy from the ambient environment and identical finite size batteries for energy storage (see Fig. 4.2). We consider block fading channel model and suppose flat fading coefficients from PU_{tx} to SU_n , PU_{tx} to AP, SU_n to PU_{rx} , and, SU_n to AP are four independent zero-mean complex Gaussian random variables, which we denote by u_n , q , z_n and h_n with variances δ_{u_n} , δ_q , δ_{z_n} and γ_n , respectively.

4.1.1 Battery and Energy Harvesting Models

We assume that SUs operate under a time-slotted scheme, with slot duration of T_f seconds, and they always have data to transmit. Each time slot is indexed by an integer t for $t = 1, 2, \dots$. The energy harvester at each SU stores randomly

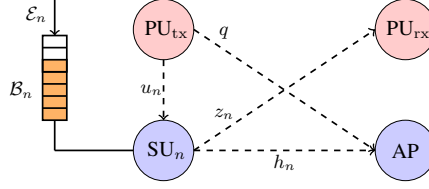


Figure 4.2: Our CR system model corresponding to SU_n for $n = 1, \dots, N_u$.

arrived energy packets in a finite size battery and consumes the stored (harvested) energy for spectrum sensing, channel estimation, and data transmission. Each battery consists of K cells (units) and the amount of energy stored in each unit is equal to e_u Joules. Thus, the battery can store up to Ke_u Joules of energy.

When k cells of the battery is charged (the amount of stored energy in the battery is ke_u Joules) we say that the battery is at state k . Let $\mathcal{B}_n^{(t)} \in \{0, 1, \dots, K\}$ denote the discrete random process indicating the battery state of SU_n at the beginning of time slot t . We define the Probability Mass Function (PMF) of the discrete random variable $\mathcal{B}_n^{(t)}$ as $\zeta_{k,n}^{(t)} = \Pr(\mathcal{B}_n^{(t)} = k)$, where $\sum_{k=0}^K \zeta_{k,n}^{(t)} = 1$. Note that $\mathcal{B}_n^{(t)} = 0$ and $\mathcal{B}_n^{(t)} = K$ represent the empty battery and full battery levels, respectively.

Let $\mathcal{E}_n^{(t)}$ denote the randomly arriving energy packets during time slot t of SU_n , where the energy packet measured in Jules is e_u Joules. The discrete random process $\mathcal{E}_n^{(t)}$ is typically modeled as a sequence of independent and identically distributed (i.i.d) random variables [53], regardless of the spectrum occupancy state of PU_{tx} . We assume that the discrete random variables $\mathcal{E}_n^{(t)}$'s are i.i.d. over time and independent across sensors. We model $\mathcal{E}_n^{(t)}$ as a Poisson random variable with the PMF $f_{\mathcal{E}_n}(r) = \Pr(\mathcal{E} = r) = e^{-\rho_n} \rho_n^r / r!$ for $r = 0, 1, \dots, \infty$, where ρ_n denotes the average number of arriving energy packets during one time slot of SU_n .¹ Let $\alpha_{h_n}^{(t)}$ be the number of stored (harvested) energy units in the battery at SU_n during time slot t . This harvested energy $\alpha_{h_n}^{(t)}$ cannot be used during time slot t . Since the battery has a finite capacity of K cells, we find that $\alpha_{h_n}^{(t)}$ is an element of the finite set $\{0, 1, \dots, K\}$. Also, $\alpha_{h_n}^{(t)}$ are i.i.d. over time slots and independent across sensors. Let $f_{\alpha_{h_n}}(r) = \Pr(\alpha_{h_n} = r)$ denote the PMF of $\alpha_{h_n}^{(t)}$. We can

¹We note that ρ_n does not depend on the duration of spectrum sensing phase, since we assume each node is capable of harvesting energy during the entire slot. If we limit harvesting energy to spectrum sensing phase, then ρ_n would change to $\rho_n T_{se} / T_f$. Poisson distribution for statistical modeling of ambient energy and solar energy has been applied before in [122]. We note, however, that our analysis is not tied to this specific distribution and can be applied for any discrete non-Poisson distribution.

find the PMF of $\alpha_{h_n}^{(t)}$ in terms of the PMF of $\mathcal{E}_n^{(t)}$ as the following²

$$f_{\alpha_{h_n}}(r) = \begin{cases} f_{\mathcal{E}_n}(r), & \text{if } 0 \leq r \leq K - 1 \\ \sum_{m=K}^{\infty} f_{\mathcal{E}_n}(m), & \text{if } r = K. \end{cases} \quad (4.1)$$

4.1.2 Slot Structure of SUs

Each time slot consists of three sub-slots (see Fig. 4.3), corresponding to spectrum sensing phase, channel estimation phase, and data transmission phase, with fixed durations of $T_{\text{se}} = N_{\text{se}}/f_s$, $T_{\text{tr}} = N_t/f_s$, $T_d = N_d/f_s$, respectively. Note that f_s is the sampling frequency, N_{se} is the number of collected samples during spectrum sensing phase, N_t is the number of training symbols sent during channel estimation phase, and N_d is the number of data symbols sent during data transmission phase. Also, we have $T_f = T_{\text{se}} + T_{\text{tr}} + T_d$.

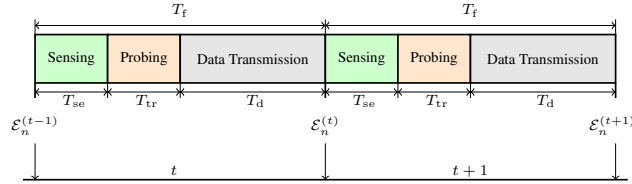


Figure 4.3: Slot structure of SUs.

During *spectrum sensing phase*, SU_n senses its pre-assigned single spectrum band to detect PU_{tx} 's activity. We model the PU_{tx} 's activity in each spectrum band as a Bernoulli random variable and we assume the statistics of PU_{tx} are i.i.d. across M spectrum bands and over time slots. Therefore, we can frame the spectrum sensing problem at SU_n as a binary hypothesis testing problem. Suppose $\mathcal{H}_1^{(t)}$ and $\mathcal{H}_0^{(t)}$ represent the binary hypotheses of PU_{tx} being active and inactive in time slot t , respectively, with prior probabilities $\Pr\{\mathcal{H}_1^{(t)}\} = \pi_1$ and $\Pr\{\mathcal{H}_0^{(t)}\} = \pi_0$. SU_n applies a binary detection rule to decide whether or not PU_{tx} is active in its pre-assigned band. Let $\hat{\mathcal{H}}_{0,n}$ and $\hat{\mathcal{H}}_{1,n}$, with probabilities $\hat{\pi}_{0,n} = \Pr\{\hat{\mathcal{H}}_{0,n}\}$ and $\hat{\pi}_{1,n} = \Pr\{\hat{\mathcal{H}}_{1,n}\}$ denote the SU_n detector outcome, i.e., the detector finds PU_{tx} active and inactive (the result of spectrum sensing is busy or idle), respectively. The accuracy of this binary detector is characterized by its false alarm and detection probabilities. The details of the binary detector are presented

²Equation (4.1) assumes that the energy storage process is lossless. For a lossy storage process, one needs to model such loss via establishing a functional relationship between α_{h_n} and \mathcal{E}_n , i.e., $\alpha_{h_n} = J_n(\mathcal{E}_n)$, where the function $J_n(\cdot)$ can be approximated using the battery type and specifications. Knowing $J_n(\cdot)$ and the pmf $f_{\mathcal{E}_n}(r)$, one can find the pmf $f_{\alpha_{h_n}}(r)$ using transformation method.

in Section 4.2.

Depending on the outcome of spectrum sensing, SU_n stays in spectrum sensing phase or enters *channel estimation phase*. In this phase, SU_n sends N_t training symbols with fixed symbol power $P_{tr} = \alpha_t e_u / T_{tr}$, to enable channel estimation at the AP, where α_t is the number of consumed cells of energy for channel estimation³. We assume that the battery always has α_t units of stored energy for channel estimation. Let $h_n^{(t)}$ denote the SU_n -AP fading coefficient in time slot t and $g_n^{(t)} = |h_n^{(t)}|^2$ be the corresponding channel power gain. Using the received signals corresponding to the training symbols, the AP estimates $\hat{h}_n^{(t)}$ and lets $\hat{g}_n^{(t)} = |\hat{h}_n^{(t)}|^2$ and shares this value with SU_n via a feedback channel. Next, SU_n enters *data transmission phase*. During this phase, SU_n sends N_d Gaussian data symbols with adaptive symbol power according to its battery state and the received information via the feedback channel about SU_n -AP link. If the battery is at state k , then SU_n allocates $\alpha_{k,n}$ cells of stored energy for each data symbol transmission, implying that the adaptive symbol power is $P_{k,n}^{(t)} = \alpha_{k,n}^{(t)} p_u$, where $p_u = e_u / T_d$. Note that since $\alpha_{k,n}^{(t)}$ is discrete, $P_{k,n}^{(t)}$ is discrete. The details of the choice of $\alpha_{k,n}^{(t)}$ according to the battery state k and the feedback information \hat{g}_n are given in Section 4.1.3 and the details of channel estimation are explained in Section 4.3.

4.1.3 Transmission Model and Battery Dynamics

As we stated, we assume that during time slot t , SU_n adapts its transmit energy per data symbol (power) according to its battery state k and the received information via the feedback channel about its channel power gain \hat{g}_n . In particular, we choose a power adaptation strategy that mimics the behavior of the rate-optimal power adaptation scheme with respect to the channel power gain [5], i.e., when \hat{g}_n is smaller than a cut-off threshold θ_n (to be optimized), the transmit energy is zero, and when \hat{g}_n exceeds θ_n , the transmit energy increases monotonically as \hat{g}_n increases until it reaches its maximum value of $\lfloor k\Omega_n \rfloor - \alpha_t$, where $\Omega_n \in [0, 1]$ (to be optimized), and $\lfloor \cdot \rfloor$ denotes the floor function. Mathematically, we express $\alpha_{k,n}^{(t)}$ for SU_n as the following

$$\alpha_{k,n}^{(t)} = \max \left\{ \bar{\alpha}_{k,n}^{(t)}, 0 \right\}, \quad \text{for } k = 0, 1, \dots, K, \quad (4.2a)$$

$$\bar{\alpha}_{k,n}^{(t)} = \left[\Omega_n k \left(1 - \frac{\theta_n}{\hat{g}_n^{(t)}} \right)^+ \right] - \alpha_t, \quad (4.2b)$$

³For ease of presentation, we assume that circuit power (energy) consumption is negligible in comparison to the consumed energy for channel estimation and data transmission. Otherwise, it can easily be incorporated into the system model.

where $(x)^+ = \max\{x, 0\}$. The parameters Ω_n and θ_n in (4.2) play key roles in balancing the energy harvesting and the energy consumption. Given θ_n , when Ω_n is large (or given Ω_n , when θ_n is small), such that the rate of energy consumption is greater than the rate of energy harvesting, SU_n may stop functioning, due to energy outage. On the other hand, given θ_n , when Ω_n is small (or given Ω_n , when θ_n is large), SU_n may fail to utilize the excess energy, due to energy overflow, and the data transmission would become limited in each slot. Note that $\bar{\alpha}_{k,n}^{(t)}$ in (4.2) ensures that the battery always has α_t units of stored energy for channel estimation. Furthermore, the transmission policy in (4.2) satisfies the causality constraint of the battery. The causality constraint restrains the energy corresponding to symbol transmit power to be less than the available stored energy in the battery, i.e., $\alpha_{k,n} \leq k - \alpha_t$. Note that $\alpha_{k,n}$ is discrete random variable and $\alpha_{k,n} \in \{0, 1, \dots, K\}$ ⁴. Let $\psi_{i,k,n}^\varepsilon = \Pr(\alpha_{k,n} = i | \mathcal{H}_\varepsilon)$ denote the conditional PMF of $\alpha_{k,n}$ given $\mathcal{H}_\varepsilon, \varepsilon = 0, 1$. We have

$$\psi_{i,k,n}^\varepsilon = \begin{cases} 1, & \text{if } 0 \leq k \leq \alpha_t, i = 0 \\ 0, & \text{if } 0 \leq k \leq \alpha_t, i \neq 0 \\ Y_{k,n}, & \text{if } k \geq \alpha_t + 1, i = 0 \\ Q_{i,k,n}, & \text{if } k \geq \alpha_t + 1, 1 \leq i \leq \lfloor k\Omega_n \rfloor - \alpha_t \\ 0, & \text{if } k \geq \alpha_t + 1, i \geq \lfloor k\Omega_n \rfloor - \alpha_t + 1 \end{cases} \quad (4.3)$$

in which

$$Q_{i,k,n} = F_{\hat{g}_n}^\varepsilon(c_{i,k,n}) - F_{\hat{g}_n}^\varepsilon(a_{i,k,n}) \quad (4.4a)$$

$$Y_{k,n} = F_{\hat{g}_n}^\varepsilon(\theta_n) + \sum_{m=1}^{\min(\lfloor k\Omega_n \rfloor, \alpha_t)} Q_{m-\alpha_t, k, n} \quad (4.4b)$$

$$a_{i,k,n} = \frac{\theta_n k \Omega_n}{k \Omega_n - \alpha_t - i}, \quad c_{i,k,n} = \frac{\theta_n k \Omega_n}{k \Omega_n - \alpha_t - i - 1}, \quad (4.4c)$$

where $F_{\hat{g}_n}^\varepsilon(x) = F_{\hat{g}_n}(x | \mathcal{H}_\varepsilon)$ is the CDF of \hat{g}_n given \mathcal{H}_ε . Note that if $c_{i,k,n} < 0$, we set $c_{i,k,n} = +\infty$.

The battery state at the beginning of time slot $t + 1$ depends on the battery state at the beginning of time slot t , the harvested energy during time slot t , the transmission symbol, as well as α_t . In particular, if at time slot t , SU_n senses

⁴Examining (4.2) we realize that the largest value that $\alpha_{k,n}^{(t)}$ can take is $K - \alpha_t$. Hence, the maximum transmit energy of SU_n is bounded by $K - \alpha_t$. The system designer can choose K such that signal distortion, due to the nonlinear behavior of power amplifiers, is prevented and the operation of power amplifiers in their linear regions is guaranteed.

its spectrum band to be idle, the state of its battery at the beginning of slot $t + 1$ is

$$\mathcal{B}_n^{(t+1)} = \min \left\{ \left(\mathcal{B}_n^{(t)} - \alpha_t - \alpha_{k,n}^{(t)} + \alpha_{h_n}^{(t)} \right)^+, K \right\}. \quad (4.5)$$

On the other hand if at time slot t , SU_n senses its spectrum band to be busy, the state of its battery at the beginning of slot $t + 1$ is

$$\mathcal{B}_n^{(t+1)} = \min \left\{ \left(\mathcal{B}_n^{(t)} + \alpha_{h_n}^{(t)} \right)^+, K \right\}, \quad (4.6)$$

since $\alpha_{k,n}^{(t)} = 0$. Considering the dynamic battery state model in (4.5) and (4.6) we note that, conditioned on $\alpha_{h_n}^{(t)}$ and $\alpha_{k,n}^{(t)}$ the value of $\mathcal{B}_n^{(t+1)}$ only depends on the value of $\mathcal{B}_n^{(t)}$ (and not the battery states of time slots before t). Hence, the battery state random process $\mathcal{B}_n^{(t)}$ can be modeled as a Markov chain (see Fig. 4.4). Let the probability vector of battery state in time slot t be $\zeta_n^{(t)} = [\zeta_{1,n}^{(t)}, \dots, \zeta_{K,n}^{(t)}]^T$. Note that the probability $\zeta_{k,n}^{(t)}$ depends on the battery state at slot $t - 1$, the number of battery units filled by the harvested energy during slot $t - 1$, the probability of spectrum band sensed idle, and, the number of energy units allocated for data transmission at slot $t - 1$ when the spectrum band is sensed idle, i.e., $\zeta_{k,n}^{(t)}$ depends on $\mathcal{B}_n^{(t-1)}$, $\alpha_{h_n}^{(t-1)}$, $\hat{\pi}_{0,n}$, $\alpha_{k,n}^{(t-1)}$, respectively. Assuming the Markov chain is time-homogeneous⁵, we let Φ_n denote the $(K + 1) \times (K + 1)$ transition probability matrix of this chain with its (i, j) -th entry $\phi_{i,j}^n = \Pr(\mathcal{B}_n^{(t)} = i | \mathcal{B}_n^{(t-1)} = j)$ given as

$$\phi_{0,j}^n = \sum_{l=0}^K \left[\psi_{l,j,n}^0 \hat{\pi}_{0,n} F_{\alpha_{h_n}}(\alpha_t + l - j) \right] + \hat{\pi}_{1,n} F_{\alpha_{h_n}}(-j) \quad (4.7a)$$

$$\phi_{K,j}^n = \sum_{l=0}^K \left[\psi_{l,j,n}^0 \hat{\pi}_{0,n} \left(1 - F_{\alpha_{h_n}}(\alpha_t + l + K - j) \right) \right] + \hat{\pi}_{1,n} \left(1 - F_{\alpha_{h_n}}(K - j) \right) \quad (4.7b)$$

$$\phi_{i,j}^n = \sum_{l=0}^K \left[\psi_{l,j,n}^0 \hat{\pi}_{0,n} f_{\alpha_{h_n}}(\alpha_t + l + i - j) \right] + \hat{\pi}_{1,n} f_{\alpha_{h_n}}(i - j), \quad \text{for } i = 1, \dots, K - 1 \quad (4.7c)$$

where $F_{\alpha_{h_n}}(\cdot)$ is the CDF of α_{h_n} . We have

$$\zeta_n^{(t+1)} = \Phi_n \zeta_n^{(t)}. \quad (4.8)$$

Since the Markov chain characterized by the transition probability matrix Φ_n is irreducible and aperiodic, there exists a unique steady-state distribution, regardless of the initial state [123]. Let $\zeta_n = \lim_{t \rightarrow \infty} \zeta_n^{(t)}$ be the unique steady-state

⁵A Markov chain is time-homogeneous (stationary) if and only if its transition probability matrix is time-invariant. Adopting homogeneous Markov chain model for studying EH-enabled communication systems is widely common [123].

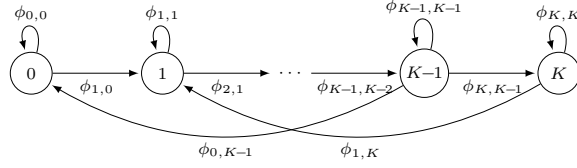


Figure 4.4: Schematics of Markov chain corresponding to the battery state random process $\mathcal{B}_n^{(t)}$.

probability vector. This vector satisfies the following equations

$$\zeta_n = \Phi_n \zeta_n, \quad (4.9a)$$

$$\zeta_n^T \mathbf{1} = \sum_{k=1}^K \zeta_{k,n} = 1, \quad (4.9b)$$

where $\mathbf{1}$ is an all-ones vector, i.e., ζ_n is the normalized eigenvector corresponding to the unit eigenvalue of Φ_n , such that the entries of ζ_n sums up to one. The closed-form expression for ζ_n is [124]

$$\zeta_n = (\Phi_n - I + B)^{-1} \mathbf{1}, \quad (4.10)$$

where B is an all-ones matrix and I is the identity matrix. From this point forward, we assume that the battery is at its steady-state and we drop the superscript t .

To illustrate our transmission model in (4.2) we consider the following simple numerical example. Assuming that the battery has $K = 7$ cells, Fig. 4.5 shows an example of $\alpha_{k,n}$ for our CR system for two sets of $\{\Omega_n, \theta_n\}$ given as $\Omega_n^{(a)} = 0.75, \theta_n^{(a)} = 0.02$ and $\Omega_n^{(b)} = 0.95, \theta_n^{(b)} = 0.02$. The corresponding transition probability matrices are given in the following

$$\Phi_n^{(a)} = \begin{pmatrix} 0.42 & 0.29 & 0.17 & 0.08 & 0.02 & 0 & 0 & 0 \\ 0.12 & 0.13 & 0.12 & 0.09 & 0.05 & 0.02 & 0 & 0 \\ 0.19 & 0.12 & 0.13 & 0.12 & 0.09 & 0.05 & 0.02 & 0 \\ 0.07 & 0.19 & 0.12 & 0.13 & 0.12 & 0.09 & 0.05 & 0.02 \\ 0.05 & 0.07 & 0.19 & 0.12 & 0.13 & 0.12 & 0.09 & 0.05 \\ 0.05 & 0.05 & 0.07 & 0.19 & 0.12 & 0.13 & 0.12 & 0.09 \\ 0.04 & 0.05 & 0.05 & 0.07 & 0.19 & 0.12 & 0.13 & 0.12 \\ 0.06 & 0.1 & 0.15 & 0.2 & 0.27 & 0.46 & 0.58 & 0.71 \end{pmatrix}, \quad \Phi_n^{(b)} = \begin{pmatrix} 0.54 & 0.43 & 0.31 & 0.18 & 0.08 & 0.03 & 0 & 0 \\ 0.18 & 0.11 & 0.13 & 0.12 & 0.1 & 0.06 & 0.02 & 0 \\ 0.04 & 0.18 & 0.11 & 0.13 & 0.12 & 0.1 & 0.06 & 0.02 \\ 0.04 & 0.04 & 0.18 & 0.11 & 0.13 & 0.12 & 0.1 & 0.06 \\ 0.05 & 0.04 & 0.04 & 0.18 & 0.11 & 0.13 & 0.12 & 0.1 \\ 0.05 & 0.05 & 0.04 & 0.04 & 0.18 & 0.11 & 0.13 & 0.12 \\ 0.04 & 0.05 & 0.05 & 0.04 & 0.04 & 0.18 & 0.11 & 0.13 \\ 0.06 & 0.1 & 0.15 & 0.2 & 0.24 & 0.28 & 0.46 & 0.57 \end{pmatrix}.$$

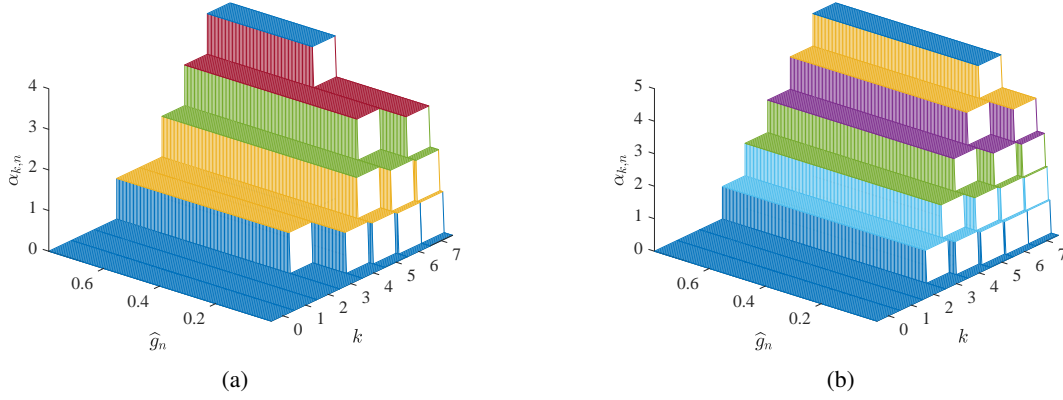


Figure 4.5: This example shows how many energy units ($\alpha_{k,n}$) SU_n spends for data transmission, given its battery state and the received information about its channel gain via feedback link. (a) $\Omega_n^{(a)} = 0.75$, $\theta_n^{(a)} = 0.02$, (b) $\Omega_n^{(b)} = 0.95$, $\theta_n^{(b)} = 0.02$.

Our goal is to find the transmission parameters $\{\Omega_n, \theta_n\}$ in (4.2b) for all SUs such that the uplink sum-rate of our CR network is maximized, subject to a constraint on the average interference that collective SUs can impose on PU_{rx} . We assume that this optimization problem is solved *offline* at AP, given the *statistical* information of (i) fading channels and noises, (ii) randomly arriving energy packets, and (iii) PU's activities, the number of samples collected during spectrum sensing phase N_{se} , the number of training symbols sent during channel probing phase N_t and power of training symbols P_{tr} . The solutions to this optimization problem, i.e., the optimal set $\{\Omega_n, \theta_n\}_{n=1}^{N_u}$ is available *a priori* at the AP and SUs, to be utilized for adapting symbol power during data transmission phase. The idea of offline power allocation optimization with a limited feedback channel has been used before for distributed detection systems in wireless sensor networks [125]. In the following sections, we describe how SUs operate during spectrum sensing phase, channel estimation phase, and data transmission phase. For the readers' convenience, we have collected the most commonly used symbols in Table 4.1.

4.2 Spectrum Sensing Phase

In order to access its spectrum band, SU_n first needs to sense its band during spectrum sensing phase, to determine whether it is busy or idle (see Fig. 4.3). We formulate the spectrum sensing at SU_n as a binary hypothesis testing

Table 4.1: Most commonly used symbols.

Symbol	Description
N_{se}	Number of collected samples during <i>spectrum sensing phase</i>
N_t	Number of training symbols during <i>channel estimation phase</i>
N_d	Number of data symbols during <i>data transmission phase</i>
P_{tr}	Power of training symbols
$h_n, \hat{h}_n, \tilde{h}_n$	Fading coefficient of SU _n -AP link, LMMSE channel estimate, and its corresponding estimation error
$\gamma_n, \hat{\gamma}_n, \tilde{\gamma}_n$	Variances of $h_n, \hat{h}_n, \tilde{h}_n$
π_0, π_1	Prior probabilities of \mathcal{H}_0 and \mathcal{H}_1
$\hat{\pi}_{0,n}, \hat{\pi}_{1,n}$	Probabilities of spectrum bands being sensed idle or busy
$\zeta_{k,n}$	Probability of SU _n battery being at state k
u_n	Fading coefficient of PU _{tx} -SU _n link with variance δ_{u_n}
q	Fading coefficient of PU _{tx} -AP link with variance δ_q
z_n	Fading coefficient of SU _n -PU _{rx} link with variance δ_{z_n}

problem, where the received signal at SU_n can be written as:

$$\begin{aligned} \mathcal{H}_0 &: y_n[m] = w_n[m], \\ \mathcal{H}_1 &: y_n[m] = u_n[m]p[m] + w_n[m], \end{aligned} \quad (4.11)$$

for $m = 1, \dots, N_{se}$, where $p[m]$ is the transmit signal of PU_{tx}, $w_n[m] \sim \mathcal{CN}(0, \sigma_{w_n}^2)$ is the Additive White Gaussian Noise (AWGN) at SU_n and $u_n[m]$ is the fading coefficient corresponding to PU_{tx}-SU_n channel. The two hypotheses \mathcal{H}_0 and \mathcal{H}_1 with probabilities π_0 and $\pi_1 = 1 - \pi_0$ denote the spectrum is truly idle and truly busy, respectively. We assume that π_0 and π_1 are known to SUs based on long-term spectrum measurements. For spectrum sensing we consider energy detector, where the decision statistics at SU_n is $Z_n = \frac{1}{N_{se}} \sum_{m=1}^{N_{se}} |y_n[m]|^2$. The accuracy of this detector is characterized by its false alarm probability $P_{fa_n} = \Pr(\hat{\mathcal{H}}_{1,n} | \mathcal{H}_0) = \Pr(Z_n > \xi_n | \mathcal{H}_0)$ and detection probability $P_{d_n} = \Pr(\hat{\mathcal{H}}_{1,n} | \mathcal{H}_1) = \Pr(Z_n > \xi_n | \mathcal{H}_1)$, where ξ_n is the local decision threshold. For large N_{se} , we can invoke central limit theorem and approximate the CDF of Z_n as Gaussian. Hence, P_{fa_n} and P_{d_n} can be expressed in terms of Q function as below [2]

$$P_{fa_n} = Q\left(\left(\frac{\xi_n}{\sigma_{w_n}^2} - 1\right)\sqrt{N_{se}}\right), \quad (4.12a)$$

$$P_{d_n} = Q\left(\left(\frac{\xi_n}{\sigma_{w_n}^2} - \nu_n - 1\right)\sqrt{\frac{N_{se}}{2\nu_n + 1}}\right), \quad (4.12b)$$

where $\nu_n = P_p \delta_{u_n} / \sigma_{w_n}^2$ and P_p is the average transmit power of PU_{tx}. For a given value of $P_{d_n} = \bar{P}_d$, the false alarm probability can be written as

$$P_{fa_n} = Q\left(\sqrt{2\nu_n + 1}Q^{-1}(\bar{P}_d) + \nu_n\sqrt{T_{\text{se}}f_s}\right). \quad (4.13)$$

The probabilities $\hat{\pi}_{0,n}$ and $\hat{\pi}_{1,n}$, are related to P_{d_n} and P_{fa_n} . In particular, we have $\hat{\pi}_{0,n} = \beta_{0,n} + \beta_{1,n}$ and $\hat{\pi}_{1,n} = 1 - \hat{\pi}_{0,n}$ where

$$\beta_{0,n} = \Pr\{\mathcal{H}_0, \hat{\mathcal{H}}_{0,n}\} = \pi_0(1 - P_{fa_n}), \quad (4.14a)$$

$$\beta_{1,n} = \Pr\{\mathcal{H}_1, \hat{\mathcal{H}}_{0,n}\} = \pi_1(1 - P_{d_n}). \quad (4.14b)$$

4.3 Channel Probing Phase

Depending on the outcome of its spectrum sensing, SU_n either stays in spectrum sensing phase (i.e., remains silent in the remaining of time slot) if its band is sensed busy (the detector outcome is $\hat{\mathcal{H}}_{1,n}$), or it enters channel estimation phase if its band is sensed idle (the detector outcome is $\hat{\mathcal{H}}_{0,n}$). During channel estimation phase, we assume SU_n sends training vector $\mathbf{x}_t = \sqrt{P_{\text{tr}}}\mathbf{1}$, where $\mathbf{1}$ is an $N_t \times 1$ all-ones vector to enable channel estimation at the AP. Let vector $\mathbf{s}_n = [s_n(1), \dots, s_n(N_t)]^T$ denote the discrete-time representation of received training symbols at the AP from SU_n. Assuming the fading coefficient h_n corresponding to SU_n–AP channel is unchanged during the entire time slot, we have

$$\begin{aligned} \mathcal{H}_0, \hat{\mathcal{H}}_{0,n}: \quad s_n[m] &= h_n\sqrt{P_{\text{tr}}} + v_n[m], \\ \mathcal{H}_1, \hat{\mathcal{H}}_{0,n}: \quad s_n[m] &= h_n\sqrt{P_{\text{tr}}} + q[m]p[m] + v_n[m], \end{aligned} \quad (4.15)$$

for $m = 1, \dots, N_t$, $v_n[m] \sim \mathcal{CN}(0, \sigma_{v_n}^2)$ is the AWGN at the AP, and $q[m]$ is the fading coefficient corresponding to PU_{tx}–AP channel. The LMMSE estimate of h_n given $\hat{\mathcal{H}}_{0,n}$ is [5, 117]

$$\hat{h}_n = C_{h_n \mathbf{s}_n} C_{\mathbf{s}_n}^{-1} \mathbf{s}_n, \quad (4.16a)$$

$$C_{h_n \mathbf{s}_n} = \mathbb{E}\{h_n \mathbf{s}_n^H | \hat{\mathcal{H}}_{0,n}\} = \gamma_n \sqrt{P_{\text{tr}}}\mathbf{1}, \quad (4.16b)$$

$$C_{\mathbf{s}_n} = \mathbb{E}\left\{\mathbf{s}_n \mathbf{s}_n^H | \hat{\mathcal{H}}_{0,n}\right\} = \omega_{0,n} \mathbb{E}\left\{\mathbf{s}_n \mathbf{s}_n^H | \mathcal{H}_0, \hat{\mathcal{H}}_{0,n}\right\} + \omega_{1,n} \mathbb{E}\left\{\mathbf{s}_n \mathbf{s}_n^H | \mathcal{H}_1, \hat{\mathcal{H}}_{0,n}\right\}, \quad (4.16c)$$

where

$$\omega_{0,n} = \Pr\{\mathcal{H}_0|\widehat{\mathcal{H}}_{0,n}\} = \frac{\pi_0(1 - P_{\text{fa}_n})}{\widehat{\pi}_{0,n}} = \frac{\beta_{0,n}}{\widehat{\pi}_{0,n}}, \quad (4.17a)$$

$$\omega_{1,n} = \Pr\{\mathcal{H}_1|\widehat{\mathcal{H}}_{0,n}\} = \frac{\pi_1(1 - P_{\text{d}_n})}{\widehat{\pi}_{0,n}} = \frac{\beta_{1,n}}{\widehat{\pi}_{0,n}}, \quad (4.17b)$$

and

$$\mathbb{E}\left\{s_n s_n^H | \mathcal{H}_0, \widehat{\mathcal{H}}_{0,n}\right\} = (\widehat{\gamma}_n^0 P_{\text{tr}} + \sigma_{v_n}^2) \mathbf{I}, \quad (4.18a)$$

$$\mathbb{E}\left\{s_n s_n^H | \mathcal{H}_1, \widehat{\mathcal{H}}_{0,n}\right\} = (\widehat{\gamma}_n^1 P_{\text{tr}} + \sigma_{v_n}^2 + \sigma_p^2) \mathbf{I}. \quad (4.18b)$$

After substituting (4.17) into (4.16), \widehat{h}_n reduces to

$$\widehat{h}_n = \frac{\gamma_n \sqrt{P_{\text{tr}}}}{\gamma_n P_{\text{tr}} N_t + \sigma_{v_n}^2 + \omega_{1,n} \sigma_p^2} \sum_{m=1}^{N_t} s_n[m], \quad (4.19)$$

where $\sigma_p^2 = P_p \delta_q$. The estimation error is $\widetilde{h}_n = h_n - \widehat{h}_n$, where \widehat{h}_n and \widetilde{h}_n are orthogonal random variables [117], and \widehat{h}_n and \widetilde{h}_n are zero mean. Approximating $q[m]p[m]$ as a zero-mean Gaussian random variable with variance σ_p^2 , we find that the estimate \widehat{h}_n given $\widehat{\mathcal{H}}_{0,n}$ is distributed as a Gaussian mixture random variable [5]. Let $\widehat{\gamma}_n$ and $\widetilde{\gamma}_n$, represent the variances of \widehat{h}_n and \widetilde{h}_n , respectively. Also, Let $\widehat{\gamma}_n^0$ and $\widehat{\gamma}_n^1$ represent the variances of \widehat{h}_n under $\{\mathcal{H}_0, \widehat{\mathcal{H}}_{0,n}\}$ and $\{\mathcal{H}_1, \widehat{\mathcal{H}}_{0,n}\}$, respectively. We have

$$\widehat{\gamma}_n^0 = \text{VAR}\{\widehat{h}_n | \mathcal{H}_0, \widehat{\mathcal{H}}_{0,n}\} = \frac{\gamma_n^2 P_{\text{tr}} N_t \left(\gamma_n P_{\text{tr}} N_t + \sigma_{v_n}^2 \right)}{\left(\gamma_n P_{\text{tr}} N_t + \sigma_{v_n}^2 + \omega_{1,n} \sigma_p^2 \right)^2}, \quad (4.20a)$$

$$\widehat{\gamma}_n^1 = \text{VAR}\{\widehat{h}_n | \mathcal{H}_1, \widehat{\mathcal{H}}_{0,n}\} = \frac{\gamma_n^2 P_{\text{tr}} N_t \left(\gamma_n P_{\text{tr}} N_t + \sigma_{v_n}^2 + \sigma_p^2 \right)}{\left(\gamma_n P_{\text{tr}} N_t + \sigma_{v_n}^2 + \omega_{1,n} \sigma_p^2 \right)^2}. \quad (4.20b)$$

Therefore, $\hat{\gamma}_n = \omega_{0,n}\hat{\gamma}_n^0 + \omega_{1,n}\hat{\gamma}_n^1$. Also, let $\tilde{\gamma}_n^0$ and $\tilde{\gamma}_n^1$ indicate the variances of \tilde{h}_n under $\{\mathcal{H}_0, \hat{\mathcal{H}}_{0,n}\}$ and $\{\mathcal{H}_1, \hat{\mathcal{H}}_{0,n}\}$, respectively. We have

$$\tilde{\gamma}_n^0 = \text{VAR}\{\tilde{h}_n|\mathcal{H}_0, \hat{\mathcal{H}}_{0,n}\} = \gamma_n - \hat{\gamma}_n^0, \quad (4.21a)$$

$$\tilde{\gamma}_n^1 = \text{VAR}\{\tilde{h}_n|\mathcal{H}_1, \hat{\mathcal{H}}_{0,n}\} = \gamma_n - \hat{\gamma}_n^1. \quad (4.21b)$$

Hence, $\tilde{\gamma}_n = \omega_{0,n}\tilde{\gamma}_n^0 + \omega_{1,n}\tilde{\gamma}_n^1$. For ideal spectrum sensing, we get $\omega_{0,n} = 1$ and $\omega_{1,n} = 0$ and \hat{h}_n becomes Gaussian. Let $F_{\hat{g}_n}^\varepsilon(x)$ denote the CDF of \hat{g}_n under $\{\mathcal{H}_\varepsilon, \hat{\mathcal{H}}_{0,n}\}$ for $\varepsilon = 0, 1$. Note that under $\{\mathcal{H}_\varepsilon, \hat{\mathcal{H}}_{0,n}\}$ for $\varepsilon = 0, 1$, \hat{h}_n is zero mean complex Gaussian. Hence, under $\{\mathcal{H}_\varepsilon, \hat{\mathcal{H}}_{0,n}\}$ for $\varepsilon = 0, 1$, \hat{g}_n is an exponential random variable with mean $\hat{\gamma}_n^\varepsilon$ and CDF

$$F_{\hat{g}_n}^\varepsilon(x) = 1 - e^{-\frac{x}{\hat{\gamma}_n^\varepsilon}}. \quad (4.22)$$

The CDF of \hat{g}_n , denoted as $F_{\hat{g}_n}^\varepsilon(x)$, can be expressed in terms of $F_{\hat{g}_n}^0(x)$ and $F_{\hat{g}_n}^1(x)$ as the following:

$$F_{\hat{g}_n}(x) = \omega_{0,n}F_{\hat{g}_n}^0(x) + \omega_{1,n}F_{\hat{g}_n}^1(x). \quad (4.23)$$

After channel estimation, the AP feeds back the channel gains $\hat{g}_n = |\hat{h}_n|^2$ over a feedback link to SU_n .

4.4 Data Transmission Phase

After channel estimation phase, SU_n enters this phase. We note that entering this phase is only possible, if in spectrum sensing phase the outcome of the binary detector is $\hat{\mathcal{H}}_{0,n}$. During this phase, SU_n sends Gaussian data symbols to the AP, while it adapts its transmission power according to information provided by the AP through the feedback channel about SU_n -AP link as well as its battery state. In particular, SU_n transmits N_d zero-mean i.i.d. complex Gaussian symbols $x_n[m]$ for $m = 1, \dots, N_d$ with power $P_{k,n} = \alpha_{k,n}p_u$, when the battery is at state k and $\alpha_{k,n}$ is given in (4.2). Let $s_n[m]$ denote the discrete-time representation of received signal at the AP from SU_n . Due to error in spectrum sensing, we need to distinguish the signal model for $s_n[m]$ under \mathcal{H}_0 and \mathcal{H}_1 . We have

$$\mathcal{H}_0, \hat{\mathcal{H}}_{0,n}: s_n[m] = h_n x_n[m] + v_n[m], \quad (4.24)$$

$$\mathcal{H}_1, \hat{\mathcal{H}}_{0,n}: s_n[m] = h_n x_n[m] + q[m]p[m] + v_n[m].$$

Substituting $h_n = \hat{h}_n + \tilde{h}_n$ in (4.24), we reach at⁶

$$\begin{aligned} \mathcal{H}_0, \hat{\mathcal{H}}_{0,n}: s_n[m] &= \hat{h}_n x_n[m] + \overbrace{\tilde{h}_n x_n[m] + v_n[m]}^{\text{new noise } \eta_{n,0}[m]}, \\ \mathcal{H}_1, \hat{\mathcal{H}}_{0,n}: s_n[m] &= \hat{h}_n x_n[m] + \overbrace{\tilde{h}_n x_n[m] + q[m]p[m] + v_n[m]}^{\text{new noise } \eta_{n,1}[m]}, \end{aligned} \quad (4.25)$$

where the new noise terms depend on \tilde{h}_n . Given \hat{g}_n at the AP, we obtain an achievable rate expression for a time slot by considering symbol-wise mutual information between channel input and output over the duration of N_d data symbols as follows

$$R_n = \frac{WD_d}{N_d} \sum_{m=1}^{N_d} \left[\beta_{0,n} \mathbb{E} \left\{ I(x_n[m]; s_n[m] | \hat{g}_n, \mathcal{H}_0, \hat{\mathcal{H}}_{0,n}) \right\} + \beta_{1,n} \mathbb{E} \left\{ I(x_n[m]; s_n[m] | \hat{g}_n, \mathcal{H}_1, \hat{\mathcal{H}}_{0,n}) \right\} \right], \quad (4.26)$$

where $D_d = T_d/T_f$ is the fraction of the time slot used for data transmission and the expectations in (4.26) are taken over the conditional PDFs of \hat{g}_n given $\{\mathcal{H}_\varepsilon, \hat{\mathcal{H}}_{0,n}\}$ for $\varepsilon = 0, 1$. To characterize R_n in (4.26) we need to find $\mathbb{E}\{I(x_n[m]; s_n[m] | \hat{g}_n, \mathcal{H}_\varepsilon, \hat{\mathcal{H}}_{0,n})\}$. Exploiting the chain rule we can rewrite this expectation as follows

$$\mathbb{E} \left\{ I(x_n[m]; s_n[m] | \hat{g}_n, \mathcal{H}_\varepsilon, \hat{\mathcal{H}}_{0,n}) \right\} = \sum_{k=0}^K \zeta_{k,n} I(x_n[m]; s_n[m] | \hat{g}_n, k, \mathcal{H}_\varepsilon, \hat{\mathcal{H}}_{0,n}). \quad (4.27)$$

Note that $I(x_n[m]; s_n[m] | \hat{g}_n, \mathcal{H}_\varepsilon, \hat{\mathcal{H}}_{0,n})$ in (4.27) is the mutual information between $x_n[m]$ and $s_n[m]$ when the battery state is k , given \hat{g}_n and $\{\mathcal{H}_\varepsilon, \hat{\mathcal{H}}_{0,n}\}$. From now on, we drop the variable m in $x_n[m]$ and $s_n[m]$ for brevity of the presentation. Focusing on $I(x_n; s_n | \hat{g}_n, \mathcal{H}_\varepsilon, \hat{\mathcal{H}}_{0,n})$, we have

$$I(x_n; s_n | \hat{g}_n, k, \mathcal{H}_\varepsilon, \hat{\mathcal{H}}_{0,n}) = h(x_n | \hat{g}_n, k, \hat{\mathcal{H}}_{0,n}, \mathcal{H}_\varepsilon) - h(x_n | s_n, \hat{g}_n, k, \hat{\mathcal{H}}_{0,n}, \mathcal{H}_\varepsilon), \quad (4.28)$$

where $h(\cdot)$ is the differential entropy. Consider the first term in (4.28). Since $x_n \sim \mathcal{CN}(0, P_{k,n})$ we have $h(x_n | \hat{g}_n, k, \hat{\mathcal{H}}_{0,n}, \mathcal{H}_\varepsilon) = \log_2(\pi e P_{k,n})$. Consider the second term in (4.28). Due to channel estimation error, the new noises $\eta_{n,\varepsilon}$'s in (4.25) are non-Gaussian and this term does not have a closed form expression. Hence, similar to [107, 111, 118] we employ bounding techniques to find an upper bound on this term. This term is upper bounded by the entropy of a Gaussian

⁶We note that under \mathcal{H}_ε , our channel model $h_n = \hat{h}_n + \tilde{h}_n$ can be extended to include both the effects of channel estimation error and delayed feedback due to SU_n 's mobility. In particular, we can model $h_n = \chi \tilde{h}_n + z_n$, where the parameter $\chi = J_0(2\pi v T_f / \lambda)$ is from Jakes' model for Rayleigh fading [115], v is the velocity of SU_n , and λ is the wavelength of transmit signal, \tilde{h}_n is the outdated CSI available at SU_n , and $z_n \sim \mathcal{CN}(0, (1 - \chi^2)\tilde{\gamma}_n^\varepsilon + \tilde{\gamma}_n^\varepsilon)$. Substituting this channel model in (4.24) we reach at a signal model that is different from (4.25), which can be used to derive a new rate lower bound $R_{n,\text{LB}}$.

random variable with the variance $\Theta_M^{n,\varepsilon}$

$$\Theta_M^{n,\varepsilon} = \mathbb{E} \left\{ \left| x_n - \mathbb{E} \left\{ x_n \mid \hat{g}_n, k, \hat{\mathcal{H}}_{0,n}, \mathcal{H}_\varepsilon \right\} \right|^2 \right\}, \quad (4.29)$$

where the expectations are taken over the conditional pdf of x_n given $s_n, \hat{g}_n, k, \hat{\mathcal{H}}_{0,n}, \mathcal{H}_\varepsilon$. In fact, $\Theta_M^{i,\varepsilon}$ is the MSE of the MMSE estimate of x_n given $s_n, \hat{g}_n, k, \hat{\mathcal{H}}_{0,n}, \mathcal{H}_\varepsilon$. Using minimum variance property of MMSE estimator, we have $\Theta_M^{n,\varepsilon} \leq \Theta_L^{n,\varepsilon}$, where $\Theta_L^{n,\varepsilon}$ is the MSE of the LMMSE estimate of x_n given $s_n, \hat{g}_n, k, \hat{\mathcal{H}}_{0,n}, \mathcal{H}_\varepsilon$. Combining all, we find $h(x_n | s_n, \hat{g}_n, k, \hat{\mathcal{H}}_{0,n}, \mathcal{H}_\varepsilon) \leq \log_2(\pi e \Theta_L^{n,\varepsilon})$ and $I(x_n; s_n | \hat{g}_n, k, \hat{\mathcal{H}}_{0,n}, \mathcal{H}_\varepsilon) \geq \log_2(P_{k,n}/\Theta_L^{n,\varepsilon})$ where

$$\Theta_L^{n,\varepsilon} = \frac{P_{k,n} \sigma_{\eta_{n,\varepsilon}}^2}{\sigma_{\eta_{n,\varepsilon}}^2 + \hat{g}_n P_{k,n}}, \quad (4.30)$$

$$\sigma_{\eta_{n,\varepsilon}}^2 = \tilde{\gamma}_n^\varepsilon P_{k,n} + \sigma_{v_n}^2 + \varepsilon \sigma_p^2. \quad (4.31)$$

At the end, we obtain the lower bounds as follow

$$I(x_n; s_n | \hat{g}_n, k, \hat{\mathcal{H}}_{0,n}, \mathcal{H}_0) \geq \log_2 \left(1 + \hat{g}_n b_{k,n}^0 \right), \quad (4.32a)$$

$$I(x_n; s_n | \hat{g}_n, k, \hat{\mathcal{H}}_{0,n}, \mathcal{H}_1) \geq \log_2 \left(1 + \hat{g}_n b_{k,n}^1 \right), \quad (4.32b)$$

where

$$b_{k,n}^0 = \frac{P_{k,n}}{(\tilde{\gamma}_n^0 P_{k,n} + \sigma_{v_n}^2)}, \quad b_{k,n}^1 = \frac{P_{k,n}}{(\tilde{\gamma}_n^1 P_{k,n} + \sigma_{v_n}^2 + \sigma_p^2)}. \quad (4.33)$$

Substituting equations (4.27) and (4.32) in (4.26) and noting that the symbol-wise mutual information between channel input and output for N_d data symbols are equal we reach at

$$\begin{aligned} R_n \geq R_{n,\text{LB}} &= D_d \beta_{0,n} W \sum_{k=0}^K \zeta_{k,n} \mathbb{E} \left\{ \log_2 \left(1 + \hat{g}_n b_{k,n}^0 \right) \mid \mathcal{H}_0 \right\} \\ &+ D_d \beta_{1,n} W \sum_{k=0}^K \zeta_{k,n} \mathbb{E} \left\{ \log_2 \left(1 + \hat{g}_n b_{k,n}^1 \right) \mid \mathcal{H}_1 \right\}. \end{aligned} \quad (4.34)$$

Next, we compute the conditional expectations in (4.34), in which we take average over \hat{g}_n , given \mathcal{H}_ε . Using (4.3) and (4.4c) we have

$$\mathbb{E} \left\{ \log_2 \left(1 + \hat{g}_n b_{k,n}^\varepsilon \right) | \mathcal{H}_\varepsilon \right\} = \sum_{i=1}^{\lfloor k\Omega_n \rfloor - \alpha_t} \int_{a_{i,k,n}}^{c_{i,k,n}} \log_2 \left(1 + \mathbf{S}_{i,n}^\varepsilon x \right) f_{\hat{g}_n}^\varepsilon(x) dx = \sum_{i=1}^{\lfloor k\Omega_n \rfloor - \alpha_t} V_k(\mathbf{S}_{i,n}^\varepsilon, \hat{\gamma}_n^\varepsilon) \quad (4.35a)$$

in which

$$\mathbf{S}_{i,n}^0 = \frac{i p_u}{(\hat{\gamma}_n^0 i p_u + \sigma_{v_n}^2)}, \quad \mathbf{S}_{i,n}^1 = \frac{i p_u}{(\hat{\gamma}_n^1 i p_u + \sigma_{v_n}^2 + \sigma_p^2)}, \quad (4.35b)$$

$$V_k(\mathbf{S}_{i,n}, \hat{\gamma}_n) = M(c_{i,k,n}, \mathbf{S}_{i,n}, \hat{\gamma}_n) - M(a_{i,k,n}, \mathbf{S}_{i,n}, \hat{\gamma}_n), \quad (4.35c)$$

and

$$M(x, \mathbf{S}, w) = \int \log_2(1 + \mathbf{S}x) \frac{e^{-\frac{x}{w}}}{w} dx = \frac{e^{\frac{1}{\mathbf{S}w}}}{\ln(2)} \text{Ei} \left(\frac{-x}{w} - \frac{1}{\mathbf{S}w} \right) - e^{-\frac{x}{w}} \log_2(1 + \mathbf{S}x). \quad (4.36)$$

Also, $c_{i,k,n}$ and $a_{i,k,n}$ are given in (4.4c). Substituting (4.35a) in (4.34) we reach to

$$R_{n,\text{LB}} = D_d \beta_{0,n} W \sum_{k=\alpha_t+1}^K \sum_{i=1}^{\lfloor k\Omega_n \rfloor - \alpha_t} \zeta_{k,n} V_k(\mathbf{S}_{i,n}^0, \hat{\gamma}_n^0) + D_d \beta_{1,n} W \sum_{k=\alpha_t+1}^K \sum_{i=1}^{\lfloor k\Omega_n \rfloor - \alpha_t} \zeta_{k,n} V_k(\mathbf{S}_{i,n}^1, \hat{\gamma}_n^1). \quad (4.37)$$

We note that the lower bounds in (4.32) are achieved when the new noises $\eta_{n,0}, \eta_{n,1}$ in (4.25) are regarded as worst-case Gaussian noise and hence the MMSE and LMMSE of x_n given $s_n, \hat{g}_n, k, \hat{\mathcal{H}}_{0,n}, \mathcal{H}_\varepsilon$ coincide. Given the rate lower bound $R_{n,\text{LB}}$ for SU_n , the uplink sum-rate lower bound for all SU_n 's is

$$R_{\text{LB}} = \sum_{n=1}^{N_u} R_{n,\text{LB}}. \quad (4.38)$$

So far, we have established a sum-rate lower bound on the achievable sum-rate. Next, we characterize the average AIC. Suppose \bar{I}_{av} is the maximum allowed average interference, i.e., the average interference that collective SUs impose on PU_{rx} cannot exceed \bar{I}_{av} . To satisfy AIC, we have

$$\sum_{n=1}^{N_u} I_n \leq \bar{I}_{\text{av}}, \quad (4.39)$$

where I_n is the average interference power that SU_n imposes on PU_{rx} . We find

$$I_n = \beta_{1,n} \mathbb{E}\{z_n\} \left[D_d \mathbb{E} \left\{ P_n(\hat{g}_n) \right\} + D_{\text{tr}} P_{\text{tr}} \right] \quad (4.40)$$

where $D_{\text{tr}} = T_{\text{tr}}/T_{\text{f}}$ and the expectation is over the conditional pdfs of \hat{g}_n under $\{\mathcal{H}_1, \hat{\mathcal{H}}_{0,n}\}$. Considering the right side of (4.40), we note that the first term is the average interference power imposed on PU_{rx} when SU_n transmits data symbols, and the second term is the average interference imposed on PU_{rx} when SU_n sends training symbols for channel estimation at the AP. Using (4.3) we compute the term with expectation inside (4.40) as follows

$$\mathbb{E}\left\{P_n(\hat{g}_n)\right\} = \sum_{k=0}^K \zeta_{k,n} \sum_{i=0}^K \Pr(\alpha_{k,n} = i | \mathcal{H}_1) i p_{\text{u}} = \sum_{k=\alpha_t+1}^K \zeta_{k,n} \sum_{i=1}^{\lfloor k\Omega_n \rfloor - \alpha_t} \psi_{i,k,n}^1 i p_{\text{u}}. \quad (4.41)$$

Substituting (4.41) into (4.39), we can rewrite the AIC in (4.39) as

$$\sum_{n=1}^{N_{\text{u}}} \beta_{1,n} \delta_{z_n} \left[\sum_{k=\alpha_t+1}^K \zeta_{k,n} \sum_{i=1}^{\lfloor k\Omega_n \rfloor - \alpha_t} \psi_{i,k,n}^1 i p_{\text{u}} + D_{\text{tr}} P_{\text{tr}} \right] \leq \bar{I}_{\text{av}}. \quad (4.42)$$

For ideal spectrum sensing we get $\beta_{1,n} = 0$ in (4.14), implying that data transmission from SUs to the AP does not cause interference on PU_{rx} and the left-hand side of (4.42) becomes zero, i.e., the AIC is always satisfied.

Next, we examine how spectrum sensing error and channel estimation error affect R_{LB} and AIC expressions. First, spectrum sensing error affects AIC via $\beta_{1,n}$, and R_{LB} via $\beta_{0,n}$ and $\beta_{1,n}$. Recall $\beta_{0,n}, \beta_{1,n}$ depend on $\pi_0, P_{\text{fa},n}, P_{\text{d},n}$ (see (4.14)). Second, channel estimation error affects AIC via $D_{\text{tr}}, \psi_{i,k,n}^1$, and R_{LB} via $\tilde{\gamma}_n^\varepsilon$.

Having the mathematical expressions for R_{LB} and AIC, our goal is to optimize the set of transmission parameters $\{\Omega_n, \theta_n\}$ for all SUs such that R_{LB} is maximized, subject to the AIC. To inspect the underlying trade-offs between decreasing the average interference imposed by SU_n 's on PU_{rx} and increasing the sum-rate lower bound R_{LB} , we note that increasing data symbol transmission power $P_{k,n}$ increases R_{LB} . However, it increases the average interference. Aiming to strike a balance between increasing R_{LB} and decreasing the imposed average interference, we seek the optimal $\{\Omega_n, \theta_n\}_{n=1}^{N_{\text{u}}}$ such that R_{LB} in (4.34) is maximized, subject to AIC given in (4.42). In other words, we are

interested in solving the following constrained optimization problem

$$\begin{aligned}
& \underset{\{\Omega_n, \theta_n\}_{n=1}^{N_u}}{\text{Maximize}} \quad R_{\text{LB}} & (4.P1) \\
& \text{s.t.:} \quad \Omega_n \in [0, 1], \forall n \\
& \quad \theta_n \geq 0, \forall n \\
& \quad \zeta_n = \left(\Phi_n - \mathbf{I} + \mathbf{B} \right)^{-1} \mathbf{1}, \forall n \\
& \quad \text{AIC in (4.42) is satisfied.}
\end{aligned}$$

Problem (4.P1) is not convex with respect to $\{\Omega_n, \theta_n\}_{n=1}^{N_u}$. Unfortunately, the objective function and the constraints in (4.P1) are *not differentiable* with respect to $\{\Omega_n, \theta_n\}_{n=1}^{N_u}$. Hence, existing gradient-based algorithms for solving non-convex optimization problems cannot be used to solve (4.P1). We resort to a grid-based search method, which requires $2N_u$ -dimensional search over the search space $[0, 1]^{N_u} \times [0, \infty)^{N_u}$.

To reduce the computation complexity of solving (4.P1), we propose to decompose (4.P1) to N_u sub-problems corresponding to N_u SUs. To achieve such decomposition, we assume that I_n in (4.40) cannot exceed \bar{I}_{av}/N_u . Let (4.SP1-SU $_n$) refer to the sub-problem corresponding to SU $_n$. We have

$$\begin{aligned}
& \underset{\{\Omega_n, \theta_n\}}{\text{Maximize}} \quad R_{n,\text{LB}} & (4.SP1-SU_n) \\
& \text{s.t.:} \quad \Omega_n \in [0, 1], \\
& \quad \theta_n \geq 0, \\
& \quad \zeta_n = \left(\Phi_n - \mathbf{I} + \mathbf{B} \right)^{-1} \mathbf{1}, \\
& \quad I_n \leq \bar{I}_{\text{av}}/N_u.
\end{aligned}$$

We solve sub-problem (4.SP1-SU $_n$) for $n = 1, \dots, N_u$, using a grid-based search method, which requires 2-dimensional search over the search space $[0, 1] \times [0, \infty)$. To curb the computational complexity of these searches, we can limit θ_n 's to a maximum value, denoted as θ_{max} . We refer to the solutions obtained from solving (4.P1) and solving N_u sub-problems, respectively, the ‘‘optimal’’ and the ‘‘sub-optimal’’ solutions. Clearly, the accuracy of these solutions depend on the resolution of the grid-based searches. We call the former solution the ‘‘optimal’’, in the sense that it is the best achievable solution, and the latter solution the ‘‘sub-optimal’’, in the sense that solving N_u sub-problems always

yield a sub-optimal solution, with respect to solving (4.P1), since AIC in (4.P1) is coupled across all SUs. When \bar{T}_{av} in (4.39) is large enough such that AIC is not active, the “optimal” and “sub-optimal” solutions become identical. In the following, we compare the computational complexity of finding the “optimal” and “sub-optimal” solutions.

For finding both the “optimal” and the “sub-optimal” solutions, SU_n needs to perform two tasks for each point in its grid-based search: task (i) forming Φ_n and solving (4.10) to find ζ_n , task (ii) calculating $R_{n,LB}$ and I_n . Our numerical results show that for a fixed Ω_n, θ_n , the computational complexity of task (i) and task (ii) are $\mathcal{O}(K^{3.1})$ and $\mathcal{O}(K^{2.1})$, respectively. Assuming that the intervals $[0, 1]$ and $[0, \theta_{max}]$ are divided into N_Ω and N_θ sub-intervals, respectively, we realize that SU_n needs to perform task (i) and task (ii) for $N_\Omega N_\theta$ times in total. Therefore, the computational complexity of finding the “sub-optimal” solution is $\mathcal{O}(N_u N_\Omega N_\theta (K^{3.1} + K^{2.1}))$, which can be simplified to $\mathcal{O}(N_u N_\Omega N_\theta K^{3.1})$.

To solve (4.P1), however, the leftmost summation in (4.42) must be computed for all combinations of $\{\Omega_n, \theta_n\}_{n=1}^{N_u}$ and its computational complexity is $\mathcal{O}((N_\Omega N_\theta K^{2.1})^{N_u})$. Therefore, the computational complexity of finding the “optimal” solution is $\mathcal{O}((N_\Omega N_\theta K^{2.1})^{N_u} + N_u N_\Omega N_\theta K^{3.1})$, which for $N_u \geq 2$ can be simplified to $\mathcal{O}((N_\Omega N_\theta K^{2.1})^{N_u})$. We note that the computational complexity of obtaining the “optimal” and the “sub-optimal” solutions grow exponentially and linearly, respectively, in N_u .

4.5 Simulation Results

In this section we corroborate our analysis on constrained maximization of the achievable uplink sum-rate lower bound with Matlab simulations, and examine how the optimized uplink sum-rate lower bound depends on the average number of harvesting energy packets ρ_n , the maximum allowed average interference power \bar{T}_{av} , the duration of spectrum sensing phase T_{se} , the number of consumed cells of energy for channel probing α_t , and the size of the battery K . Our simulation parameters are given in Table 4.2.

• **Spectrum sensing-channel probing-data transmission trade-offs:** To explore these trade-offs, in this section we let $N_u = 1$ and examine how the rate lower bound R_{LB} in (4.38) for a single user changes when we vary T_{se} , or α_t . The simulation parameters, except for $\alpha_t, T_{se}, \sigma_w^2, \sigma_v^2$ are given in Table 4.2 ⁷.

⁷Note that the variances of channel estimate and corresponding estimation error in (4.20) depend on the product $P_{tr} N_t = \alpha_t e_u f_s$ and is independent of T_{tr} . That is the reason, instead of T_{tr} , we consider varying α_t , to understand channel probing trade-offs.

Table 4.2: Simulation Parameters

Parameter	Value	Parameter	Value
P_p	1 watts	$\sigma_{v_n}^2$	1
π_0	0.7	$\sigma_{w_n}^2$	1
T_{tr}	0.1 ms	α_t	1
T_{se}	1 ms	\bar{P}_d	0.85
T_f	10 ms	W	10 KHz
e_u	0.01	δ_q	1

Fig. 4.6a shows R_{LB} versus T_{se} for two values of the energy harvesting parameter $\rho = 15, 16$, $\sigma_w^2 = \sigma_v^2 = 1$ and $\alpha_t = 1$. This figure suggests that there exists a trade-off between T_{se} and R_{LB} . On the positive side, as T_{se} (or equivalently N_{se}) increases, the accuracy of the energy detector for spectrum sensing increases (i.e., P_{fa_n} in (4.12b) decreases). A more accurate spectrum sensing can reveal new opportunities for SU_n to be exploited for its data transmission, that can increase R_{LB} . On the negative side, as T_{se} increases, the duration of data transmission phase $T_d = T_f - T_{se} - T_{tr}$ decreases. This trade-off between spectrum sensing and data transmission indicates that, given the parameters (including α_t), there is an optimal T_{se} , denoted as T_{se}^* in Fig. 4.6a, that maximizes R_{LB} . For instance, for $\rho = 15, 16$ we have $T_{se}^* = 0.6, 0.75$ ms.

Fig. 4.6b plots R_{LB} versus α_t for $\rho = 18, 20$, $T_{se} = 1$ ms and $\sigma_w^2 = \sigma_v^2 = 5$. This figure suggests that a trade-off exists between α_t and R_{LB} . On the positive side, as α_t increases, the accuracy of channel probing (measured by the variance of channel estimation error in (4.20)) improves. A more accurate channel probing can increase R_{LB} . On the negative side, as α_t increases, the available energy for data transmission decreases. This trade-off between channel probing and data transmission shows that, given the parameters (including T_{se}), there is an optimal α_t , denoted as α_t^* in Fig. 4.6b, that maximizes R_{LB} . For instance, for $\rho = 15, 16$ we have $\alpha_t^* = 4$. The x -axis in Fig. 4.6b can be converted to the normalized channel estimation error variance $\tilde{\gamma}/\gamma$.

• **Effect of the optimization variables Ω, θ :** In this section, we let $N_u = 1$ and we illustrate how the entries of the steady-state probability vector ζ in (4.10), R_{LB} in (4.38) for a single user, and the battery outage probability P_b^{Out} defined below, the spectral efficiency η_{SE} and the energy efficiency η_{EE} defined below, depend on the optimization variables Ω and θ . We define $P_{b_n}^{Out}$ as the steady-state probability of the battery of SU_n being equal or lower than α_t . When the battery is at outage, it cannot yield energy for data transmission or channel probing. We have

$$P_{b_n}^{Out} = \Pr(\mathcal{B}_n \leq \alpha_t) = \sum_{k=0}^{\alpha_t} \zeta_{k,n}. \quad (4.43)$$

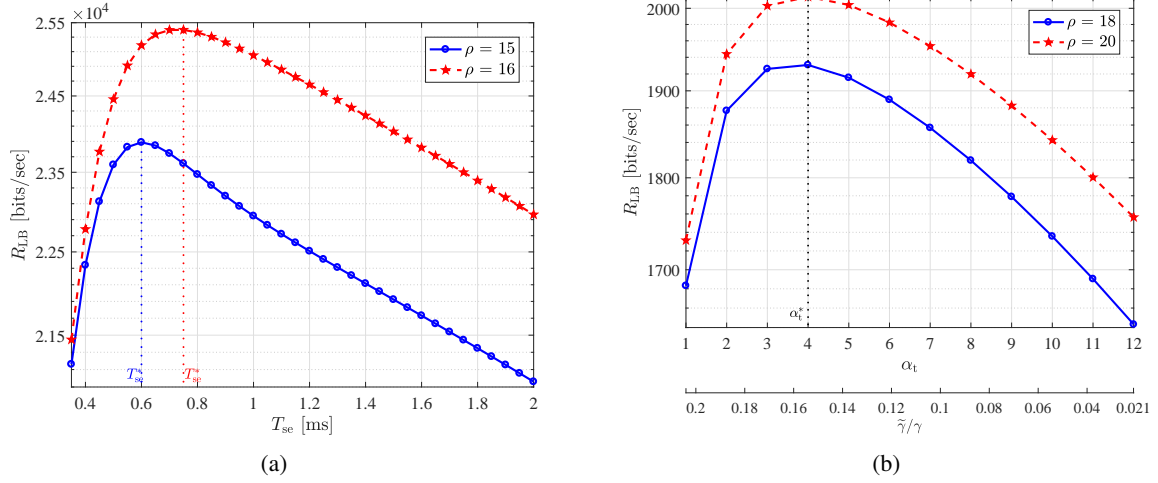


Figure 4.6: (a) R_{LB} versus T_{se} for $K = 80, \theta = 0.25, \Omega = 0.35, \sigma_w^2 = \sigma_v^2 = 1$, (b) R_{LB} versus α_t for $K = 200, \theta = 0.25, \Omega = 0.35, \sigma_w^2 = \sigma_v^2 = 5$.

We define the spectral efficiency of our CR system, denoted as η_{SE} and measured in bits/sec/Hz, as

$$\eta_{SE} = \frac{R_{LB}}{\text{total available bandwidth}} = \frac{R_{LB}}{MW} \quad (4.44)$$

Inspired by [126], we define the energy efficiency of our CR system, denoted as η_{EE} and measured in bits/Hz/Joule, as

$$\eta_{EE} = \frac{\eta_{SE}}{\text{average transmit power of all SUs}}. \quad (4.45)$$

Let \bar{P} denote the average transmit power of all SUs during channel probing and data transmission phases in our CR system. We find \bar{P} as the following

$$\bar{P} = D_d \sum_{n=1}^{N_u} \sum_{k=\alpha_t+1}^K \zeta_{k,n} \sum_{i=1}^{\lfloor k\Omega_n \rfloor - \alpha_t} i p_u \left[\beta_{0,n} \psi_{i,k,n}^0 + \beta_{1,n} \psi_{i,k,n}^1 \right] + D_{tr} P_{tr} \sum_{n=1}^{N_u} \hat{\pi}_{0,n}. \quad (4.46)$$

The simulation parameters are given in Table 4.2. Also, we let $\gamma = 2, \delta_u = 1, \delta_z = 1$. Fig. 4.7a illustrates R_{LB} for a single user versus Ω for $\rho = 15, 20$. We observe that R_{LB} is neither a convex nor a concave function of Ω . This figure suggests that there is an optimal Ω , which we denote as Ω^* , that maximizes R_{LB} . Starting from small values of Ω , as Ω increases (until it reaches the value Ω^*), R_{LB} increases, because the harvested energy can recharge the battery and

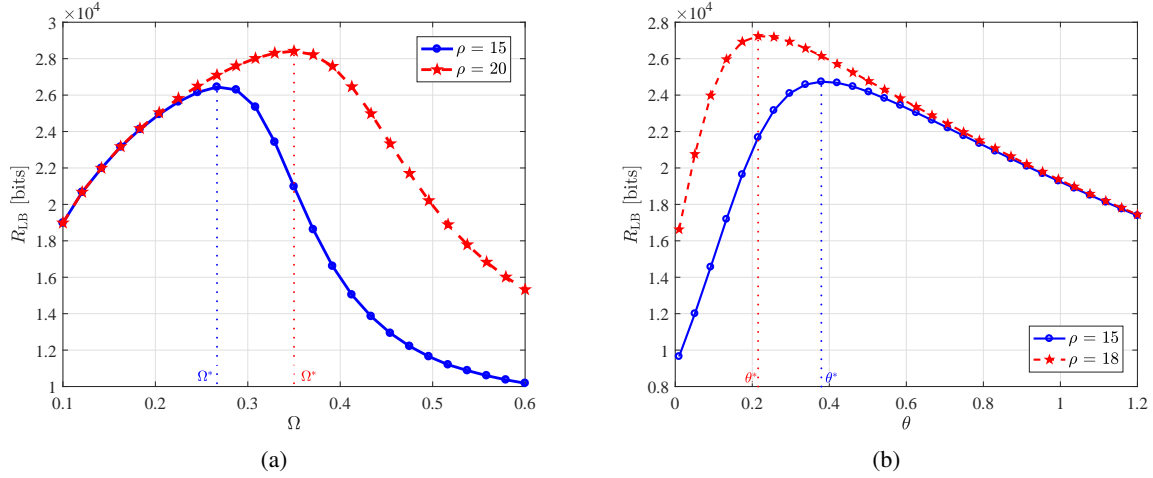


Figure 4.7: (a) R_{LB} versus Ω for $K = 80, \theta = 0.2$, (b) R_{LB} versus θ for $K = 80, \Omega = 0.35$.

can yield more power for data transmission. However, when Ω exceeds Ω^* , the harvested and stored energy cannot support the data transmission and R_{LB} decreases. Moreover, as ρ increases, R_{LB} increases as well. The behavior of R_{LB} versus θ is shown in Fig. 4.7b for $\rho = 15, 18$. We observe that R_{LB} is neither a convex nor a concave function of θ . Similar to Ω , there is an optimal θ , which we denote as θ^* , that maximizes R_{LB} . Starting from small values of θ , as θ increases (until it reaches θ^*), R_{LB} increases. However, when θ exceeds θ^* , R_{LB} decreases.

Fig. 4.8 plots the entries of the steady-state probability vector ζ versus k for $\Omega = 0.45, 0.3$ and $\theta = 0.2$. Fig. 4.9 plots the entries of ζ versus k for $\theta = 0.1, 0.5$ and $\Omega = 0.35$. To quantify the effect of Ω and θ on the entries of ζ we define the average energy stored at the battery of SU_n as

$$\bar{B}_n = \mathbb{E}\{\mathcal{B}_n\} = \sum_{k=0}^K k \zeta_{k,n}, \quad (4.47)$$

where the largest possible value for \bar{B}_n is K . Considering Figs. 4.8a and 4.8b, we find $\bar{B}^{(a)} = 16.97$ for $\Omega = 0.45$, implying that the battery is near empty, and $\bar{B}^{(b)} = 66.30$ for $\Omega = 0.30$, implying that the battery is near full. Considering Figs. 4.9a and 4.9b, we find $\bar{B}^{(a)} = 24.08$ for $\theta = 0.1$ and $\bar{B}^{(b)} = 71.55$ for $\theta = 0.5$. Clearly, the values of Ω and θ affect \bar{B} . Given θ , when Ω is large, data transmit energy α_k in (4.2) is large. Due to large energy consumption for data transmission, compared to energy harvesting, the battery becomes near empty at its steady-state and SU may stop functioning, due to energy outage. When Ω is small, α_k in (4.2) is small. Due to small energy

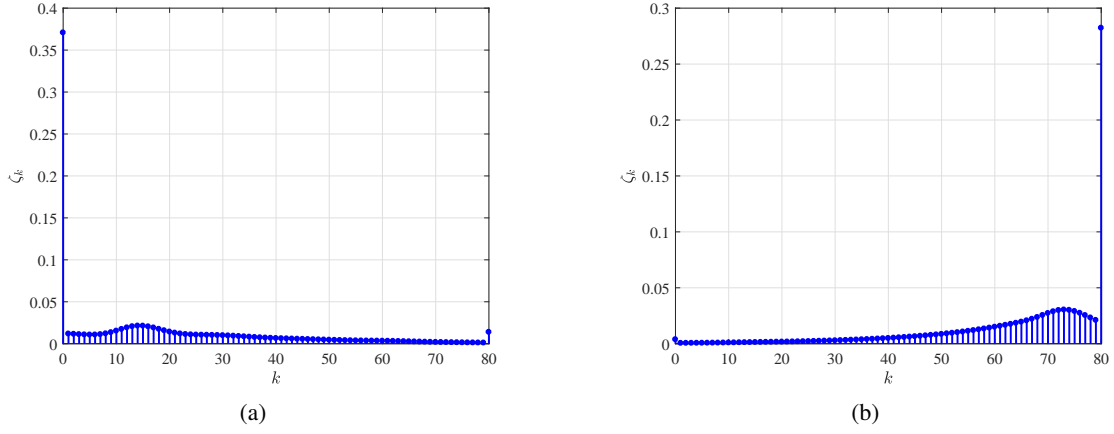


Figure 4.8: ζ_k versus k for $K = 80, \rho = 15, \theta = 0.2$, (a) $\Omega = 0.45$, (b) $\Omega = 0.30$.

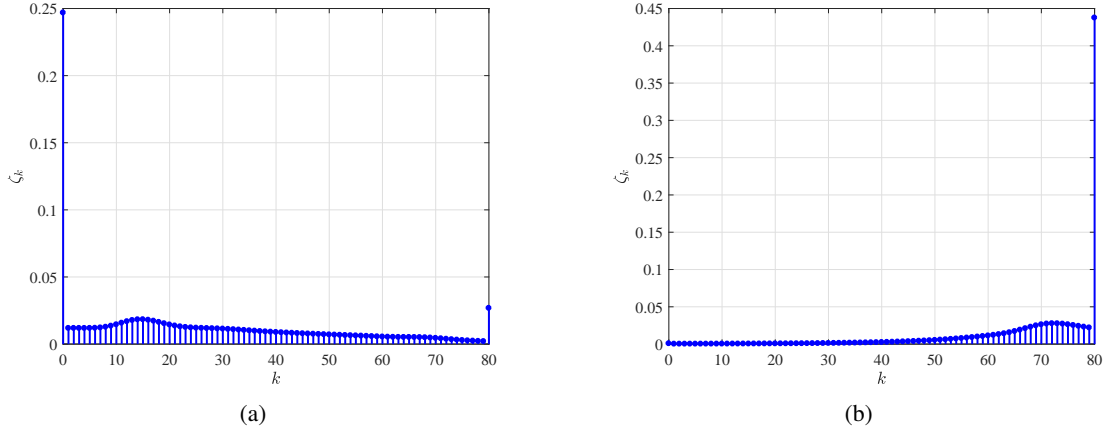


Figure 4.9: ζ_k versus k for $K = 80, \rho = 15, \Omega = 0.35$, (a) $\theta = 0.1$, (b) $\theta = 0.5$.

consumption for data transmission, compared to energy harvesting, the battery becomes near full at its steady-state, indicating that SU has failed to utilize the excess energy. Both cases inevitably hinder data transmission, leading to a reduction in R_{LB} . Similar argument holds true, when θ varies and Ω is given. In particular, when θ is small, transmit energy α_k in (4.2) is large, and when θ is large, transmit energy α_k in (4.2) is small. Again, both cases impede data transmission, leading to a lower R_{LB} . Overall, the observations we make in Figs. 4.7, 4.8, 4.9 confirm that optimizing both Ω and θ to achieve a balance between the energy harvesting and the energy consumption for data transmission is of high importance.

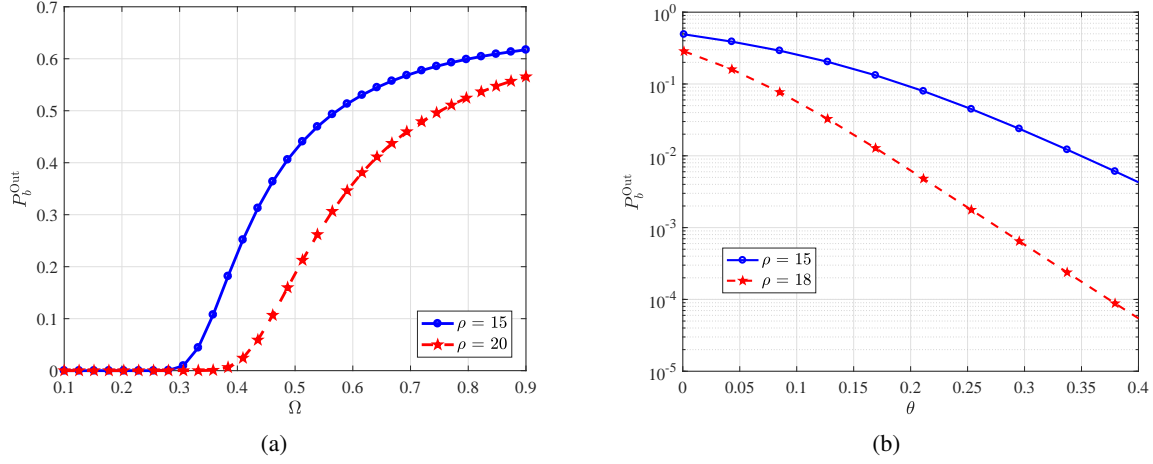


Figure 4.10: (a) P_b^{Out} versus Ω for $K = 80, \theta = 0.05$, (b) P_b^{Out} versus θ for $K = 80, \Omega = 0.35$.

Fig. 4.10a illustrates the behavior of P_b^{Out} for a single user in terms of Ω for $\theta = 0.05$. Fig. 4.10b plots P_b^{Out} versus θ for $\Omega = 0.35$. For $\alpha_t = 1$, P_b^{Out} in (4.43) reduces to $P_b^{\text{Out}} = \zeta_0 + \zeta_1$, i.e., P_b^{Out} depends on Ω and θ , via only the first two entries of vector ζ . Fig. 4.10a shows that, as Ω increases, P_b^{Out} increases as well. This is because as Ω increases, given θ , α_k in (4.2) increases. Due to large energy consumption for data transmission the chance of the battery depletion and hence P_b^{Out} increase. Fig. ?? demonstrates that, as θ increases, P_b^{Out} decreases. This is because as θ increases, given Ω , α_k in (4.2) decreases. Due to small energy consumption for data transmission the chance of the battery depletion and hence P_b^{Out} decrease.

Fig. 4.11a shows how η_{EE} and η_{SE} vary as Ω changes. As Ω increases, both η_{EE} and η_{SE} increase, until Ω reaches a certain value, denoted as Ω_{EE}^* . We note that at $\Omega = \Omega_{\text{EE}}^*$, η_{EE} achieves its maximum value. When Ω exceeds Ω_{EE}^* , η_{EE} decreases while η_{SE} increases. This trend continues until Ω reaches another certain value, denoted as Ω_{SE}^* . We note that at $\Omega = \Omega_{\text{SE}}^*$, η_{SE} achieves its maximum value. When Ω exceeds Ω_{SE}^* , both η_{EE} and η_{SE} decrease. We also observe that $\Omega_{\text{SE}}^* > \Omega_{\text{EE}}^*$.

Fig. 4.11b shows how η_{EE} and η_{SE} vary as θ changes. As θ increases, both η_{EE} and η_{SE} increase, until θ reaches a certain value, denoted as θ_{SE}^* . We observe that at $\theta = \theta_{\text{SE}}^*$, η_{SE} achieves its maximum value. When θ exceeds θ_{SE}^* , η_{SE} decreases while η_{EE} increases. This trend continues until θ reaches another certain value, denoted as θ_{EE}^* . When θ exceeds θ_{EE}^* , both η_{EE} and η_{SE} decrease. We also observe that $\theta_{\text{SE}}^* < \theta_{\text{EE}}^*$.

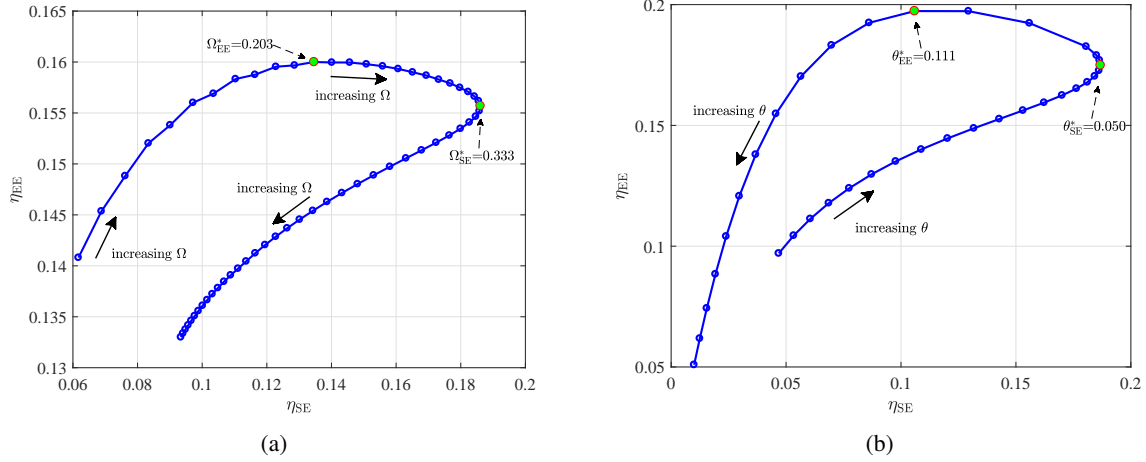


Figure 4.11: (a) η_{EE} versus η_{SE} for different values of Ω and $\theta = 0.02$, (b) η_{EE} versus η_{SE} for different values of θ and $\Omega = 0.6$.

Motivated by [126] we define a new metric, denoted as Z below, which is a weighted summation of η_{SE} and η_{EE}

$$Z = \kappa \eta_{SE} + (1 - \kappa) \eta_{EE}. \quad (4.48)$$

where $0 \leq \kappa \leq 1$ is the weighting factor. When $\kappa = 1$, maximizing Z defined in (4.48) becomes equal to maximizing the spectral efficiency (our problem in (4.P1)). When $\kappa = 0$, maximizing Z becomes equal to maximizing the energy efficiency. Fig. 4.12a illustrates Z versus Ω for different values of κ . We observe that the value of Ω which maximizes Z is different for different values of κ . Fig. 4.12b illustrates Z versus θ for different values of κ . We observe that the value of θ which maximizes Z is different for different values of κ .

• **Solving Problem (4.P1):** Next, we consider solving the constrained optimization problem (4.P1) and (4.SP1-SU $_n$) and plot the maximized R_{LB} , denoted as R_{LB}^* (R_{LB}^* is R_{LB} evaluated at the solutions obtained from solving (4.P1) and (4.SP1-SU $_n$)).

Fig. 4.13 depicts R_{LB}^* obtained by solving (4.P1) and (4.SP1-SU $_n$) versus \bar{I}_{av} for $N_u = 3, \pi_0 = 0.7, 0.8$. We let the statistics of fading coefficients be different across SUs, $\gamma = [2, 2.2, 2.1], \delta_u = [1, 0.8, 1.2], \delta_z = [1, 0.5, 0.8]$ and $K = 60, \rho = 10$ be equal for all SUs. We observe that for small \bar{I}_{av} the “sub-optimal” solution obtained from solving (4.SP1-SU $_n$) yields a lower sum-rate in comparison to the “optimal” solution obtained from solving (4.P1). However, for large \bar{I}_{av} , when AIC is not active these two solutions become identical. As π_0 increases, the probability

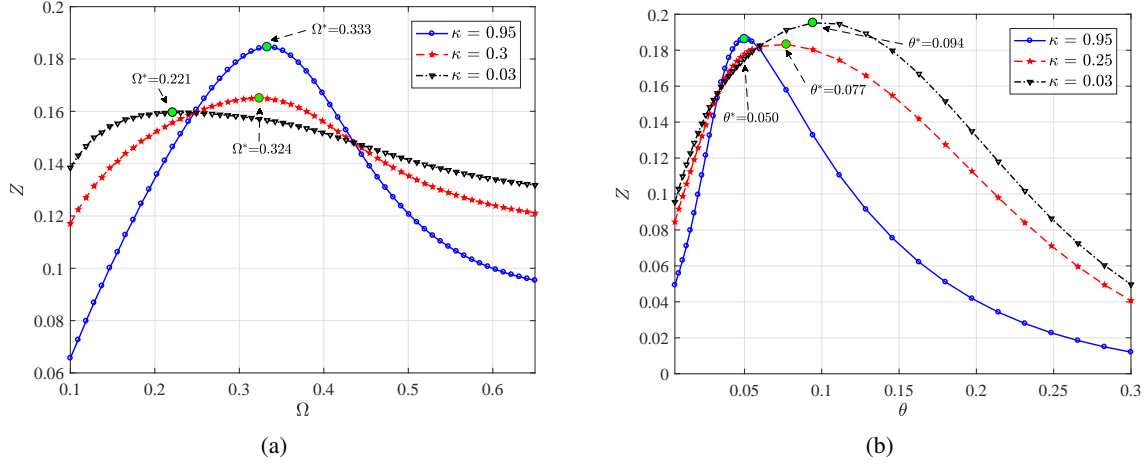


Figure 4.12: (a) Z versus Ω for $\theta = 0.02$, (b) Z versus θ for $\Omega = 0.6$.

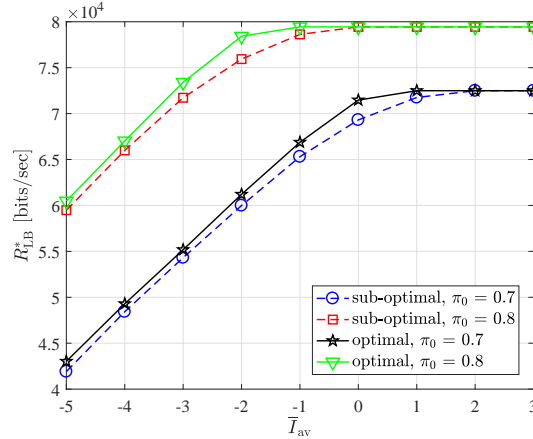


Figure 4.13: R_{LB}^* versus \bar{I}_{av} for $K = 60$, $\rho = 10$, $N_u = 3$.

of the spectrum being actually idle increases and the opportunity for SUs to utilize the spectrum for data transmission increases. Consequently, the sum-rate lower bound increases as π_0 increases, for a given \bar{I}_{av} .

Fig. 4.14 depicts R_{LB}^* versus K for $N_u = 3$, $\rho = 30, 40$. We observe that as K increases, R_{LB}^* increases. This is expected, since as K increases the chance of energy overflow decreases, leading to a larger amount of stored energy in the battery, which can be utilized to support a higher data rate transmission. Fig. 4.15 shows R_{LB}^* versus \bar{I}_{av} for $K = 80$, $\rho = 10, 15$ and $N_u = 3$. For small \bar{I}_{av} , the AIC in (4.42) is active and consequently, it limits transmit power

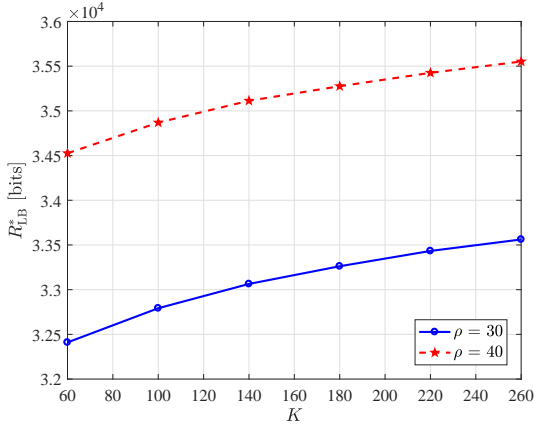


Figure 4.14: R_{LB}^* versus K for $\bar{T}_{av} = 2$ dB.

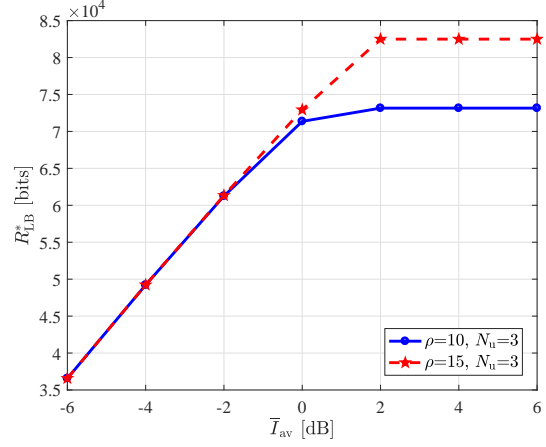


Figure 4.15: R_{LB}^* versus \bar{T}_{av} for $N_u = 3, K = 80$.

of SUs. As \bar{T}_{av} increases, SUs can transmit at higher power levels and R_{LB}^* increases, until R_{LB}^* reaches its maximum value. Increasing \bar{T}_{av} any further, beyond the knee point in Fig. 4.15, does not increase R_{LB}^* . This is because for large \bar{T}_{av} , transmit power levels are restricted by the amount of harvested and stored energy in the battery (i.e., they are not restricted by AIC). Therefore, increasing \bar{T}_{av} beyond the knee point has no effect on R_{LB}^* . Moreover, for small \bar{T}_{av} where the AIC is active, increasing ρ has no effect on R_{LB}^* . On the other hand, for large \bar{T}_{av} , when ρ increases, R_{LB}^* increases.

Considering SU_1 , Fig 4.16 depicts $P_{b_1}^{Out}$ of this user versus K where the optimization variables Ω_1 and θ_1 are obtained by solving (4.P1) and maximizing R_{LB} and then substituting the optimized variables in (4.43) to calculate $P_{b_1}^{Out}$. We observe that increasing K leads to a lower $P_{b_1}^{Out}$.

We define the transmission outage probability $P_{\alpha_n}^{Out}$ as the probability of SU_n not being able to transmit data to the AP, due to either a weak SU_n -AP link with small fading coefficient or insufficient amount of stored energy at the battery.

We have

$$P_{\alpha_n}^{Out} = \Pr(P_n = 0 | \hat{\mathcal{H}}_{0,n}) = \omega_{0,n} \Pr(P_n = 0 | \hat{\mathcal{H}}_{0,n}, \mathcal{H}_0) + \omega_{1,n} \Pr(P_n = 0 | \hat{\mathcal{H}}_{0,n}, \mathcal{H}_1), \quad (4.49)$$

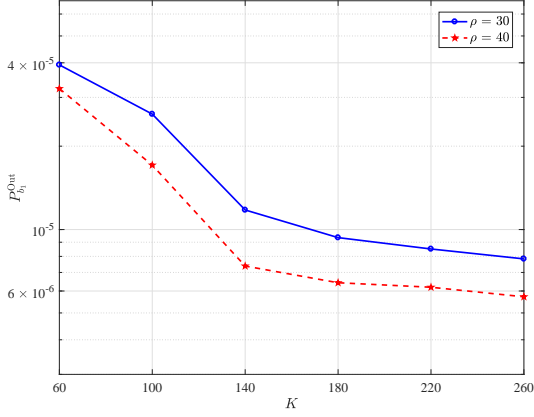


Figure 4.16: $P_{b_1}^{Out}$ for SU_1 versus K when $\bar{I}_{av} = 2$ dB.

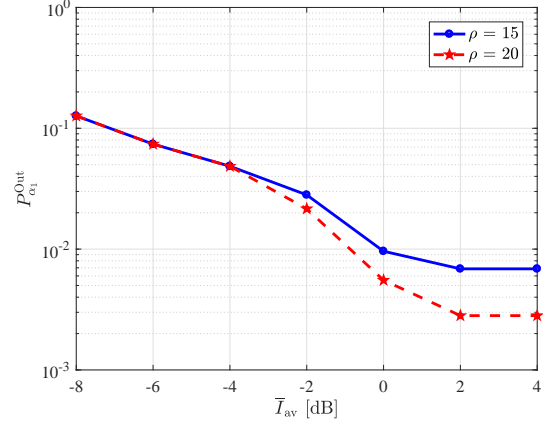


Figure 4.17: $P_{\alpha_1}^{Out}$ for SU_1 versus \bar{I}_{av} for SU_1 when $K = 100$.

where

$$\begin{aligned} & \Pr(P_n = 0 | \hat{\mathcal{H}}_{0,n}, \mathcal{H}_\varepsilon) \\ &= \sum_{k=0}^{\alpha_t} \zeta_{k,n} \Pr(\alpha_{k,n} = 0 | \hat{\mathcal{H}}_{0,n}, \mathcal{H}_\varepsilon, \mathcal{B}_n \leq \alpha_t) + \sum_{k=\alpha_t+1}^K \zeta_{k,n} \Pr(\alpha_{k,n} = 0 | \hat{\mathcal{H}}_{0,n}, \mathcal{H}_\varepsilon, \mathcal{B}_n \geq \alpha_t + 1). \end{aligned} \quad (4.50)$$

Substituting (4.3) and (4.50) in (4.49) we get

$$P_{\alpha_n}^{Out} = \sum_{k=0}^{\alpha_t} \zeta_{k,n} + \sum_{k=\alpha_t+1}^K \zeta_{k,n} Y_{k,n}. \quad (4.51)$$

Fig. 4.17 shows $P_{\alpha_1}^{Out}$ for SU_1 versus \bar{I}_{av} where the optimization variables Ω_1 and θ_1 are obtained by solving (4.P1) and maximizing R_{LB} and then substituting the optimized variables in (4.51) to compute $P_{\alpha_1}^{Out}$. Starting from small \bar{I}_{av} , as \bar{I}_{av} increases, SUs can transmit at higher power levels and $P_{\alpha_1}^{Out}$ decreases, until $P_{\alpha_1}^{Out}$ reaches its minimum value. Increasing \bar{I}_{av} any further, beyond the knee point in Fig. 4.17, does not reduce $P_{\alpha_1}^{Out}$. This is because for large \bar{I}_{av} transmit power levels are restricted by the amount of harvested and stored energy in the battery (i.e., they are not restricted by AIC). Therefore, increasing \bar{I}_{av} beyond the knee point has no effect on $P_{\alpha_1}^{Out}$.

4.6 Conclusion

We considered an uplink opportunistic CR network, that can access a spectrum band licensed to a primary network. Each SU is equipped with a finite size battery, for storing energy. Modeling the dynamics of the battery as a finite state Markov chain, we established a lower bound on the achievable uplink sum-rate of SUs–AP links, in the presence of both spectrum sensing and channel estimation errors. We proposed a parameterized transmit power control strategy that allows each SU to adapt its power, according to the received feedback information from the AP regarding its link fading coefficient and its stored energy in the battery. We optimized the transmit parameters such that the derived uplink sum-rate lower bound is maximized, subject to AIC. Since the proposed constrained optimization problem is not convex and the objective function and the constraints are not differentiable with respect to the optimization parameters, we resorted to grid-based search methods to solve the problem. We explored the trade-offs between R_{LB} , spectrum sensing duration, and channel estimation error. We also illustrated the trade-offs between spectral efficiency and energy efficiency for our CR system. As future work, we plan to study how a non-ideal feedback channel, combined with spectrum sensing and channel estimation errors, will affect our sum-rate maximization problem. In particular, we will consider the effects of SU_n 's mobility and bandwidth-limited feedback channel on our optimization problem and its solution.

CHAPTER 5: THROUGHPUT-OPTIMAL D2D MMWAVE COMMUNICATION: JOINT COALITION FORMATION, POWER, AND BEAM OPTIMIZATION

In this chapter, we explore a throughput-optimal design for a D2D MMWAVE network, where the nodes employ *directional antennas* for wireless communication. In particular, we consider a MMWAVE network with a total available bandwidth of B_c Hz, that supports communication of N cooperative pairs of transmitters and receivers over fading channels. We assume the available spectrum band is divided into N_c non-overlapping sub-bands, where each sub-band has a bandwidth of $W = B_c/N_c$ Hz. Also, we assume $N_c \ll N$. Each node is capable of steering its beam within the range of its field of view (FOV) [1, 5]. Also, each transmitter node can adjust its transmit power. The transmitter-receiver pairs can form up to N_c disjoint coalitions, such that the pairs in a particular coalition share the same sub-band for communication. Therefore, the pairs within a coalition cause co-channel interference, whereas the pairs in different coalitions do not interfere.

The questions we address are: What is the best coalition among the pairs? What are the optimal beam steering angles of directional antennas of the pairs within each coalition, and what are the optimal transmit powers such that the network throughput, defined as the sum-rate of all N transmitter-receiver pairs in N_c coalitions, is maximized? We combine the concepts of coalition formation among cooperative transmitter-receiver pairs and directional MMWAVE bands, and we take full advantage of adaptive beam steering and adaptive transmit power to improve the spectral efficiency and maximize the network throughput.

5.1 System Overview

5.1.1 System Model

To describe our system model, suppose link i denotes the wireless communication link between transmitter t_i and receiver r_i of pair i , for $i = 1, \dots, N$ (see Fig. 5.1). Our wireless channel propagation model encompasses both flat fading and path loss. Suppose nodes t_i and r_j are located at Cartesian locations (X_{t_i}, Y_{t_i}) and (X_{r_j}, Y_{r_j}) , respectively. Let the angles ϕ_{t_i} and ϕ_{r_j} (measured in radian) denote the the antenna orientations of nodes t_i and r_j in their local

coordinates, respectively. Also, let the angle $\theta_{t_i r_j}$ denote the orientation of the line connecting nodes t_i and r_j where

$$\theta_{t_i r_j} = \tan^{-1} \left(\frac{Y_{t_i} - Y_{r_j}}{X_{t_i} - X_{r_j}} \right). \quad (5.1)$$

Suppose $A_\ell(\phi)$ denotes the antenna gain of node ℓ (which can be either a transmitter or receiver) at an arbitrary angle ϕ . Suppose pair i is in coalition c , i.e., the pair is communicating over sub-band c , for $c = 1, \dots, N_c$. The received signal power at node r_i from node t_i can be written as

$$P_{t_i r_i}^c = P^c g_{t_i r_i}^c G_{t_i r_i}(\phi_{t_i}, \phi_{r_i}), \quad (5.2)$$

where P^c is the transmit power of t_i , $g_{t_i r_i}^c$ is the power of fading channel between t_i and r_i corresponding to sub-band c . We model $g_{t_i r_i}^c$ as an Exponential random variable with mean $E\{g_{t_i r_i}^c\} = \frac{d_0}{(d_{t_i r_i})^\alpha}$, where d_0 is the reference distance, $d_{t_i r_i} = \sqrt{(X_{t_i} - X_{r_i})^2 + (Y_{t_i} - Y_{r_i})^2}$ is the Euclidean distance between t_i and r_i , and α is the path loss exponent. Also, $G_{t_i r_i}(\phi_{t_i}, \phi_{r_i})$ is the product of antenna gains of t_i and r_i when the antenna orientations of t_i and r_i in their local coordinates are ϕ_{t_i} and ϕ_{r_i} , respectively. We have

$$G_{t_i r_i}(\phi_{t_i}, \phi_{r_i}) = A_{t_i}(\phi_{t_i} - \theta_{t_i r_i}) A_{r_i}(\phi_{r_i} - \pi - \theta_{t_i r_i}). \quad (5.3)$$

Note that communication of pair i in coalition c causes co-channel interference on other receiver nodes in this coalition. Similarly, communication of other pairs in coalition c causes co-channel interference on node r_i in this coalition. Suppose $I_{t_j r_i}^c$ denotes the interference power imposed on r_i from t_j in coalition c . This interference power can be written as

$$I_{t_j r_i}^c = P^c g_{t_j r_i}^c G_{t_j r_i}(\phi_{t_j}, \phi_{r_i}), \quad (5.4)$$

where $g_{t_j r_i}^c$ is the power of fading channel between t_j and r_i corresponding to sub-band c , and

$$G_{t_j r_i}(\phi_{t_j}, \phi_{r_i}) = A_{t_j}(\phi_{t_j} - \theta_{t_j r_i}) A_{r_i}(\phi_{r_i} - \pi - \theta_{t_j r_i}). \quad (5.5)$$

To simplify the presentation, we let the binary variable a_i^c indicate whether or not transmitter-receiver pair i is in coalition c , i.e., if $a_i^c = 1$ then pair i is in coalition c and thus link i operates in sub-band c , otherwise, $a_i^c = 0$. The

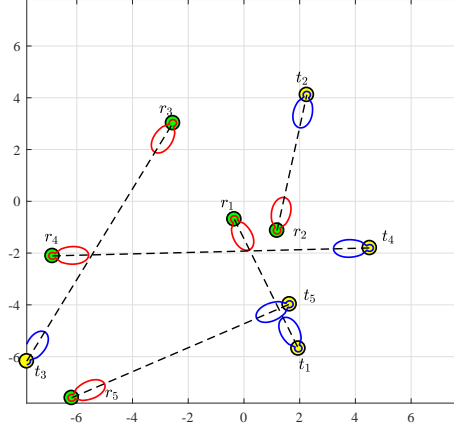


Figure 5.1: An example of 5 transmitter-receiver pairs in a coalition. In each pair, the directional antennas of transmitter and receiver are exactly along the center of their main lobes (which is not necessarily throughput-optimal).

rate of link i operating over sub-band c can be written as

$$R_i^c = W \log_2 \left(1 + \frac{a_i^c P_{t_i r_i}^c}{N_0 W + \sum_{j=1, j \neq i}^N a_j^c I_{t_j r_i}^c} \right), \quad (5.6)$$

where N_0 is the power spectral density of the receiver additive white Gaussian noise. Then, the sum-rate of all pairs in coalition c can be written as

$$R^c = \sum_{i=1}^N R_i^c. \quad (5.7)$$

Consequently, the network throughput is $\sum_{c=1}^{N_c} R^c = \sum_{c=1}^{N_c} \sum_{i=1}^N R_i^c$.

Clearly, the network throughput depends on the coalition formation among the pairs, beam steering angles of directional antennas of the pairs within each coalition, and transmit powers. We ask the following questions: How does the throughput-optimal coalition formation look like? In other words, given each sub-band c , which transmitter-receiver pairs should operate over this sub-band? Furthermore, within each coalition, what are the best beam steering angles of directional antennas of the pairs and the best transmit power, in terms of maximizing the network throughput?

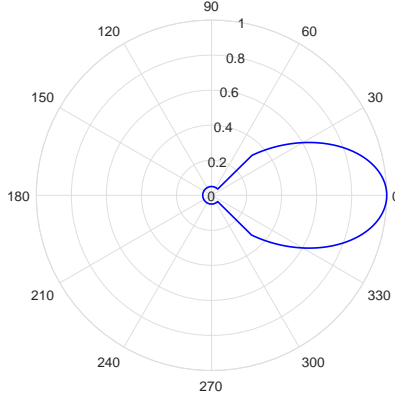


Figure 5.2: An example of $A_\ell(\phi)$.

5.1.2 Antenna Model

Let $A_\ell(\phi)$ denote the gain of directional antenna of node ℓ (which can be a transmitter or a receiver). We express $A_\ell(\phi)$ as the following

$$A_\ell(\phi) = \begin{cases} A_{\text{ml}}^\ell e^{-B\left(\frac{\phi}{\phi_{3\text{dB}}^\ell}\right)^2}, & |\phi| \leq \phi_{\text{ml}}^\ell \\ A_{\text{sl}}^\ell, & |\phi| > \phi_{\text{ml}}^\ell \end{cases} \quad (5.8)$$

where ϕ denotes an arbitrary angle within the FOV range $[-\phi_{\text{FOV}}^\ell, \phi_{\text{FOV}}^\ell]$, ϕ_{ml}^ℓ denotes the main lobe width, $\phi_{3\text{dB}}^\ell$ is the half-power beamwidth, A_{ml}^ℓ is the maximum antenna gain, A_{sl}^ℓ is the sidelobe gain and $B = \ln(2)$. We adopt our antenna gain pattern in (5.8) from [127]. This is a realistic model for directional antennas with sidelobe gain. Fig. 5.2 illustrates an example of $A_\ell(\phi)$ for $A_{\text{ml}}^\ell = 1$, $A_{\text{sl}}^\ell = 0.05$, $\phi_{\text{ml}}^\ell = 45^\circ$, $\phi_{3\text{dB}}^\ell = 35^\circ$.

5.1.3 Problem Formulation

To formulate the network throughput maximization problem, we need to incorporate the constraints on the binary variable a_i^c in (5.6). Since each transmitter-receiver pair can belong to at most one coalition, we have

$$\sum_{c=1}^{N_c} a_i^c \leq 1, \quad \text{for } i = 1, \dots, N. \quad (5.9)$$

Let P_{\max} indicate the maximum allowed total transmit power of all transmitter nodes in the network. To satisfy this power constraint, we need to have

$$\sum_{c=1}^{N_c} \sum_{i=1}^N P^c a_i^c \leq P_{\max}. \quad (5.10)$$

Finally, we note that the beam steering angle ϕ of node ℓ is limited to be within its field of view range $[-\phi_{\text{FOV}}^\ell, \phi_{\text{FOV}}^\ell]$.

Therefore, the beam steering angles of nodes t_i and r_i in pair i are limited as the following:

$$\phi_{t_i} \in [\phi_{t_i}^{(\text{low})}, \phi_{t_i}^{(\text{up})}], \quad \phi_{r_i} \in [\phi_{r_i}^{(\text{low})}, \phi_{r_i}^{(\text{up})}], \quad \forall i \quad (5.11)$$

where

$$\begin{aligned} \phi_{t_i}^{(\text{low})} &= \theta_{t_i r_i} - \phi_{\text{FOV}}^{t_i}, & \phi_{t_i}^{(\text{up})} &= \theta_{t_i r_i} + \phi_{\text{FOV}}^{t_i}, \\ \phi_{r_i}^{(\text{low})} &= \pi + \theta_{t_i r_i} - \phi_{\text{FOV}}^{r_i}, & \phi_{r_i}^{(\text{up})} &= \pi + \theta_{t_i r_i} + \phi_{\text{FOV}}^{r_i}. \end{aligned}$$

Our goal is to find the set of binary variables $\{a_i^c\}, \forall i, c$, the transmit powers $\{P^c\}, \forall c$, and the set of beam steering angles of directional antennas of all pairs $\{\phi_{t_i}, \phi_{r_i}\}, \forall i$ such that the network throughput is maximized, subject to the constraints in (5.9), (5.10) and (5.11). In other words, we are interested to solve the following constrained optimization problem

$$\begin{aligned} & \underset{\{a_i^c\}, \forall i, c, \{P^c\}, \forall c, \{\phi_{t_i}, \phi_{r_i}\}, \forall i}{\text{Maximize}} && \sum_{c=1}^{N_c} R^c && (5.P1) \\ \text{s.t.} & \sum_{c=1}^{N_c} a_i^c \leq 1, && \forall i, \\ & \sum_{c=1}^{N_c} \sum_{i=1}^N P^c a_i^c \leq P_{\max}, \\ & \phi_{t_i} \in [\phi_{t_i}^{(\text{low})}, \phi_{t_i}^{(\text{up})}], && \phi_{r_i} \in [\phi_{r_i}^{(\text{low})}, \phi_{r_i}^{(\text{up})}], && \forall i. \end{aligned}$$

We note that (5.P1) is a mixed-integer nonlinear programming problem with exorbitant computational complexity [128]. Even if the binary variables $\{a_i^c\}, \forall i, c$ are relaxed to be in the interval $[0, 1]$, the optimal solution of (5.P1) cannot be obtained via the gradient descent algorithm, due to the constraints on a_i^c . Even if the beam steering angles $\{\phi_{t_i}, \phi_{r_i}\}, \forall i$ and the transmit powers $\{P^c\}, \forall c$ are given in (5.P1), still the computational complexity of finding the optimal binary variables $\{a_i^c\}, \forall i, c$ is NP-hard, and it can only be found for a small network with small N and N_c .

5.2 Solving Problem

We propose an iterative method based on the BCD algorithm to solve (5.P1) [129]. The underlying principle of the BCD algorithm is that, at each iteration one variable is optimized, while the remaining variables are fixed. The iteration continues until it converges to a stationary point of (5.P1) [5, 109]. To apply the principle of the BCD algorithm to (5.P1), we decompose (5.P1) into three sub-problems, which we refer to as (5.SP1), (5.SP2), and (5.SP3). In (5.SP1), we search for the binary variables $\{a_i^c\}, \forall i, c$, given $\{P^c\}, \forall c$ and $\{\phi_{t_i}, \phi_{r_i}\}, \forall i$. In other words, we solve the following problem

$$\begin{aligned} &\text{Given } \{P^c\}, \forall c \text{ and } \{\phi_{t_i}, \phi_{r_i}\}, \forall i && (5.SP1) \\ &\text{Maximize } \sum_{c=1}^{N_c} R^c \\ &\quad \{a_i^c\}, \forall i, c \\ &\text{s.t. } \sum_{c=1}^{N_c} a_i^c \leq 1, \quad \forall i. \end{aligned}$$

To solve (5.SP1), we take a coalitional game approach. The approach and the algorithm are discussed in Section 5.2.1. In (5.SP2), we search for the transmit powers $\{P^c\}, \forall c$ given $\{a_i^c\}, \forall i, c$ and $\{\phi_{t_i}, \phi_{r_i}\}, \forall i$. In other words, we solve the following problem

$$\begin{aligned} &\text{Given } \{a_i^c\}, \forall i, c \text{ and } \{\phi_{t_i}, \phi_{r_i}\}, \forall i && (5.SP2) \\ &\text{Maximize } \sum_{c=1}^{N_c} R^c \\ &\quad \{P^c\}, \forall c \\ &\text{s.t. } \sum_{c=1}^{N_c} \sum_{i=1}^N P^c a_i^c \leq P_{\max}. \end{aligned}$$

We note that (5.SP2) is a jointly concave function of $\{P^c\}, \forall c$. Hence, we use the Lagrange multiplier method and solve the corresponding KKT conditions to find the solution. The details are explained in Section 5.2.2. In (5.SP3), we search for the beam steering angles $\{\phi_{t_i}, \phi_{r_i}\}, \forall i$, given $\{P^c\}, \forall c$ and $\{a_i^c\}, \forall i, c$. In other words, we solve the

following problem

$$\begin{aligned}
& \text{Given } \{P^c\}, \forall c, \{a_i^c\}, \forall i, c & (5.SP3) \\
& \text{Maximize } \sum_{c=1}^{N_c} R^c \\
& \text{s.t. } \phi_{t_i} \in [\phi_{t_i}^{(\text{low})}, \phi_{t_i}^{(\text{up})}], \quad \phi_{r_i} \in [\phi_{r_i}^{(\text{low})}, \phi_{r_i}^{(\text{up})}], \quad \forall i.
\end{aligned}$$

We note that (5.SP3) is neither a convex nor a concave function with respect to $\{\phi_{t_i}, \phi_{r_i}\}, \forall i$. We use interior-point method to solve (5.SP3). Section 5.2.3 provides more details on how we solve (5.SP3). We iterate between solving (5.SP1), (5.SP2), and (5.SP3) until we converge to a stationary point of (5.P1), which is our solution.

5.2.1 Solving Sub-problem (5.SP1)

To solve (5.SP1), we take a coalitional game approach, where N transmitter-receiver pairs in the MMWAVE network are regarded as the players of the game [127, 130]. In the following, we briefly mention some definitions of the coalitional game approach, that are important for designing the coalition formation algorithm.

Our coalitional game is defined by (\mathcal{I}, U) , where \mathcal{I} is the set of game players (i.e., the set of N cooperative transmitter-receiver pairs) and U is the utility function (i.e., the sum-rate of the pairs in a coalition). A sub-set $S_c \subseteq \mathcal{I}$ indicates the set of transmitter-receiver pairs in coalition c which communicates over sub-band c . Then $U(S_c)$ represents the value of coalition c , i.e., $U(S_c) = R^c$ is equal to the sum-rate of the pairs in set S_c . Different coalitions in our MMWAVE network satisfy the following constraints:

$$\mathcal{I} = \bigcup_{c=1}^{N_c} S_c, \quad S_c \cap S_{c'} = \emptyset, \quad \forall c, c' \text{ and } c \neq c'.$$

We notice that the transmitter-receiver pairs are not motivated to form a grand coalition, where all the pairs communicate over only one sub-band, since the co-channel interference will become very large and will negatively impact the coalition value. In fact, the transmitter-receiver pairs prefer to form as many disjoint coalitions as possible, to maximize the overall coalition value. Since there are N_c sub-bands in our MMWAVE network, the pairs are motivated to form N_c disjoint coalitions.

A coalitional partition is defined as the set $\Pi = \{S_1, \dots, S_{N_c}\}$, which partitions the set of game players \mathcal{I} into disjoint

subsets S_c 's. The total utility of this partition is

$$U(\Pi) = \sum_{c=1}^{N_c} U(S_c). \quad (5.13)$$

The players of the game prefer the coalitional partition $\Pi' = \{S'_1, \dots, S'_{N_c}\}$ instead of $\Pi = \{S_1, \dots, S_{N_c}\}$ if the total utility achieved by Π' is strictly greater than by Π , i.e.

$$\sum_{c=1}^{N_c} U(S'_c) > \sum_{c=1}^{N_c} U(S_c). \quad (5.14)$$

The players of the game decide to join or leave a coalition based on a defined *preference relation*. For any player $i \in \mathcal{I}$, the preference relation $S_p \succ_i S_q$ means player i strictly prefers being a member of coalition S_p over being a member of coalition S_q , where $S_p, S_q \subseteq \mathcal{I}$ and $S_p \neq S_q$. The preference relation $S_p \succ_i S_q$ is quantified as the following

$$U(S_p \cup i) + U(S_q \setminus i) > U(S_p) + U(S_q). \quad (5.15)$$

Given a coalitional partition $\Pi = \{S_1, \dots, S_{N_c}\}$, if player i switches from coalition S_q to coalition S_p , then the current coalitional partition Π of \mathcal{I} is modified into a new coalitional partition $\Pi' = (\Pi \setminus \{S_q, S_p\}) \cup \{S_q \setminus i\} \cup \{S_p \cup i\}$. Player i is allowed to switch from coalition S_q to coalition S_p (i.e., player i leaves S_q and joins S_p) if and only if $S_p \succ_i S_q$.

Algorithm 2 summarizes our approach to solve (5.SP1), which is based on the above definitions and the switching rule. The iterations in Algorithm 2 stop when the partition converges to the final Nash-stable coalitional partition $\Pi_{\text{Nash}} = \{S''_1, \dots, S''_{N_c}\}$. The partition Π_{Nash} satisfies the following. For any player $i \in \mathcal{I}$, if i is a member of coalition S_p , then $S_p \succ_i S_q$ for any $q \neq p$.

5.2.2 Solving Sub-problem (5.SP2)

We solve (5.SP2) using the Lagrangian multiplier method. Let $\mathcal{L}(\{P^c\}, \forall c, \lambda)$ be the Lagrangian for (5.SP2), where λ is the Lagrange multiplier. The Lagrangian is

$$\mathcal{L}(\{P^c\}, \forall c, \lambda) = - \sum_{c=1}^{N_c} R^c + \lambda \left(\sum_{c=1}^{N_c} \sum_{i=1}^N a_i^c P^c - P_{\max} \right), \quad (5.16)$$

Algorithm 2: Algorithm for Solving (5.SP1)

- 1: Given $\{P^c\}, \forall c$ and $\{\phi_{t_i}, \phi_{r_i}\}, \forall i$,
 - 2: Initialize the system by any random partition Π_{ini} . Set the current partition $\Pi_{\text{cur}} = \Pi_{\text{ini}}$,
 - 3: **repeat**
 - 4: Randomly choose a link $i \in \mathcal{I}$, and denote its current coalition as $S_p \in \Pi_{\text{cur}}$,
 - 5: Randomly choose another coalition $S_q \in (\Pi_{\text{cur}} \cup \{\emptyset\})$, such that $S_p \neq S_q$,
 - 6: **if** the switch operation from S_p to S_q satisfying $S_q \succ_i S_p$
 - 7: $\Pi_{\text{cur}} = (\Pi_{\text{cur}} \setminus \{S_p, S_q\}) \cup \{S_p \setminus \{i\}\} \cup \{S_q \cup i\}$
 - 8: **else**
 - 9: $\Pi_{\text{tmp}} = (\Pi_{\text{cur}} \setminus \{S_p, S_q\}) \cup \{S_p \setminus \{i\}\} \cup \{S_q \cup i\}$
 - 10: Randomly choose one link $i' \in \mathcal{I}$, and denote its current coalition as $S_{p'} \in \Pi_{\text{tmp}}$,
 - 11: Randomly choose another coalition, $S_{q'} \in (\Pi_{\text{tmp}} \cup \{\emptyset\})$, $S_{p'} \neq S_{q'}$
 - 12: Obtain the partition Π'_{tmp} as $\Pi'_{\text{tmp}} = (\Pi_{\text{cur}} \setminus \{S_{p'}, S_{q'}\}) \cup \{S_{p'} \setminus \{i'\}\} \cup \{S_{q'} \cup i'\}$
 - 13: **if** $U(\Pi'_{\text{tmp}}) > U(\Pi_{\text{cur}})$
 - 14: $\Pi_{\text{cur}} = \Pi'_{\text{tmp}}$
 - 15: **end**
 - 16: **end**
 - 17: **until** the partition converges to a final Nash-stable partition.
-

The optimal set $\{P^c\}, \forall c$ that minimizes (5.16) is the solution to the KKT optimality necessary and sufficient conditions. The KKT conditions are the first derivatives of \mathcal{L} with respect to P^c , λ being equal to zero. We have

$$\frac{\partial \mathcal{L}}{\partial P^c} = -\frac{\partial R^c}{\partial P^c} + \lambda \sum_{i=1}^N a_i^c = 0, \quad \forall c \quad (5.17a)$$

$$\lambda \left(\sum_{c=1}^{N_c} \sum_{i=1}^N a_i^c P^c - P_{\max} \right) = 0, \quad (5.17b)$$

where $\partial R^c / \partial P^c$ is

$$\frac{\partial R^c}{\partial P^c} = W \sum_{i=1}^N \frac{a_i^c g_{t_i r_i}^c G_{t_i r_i} N_0 W}{\left(N_0 W + \sum_{j \neq i} a_j^c I_{t_j r_i}^c \right) \left(N_0 W + P^c a_i^c g_{t_i r_i}^c G_{t_i r_i} + \sum_{j \neq i} a_j^c I_{t_j r_i}^c \right)}. \quad (5.18)$$

Since the closed-form analytical solution for (5.17a) cannot be found, we solve these equations numerically, via the following iterative method. We first initialize λ and then find P^c for $c = 1, \dots, N_c$ using (5.17a). Next, we update λ

Algorithm 3: Algorithm for Solving (5.SP2)

- 1: Given $\{a_i^c\}, \forall i, c$ and $\{\phi_{t_i}, \phi_{r_i}\}, \forall i$ and λ_{ini} ,
 - 2: Set $n = 0, \lambda^{(0)} = \lambda_{\text{ini}}$,
 - 3: **repeat**
 - 4: Calculate $P^{c,(n)}$ by solving (5.17a) for $c = 1, \dots, N_c$,
 - 5: Calculate $\lambda^{(n+1)}$ using (5.19),
 - 6: $n \leftarrow n + 1$;
 - 7: **until** (5.20) is satisfied.
-

using the subgradient method

$$\lambda^{(n+1)} = \left[\lambda^{(n)} + t_0 \left(\sum_{c=1}^{N_c} \sum_{i=1}^N a_i^c P^c - P_{\max} \right) \right]^+, \quad (5.19)$$

where t_0 is the step size and $[x]^+ = \max\{x, 0\}$. Using the updated λ , we find $\{P^c\}, \forall c$ again using (5.17a). We repeat this procedure until λ converges, i.e., the following pre-determined stopping criterion is met for a given small number δ

$$\lambda^{(n)} \left| \sum_{c=1}^{N_c} \sum_{i=1}^N a_i^c P^c - P_{\max} \right| \leq \delta. \quad (5.20)$$

Algorithm 3 summarizes our approach to solve (5.SP2).

5.2.3 Solving Sub-problem (5.SP3)

Considering (5.SP3) we note that it is neither a convex nor a concave function with respect to $\{\phi_{t_i}, \phi_{r_i}\}, \forall i$. Since the optimization variables are continuous-valued, we can solve (5.SP3) using gradient descent-based algorithms. We choose interior-point method to solve (5.SP3). Note that the solution of interior-point method depends on the initial values for $\{\phi_{t_i}, \phi_{r_i}\}, \forall i$. Hence, we randomly choose N_ϕ sets of initial values for $\{\phi_{t_i}, \phi_{r_i}\}, \forall i$ and run the interior-point algorithm N_ϕ times and find N_ϕ sets of solutions. Among these sets, we let the set that provides the largest network throughput be the solution of (5.SP3).

5.3 Numerical Performance Evaluations

In this section, we corroborate our analysis on constrained maximization of the network throughput with Matlab simulations. We assume that the antenna gain $A_\ell(\phi), \forall \ell$ are the same. In our simulations, all transmitters and receivers are uniformly distributed in a circle with radius of 30 meters. The simulation parameters are given in Table 5.1.

Table 5.1: Simulation Parameters

Parameter	Value	Parameter	Value
A_{s1}	1	ϕ_{FOV}	60°
A_{m1}	0.05	N_0	-110 dBm/Hz
ϕ_{3dB}	35°	B_c	400 MHz
ϕ_{m1}	45°	δ	0.001

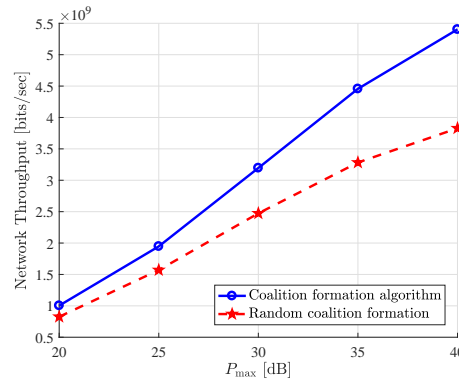


Figure 5.3: Network throughput versus P_{max} for $N = 20, N_c = 4$.

- *Impact of coalition formation optimization on throughput maximization:* Fig. 5.3 plots the network throughput versus P_{max} for $N = 20, N_c = 4$, considering two scenarios: the scenario where Algorithm 2 is employed to optimize the coalition formation among the transmitter-receiver pairs, and the scenario where the pairs form coalitions randomly, without any optimization (i.e., the pairs are randomly assigned to a coalition). In both scenarios, the beam steering angles and the transmit powers are optimized. The gap between the two curves in Fig. 5.3 indicate the impact of coalition formation optimization on the throughput maximization. We note that, as P_{max} increases, this performance gap increases. For both scenarios as P_{max} increases, the throughput increases, since the transmitters in all coalitions are allowed to transmit at higher transmit powers.

- *Impact of transmit power optimization on throughput maximization:* Fig. 5.4 plots the network throughput versus P_{max} for $N = 20, N_c = 4$, considering two scenarios: the scenario where Algorithm 3 is employed to optimize the transmit powers, and the scenario where P_{max} is uniformly distributed among N transmitters in the network, without any optimization. In both scenarios, the coalition formation and the beam steering angles are optimized. The gap between the two curves in Fig. 5.4 illustrates the impact of transmit power optimization on the throughput maximization.

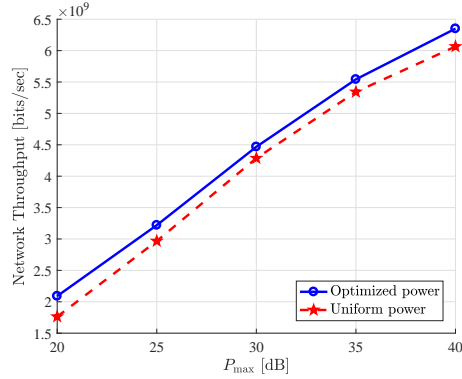


Figure 5.4: Network throughput versus P_{\max} for $N = 20, N_c = 4$.

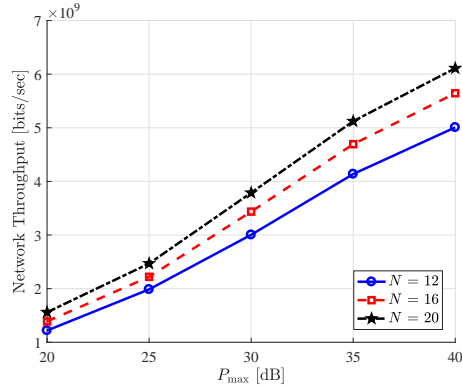


Figure 5.5: Network throughput versus P_{\max} for $N_c = 4$.

- *Impact of N on throughput maximization:* Fig. 5.5 shows the network throughput versus P_{\max} for $N = 12, 16, 20, N_c = 4$. Given a P_{\max} value, as N increases, the network throughput increases. We conjecture that this trend would change when N becomes very large (e.g., $N = 100$). We expect that as N increases further, the network throughput decreases (since the total transmit power and the total bandwidth are fixed).

- *Impact of N_c on throughput maximization:* Fig. 5.6 shows the network throughput versus N_c for $N = 30, P_{\max} = 30$ dB. This figure suggests that there is a trade-off between N_c and the network throughput. On the one hand, as the number of sub-bands N_c increases, the number of coalitions increases and the co-channel interference generated in each coalition decreases, which can lead into increasing the sum-rate in each coalition and thus increasing the network throughput. On the other hand, as N_c increases, the bandwidth W of each sub-band decreases, which can lead into decreasing the network throughput. Therefore, given N one can find the optimal N_c that provides the highest network

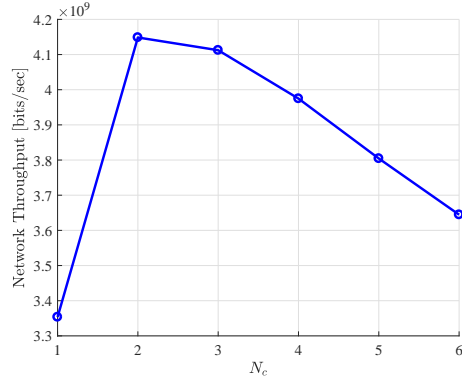


Figure 5.6: Network throughput versus N_c for $N = 30$, $P_{\max} = 30$ dB.

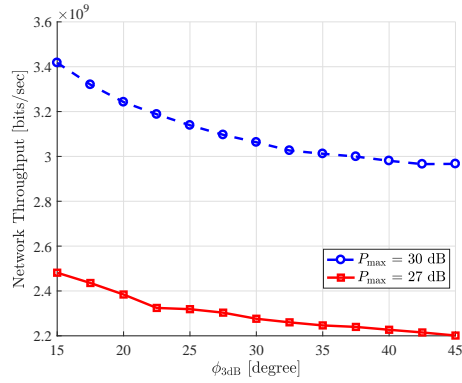


Figure 5.7: Network throughput versus $\phi_{3\text{dB}}$ for $N = 20$, $N_c = 4$.

throughput. For instance, in Fig. 5.6, $N_c = 2$ yields the highest network throughput.

- *Impact of half-power beamwidth $\phi_{3\text{dB}}$ on throughput maximization:* Fig. 5.7 shows the effect of $\phi_{3\text{dB}}$ on the network throughput for $P_{\max} = 27, 30$ dB. We note that as $\phi_{3\text{dB}}$ increases the network throughput decreases. This is because as $\phi_{3\text{dB}}$ increases, the transmitters within a particular coalition impose a stronger co-channel interference on the non-intended receivers within the same coalition.

5.4 Conclusion

We considered a D2D MMWAVE network with bandwidth of $B_c = WN_c$ Hz, where N cooperative transmitter-receiver pairs form N_c coalitions and communicate over N_c non-overlapping sub-bands, each with bandwidth of W Hz. Each node is equipped with a directional antenna that has beam steering capability. Also, each transmitter can adjust its transmit power. We formulated the network throughput maximization problem, subject to certain constraints, and we proposed a BCD algorithm, to find the optimal coalition among the transmitter-receiver pairs, the optimal beam steering angles of directional antennas of the pairs within each coalition, and the optimal transmit powers. Through numerical simulations, we investigated the effects of $N, N_c, P_{\max}, \phi_{3\text{dB}}$ on the network throughput maximization. Our simulations show that, given N, P_{\max} there is an optimal N_c value that provides the highest network throughput. Also, we showed that a lower $\phi_{3\text{dB}}$ yields a higher network throughput.

CHAPTER 6: CONCLUSION

In this dissertation we studied the effects of several factors, including spectrum sensing error, channel estimation error, channel quantization error, errors due to incorrect detection of the beam corresponding to PU's location and incorrect selection of the strongest beam for data transmission on the performance of opportunistic CR systems. We derived the achievable rate of a CR system and optimized some parameters, including durations of spectrum sensing T_{se} and channel training T_{tr} as well as data symbol transmission power at SU_{tx} such that the derived rate is maximized, subject to ATPC and AIC.

In the following, we summarize our contributions in Chapters 2-4.

6.1 Conclusions

In Chapter 2, we proposed a holistic system design for integrated sector-based spectrum sensing and sector-based data communication for an opportunistic CR system consisting of a PU, SU_{tx} , and SU_{rx} , where SU_{tx} is equipped with an ESPAR antenna that has M parasitic elements, and there is an error-free bandwidth limited feedback channel from SU_{rx} to SU_{tx} . Different from the state-of-the-art, our proposed integrated design incorporates induced errors due to: (i) imperfect spectrum sensing and determining the correct beam corresponding to PU's location, such errors affect the interference imposed on PU; (ii) selecting the best beam for data communication over SU_{tx} - SU_{rx} link. We formulated a constrained optimization problem, where the ergodic capacity for SU_{tx} - SU_{rx} link is maximized, subject to ATPC and AIC, and the optimization variables are spectrum sensing duration, quantization thresholds at SU_{rx} , and discrete power levels at SU_{tx} . We developed an iterative suboptimal algorithm with a low computational complexity, based on the BCD algorithm, that finds a unique and locally optimal solution for the constrained problem. In addition, we derived closed form expressions for outage and symbol error probabilities of our opportunistic CR system. We corroborated our mathematical analyses with extensive simulations. Our numerical results demonstrate that our proposed CR system with the ESPAR antenna at SU_{tx} yields a significantly higher capacity, a lower outage probability, and a lower symbol error probability, compared with a CR system that its SU_{tx} has an omni-directional antenna. The capacity improvement varies as the ATPC and AIC change. Furthermore, we showed that with only a small number of feedback bits the capacity of our CR system approaches to its baseline, which assumes the full knowledge of unquantized channel gain.

In Chapter 3, we studied the combined effects of spectrum sensing error and imperfect CSI of SU_{tx} – SU_{rx} link on the achievable rates of an opportunistic CR system with a RA at SU_{tx} . We considered an opportunistic CR system consisting of a PU, SU_{tx} , and SU_{rx} , where SU_{tx} is equipped with a RA that has M beams, and there is an error-free low-rate feedback channel from SU_{rx} to SU_{tx} . Utilizing the beam steering capability of the RA, we regarded a design framework for integrated sector-based spectrum sensing and data communication. In this framework, SU_{tx} senses the spectrum and detects the beam corresponding to active PU's location. SU_{tx} also sends training symbols (prior to data symbols), to enable channel estimation at SU_{rx} and selection of the strongest beam between SU_{tx} – SU_{rx} for data transmission. We established a lower bound on the achievable rates of SU_{tx} – SU_{rx} link, in the presence of spectrum sensing and channel estimation errors, and errors due to incorrect detection of the beam corresponding to PU's location and incorrect selection of the strongest beam for data transmission. We formulated a constrained optimization problem, where a lower bound on the achievable rate of SU_{tx} – SU_{rx} link is maximized, subject to ATPC and AIC, with the optimization variables being the durations of spatial spectrum sensing T_{se} and channel training T_{tr} as well as data symbol transmission power at SU_{tx} . Moreover, we proposed two alternative power adaptation schemes that are simpler to implement. We solved the proposed constrained optimization problems using iterative methods based on the BCD algorithm. Our simulation results demonstrate that one can increase the achievable rates of SU_{tx} – SU_{rx} link significantly, via implementing these optimizations, while maintaining the ATPC and AIC. They also showed that the achievable rates obtained from employing simple schemes 1 and 2 are very close to the one produced by the optimized transmit power. Our numerical results also showed that between optimizing T_{se} and T_{tr} , optimizing the latter has a larger effect on increasing the achievable rates in our system.

In Chapter 4, we considered the problem of sum-rate maximization in an opportunistic EH-enabled CR network. The CR network consists of N_u SUs and an AP, that can access a wideband spectrum licensed to a primary network. Each SU is capable of harvesting energy from natural ambient energy sources, and is equipped with a finite size rechargeable battery, to store the harvested energy. The SUs operate under a time-slotted scheme, where each time slot consists of three non-overlapping phases: spectrum sensing phase, channel estimation phase, and data transmission phase. The AP feeds back its estimates of fading coefficients of SUs–AP link to SUs. Our main *objectives* were (i) to study how the achievable sum-rate of SUs is impacted by the *combined effects* of spectrum sensing error and imperfect CSI of SUs–AP links (due to channel estimation error), and (ii) to design an energy management strategy that maximizes the achievable sum-rate of SUs, subject to a constraint on the average interference that SUs can impose on the PU. Modeling the randomly arriving energy packets during a time slot as a Poisson process, and the dynamics of the battery as a finite state Markov chain, we established a lower bound on the achievable sum-rate of SUs–AP

links, in the presence of both spectrum sensing and channel estimation errors. To strike a balance between the energy harvesting and the energy consumption, we proposed a parametrized power control strategy that allows each SU to adapt its power, according to the feedback information and its stored energy. We optimized the parameters of the proposed power control strategy, such that the derived sum-rate lower bound is maximized, subject to the AIC. We validated our analysis via Matlab simulations and explored spectrum sensing-channel estimation-data transmission trade-offs. We also illustrated how the AIC, the harvesting parameter, and the battery size impact the sum-rate, as well as transmission outage probability.

In Chapter 5, we considered a D2D MMWAVE network with bandwidth of $B_c = WN_c$ Hz, where N cooperative transmitter-receiver pairs form N_c coalitions and communicate over N_c non-overlapping sub-bands, each with bandwidth of W Hz. Each node is equipped with a directional antenna that has beam steering capability. Also, each transmitter can adjust its transmit power. We formulated the network throughput maximization problem, subject to certain constraints, and we proposed a BCD algorithm, to find the optimal coalition among the transmitter-receiver pairs, the optimal beam steering angles of directional antennas of the pairs within each coalition, and the optimal transmit powers. Through numerical simulations, we investigated the effects of $N, N_c, P_{\max}, \phi_{3\text{dB}}$ on the network throughput maximization. Our simulations show that, given N, P_{\max} there is an optimal N_c value that provides the highest network throughput. Also, we showed that a lower $\phi_{3\text{dB}}$ yields a higher network throughput.

APPENDIX A: APPENDIX FOR CHAPTER 3

A.1 Showing that $\partial R_{\text{LB}}/\partial T_{\text{se}} = 0$ has one solution in the interval $(0, T_f - T_{\text{tr}})$

Let $R_{\text{LB}} = C_0 + C_1$ where $C_0 = D_d \beta_0 R_0$ and $C_1 = D_d \beta_1 R_1$. To calculate $\partial R_{\text{LB}}/\partial T_{\text{se}}$ we need the following derivatives:

$$\begin{aligned}\frac{\partial C_0}{\partial T_{\text{se}}} &= R_0 \left[\beta_0 \frac{\partial D_d}{\partial T_{\text{se}}} + D_d \frac{\partial \beta_0}{\partial T_{\text{se}}} \right] = R_0 \left[\frac{-\beta_0}{T_f} + D_d \frac{\partial \beta_0}{\partial T_{\text{se}}} \right], \\ \frac{\partial C_1}{\partial T_{\text{se}}} &= R_1 \left[\beta_1 \frac{\partial D_d}{\partial T_{\text{se}}} + D_d \frac{\partial \beta_1}{\partial T_{\text{se}}} \right] = R_1 \left[\frac{-\beta_1}{T_f} + D_d \frac{\partial \beta_1}{\partial T_{\text{se}}} \right].\end{aligned}$$

Recall $\beta_0 = \pi_0(1 - \bar{P}_{\text{fa}})$ and $\beta_1 = \pi_1(1 - \bar{P}_{\text{d}})$ in (3.11). We assume \bar{P}_{d} is given, hence $\partial \beta_1/\partial T_{\text{se}} = 0$. On the other hand, \bar{P}_{fa} in (3.8) is variable w.r.t. T_{se} , and hence we have

$$\frac{\partial \beta_0}{\partial T_{\text{se}}} = \pi_0 f_{\text{TW2}} \left(\frac{\eta - \theta_{\text{sen}}}{\sigma_{\text{sen}}} \right) \frac{\partial}{\partial T_{\text{se}}} \left(\frac{\eta - \theta_{\text{sen}}}{\sigma_{\text{sen}}} \right) \quad (\text{A.1})$$

where f_{TW2} denotes the PDF of the Tracy-Widom distribution of order 2, and, $\theta_{\text{sen}}, \sigma_{\text{sen}}$ are given in (3.9). Evaluating $\frac{\partial C_0}{\partial T_{\text{se}}}$ and $\frac{\partial C_1}{\partial T_{\text{se}}}$ when $T_{\text{se}} \rightarrow 0$ we have

$$\lim_{T_{\text{se}} \rightarrow 0} \frac{\partial C_0}{\partial T_{\text{se}}} = \lim_{T_{\text{se}} \rightarrow 0} \frac{-\beta_0}{T_f} R_0 + \frac{(T_f - T_{\text{tr}})}{T_f} R_0 \left(\underbrace{\lim_{T_{\text{se}} \rightarrow 0} \frac{\partial \beta_0}{\partial T_{\text{se}}}}_{=+\infty} \right) = +\infty, \quad (\text{A.2a})$$

$$\lim_{T_{\text{se}} \rightarrow 0} \frac{\partial C_1}{\partial T_{\text{se}}} = \lim_{T_{\text{se}} \rightarrow 0} \frac{-\beta_1}{T_f} R_1 + \frac{(T_f - T_{\text{tr}})}{T_f} R_1 \left(\underbrace{\lim_{T_{\text{se}} \rightarrow 0} \frac{\partial \beta_1}{\partial T_{\text{se}}}}_{=0} \right) < 0. \quad (\text{A.2b})$$

Evaluating $\frac{\partial C_0}{\partial T_{\text{se}}}$ and $\frac{\partial C_1}{\partial T_{\text{se}}}$ when $T_{\text{se}} \rightarrow T_f - T_{\text{tr}}$ we have

$$\lim_{T_{\text{se}} \rightarrow T_f - T_{\text{tr}}} \frac{\partial C_0}{\partial T_{\text{se}}} = \lim_{T_{\text{se}} \rightarrow T_f - T_{\text{tr}}} \frac{-\beta_0}{T_f} R_0 + R_0 \left(\underbrace{\lim_{T_{\text{se}} \rightarrow T_f - T_{\text{tr}}} D_d}_{=0} \right) \left(\lim_{T_{\text{se}} \rightarrow T_f - T_{\text{tr}}} \frac{\partial \beta_0}{\partial T_{\text{se}}} \right) < 0, \quad (\text{A.3a})$$

$$\lim_{T_{\text{se}} \rightarrow T_f - T_{\text{tr}}} \frac{\partial C_1}{\partial T_{\text{se}}} = \lim_{T_{\text{se}} \rightarrow T_f - T_{\text{tr}}} \frac{-\beta_1}{T_f} R_1 + R_1 \left(\underbrace{\lim_{T_{\text{se}} \rightarrow T_f - T_{\text{tr}}} D_d}_{=0} \right) \left(\lim_{T_{\text{se}} \rightarrow T_f - T_{\text{tr}}} \frac{\partial \beta_1}{\partial T_{\text{se}}} \right) < 0. \quad (\text{A.3b})$$

The inequalities in (A.2a) and (A.2b) show that $\lim_{T_{\text{se}} \rightarrow 0} \frac{\partial R_{\text{LB}}}{\partial T_{\text{se}}} > 0$. On the other hand, the inequalities in (A.3a) and (A.3b) show that $\lim_{T_{\text{se}} \rightarrow T_f - T_{\text{tr}}} \frac{\partial R_{\text{LB}}}{\partial T_{\text{se}}} < 0$. Together, these indicate that the equation $\partial R_{\text{LB}}/\partial T_{\text{se}} = 0$ has one solution in the interval $(0, T_f - T_{\text{tr}})$. This solution can be found using bisection search method.

A.2 Showing that $\partial R_{LB}/\partial T_{tr} = 0$ has one solution in the interval $(0, T_f - T_{se})$

To calculate $\partial R_{LB}/\partial T_{tr}$ we need the following derivatives:

$$\frac{\partial C_0}{\partial T_{tr}} = \beta_0 \left[D_d \frac{\partial R_0}{\partial T_{tr}} + \frac{\partial D_d}{\partial T_{tr}} R_0 \right] = \beta_0 \left[D_d \sum_{m=1}^M \frac{\partial R_0}{\partial \hat{\alpha}_m^0} \frac{\partial \hat{\alpha}_m^0}{\partial T_{tr}} - \frac{R_0}{T_f} \right],$$

$$\frac{\partial C_1}{\partial T_{tr}} = \beta_1 \left[D_d \frac{\partial R_1}{\partial T_{tr}} + \frac{\partial D_d}{\partial T_{tr}} R_1 \right] = \beta_1 \left[D_d \sum_{m=1}^M \frac{\partial R_1}{\partial \hat{\alpha}_m^1} \frac{\partial \hat{\alpha}_m^1}{\partial T_{tr}} - \frac{R_1}{T_f} \right].$$

Evaluating $\frac{\partial C_0}{\partial T_{tr}}$ and $\frac{\partial C_1}{\partial T_{tr}}$ when $T_{tr} \rightarrow 0$ we have

$$\lim_{T_{tr} \rightarrow 0} \frac{\partial C_0}{\partial T_{tr}} = \frac{-\beta_0}{T_f} \left(\underbrace{\lim_{T_{tr} \rightarrow 0} R_0}_{=0} \right) + \beta_0 \frac{(T_f - T_{se})}{T_f} \sum_{m=1}^M \left(\underbrace{\lim_{T_{tr} \rightarrow 0} \frac{\partial R_0}{\partial \hat{\alpha}_m^0}}_{>0} \right) \left(\underbrace{\lim_{T_{tr} \rightarrow 0} \frac{\partial \hat{\alpha}_m^0}{\partial T_{tr}}}_{>0} \right) > 0 \quad (\text{A.4a})$$

$$\lim_{T_{tr} \rightarrow 0} \frac{\partial C_1}{\partial T_{tr}} = \frac{-\beta_1}{T_f} \left(\underbrace{\lim_{T_{tr} \rightarrow 0} R_1}_{=0} \right) + \beta_1 \frac{(T_f - T_{se})}{T_f} \sum_{m=1}^M \left(\underbrace{\lim_{T_{tr} \rightarrow 0} \frac{\partial R_1}{\partial \hat{\alpha}_m^1}}_{>0} \right) \left(\underbrace{\lim_{T_{tr} \rightarrow 0} \frac{\partial \hat{\alpha}_m^1}{\partial T_{tr}}}_{>0} \right) > 0. \quad (\text{A.4b})$$

Evaluating $\frac{\partial C_0}{\partial T_{tr}}$ and $\frac{\partial C_1}{\partial T_{tr}}$ when $T_{tr} \rightarrow T_f - T_{se}$ we have

$$\lim_{T_{tr} \rightarrow T_f - T_{se}} \frac{\partial C_0}{\partial T_{tr}} = \lim_{T_{tr} \rightarrow T_f - T_{se}} \frac{-\beta_0 R_0}{T_f} + \beta_0 \left(\underbrace{\lim_{T_{tr} \rightarrow T_f - T_{se}} D_d}_{=0} \right) \left(\lim_{T_{tr} \rightarrow T_f - T_{se}} \sum_{m=1}^M \frac{\partial R_0}{\partial \hat{\alpha}_m^0} \frac{\partial \hat{\alpha}_m^0}{\partial T_{tr}} \right) < 0 \quad (\text{A.5a})$$

$$\lim_{T_{tr} \rightarrow T_f - T_{se}} \frac{\partial C_1}{\partial T_{tr}} = \lim_{T_{tr} \rightarrow T_f - T_{se}} \frac{-\beta_1 R_1}{T_f} + \beta_1 \left(\underbrace{\lim_{T_{tr} \rightarrow T_f - T_{se}} D_d}_{=0} \right) \left(\lim_{T_{tr} \rightarrow T_f - T_{se}} \sum_{m=1}^M \frac{\partial R_1}{\partial \hat{\alpha}_m^1} \frac{\partial \hat{\alpha}_m^1}{\partial T_{tr}} \right) < 0 \quad (\text{A.5b})$$

The inequalities in (A.4a) and (A.4b) show that $\lim_{T_{tr} \rightarrow 0} \frac{\partial R_{LB}}{\partial T_{tr}} > 0$. On the other hand, the inequalities in (A.5a) and (A.5b) show that $\lim_{T_{tr} \rightarrow T_f - T_{se}} \frac{\partial R_{LB}}{\partial T_{tr}} < 0$. Together, these indicate that the equation $\partial R_{LB}/\partial T_{tr} = 0$ has one solution in this interval, which can be found numerically using bisection search method.

APPENDIX B: BIOGRAPHICAL SKETCH

The author was born in Darab, Iran in 1987. He received his Bachelor of Science (honors) degree from Shiraz University of Technology, Shiraz, Iran in 2009 and his Master of Science degree from University of Tehran, Tehran, Iran in 2012; both in Electrical Engineering. In his master's program, he worked on the problem of whitening matched filter design for ultra-wide bandwidth communication systems. In January 2016, he joined the Department of Electrical Engineering and Computer Science in University of Central Florida as a Ph.D. student under direction of Dr. Azadeh Vosoughi. His current research interests include cognitive radio, statistical signal processing, energy harvesting in wireless sensor networks, and array signal processing.

APPENDIX C: PUBLICATIONS

Journal papers

- H. Yazdani, A. Vosoughi, and X. Gong, “Achievable rates of opportunistic cognitive radio systems using reconfigurable antennas with imperfect sensing and channel estimation,” in *IEEE Transactions on Cognitive Communications and Networking*, doi: 10.1109/TCCN.2021.3056691.
- H. Yazdani, A. Vosoughi, and X. Gong, “Beam selection and discrete power allocation in opportunistic cognitive radio systems with limited feedback using ESPAR antennas,” *IEEE Transactions on Cognitive Communications and Networking*, vol. 6, no. 1, pp. 325–339, 2020.
- H. Yazdani and A. Vosoughi, “Steady-State Rate-Optimal Power Adaptation in Energy Harvesting Opportunistic Cognitive Radios with Spectrum Sensing and Channel Estimation Errors,” *IEEE Transactions on Green Communications and Networking*, doi: 10.1109/TGCN.2021.3087456.

Conference papers

- H. Yazdani, S. Seth, A. Vosoughi, and M. Yuksel, “Throughput-optimal D2D mmWave communication: Joint coalition formation, power, and beam optimization,” submitted to *2021 IEEE Global Communications Conference (GLOBECOM)*.
- M. Joneidi, H. Yazdani, A. Vosoughi and N. Rahnavard, “Source localization and tracking for dynamic radio cartography using directional antennas,” *2019 16th Annual IEEE International Conference on Sensing, Communication, and Networking (SECON)*, Boston, MA, USA, 2019, pp. 1-9.
- G. Ardeshiri, H. Yazdani and A. Vosoughi, “Power adaptation for distributed detection in energy harvesting WSNs with finite-capacity battery,” in *2019 IEEE Global Communications Conference (GLOBECOM)*, 2019, pp. 1–6.
- H. Yazdani and A. Vosoughi, “On the spectrum sensing, beam selection and power allocation in cognitive radio networks using reconfigurable antennas,” *2019 53rd Annual Conference on Information Sciences and Systems (CISS)*, Baltimore, MD, USA, 2019, pp. 1-7.
- H. Yazdani and A. Vosoughi, “On optimal sensing and capacity trade-off in cognitive radio systems with directional antennas,” *2018 IEEE Global Conference on Signal and Information Processing (GlobalSIP)*, Anaheim, CA, USA,

2018, pp. 1015-1019.

- G. Ardeshiri, H. Yazdani and A. Vosoughi, “Optimal local thresholds for distributed detection in energy harvesting wireless sensor networks,” *2018 IEEE Global Conference on Signal and Information Processing (GlobalSIP)*, Anaheim, CA, USA, 2018, pp. 813-817.
- H. Yazdani and A. Vosoughi, “On the combined effect of directional antennas and imperfect spectrum sensing upon ergodic capacity of cognitive radio systems,” in *2017 51st Asilomar Conference on Signals, Systems, and Computers*, Oct 2017, pp. 1702–1706.
- H. Yazdani, A. Vosoughi, and N. Rahnavard, “Compressive sensing based direction-of-arrival estimation using reweighted greedy block coordinate descent algorithm for ESPAR antennas,” in *MILCOM 2017 - 2017 IEEE Military Communications Conference (MILCOM)*, Oct 2017, pp. 169–173.
- H. Yazdani and A. Vosoughi, “On cognitive radio systems with directional antennas and imperfect spectrum sensing,” in *2017 IEEE International Conference on Acoustics, Speech and Signal Processing (ICASSP)*, March 2017, pp. 3589–3593.

APPENDIX D: COPYRIGHT PERMISSIONS

On cognitive radio systems with directional antennas and imperfect spectrum sensing



Conference Proceedings:

2017 IEEE International Conference on Acoustics, Speech and Signal Processing (ICASSP)

Author: Hassan Yazdani; Azadeh Vosoughi

Publisher: IEEE

Date: 5-9 March 2017

Copyright © 2017, IEEE

Thesis / Dissertation Reuse

The IEEE does not require individuals working on a thesis to obtain a formal reuse license, however, you may print out this statement to be used as a permission grant:

Requirements to be followed when using any portion (e.g., figure, graph, table, or textual material) of an IEEE copyrighted paper in a thesis:

- 1) In the case of textual material (e.g., using short quotes or referring to the work within these papers) users must give full credit to the original source (author, paper, publication) followed by the IEEE copyright line © 2011 IEEE.
- 2) In the case of illustrations or tabular material, we require that the copyright line © [Year of original publication] IEEE appear prominently with each reprinted figure and/or table.
- 3) If a substantial portion of the original paper is to be used, and if you are not the senior author, also obtain the senior author's approval.

Requirements to be followed when using an entire IEEE copyrighted paper in a thesis:

- 1) The following IEEE copyright/ credit notice should be placed prominently in the references: © [year of original publication] IEEE. Reprinted, with permission, from [author names, paper title, IEEE publication title, and month/year of publication]
- 2) Only the accepted version of an IEEE copyrighted paper can be used when posting the paper or your thesis on-line.
- 3) In placing the thesis on the author's university website, please display the following message in a prominent place on the website: In reference to IEEE copyrighted material which is used with permission in this thesis, the IEEE does not endorse any of [university/educational entity's name goes here]'s products or services. Internal or personal use of this material is permitted. If interested in reprinting/republishing IEEE copyrighted material for advertising or promotional purposes or for creating new collective works for resale or redistribution, please go to http://www.ieee.org/publications_standards/publications/rights/rights_link.html to learn how to obtain a License from RightsLink.

If applicable, University Microfilms and/or ProQuest Library, or the Archives of Canada may supply single copies of the dissertation.

BACK

CLOSE WINDOW

On Optimal Sensing and Capacity Trade-off in Cognitive Radio Systems with Directional Antennas



Conference Proceedings:

2018 IEEE Global Conference on Signal and Information Processing (GlobalSIP)

Author: Hassan Yazdani; Azadeh Vosoughi

Publisher: IEEE

Date: 26-29 Nov. 2018

Copyright © 2018, IEEE

Thesis / Dissertation Reuse

The IEEE does not require individuals working on a thesis to obtain a formal reuse license, however, you may print out this statement to be used as a permission grant:

Requirements to be followed when using any portion (e.g., figure, graph, table, or textual material) of an IEEE copyrighted paper in a thesis:

- 1) In the case of textual material (e.g., using short quotes or referring to the work within these papers) users must give full credit to the original source (author, paper, publication) followed by the IEEE copyright line © 2011 IEEE.
- 2) In the case of illustrations or tabular material, we require that the copyright line © [Year of original publication] IEEE appear prominently with each reprinted figure and/or table.
- 3) If a substantial portion of the original paper is to be used, and if you are not the senior author, also obtain the senior author's approval.

Requirements to be followed when using an entire IEEE copyrighted paper in a thesis:

- 1) The following IEEE copyright/ credit notice should be placed prominently in the references: © [year of original publication] IEEE. Reprinted, with permission, from [author names, paper title, IEEE publication title, and month/year of publication]
- 2) Only the accepted version of an IEEE copyrighted paper can be used when posting the paper or your thesis on-line.
- 3) In placing the thesis on the author's university website, please display the following message in a prominent place on the website: In reference to IEEE copyrighted material which is used with permission in this thesis, the IEEE does not endorse any of [university/educational entity's name goes here]'s products or services. Internal or personal use of this material is permitted. If interested in reprinting/republishing IEEE copyrighted material for advertising or promotional purposes or for creating new collective works for resale or redistribution, please go to http://www.ieee.org/publications_standards/publications/rights/rights_link.html to learn how to obtain a License from RightsLink.

If applicable, University Microfilms and/or ProQuest Library, or the Archives of Canada may supply single copies of the dissertation.

BACK

CLOSE WINDOW

On the Spectrum Sensing, Beam Selection and Power Allocation in Cognitive Radio Networks Using Reconfigurable Antennas



Conference Proceedings:

2019 53rd Annual Conference on Information Sciences and Systems (CISS)

Author: Hassan Yazdani; Azadeh Vosoughi

Publisher: IEEE

Date: 20-22 March 2019

Copyright © 2019, IEEE

Thesis / Dissertation Reuse

The IEEE does not require individuals working on a thesis to obtain a formal reuse license, however, you may print out this statement to be used as a permission grant:

Requirements to be followed when using any portion (e.g., figure, graph, table, or textual material) of an IEEE copyrighted paper in a thesis:

- 1) In the case of textual material (e.g., using short quotes or referring to the work within these papers) users must give full credit to the original source (author, paper, publication) followed by the IEEE copyright line © 2011 IEEE.
- 2) In the case of illustrations or tabular material, we require that the copyright line © [Year of original publication] IEEE appear prominently with each reprinted figure and/or table.
- 3) If a substantial portion of the original paper is to be used, and if you are not the senior author, also obtain the senior author's approval.

Requirements to be followed when using an entire IEEE copyrighted paper in a thesis:

- 1) The following IEEE copyright/ credit notice should be placed prominently in the references: © [year of original publication] IEEE. Reprinted, with permission, from [author names, paper title, IEEE publication title, and month/year of publication]
- 2) Only the accepted version of an IEEE copyrighted paper can be used when posting the paper or your thesis online.
- 3) In placing the thesis on the author's university website, please display the following message in a prominent place on the website: In reference to IEEE copyrighted material which is used with permission in this thesis, the IEEE does not endorse any of [university/educational entity's name goes here]'s products or services. Internal or personal use of this material is permitted. If interested in reprinting/republishing IEEE copyrighted material for advertising or promotional purposes or for creating new collective works for resale or redistribution, please go to http://www.ieee.org/publications_standards/publications/rights/rights_link.html to learn how to obtain a License from RightsLink.

If applicable, University Microfilms and/or ProQuest Library, or the Archives of Canada may supply single copies of the dissertation.

BACK

CLOSE WINDOW



Beam Selection and Discrete Power Allocation in Opportunistic Cognitive Radio Systems With Limited Feedback Using ESPAR Antennas

Author: Hassan Yazdani; Azadeh Vosoughi; Xun Gong

Publication: IEEE Transactions on Cognitive Communications and Networking

Publisher: IEEE

Date: March 2020

Copyright © 2020, IEEE

Thesis / Dissertation Reuse

The IEEE does not require individuals working on a thesis to obtain a formal reuse license, however, you may print out this statement to be used as a permission grant:

Requirements to be followed when using any portion (e.g., figure, graph, table, or textual material) of an IEEE copyrighted paper in a thesis:

- 1) In the case of textual material (e.g., using short quotes or referring to the work within these papers) users must give full credit to the original source (author, paper, publication) followed by the IEEE copyright line © 2011 IEEE.
- 2) In the case of illustrations or tabular material, we require that the copyright line © [Year of original publication] IEEE appear prominently with each reprinted figure and/or table.
- 3) If a substantial portion of the original paper is to be used, and if you are not the senior author, also obtain the senior author's approval.

Requirements to be followed when using an entire IEEE copyrighted paper in a thesis:

- 1) The following IEEE copyright/ credit notice should be placed prominently in the references: © [year of original publication] IEEE. Reprinted, with permission, from [author names, paper title, IEEE publication title, and month/year of publication]
- 2) Only the accepted version of an IEEE copyrighted paper can be used when posting the paper or your thesis online.
- 3) In placing the thesis on the author's university website, please display the following message in a prominent place on the website: In reference to IEEE copyrighted material which is used with permission in this thesis, the IEEE does not endorse any of [university/educational entity's name goes here]'s products or services. Internal or personal use of this material is permitted. If interested in reprinting/republishing IEEE copyrighted material for advertising or promotional purposes or for creating new collective works for resale or redistribution, please go to http://www.ieee.org/publications_standards/publications/rights/rights_link.html to learn how to obtain a License from RightsLink.

If applicable, University Microfilms and/or ProQuest Library, or the Archives of Canada may supply single copies of the dissertation.

BACK

CLOSE WINDOW



Achievable Rates of Opportunistic Cognitive Radio Systems Using Reconfigurable Antennas with Imperfect Sensing and Channel Estimation

Author: Hassan Yazdani; Azadeh Vosoughi; Xun Gong

Publication: IEEE Transactions on Cognitive Communications and Networking

Publisher: IEEE

Date: Dec 31, 1969

Copyright © 1969, IEEE

Thesis / Dissertation Reuse

The IEEE does not require individuals working on a thesis to obtain a formal reuse license, however, you may print out this statement to be used as a permission grant:

Requirements to be followed when using any portion (e.g., figure, graph, table, or textual material) of an IEEE copyrighted paper in a thesis:

- 1) In the case of textual material (e.g., using short quotes or referring to the work within these papers) users must give full credit to the original source (author, paper, publication) followed by the IEEE copyright line © 2011 IEEE.
- 2) In the case of illustrations or tabular material, we require that the copyright line © [Year of original publication] IEEE appear prominently with each reprinted figure and/or table.
- 3) If a substantial portion of the original paper is to be used, and if you are not the senior author, also obtain the senior author's approval.

Requirements to be followed when using an entire IEEE copyrighted paper in a thesis:

- 1) The following IEEE copyright/ credit notice should be placed prominently in the references: © [year of original publication] IEEE. Reprinted, with permission, from [author names, paper title, IEEE publication title, and month/year of publication]
- 2) Only the accepted version of an IEEE copyrighted paper can be used when posting the paper or your thesis online.
- 3) In placing the thesis on the author's university website, please display the following message in a prominent place on the website: In reference to IEEE copyrighted material which is used with permission in this thesis, the IEEE does not endorse any of [university/educational entity's name goes here]'s products or services. Internal or personal use of this material is permitted. If interested in reprinting/republishing IEEE copyrighted material for advertising or promotional purposes or for creating new collective works for resale or redistribution, please go to http://www.ieee.org/publications_standards/publications/rights/rights_link.html to learn how to obtain a License from RightsLink.

If applicable, University Microfilms and/or ProQuest Library, or the Archives of Canada may supply single copies of the dissertation.

BACK

CLOSE WINDOW



Steady-State Rate-Optimal Power Adaptation in Energy Harvesting Opportunistic Cognitive Radios with Spectrum Sensing and Channel Estimation Errors

Author: Hassan Yazdani

Publication: IEEE Transactions on Green Communications and Networking

Publisher: IEEE

Date: Dec 31, 1969

Copyright © 1969, IEEE

Thesis / Dissertation Reuse

The IEEE does not require individuals working on a thesis to obtain a formal reuse license, however, you may print out this statement to be used as a permission grant:

Requirements to be followed when using any portion (e.g., figure, graph, table, or textual material) of an IEEE copyrighted paper in a thesis:

- 1) In the case of textual material (e.g., using short quotes or referring to the work within these papers) users must give full credit to the original source (author, paper, publication) followed by the IEEE copyright line © 2011 IEEE.
- 2) In the case of illustrations or tabular material, we require that the copyright line © [Year of original publication] IEEE appear prominently with each reprinted figure and/or table.
- 3) If a substantial portion of the original paper is to be used, and if you are not the senior author, also obtain the senior author's approval.

Requirements to be followed when using an entire IEEE copyrighted paper in a thesis:

- 1) The following IEEE copyright/ credit notice should be placed prominently in the references: © [year of original publication] IEEE. Reprinted, with permission, from [author names, paper title, IEEE publication title, and month/year of publication]
- 2) Only the accepted version of an IEEE copyrighted paper can be used when posting the paper or your thesis on-line.
- 3) In placing the thesis on the author's university website, please display the following message in a prominent place on the website: In reference to IEEE copyrighted material which is used with permission in this thesis, the IEEE does not endorse any of [university/educational entity's name goes here]'s products or services. Internal or personal use of this material is permitted. If interested in reprinting/republishing IEEE copyrighted material for advertising or promotional purposes or for creating new collective works for resale or redistribution, please go to http://www.ieee.org/publications_standards/publications/rights/rights_link.html to learn how to obtain a License from RightsLink.

If applicable, University Microfilms and/or ProQuest Library, or the Archives of Canada may supply single copies of the dissertation.

BACK

CLOSE WINDOW

LIST OF REFERENCES

- [1] H. Yazdani and A. Vosoughi, "On cognitive radio systems with directional antennas and imperfect spectrum sensing," in *2017 IEEE International Conference on Acoustics, Speech and Signal Processing (ICASSP)*, March 2017, pp. 3589–3593.
- [2] H. Yazdani and A. Vosoughi, "On optimal sensing and capacity trade-off in cognitive radio systems with directional antennas," in *2018 IEEE Global Conference on Signal and Information Processing (GlobalSIP)*, Nov 2018, pp. 1015–1019.
- [3] H. Yazdani and A. Vosoughi, "On the spectrum sensing, beam selection and power allocation in cognitive radio networks using reconfigurable antennas," in *2019 53rd Annual Conference on Information Sciences and Systems (CISS)*, March 2019.
- [4] H. Yazdani, A. Vosoughi, and X. Gong, "Beam selection and discrete power allocation in opportunistic cognitive radio systems with limited feedback using ESPAR antennas," *IEEE Transactions on Cognitive Communications and Networking*, vol. 6, no. 1, pp. 325–339, 2020.
- [5] H. Yazdani, A. Vosoughi, and X. Gong, "Achievable rates of opportunistic cognitive radio systems using reconfigurable antennas with imperfect sensing and channel estimation," *arXiv:2007.04390*, 2020.
- [6] H. Yazdani and A. Vosoughi, "Steady-state rate-optimal power adaptation in energy harvesting opportunistic cognitive radios with spectrum sensing and channel estimation errors," *IEEE Transactions on Green Communications and Networking*, pp. 1–1, 2021.
- [7] A. Goldsmith, S. A. Jafar, I. Maric, and S. Srinivasa, "Breaking spectrum gridlock with cognitive radios: An information theoretic perspective," *Proceedings of the IEEE*, vol. 97, no. 5, pp. 894–914, May 2009.
- [8] T. Yucek and H. Arslan, "A survey of spectrum sensing algorithms for cognitive radio applications," *IEEE Communications Surveys Tutorials*, vol. 11, no. 1, pp. 116–130, 2009.
- [9] S. Haykin, "Cognitive radio: brain-empowered wireless communications," *IEEE Journal on Selected Areas in Communications*, vol. 23, no. 2, pp. 201–220, 2005.
- [10] P. Paysarvi-Hoseini and N. C. Beaulieu, "Optimal wideband spectrum sensing framework for cognitive radio systems," *IEEE Transactions on Signal Processing*, vol. 59, no. 3, pp. 1170–1182, March 2011.

- [11] H. Bogucka, P. Kryszkiewicz, and A. Kliks, "Dynamic spectrum aggregation for future 5G communications," *IEEE Communications Magazine*, vol. 53, no. 5, pp. 35–43, 2015.
- [12] J. Zou, H. Xiong, D. Wang, and C. W. Chen, "Optimal power allocation for hybrid overlay/underlay spectrum sharing in multiband cognitive radio networks," *IEEE Transactions on Vehicular Technology*, vol. 62, no. 4, pp. 1827–1837, 2013.
- [13] T. M. C. Chu, H. Phan, and H. Zepernick, "Hybrid interweave-underlay spectrum access for cognitive cooperative radio networks," *IEEE Transactions on Communications*, vol. 62, no. 7, pp. 2183–2197, 2014.
- [14] G. Ozcan and M. C. Gursoy, "Optimal power control for underlay cognitive radio systems with arbitrary input distributions," *IEEE Transactions on Wireless Communications*, vol. 14, no. 8, pp. 4219–4233, Aug 2015.
- [15] M. M. Abdallah, A. H. Salem, M. S. Alouini, and K. A. Qaraqe, "Adaptive discrete rate and power transmission for spectrum sharing systems," *IEEE Transactions on Wireless Communications*, vol. 11, no. 4, pp. 1283–1289, April 2012.
- [16] X. Kang, Y. C. Liang, A. Nallanathan, H. K. Garg, and R. Zhang, "Optimal power allocation for fading channels in cognitive radio networks: Ergodic capacity and outage capacity," *IEEE Transactions on Wireless Communications*, vol. 8, no. 2, pp. 940–950, Feb 2009.
- [17] L. Musavian, S. Aissa, and S. Lambotharan, "Adaptive modulation in spectrum-sharing channels under delay quality-of-service constraints," *IEEE Transactions on Vehicular Technology*, vol. 60, no. 3, pp. 901–911, 2011.
- [18] L. Musavian and S. Aissa, "Capacity and power allocation for spectrum-sharing communications in fading channels," *IEEE Transactions on Wireless Communications*, vol. 8, no. 1, pp. 148–156, 2009.
- [19] G. Ozcan, M. C. Gursoy, N. Tran, and J. Tang, "Energy-efficient power allocation in cognitive radio systems with imperfect spectrum sensing," *IEEE Journal on Selected Areas in Communications*, vol. 34, no. 12, pp. 3466–3481, Dec 2016.
- [20] S. Kashyap and N. B. Mehta, "Optimal binary power control for underlay CR with different interference constraints and impact of channel estimation errors," *IEEE Transactions on Communications*, vol. 62, no. 11, pp. 3753–3764, Nov 2014.
- [21] H. V. Poor, *An introduction to signal detection and estimation*. Springer Science & Business Media, 2013.

- [22] Y. Zeng, Y.-C. Liang, A. T. Hoang, and R. Zhang, "A review on spectrum sensing for cognitive radio: challenges and solutions," *EURASIP Journal on Advances in signal Processing*, vol. 2010, pp. 1–15, 2010.
- [23] S. Srinivasa and S. A. Jafar, "Cognitive radios for dynamic spectrum access - The throughput potential of cognitive radio: A theoretical perspective," *IEEE Communications Magazine*, vol. 45, no. 5, pp. 73–79, 2007.
- [24] E. Axell, G. Leus, E. G. Larsson, and H. V. Poor, "Spectrum sensing for cognitive radio: State-of-the-art and recent advances," *IEEE Signal Processing Magazine*, vol. 29, no. 3, pp. 101–116, 2012.
- [25] F. F. Digham, M. Alouini, and M. K. Simon, "On the energy detection of unknown signals over fading channels," *IEEE Transactions on Communications*, vol. 55, no. 1, pp. 21–24, 2007.
- [26] A. Taherpour, M. Nasiri-Kenari, and S. Gazor, "Multiple antenna spectrum sensing in cognitive radios," *IEEE Transactions on Wireless Communications*, vol. 9, no. 2, pp. 814–823, February 2010.
- [27] A. Kortun, T. Ratnarajah, M. Sellathurai, Y. Liang, and Y. Zeng, "On the eigenvalue-based spectrum sensing and secondary user throughput," *IEEE Transactions on Vehicular Technology*, vol. 63, no. 3, pp. 1480–1486, March 2014.
- [28] F. Awin, E. Abdel-Raheem, and K. Tepe, "Blind spectrum sensing approaches for interweaved cognitive radio system: A tutorial and short course," *IEEE Communications Surveys Tutorials*, vol. 21, no. 1, pp. 238–259, Firstquarter 2019.
- [29] Y. He, T. Ratnarajah, E. H. Yousif, J. Xue, and M. Sellathurai, "Performance analysis of multi-antenna GLRT-based spectrum sensing for cognitive radio," *Signal Processing*, vol. 120, pp. 580–593, March 2016.
- [30] S. Akin and M. C. Gursoy, "Performance analysis of cognitive radio systems under QoS constraints and channel uncertainty," *IEEE Transactions on Wireless Communications*, vol. 10, no. 9, pp. 2883–2895, September 2011.
- [31] Z. Rezk and M. Alouini, "Ergodic capacity of cognitive radio under imperfect channel-state information," *IEEE Transactions on Vehicular Technology*, vol. 61, no. 5, pp. 2108–2119, Jun 2012.
- [32] D. Xu, Z. Feng, and P. Zhang, "On the impacts of channel estimation errors and feedback delay on the ergodic capacity for spectrum sharing cognitive radio," *Wireless Personal Communications*, vol. 72, no. 4, pp. 1875–1887, Oct 2013.

- [33] H. A. Suraweera, P. J. Smith, and M. Shafi, "Capacity limits and performance analysis of cognitive radio with imperfect channel knowledge," *IEEE Transactions on Vehicular Technology*, vol. 59, no. 4, pp. 1811–1822, May 2010.
- [34] L. Sboui, Z. Rezki, and M. Alouini, "A unified framework for the ergodic capacity of spectrum sharing cognitive radio systems," *IEEE Transactions on Wireless Communications*, vol. 12, no. 2, pp. 877–887, February 2013.
- [35] P. J. Smith, P. A. Dmochowski, H. A. Suraweera, and M. Shafi, "The effects of limited channel knowledge on cognitive radio system capacity," *IEEE Transactions on Vehicular Technology*, vol. 62, no. 2, pp. 927–933, Feb 2013.
- [36] A. Kaushik, S. K. Sharma, S. Chatzinotas, B. Ottersten, and F. K. Jondral, "On the performance analysis of underlay cognitive radio systems: A deployment perspective," *IEEE Transactions on Cognitive Communications and Networking*, vol. 2, no. 3, pp. 273–287, Sep. 2016.
- [37] L. Musavian and S. Aissa, "Fundamental capacity limits of cognitive radio in fading environments with imperfect channel information," *IEEE Transactions on Communications*, vol. 57, no. 11, pp. 3472–3480, 2009.
- [38] H. Zhang, Y. Nie, J. Cheng, V. C. M. Leung, and A. Nallanathan, "Sensing time optimization and power control for energy efficient cognitive small cell with imperfect hybrid spectrum sensing," *IEEE Transactions on Wireless Communications*, vol. 16, no. 2, pp. 730–743, Feb 2017.
- [39] S. Stotas and A. Nallanathan, "Optimal sensing time and power allocation in multiband cognitive radio networks," *IEEE Transactions on Communications*, vol. 59, no. 1, pp. 226–235, January 2011.
- [40] H. Hu, H. Zhang, and Y. C. Liang, "On the spectrum- and energy-efficiency tradeoff in cognitive radio networks," *IEEE Transactions on Communications*, vol. 64, no. 2, pp. 490–501, Feb 2016.
- [41] Y. C. Liang, Y. Zeng, E. C. Y. Peh, and A. T. Hoang, "Sensing-throughput tradeoff for cognitive radio networks," *IEEE Transactions on Wireless Communications*, vol. 7, no. 4, pp. 1326–1337, April 2008.
- [42] S. Srinivasa and A. Nallanathan, "On the throughput and spectrum sensing enhancement of opportunistic spectrum access cognitive radio networks," *IEEE Transactions on Wireless Communications*, vol. 11, no. 1, pp. 97–107, January 2012.
- [43] G. Ozcan, M. C. Gursoy, and J. Tang, "Spectral and energy efficiency in cognitive radio systems with unslotted primary users and sensing uncertainty," *IEEE Transactions on Communications*, vol. 65, no. 10, pp. 4138–4151, 2017.

- [44] S. Akin and M. C. Gursoy, “Effective capacity analysis of cognitive radio channels for quality of service provisioning,” *IEEE Transactions on Wireless Communications*, vol. 9, no. 11, pp. 3354–3364, 2010.
- [45] S. Stotas and A. Nallanathan, “On the outage and TIFR capacity of sensing enhanced spectrum sharing systems,” in *2012 IEEE International Conference on Communications (ICC)*, 2012, pp. 1848–1853.
- [46] G. Ozcan, M. C. Gursoy, and S. Gezici, “Error rate analysis of cognitive radio transmissions with imperfect channel sensing,” *IEEE Transactions on Wireless Communications*, vol. 13, no. 3, pp. 1642–1655, 2014.
- [47] N. Janatian, S. Sun, and M. Modarres-Hashemi, “Joint optimal spectrum sensing and power allocation in cdma-based cognitive radio networks,” *IEEE Transactions on Vehicular Technology*, vol. 64, no. 9, pp. 3990–3998, 2015.
- [48] A. Kaushik, S. K. Sharma, S. Chatzinotas, B. Ottersten, and F. K. Jondral, “Sensing-throughput tradeoff for interweave cognitive radio system: A deployment-centric viewpoint,” *IEEE Transactions on Wireless Communications*, vol. 15, no. 5, pp. 3690–3702, May 2016.
- [49] L. Zhang, M. Xiao, G. Wu, S. Li, and Y. Liang, “Energy-efficient cognitive transmission with imperfect spectrum sensing,” *IEEE Journal on Selected Areas in Communications*, vol. 34, no. 5, pp. 1320–1335, 2016.
- [50] K. Wu, H. Jiang, and C. Tellambura, “Sensing, probing, and transmitting strategy for energy harvesting cognitive radio,” in *2017 IEEE International Conference on Communications (ICC)*, May 2017, pp. 1–6.
- [51] W. Chung, S. Park, S. Lim, and D. Hong, “Optimal transmit power control for energy-harvesting cognitive radio system,” in *2013 IEEE 78th Vehicular Technology Conference (VTC Fall)*, Sep. 2013, pp. 1–5.
- [52] A. Sultan, “Sensing and transmit energy optimization for an energy harvesting cognitive radio,” *IEEE Wireless Communications Letters*, vol. 1, no. 5, pp. 500–503, October 2012.
- [53] F. Zhang, T. Jing, Y. Huo, and K. Jiang, “Throughput maximization for energy harvesting cognitive radio networks with finite horizon,” in *2017 9th International Conference on Wireless Communications and Signal Processing (WCSP)*, Oct 2017, pp. 1–7.
- [54] M. Ku, W. Li, Y. Chen, and K. J. Ray Liu, “Advances in energy harvesting communications: Past, present, and future challenges,” *IEEE Communications Surveys Tutorials*, vol. 18, no. 2, pp. 1384–1412, 2016.

- [55] G. Ardeshiri, H. Yazdani, and A. Vosoughi, "Optimal local thresholds for distributed detection in energy harvesting wireless sensor networks," in *2018 IEEE Global Conference on Signal and Information Processing (GlobalSIP)*, Nov 2018, pp. 813–817.
- [56] —, "Power adaptation for distributed detection in energy harvesting WSNs with finite-capacity battery," in *2019 IEEE Global Communications Conference (GLOBECOM)*, 2019, pp. 1–6.
- [57] S. Park, H. Kim, and D. Hong, "Cognitive radio networks with energy harvesting," *IEEE Transactions on Wireless Communications*, vol. 12, no. 3, pp. 1386–1397, March 2013.
- [58] S. Park and D. Hong, "Achievable throughput of energy harvesting cognitive radio networks," *IEEE Transactions on Wireless Communications*, vol. 13, no. 2, pp. 1010–1022, February 2014.
- [59] D. Zhang, Z. Chen, J. Ren, N. Zhang, M. K. Awad, H. Zhou, and X. S. Shen, "Energy-harvesting-aided spectrum sensing and data transmission in heterogeneous cognitive radio sensor network," *IEEE Transactions on Vehicular Technology*, vol. 66, no. 1, pp. 831–843, 2017.
- [60] D. Niyato, P. Wang, and D. I. Kim, "Performance analysis of cognitive radio networks with opportunistic RF energy harvesting," in *2014 IEEE Global Communications Conference*, 2014, pp. 1096–1101.
- [61] D. Altinel and G. K. Kurt, "Finite-state markov channel based modeling of RF energy harvesting systems," *IEEE Transactions on Vehicular Technology*, vol. 67, no. 2, pp. 1713–1725, 2018.
- [62] A. H. Sakr and E. Hossain, "Cognitive and energy harvesting-based D2D communication in cellular networks: Stochastic geometry modeling and analysis," *IEEE Transactions on Communications*, vol. 63, no. 5, pp. 1867–1880, 2015.
- [63] H. S. Lee, M. E. Ahmed, and D. I. Kim, "Optimal spectrum sensing policy in RF-powered cognitive radio networks," *IEEE Transactions on Vehicular Technology*, vol. 67, no. 10, pp. 9557–9570, 2018.
- [64] S. Park, J. Heo, B. Kim, W. Chung, H. Wang, and D. Hong, "Optimal mode selection for cognitive radio sensor networks with RF energy harvesting," in *2012 IEEE 23rd International Symposium on Personal, Indoor and Mobile Radio Communications - (PIMRC)*, 2012, pp. 2155–2159.
- [65] S. Mao, M. H. Cheung, and V. W. S. Wong, "Joint energy allocation for sensing and transmission in rechargeable wireless sensor networks," *IEEE Transactions on Vehicular Technology*, vol. 63, no. 6, pp. 2862–2875, 2014.

- [66] S. Yin, Z. Qu, and S. Li, "Achievable throughput optimization in energy harvesting cognitive radio systems," *IEEE Journal on Selected Areas in Communications*, vol. 33, no. 3, pp. 407–422, 2015.
- [67] R. Ma and W. Zhang, "Optimal power allocation for energy harvesting communications with limited channel feedback," in *2014 IEEE Global Conference on Signal and Information Processing (GlobalSIP)*, 2014, pp. 193–197.
- [68] M. R. Zenaïdi, Z. Rezkî, and M. Alouini, "On communications under stochastic energy harvesting with noisy channel state information," in *2016 IEEE Global Communications Conference (GLOBECOM)*, 2016, pp. 1–6.
- [69] —, "Performance limits of online energy harvesting communications with noisy channel state information at the transmitter," *IEEE Access*, vol. 5, pp. 1239–1249, 2017.
- [70] M. Ku, Y. Chen, and K. J. R. Liu, "Data-driven stochastic models and policies for energy harvesting sensor communications," *IEEE Journal on Selected Areas in Communications*, vol. 33, no. 8, pp. 1505–1520, 2015.
- [71] G. Zhao, J. Ma, G. Y. Li, T. Wu, Y. Kwon, A. Soong, and C. Yang, "Spatial spectrum holes for cognitive radio with relay-assisted directional transmission," *IEEE Transactions on Wireless Communications*, vol. 8, no. 10, pp. 5270–5279, October 2009.
- [72] M. Joneidi, H. Yazdani, A. Vosoughi, and N. Rahnavard, "Source localization and tracking for dynamic radio cartography using directional antennas," in *2019 16th Annual IEEE International Conference on Sensing, Communication, and Networking (SECON)*, 2019, pp. 1–9.
- [73] H. Yazdani and A. Vosoughi, "On the combined effect of directional antennas and imperfect spectrum sensing upon ergodic capacity of cognitive radio systems," in *2017 51st Asilomar Conference on Signals, Systems, and Computers*, Oct 2017, pp. 1702–1706.
- [74] S. M. Sánchez, S. B. Mafra, R. D. Souza, and E. M. G. Fernandez, "Power-rate control with directional transmission and reception in a cognitive radio network," in *2014 International Telecommunications Symposium (ITS)*, Aug 2014, pp. 1–5.
- [75] L. Zhang, Y. Liang, Y. Xin, and H. V. Poor, "Robust cognitive beamforming with partial channel state information," *IEEE Transactions on Wireless Communications*, vol. 8, no. 8, pp. 4143–4153, August 2009.
- [76] V. Nguyen, C. T. Nguyen, H. V. Nguyen, and O. Shin, "Joint beamforming and antenna selection for sum rate maximization in cognitive radio networks," *IEEE Communications Letters*, vol. 21, no. 6, pp. 1369–1372, 2017.

- [77] L. Zhang, Y. Liang, and Y. Xin, "Joint beamforming and power allocation for multiple access channels in cognitive radio networks," *IEEE Journal on Selected Areas in Communications*, vol. 26, no. 1, pp. 38–51, 2008.
- [78] F. Gao, R. Zhang, Y. Liang, and X. Wang, "Design of learning-based MIMO cognitive radio systems," *IEEE Transactions on Vehicular Technology*, vol. 59, no. 4, pp. 1707–1720, May 2010.
- [79] R. Sarvendranath and N. B. Mehta, "Transmit antenna selection for interference-outage constrained underlay CR," *IEEE Transactions on Communications*, vol. 66, no. 9, pp. 3772–3783, Sep. 2018.
- [80] S. Akin and M. C. Gursoy, "On the throughput and energy efficiency of cognitive MIMO transmissions," *IEEE Transactions on Vehicular Technology*, vol. 62, no. 7, pp. 3245–3260, Sep. 2013.
- [81] G. A. Ropokis, M. C. Filippou, A. A. Rontogiannis, L. A. DaSilva, N. Marchetti, V. Frascolla, and P. T. Mathiopoulos, "Optimal sensing and power allocation in pilot-aided shared access systems: A BER minimization approach," in *2016 IEEE 17th International Workshop on Signal Processing Advances in Wireless Communications (SPAWC)*, July 2016, pp. 1–6.
- [82] M. Shirazi, T. Li, J. Huang, and X. Gong, "A reconfigurable dual-polarization slot-ring antenna element with wide bandwidth for array applications," *IEEE Transactions on Antennas and Propagation*, vol. 66, no. 11, pp. 5943–5954, Nov 2018.
- [83] M. Shirazi, J. Huang, T. Li, and X. Gong, "A switchable-frequency slot-ring antenna element for designing a reconfigurable array," *IEEE Antennas and Wireless Propagation Letters*, vol. 17, no. 2, pp. 229–233, Feb 2018.
- [84] W. Ouyang and X. Gong, "A 20-element cavity-backed slot electronically steerable parasitic array radiator (ESPAR) with 2-D beamsteering and minimized beam squint," *IEEE Antennas and Wireless Propagation Letters*, pp. 1–1, 2020.
- [85] W. Ouyang, A. Vosoughi, and X. Gong, "A frequency-reconfigurable electronically-steerable parasitic array radiator using microstrip patch antennas," *Microwave and Optical Technology Letters*, vol. 62, no. 3, pp. 1409–1422, 2020.
- [86] W. Ouyang and X. Gong, "An electronically steerable parasitic array radiator (ESPAR) using cavity-backed slot antennas," *IEEE Antennas and Wireless Propagation Letters*, vol. 18, no. 4, pp. 757–761, 2019.
- [87] M. A. Hossain, I. Bahceci, and B. A. Cetiner, "Parasitic layer-based radiation pattern reconfigurable antenna for 5G communications," *IEEE Transactions on Antennas and Propagation*, vol. 65, no. 12, pp. 6444–6452, 2017.

- [88] *Key Technologies for 5G Wireless Systems*. Cambridge University Press, 2017.
- [89] D. Wilcox, E. Tsakalaki, A. Kortun, T. Ratnarajah, C. B. Papadias, and M. Sellathurai, “On spatial domain cognitive radio using single-radio parasitic antenna arrays,” *IEEE Journal on Selected Areas in Communications*, vol. 31, no. 3, pp. 571–580, March 2013.
- [90] C. Liu and M. Jin, “Maximum-minimum spatial spectrum detection for cognitive radio using parasitic antenna arrays,” in *2014 IEEE/CIC International Conference on Communications in China (ICCC)*, Oct 2014, pp. 365–369.
- [91] C. Liu, M. Li, and M. L. Jin, “Blind energy-based detection for spatial spectrum sensing,” *IEEE Wireless Communications Letters*, vol. 4, no. 1, pp. 98–101, Feb 2015.
- [92] H. Yazdani, A. Vosoughi, and N. Rahnavard, “Compressive sensing based direction-of-arrival estimation using reweighted greedy block coordinate descent algorithm for ESPAR antennas,” in *MILCOM 2017 - 2017 IEEE Military Communications Conference (MILCOM)*, Oct 2017, pp. 169–173.
- [93] W. Ouyang and X. Gong, “A cavity-backed slot ESPAR E-plane array,” in *2017 IEEE 18th Wireless and Microwave Technology Conference (WAMICON)*, April 2017, pp. 1–3.
- [94] R. Qian, M. Sellathurai, and T. Ratnarajah, “Directional spectrum sensing for cognitive radio using ESPAR arrays with a single RF chain,” in *2014 European Conference on Networks and Communications (EuCNC)*, June 2014, pp. 1–5.
- [95] A. M. Alaa, M. H. Ismail, and H. Tawfik, “Random aerial beamforming for underlay cognitive radio with exposed secondary users,” *IEEE Transactions on Vehicular Technology*, vol. 65, no. 7, pp. 5364–5383, July 2016.
- [96] R. Qian and M. Sellathurai, “On the implementation of blind interference alignment with single-radio parasitic antennas,” *IEEE Transactions on Vehicular Technology*, vol. 65, no. 12, pp. 10 180–10 184, Dec 2016.
- [97] M. Artuso, D. Boviz, A. Checko, H. L. Christiansen, B. Clerckx, L. Cottatellucci, D. Gesbert, B. Gizas, A. Gopalasingham, F. Khan, J. Kelif, R. Muller, D. Ntaikos, K. Ntougias, C. B. Papadias, B. Rassouli, M. A. Sedaghat, T. Ratnarajah, L. Roullet, S. Senecal, H. Yin, and L. Zhou, “Enhancing LTE with cloud-RAN and load-controlled parasitic antenna arrays,” *IEEE Communications Magazine*, vol. 54, no. 12, pp. 183–191, December 2016.

- [98] Z. Bouida, H. El-Sallabi, A. Ghrayeb, and K. A. Qaraqe, "Reconfigurable antenna-based space-shift keying (SSK) for MIMO Rician channels," *IEEE Transactions on Wireless Communications*, vol. 15, no. 1, pp. 446–457, Jan 2016.
- [99] Z. Bouida, H. El-Sallabi, M. Abdallah, A. Ghrayeb, and K. A. Qaraqe, "Reconfigurable antenna-based space-shift keying for spectrum sharing systems under Rician fading," *IEEE Transactions on Communications*, vol. 64, no. 9, pp. 3970–3980, Sept 2016.
- [100] R. Senanayake, P. J. Smith, P. A. Martin, and J. S. Evans, "Performance analysis of reconfigurable antenna arrays," *IEEE Transactions on Communications*, vol. 65, no. 6, pp. 2726–2739, June 2017.
- [101] P. J. Smith, A. Firag, P. A. Martin, and R. Murch, "SNR performance analysis of reconfigurable antennas," *IEEE Communications Letters*, vol. 16, no. 4, pp. 498–501, April 2012.
- [102] M. H. Yilmaz, M. M. Abdallah, H. M. El-Sallabi, J. F. Chamberland, K. A. Qaraqe, and H. Arslan, "Joint sub-carrier and antenna state selection for cognitive heterogeneous networks with reconfigurable antennas," *IEEE Transactions on Communications*, vol. 63, no. 11, pp. 4015–4025, Nov 2015.
- [103] A. Abdalrazik, H. Soliman, M. F. Abdelkader, and T. M. Abuelfadl, "Power performance enhancement of underlay spectrum sharing using microstrip patch ESPAR antenna," in *2016 IEEE Wireless Communications and Networking Conference*, April 2016, pp. 1–6.
- [104] C. Sun, A. Hirata, T. Ohira, and N. C. Karmakar, "Fast beamforming of electronically steerable parasitic array radiator antennas: theory and experiment," *IEEE Transactions on Antennas and Propagation*, vol. 52, no. 7, pp. 1819–1832, July 2004.
- [105] R. Qian, M. Sellathurai, and D. Wilcox, "A study on MVDR beamforming applied to an ESPAR antenna," *IEEE Signal Processing Letters*, vol. 22, no. 1, pp. 67–70, Jan 2015.
- [106] H. Du, Y. Sun, and Z. Wu, "Robust beamforming for ESPAR-based cognitive radio MIMO system," in *2017 IEEE/CIC International Conference on Communications in China (ICCC)*, Oct 2017, pp. 1–5.
- [107] B. Hassibi and B. M. Hochwald, "How much training is needed in multiple-antenna wireless links?" *IEEE Transactions on Information Theory*, vol. 49, no. 4, pp. 951–963, April 2003.
- [108] M. Medard, "The effect upon channel capacity in wireless communications of perfect and imperfect knowledge of the channel," *IEEE Transactions on Information Theory*, vol. 46, no. 3, pp. 933–946, 2000.

- [109] M. Shirazi and A. Vosoughi, “On distributed estimation in hierarchical power constrained wireless sensor networks,” *IEEE Transactions on Signal and Information Processing over Networks*, vol. 6, pp. 442–459, 2020.
- [110] H. R. Ahmadi and A. Vosoughi, “Impact of wireless channel uncertainty upon distributed detection systems,” *IEEE Transactions on Wireless Communications*, vol. 12, no. 6, pp. 2566–2577, 2013.
- [111] A. Vosoughi and Y. Jia, “How does channel estimation error affect average sum-rate in two-way amplify-and-forward relay networks?” *IEEE Transactions on Wireless Communications*, vol. 11, no. 5, pp. 1676–1687, 2012.
- [112] Y. Jia and A. Vosoughi, “Transmission resource allocation for training based amplify-and-forward relay systems,” *IEEE Transactions on Wireless Communications*, vol. 10, no. 2, pp. 450–455, 2011.
- [113] J. Werner, J. Wang, A. Hakkarainen, D. Cabric, and M. Valkama, “Performance and Cramér–Rao bounds for DoA/RSS estimation and transmitter localization using sectorized antennas,” *IEEE Transactions on Vehicular Technology*, vol. 65, no. 5, pp. 3255–3270, May 2016.
- [114] X. Guo, Y. He, S. Atapattu, S. Dey, and J. S. Evans, “Power allocation for distributed detection systems in wireless sensor networks with limited fusion center feedback,” *IEEE Transactions on Communications*, vol. 66, no. 10, pp. 4753–4766, Oct 2018.
- [115] A. Goldsmith, *Wireless Communications*. Cambridge University Press, 2005.
- [116] T. M. Cover and J. A. Thomas, *Elements of Information Theory (Wiley Series in Telecommunications and Signal Processing)*, 2nd ed. New York, NY, USA: Wiley-Interscience, 2006.
- [117] S. M. Kay, *Fundamentals of statistical signal processing*. Prentice Hall PTR, 1993.
- [118] A. Vosoughi and A. Scaglione, “On the effect of receiver estimation error upon channel mutual information,” *IEEE Transactions on Signal Processing*, vol. 54, no. 2, pp. 459–472, 2006.
- [119] D. P. Bertsekas and A. Scientific, *Convex optimization algorithms*. Athena Scientific Belmont, 2015.
- [120] D. G. Luenberger, Y. Ye *et al.*, *Linear and nonlinear programming*, 4th ed. Springer, 2015.
- [121] S. Stotas and A. Nallanathan, “Optimal sensing time and power allocation in multiband cognitive radio networks,” *IEEE Transactions on Communications*, vol. 59, no. 1, pp. 226–235, January 2011.

- [122] Y. Dong, J. Wang, B. Shim, and D. I. Kim, "DEARER: A distance-and-energy-aware routing with energy reservation for energy harvesting wireless sensor networks," *IEEE Journal on Selected Areas in Communications*, vol. 34, no. 12, pp. 3798–3813, 2016.
- [123] J. F. Shortle, J. M. Thompson, D. Gross, and C. M. Harris, *Fundamentals of queueing theory*. John Wiley & Sons, 2018, vol. 399.
- [124] R. Zhang, H. Chen, P. L. Yeoh, Y. Li, and B. Vucetic, "Full-duplex cooperative cognitive radio networks with wireless energy harvesting," in *2017 IEEE International Conference on Communications (ICC)*, 2017, pp. 1–6.
- [125] X. Guo, Y. He, S. Atapattu, S. Dey, and J. S. Evans, "Power allocation for distributed detection systems in wireless sensor networks with limited fusion center feedback," *IEEE Transactions on Communications*, vol. 66, no. 10, pp. 4753–4766, 2018.
- [126] T. Q. Wu, H. C. Yang, and Y. C. Liang, "Cooperative secondary beam selection for cognitive multiuser MIMO transmission with random beamforming," *IEEE Transactions on Cognitive Communications and Networking*, vol. 2, no. 2, pp. 141–149, June 2016.
- [127] Y. Wang, Y. Niu, H. Wu, Z. Han, B. Ai, and Q. Wang, "Sub-channel allocation for device-to-device underlaying full-duplex mmwave small cells using coalition formation games," *IEEE Transactions on Vehicular Technology*, vol. 68, no. 12, pp. 11 915–11 927, 2019.
- [128] D. Li and X. Sun, *Nonlinear integer programming*. Springer Science & Business Media, 2006, vol. 84.
- [129] S. Boyd, S. P. Boyd, and L. Vandenberghe, *Convex optimization*. Cambridge university press, 2004.
- [130] S. Seth, D. Roy, and M. Yuksel, "Spectrum sharing secondary users in presence of multiple adversaries," in *Proceedings of International Conference on NETwork Games, Control and Optimization (NetGCoop)*, 2020.